NOTICE

The quality of this microform is heavily dependent upon the quality of the original thesis submitted for microfilming. Every effort has been made to ensure the highest quality of reproduction possible.

If pages are missing, contact the university which granted the degree.

Some pages may have indistinct print especially if the original pages were typed with a poor typewriter ribbon or if the university sent us an inferior photocopy.

Reproduction in full or in part of this microform is governed by the Canadian Copyright Act, R.S.C. 1970, c. C-30, and subsequent amendments.

AVIS

La qualité de cette microforme dépend grandement de la qualité de la thèse soumise au microfilmage. Nous avons tout fait pour assurer une qualité supérieure de reproduction.

S'il manque des pages, veuillez communiquer avec l'université qui a conféré le grade.

La qualité d'impression de certaines pages peut laisser à désirer, surtout si les pages originales ont été dactylographiées à l'aide d'un ruban usé ou si l'université nous a fait parvenir une photocopie de qualité inférieure.

La reproduction, même partielle, de cette microforme est soumise à la Loi canadienne sur le droit d'auteur, SRC 1970, c. C-30, et ses amendements subséquents.

SYNRIFT SEDIMENTATION IN THE UPPER CARBONIFEROUS CANYON FIORD FORMATION, SW ELLESMERE ISLAND, CANADIAN ARCTIC

by

Pierre Thériault

A Thesis

Submitted to the School of Graduate Studies and Research

in Partial Fulfillment of the Requirements for the

Degree of Master of Science

in Geology

Ottawa-Carleton Geoscience Centre

University of Ottawa

Ottawa, Ontario

ISBN 0-315-68019-9

UNIVERSITÉ D'OTTAWA
UNIVERSITY OF OTTAWA

ABSTRACT

The Upper Carboniferous Canyon Fiord Formation is genetically related to continental rifting during the early history of Sverdrup Basin. The basal part of the formation, which represents the oldest synrift deposits of the study area on southwestern Ellesmere Island, has been subdivided into five distinct facies assemblages: i) a lower sandstone assemblage, deposited in the floodplain environment of high sinuosity streams, and locally in lacustrine and paludal environments; ii) a conglomerate assemblage, deposited in the alluvial fan to proximal braided stream environment; iii) an upper sandstone assemblage, deposited in braided stream and coastal plain environments; iv) an evaporite assemblage, deposited in a local coastal playa and hypersaline lagoon; and v) a limestone assemblage, deposited in restricted to relatively open, shallow marine environments. These assemblages are exposed within two N-S-oriented outcrop belts, informally called the Trold Fiord belt and the Blind Fiord belt. The outcrop belts are separated by a N-S oblique strike-slip fault of Tertiary age, and are associated with two distinct, Late Carboniferous half-grabens of opposite polarity: i) the Trold Fiord Depression, situated in the northeastern part of the study area; and ii) the Blind Fiord Depression, situated in the southwestern part of the study area.

The characteristics of the Trold Fiord and Blind Fiord basin-fill successions indicate that sedimentation was controlled by at least two tectono-sedimentary episodes (TSE-1 and TSE-2). In response to these episodes, the paleogeography of the Trold Fiord and Blind Fiord depressions evolved as follows: i) continental half-grabens with interior drainage during Early TSE-1 (late Bashkirian ?); ii) continental half-grabens with local fault-scarp drainage and regional axial drainage during Late TSE-1 (early Moscovian ?); iii) continental/marine half-grabens with local fault-scarp drainage and regional axial drainage in the central to northern Trold Fiord Depression, and nearshore shallow marine processes in the southern Trold Fiord Depression and throughout the Blind Fiord Depression, during Earliest TSE-2 (middle / late middle Moscovian); iv) marine half-grabens with nearshore shallow marine processes, and local coastal playa to hypersaline lagoon processes in the southern Trold Fiord Depression, during Early TSE-2 (middle / early late Moscovian); and v) marine half-grabens with coastal to open platform processes during Late TSE-2 (latest Moscovian), and probably during TSE-3, TSE-4, etc. (latest Carboniferous to Early Permian ?).

RÉSUMÉ

La Formation de Canyon Fiord d'âge Carbonifère tardif est génétiquement reliée à une phase de rifting au début de la formation du bassin de Sverdrup. La partie basale de cette formation, qui constitue les plus anciens dépôts synrifts de la région d'étude dans le sud-ouest de l'île d'Ellesmere, a été subdivisée en cinq faciès sédimentaires: i) un faciès inférieur à grès, formé dans un milieu de plaines d'inondations associé à des rivières fortement sinueuses, et localement dans des milieux lacustres et paludaux; ii) un faciès à conglomérats, formé dans un milieu de cônes de déjection à rivières en tresses proximales; iii) un faciès supérieur à grès, formé dans des milieux de rivières en tresse et de plaines côtières ; iv) un faciès à évaporites, formé localement dans un playa côtier à lagon hypersalin; et v) un faciès à calcaires, formé dans un milieu marin peu profond variant de restraint à relativement ouvert. Ces assemblages sédimentaires affleurent à l'intérieur de deux ceintures d'affleurements d'orientation nord-sud, appellées la ceinture Trold Fiord et la ceinture Blind Fiord. Ces ceintures d'affleurements sont séparées par une faille de décrochement oblique d'âge Tertiaire et d'orientation nord-sud, et sont associées à deux demi-grabens Carbonifères de polarité opposée: i) le Trold Fiord Depression, situé dans la partie sud-ouest de la région d'étude; et ii) le Blind Fiord Depression, situé dans la partie nord-est de la région d'étude.

La séquence sédimentaire caractérisant chacun des demi-grabens indique que la sédimentation fut controllée par au moins deux épisodes tectono-sédimentaires, nommés TSE-1 et TSE-2. En réponse à ces deux épisodes tectono-sédimentaires, la paléogéographie du Trold Fiord Depression et du Blind Fiord Depression a évoluée comme suit: i) demi-grabens continentaux avec drainage interne durant le début de TSE-1 (Bashkirien tardif?); ii) demi-grabens continentaux avec drainage d'escarpement de faille local et drainage axial regional durant la fin de TSE-1 (Moscovien précoce?); iii) demi-grabens continentaux/ marins avec drainage d'escarpement de faille local et drainage axial régional dans la partie centrale et nord du Trold Fiord Depression, et processus côtiers dans la partie sud du Trold Fiord Depression ainsi qu'à la grandeur du Blind Fiord Depression, durant l'initiation de TSE-2 (Moscovien moyen à moyen tardif); iv) demi-grabens marins avec processus côtiers, et localement avec processus de playa côtier à lagon hypersalin dans le sud du Trold Fiord Depression, durant le début de TSE-2 (Moscovien moyen à tardif); et v) demi-grabens marins avec processus côtiers à plate-forme ouverte durant la fin de TSE-2 (Moscovien tardif), et se poursuivant probablement durant TSE-3, TSE-4, etc. (Carbonifère tardif à Permien précoce?).

ACKNOWLEDGEMENTS

I would first like to thank my supervisors, Drs. Benoît Beauchamp, Brian Rust, and André Desrochers for their invaluable guidance, support, and motivation throughout the course of this project. Their contribution in improving the organization, scientific rigour, and "English" of early drafts, although invaluable, is only second to what I learned from them by their example: their professionalism and work intensity will always remain an inspiration to me. I will miss Brian, who died of malaria in June 1990. I am also thankful to the following scientists, technicians, field assistants, friends, and relatives for their help, encouragement, and support: Wayne Bamber, Georges Beaudoin, Jon Devaney, Owen Dixon, Al Donaldson, Gene Dougherty, Ashton Embry, Denis Fillion, Keiko Hattori, Edward Hearn, Charles Henderson, Roy Krouse, François Lalonde, Julie Lamirande, Alyne Lemieux, Jean Morin, Kevin Mutterback, Walter Nassichuk, Alain Plouffe, Patrick Plouffe, Martine Savard, Colleen Sherry, Jean-François Tardif, Robert Thériault, Carol Wallace, Don Watanabe and Ray Yole.

Financial and logistical field support was provided by the following organizations: Fonds pour la Formation de Chercheurs et l'Aide à la Recherche (Postgraduate Scholarship); Geological Survey of Canada (Institute of Sedimentary and Petroleum Geology); Natural Sciences and Engineering Research Council of Canada (Grants to Drs. B.R. Rust and A. Desrochers); Northern Scientific Training Program Funds; Polar Continental Shelf Project; University of Ottawa (Postgraduate Scholarship).

"How many years can a mountain exist,
before it is washed to the sea ?.....
The answer, my friend, is blowin' in the wind"

Bob Dylan

TABLE OF CONTENTS

LIST OF FIGURES

LIST OF PLATES

CHAPTER 1: INTRODUCTION

1.1 Purpose and Objectives

The Upper Carboniferous Canyon Fiord Formation is a clastic-dominated unit that outcrops as a narrow band along the margin of Sverdrup Basin, a rift basin underlying the Canadian Arctic Archipelago (Fig. 1). Exposures are known from northern Melville Island, northwestern Devon Island, and many areas of Ellesmere Island. The formation was deposited in response to an active phase of continental extension at the basin margin, associated with Late Carboniferous to Early Permian rifting. In a detailed study of the upper Paleozoic succession on Raanes Peninsula, southwestern Ellesmere Island, Beauchamp (1987) subdivided the Canyon Fiord Formation into three informal members: i) a lower clastic member, consisting of fluvial conglomerate and sandstone; ii) a middle limestone member, consisting of shallow marine limestone; and iii) an upper clastic member, consisting of shallow marine sandstone and subordinate limestone. Whereas the middle limestone and upper clastic members have been extensively studied, the lower clastic member has not yet been investigated in detail, and its sedimentology remains poorly understood.

The present study focusses on the lower clastic member of the Canyon Fiord Formation, and its transition with the overlying limestone member. The specific objectives are:

1. To identify distinct facies assemblages, and determine their spatial distribution
2. To describe the various facies assemblages, and interpret their depositional environments

Figure 1: Exposures of Canyon Fiord Formation at margin of Sverdrup Basin. The study area is located in the northern part of #7, on Raanes Peninsula (from Beauchamp et al., 1989a).

SVERDRUP BASIN

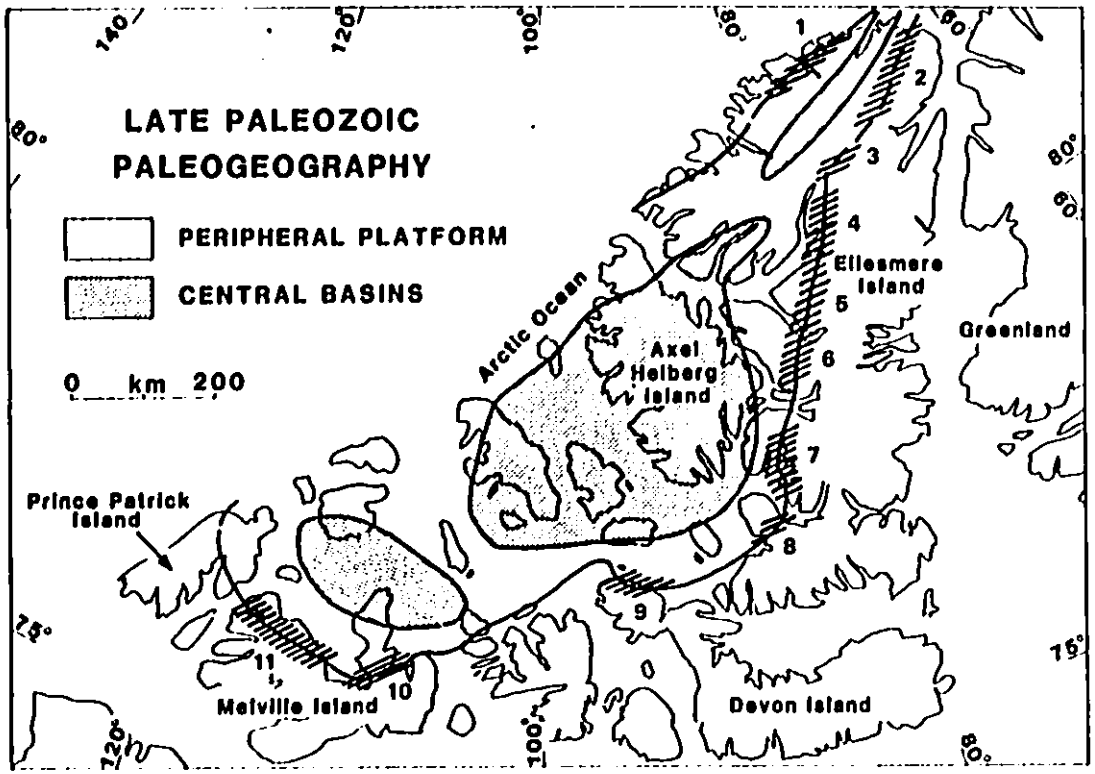

1. M'Clintock Inlet - Markham Fiord
2. Clements Markham Inlet/River
3. Henrietta Nesmith Glacier
4. North Greely Fiord
5. Hamilton Peninsula
6. Fosheim Peninsula
7. Raanes/Svendsen peninsulas
8. Bjorne Peninsula
9. Grinnell Peninsula
10. Sabine Peninsula
11. Marie Bay - McCormick Inlet

3. To reconstruct the paleogeography of the study area during its Late Carboniferous synrift history
4. To infer the tectono-sedimentary evolution of the basal Canyon Fiord Formation.

This study complements that of Beauchamp (1987), and sheds new light on the early rifting history on Raanes Peninsula, shown here to have been characterized by the development of two subbasins in which continental sedimentation was rapidly succeeded by marine sedimentation.

1.2 Geographic Situation

The Canyon Fiord Formation, exposed at the periphery of Sverdrup Basin, unconformably overlies either the Lower Carboniferous Emma Fiord Formation (the oldest deposits in the basin), or Ordovician to Devonian basement rocks of the Franklinian Mobile Belt (Fig. 2). The formation is exposed on northern Melville Island, on north vestern Devon Island, and on southwestern to northern Ellesmere Island (Fig. 1). The type section of the Canyon Fiord Formation, on the north shore of Cañon Fiord, west-central Ellesmere Island, was first described by Troelsen (1950), and later emended by Thorsteinsson (1974). J.C. Troelsen's spelling of the formation ("Canyon") differs from the original spelling of the fiord ("Cañon"; Sverdrup, 1904), as several maps published after Otto Sverdrup's geographic discovery used the alternate orthography "Canyon" (Thorsteinsson, 1974). No exposures of equivalent strata have been reported at the western margin of the basin, where Paleozoic and Mesozoic rocks are mainly covered by the younger Cenozoic arctic coastal plain and continental shelf.

The study area is in the eastern part of Raanes Peninsula (southwestern Ellesmere Island), which is bounded by Bay Fiord to the north, Eureka Sound to the west, Baumann

Figure 2: Transgressive-regressive sequences of second- and third-order in the Carboniferous to Lower Triassic succession of Sverdrup Basin (from Beauchamp et al., 1989b). The Borup Fiord Formation is now thought to form a distinct sequence (Sequence 2) between the locally exposed Emma Fiord Formation (Sequence 1) and the younger Antoinette, Nansen, and Otto Fiord formations (now Sequence 3).

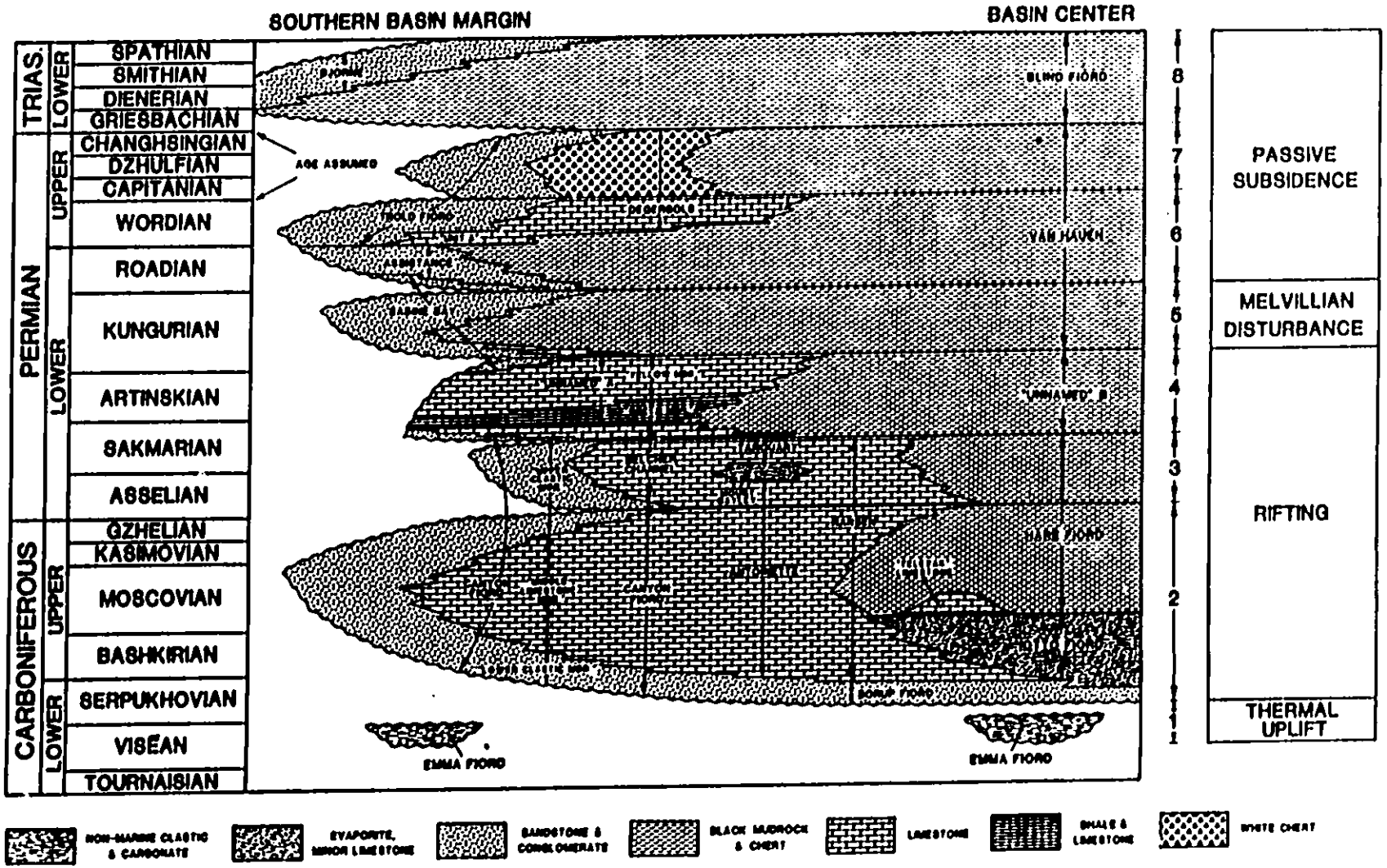
SOUTHERN BASIN MARGIN
BASIN CENTER
TRIAS.
LOWER
SPATHIAN
SMITHIAN
DIENERIAN
GRIESBACHIAN
PERMIAN
UPPER
CHANGHSINGIAN
DZHULFIAN
CAPITANIAN
WORDIAN
LOWER
ROADIAN
KUNGURIAN
ARTINSKIAN
SAKMARIAN
ASSELIAN
CARBONIFEROUS
UPPER
GZHELIAN
KASIMOVIAN
MOSCOVIAN
BASHKIRIAN
LOWER
SERPUKHOVIAN
VISEAN
TOURNAISIAN
AGE ASSUMED
BLIND FIORD
VAN HAUEN
"UNNAMED" B
HARE FIORD
EMMA FIORD
EMMA FIORD
8
7
6
5
4
3
2
1
PASSIVE SUBSIDENCE
MELVILLIAN DISTURBANCE
RIFTING
THERMAL UPLIFT
NON-MARINE CLASTIC & CARBONATE
EVAPORITE, MINOR LIMESTONE
SANDSTONE & CONGLOMERATE
BLACK MUDROCK & CHERT
LIMESTONE
SHALE & LIMESTONE
WHITE CHERT

Fiord to the south, and Trold Fiord to the southeast (Fig. 3). The peninsula is partly bisected by Blind Fiord, a north-south oriented inlet to the west of and parallel to Trold Fiord. The study area is situated between 78°16'N and 78°38'N of latitude, and between 84°33'W and 85°20'W of longitude.

1.3 Methods

Field work on southwestern Ellesmere Island was carried out between June 15 and August 15 of 1989, with the support of the Institute of Sedimentary and Petroleum Geology (Geological Survey of Canada). A total of 28 stratigraphic sections (Appendix 1), ranging in thickness from 10m to 250m, were measured, described, and sampled (Appendix 5) within an area of approximately 250 km^2 (Fig. 4; Appendix 2).

Samples were collected for conodont biostratigraphy, isotopic geochemistry, and petrography. Conodont processing and identification was performed at the Institute of Sedimentary and Petroleum Geology in Calgary by Dr. Charles Henderson. Oxygen, carbon, and sulphur isotopic analyses of carbonate and evaporite samples were done under the supervision of Dr. Roy Krouse, at the University of Calgary. Polished hand specimens and standard petrographic thin sections were produced at the University of Ottawa for petrographic observations.

1.4 Previous Work

Preliminary geological investigations in the Canadian Arctic Archipelago started early in the 1800's, when British naval expeditions entered Baffin Bay in search of the Northwest Passage (Dawes and Christie, 1982). Half a century later, and following the ill-fated Franklin expedition in 1845, several rescue operations were organized, from which coastline maps as well as fossil and rock collections were upgraded (Harker and

Figure 3: Simplified geological map of study area and adjacent areas on Raanes Peninsula, southwestern Ellesmere Island. Pre-Cenozoic strata are progressively younger towards the west. The two faults, shown as thrusts, are now thought to be dextral strike-slip faults (modified from Thorsteinsson, 1974; Map 1300A).

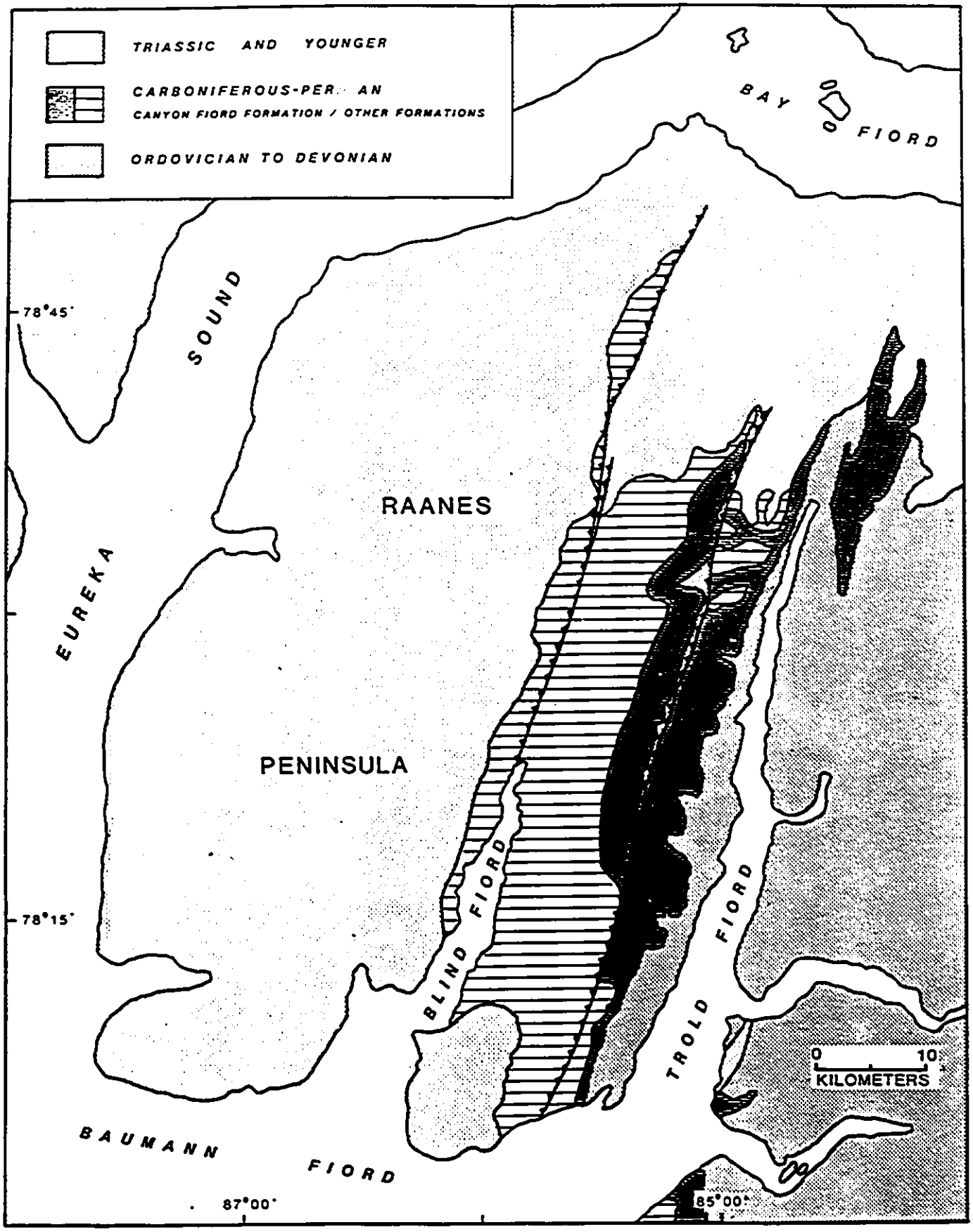
TRIASSIC AND YOUNGER
CARBONIFEROUS-PERMIAN
CANYON FIORD FORMATION / OTHER FORMATIONS
ORDOVICIAN TO DEVONIAN
BAY
FIORD
78°45'
SOUND
RAANES
EUREKA
PENINSULA
78°15'
BLIND FIORD
TROLD FIORD
0
10
KILOMETERS
BAUMANN
FIORD
87°00'
85°00'

Figure 4: Map showing location of measured stratigraphic sections. Exposures of the Canyon Fiord Formation occur within two narrow bands called the Blind Fiord belt (to the west) and the Trold Fiord belt (to the east). Section 10 is included in the Trold Fiord belt.

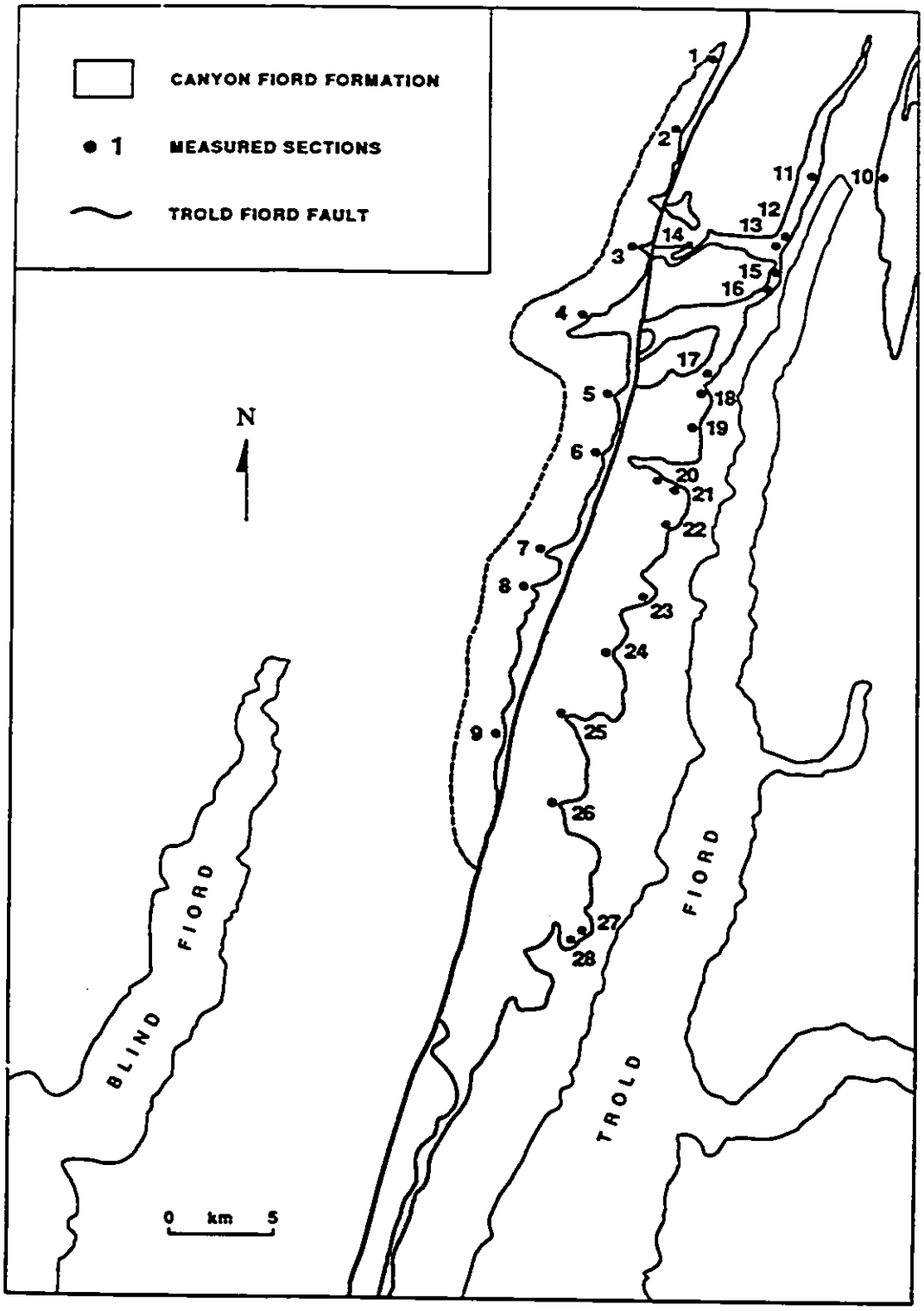
CANYON FIORD FORMATION
1 MEASURED SECTIONS
TROLD FIORD FAULT
N
BLIND FIORD
TROLD FIORD
0 km 5
1
2
3
4
5
6
7
8
9
10
11
12
13
14
15
16
17
18
19
20
21
22
23
24
25
26
27
28

Thorsteinsson, 1960). The geological knowledge of Ellesmere and eastern Axel Heiberg islands was considerably improved as a result of an expedition commanded by Capt. Otto Sverdrup, between 1898 and 1902. Per Shei, a geologist attached to this expedition, subsequently published sketch maps of, and reports describing, the Precambrian basement and overlying Paleozoic and Mesozoic stratigraphy (Shei, 1903). The next important contribution to the geology of northeastern Arctic regions came from the Danish Thule-Ellesmere Land Expedition in 1939-41, when J.C. Troelsen undertook coastline and inland investigations by dogsled (Troelsen, 1950). He later produced evidence for at least two deformational events on Ellesmere Island (Troelsen, 1952).

Geologists attached to Operation Franklin, a reconnaissance GSC survey in 1955, performed extensive stratigraphical and structural investigations in order to evaluate the hydrocarbon potential of the High Arctic (Fortier et al., 1963). Thorsteinsson (1974) later produced a comprehensive account of the upper Paleozoic stratigraphy of Axel Heiberg and western Ellesmere Island, which was the result of a regional project operated by the Geological Survey of Canada between 1956 and 1963. Minor modifications to Thorsteinsson's concepts were proposed by W.W. Nassichuk, who refined the stratigraphic framework for Raanes Peninsula (Nassichuk, 1975a,b; Nassichuk and Wilde, 1977). More recently, a detailed investigation was carried out by B. Beauchamp on Raanes Peninsula in the course of his Ph.D. thesis (Beauchamp, 1987). This study evolved into a long-term, ongoing GSC project dealing with the upper Paleozoic stratigraphy of Sverdrup Basin (Beauchamp et al., 1989a,b). The present M.Sc. study on the basal part of the Canyon Fiord Formation has been sponsored by the GSC through that project.

The Canyon Fiord Formation was first documented and named by Troelsen (1950) for an occurrence at Caledonian Bay, on the east coast of Cañon Fiord, west-central Ellesmere Island (see Hamilton Peninsula; Fig. 1). Additional exposures were found by members of Operation Franklin in the vicinity of Trold Fiord (Tozer, 1963) and Eids Fiord (McLaren, 1963) on southwestern Ellesmere Island, and on Sabine Peninsula, Melville

Island (Tozer, 1963). The type section at Caledonian Bay was emended and described in much detail by Thorsteinsson (1974). The formation has been studied elsewhere on Ellesmere Island (Fig. 1), namely on Fosheim and Hamilton peninsulas, and along Tanquary Fiord, Clements Markham River, Clements Markham Inlet, Markham Fiord, M'Clintock Inlet, and the Henrietta Nesmith Glacier (Trettin, 1969; Thorsteinsson, 1974; Mayr, in press). Exposures of the Canyon Fiord Formation have been also reported on Grinnell Peninsula, Devon Island (Nassichuk, 1965), an area where the unit was originally included in the type section of the Belcher Channel Formation (Harker and Thorsteinsson, 1960). Recent work by Harrison and Riediger (in press) on northern Melville Island, and by Thériault and Beauchamp (1991) on west-central Ellesmere Island, has focussed on establishing preliminary depositional models and understanding the tectonic setting of the formation.

1.5 Geological Setting

1.5.1 Canadian Arctic Archipelago

Lying at the northern tip of North America, the Canadian Arctic Archipelago consists of a land area of approximately $3X10^6$ km^2 segmented by numerous inter-island channels and fiords. The archipelago is underlain predominantly by Upper Proterozoic to Cenozoic sedimentary rocks that rest on the Canadian Shield to the south (Fig. 5). Six distinct geological provinces are recognized (Trettin, 1989): i) the Canadian Shield; ii) the Interior Platform; iii) the Franklinian Mobile Belt; iv) Sverdrup Basin; x) the Arctic Platform; and xi) the Arctic Continental Terrace Wedge.

The **Canadian Shield** is present as continuous exposures in the eastern part of the archipelago, and as outliers on the western islands. It comprises Archean to Lower Proterozoic crystalline basement, and a rift-related sedimentary/volcanic succession of late Early Proterozoic to Late Proterozoic age (Frisch, 1983; Trettin, 1989).

Figure 5: Map of geological provinces of the Canadian Arctic Archipelago (modified from Trettin, 1989).

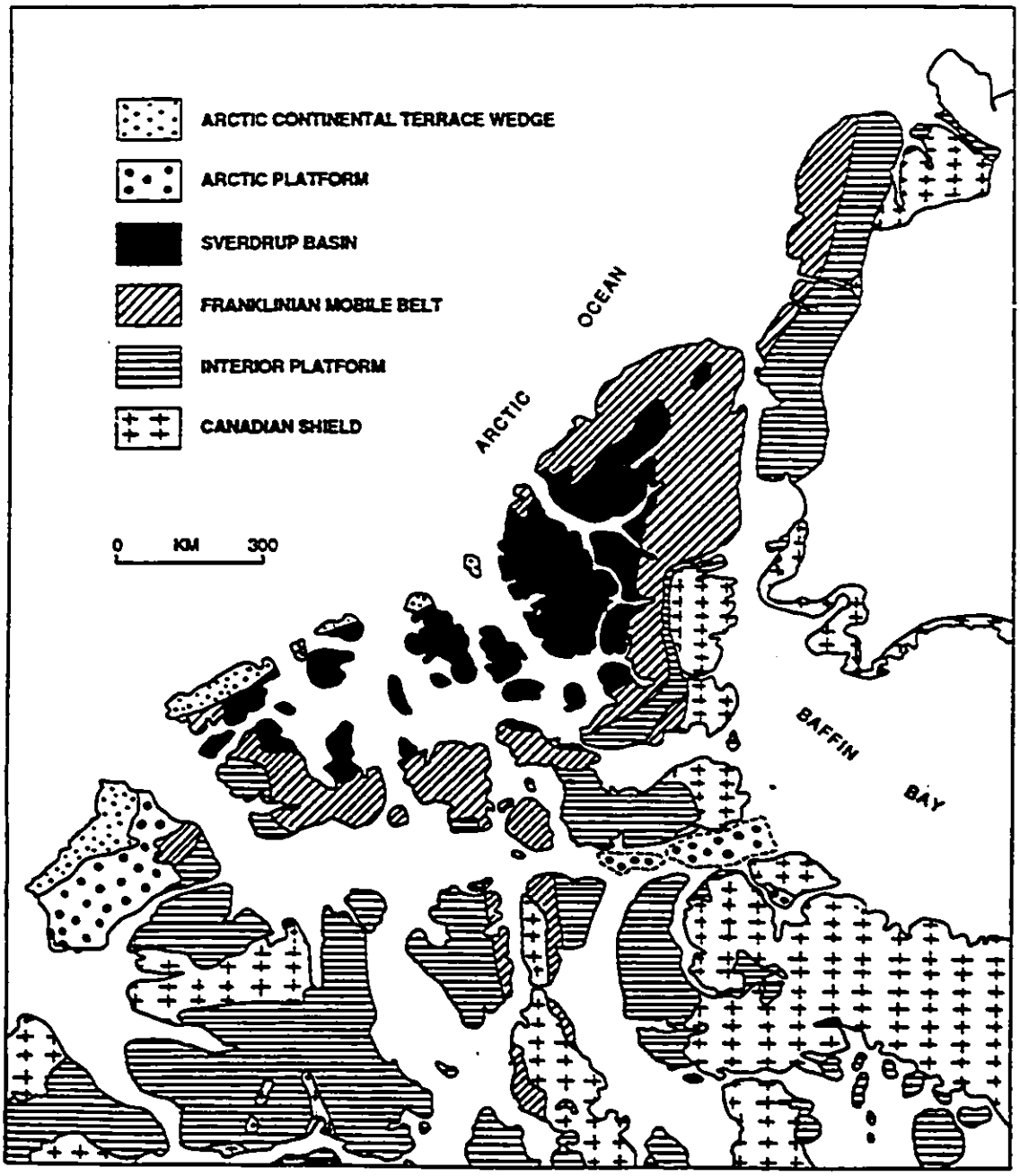
ARCTIC CONTINENTAL TERRACE WEDGE
ARCTIC PLATFORM
SVERDRUP BASIN
FRANKLINIAN MOBILE BELT
INTERIOR PLATFORM
CANADIAN SHIELD
0 KM 300
ARCTIC
OCEAN
BAFFIN
BAY

The Cambrian to Devonian **Interior Platform** directly overlies the shield and delineates its northernmost extension at the surface. This province is composed mainly of flat-lying, shallow marine carbonates that are laterally continuous with contemporaneous shelf deposits more severely affected by orogenic activity in the Franklinian Mobile Belt (Trettin, 1989).

The **Franklinian Mobile Belt** is widely exposed in the northern part of the archipelago on Ellesmere Island, Bathurst Island, and Melville Island. It also extends south as flanking beds on the Boothia Uplift, a compressional structure of N-S orientation. The Franklinian Mobile Belt comprises a shelf succession dominated by carbonate sediments, and a deep basinal succession consisting of fine-grained clastics and volcanic units. The volcanics are intermediate to felsic in composition, and have island-arc affinities. The Franklinian Mobile Belt, initiated probably by rifting in the Late Proterozoic, was first deformed following the oblique accretion of the Pearya terrane (now exposed in northern Ellesmere Island) in the Late Silurian, and subsequently experienced local compressional uplifts in the Late Silurian-Early Devonian. Its depositional history ended with the Late Devonian-Early Carboniferous Ellesmerian Orogeny (Miall, 1986; Trettin, 1989).

A continental rifting event led to the development of **Sverdrup Basin**, which was was initiated in the Early Carboniferous by extension and collapse of the Franklinian Mobile Belt, and ended in the middle Tertiary with the onset of the Eurekan Orogeny. Sverdrup Basin has long been interpreted as a rift basin, based primarily on its intracontinental position, the nature of its thick and nearly continuous Lower Carboniferous to middle Tertiary succession, and the presence of associated volcanic rocks of extensional origin (Thorsteinsson, 1974; Cameron, 1989; Davies and Nassichuk, 1990). Additional features suggest that Sverdrup Basin was initiated by passive rifting, including the lack of evidence supporting domal uplift, the presence of only minor volcanics in very localized areas, and the thick nature of its sedimentary succession. The rifting event lasted from Early Carboniferous to middle Permian time, the early phase of which led to the deposition

of: i) the Emma Fiord Formation, in lacustrine and floodplain environments, locally throughout the basin in Early Carboniferous time; ii) the Borup Fiord Formation, in fluvial and shallow marine environments, at the basin centre in latest Early Carboniferous time; and iii) the basal Canyon Fiord Formation, mainly in fluvial environments, in a series of fault-bounded subbasins restricted to the basin margin in Late Carboniferous time (Harrison et al., 1988; Harrison and Riediger, in press; Thériault and Beauchamp, 1991). These partially infilled subbasins were subsequently covered by marine carbonates (i.e. middle limestone member of the Canyon Fiord Formation) during a basin-wide transgression. This transgression was part of the third of eight, low-order transgressive-regressive sequences that affected the upper Paleozoic succession of Sverdrup Basin (Fig. 2). The overlying Mesosoic to middle Tertiary succession comprises more than thirty similar low-order cycles, deposited during an episode of passive subsidence from the Early Triassic to the earliest Cretaceous, an episode of rifting in the Early Cretaceous, and an episode of passive subsidence from the Late Cretaceous to the middle Tertiary (Stephenson et al., 1987; Embry, 1988; Trettin, 1989). Sedimentation in Sverdrup Basin ended with the middle Tertiary Eurekan Orogeny, related to rotational sea-floor spreading in Labrador Basin (Kerr, 1982; Miall, 1983).

The **Arctic Platform** consists of Mesozoic to Paleogene strata deposited in small basins south of the Sverdrup sea. These basins include Banks Basin, Eglington Sound Basin, and Bylot Trough (Kerr, 1981; Trettin, 1989). Their tectonic setting has not yet been determined.

The **Arctic Continental Terrace Wedge** is a post-Eocene clastic succession, exposed on the northwesternmost islands, which extends offshore as the modern continental shelf of the Arctic Ocean (Devaney and Fyles, 1988; Fyles, 1990). Sediments of this province were deposited following the middle Tertiary Eurekan Orogeny.

1.5.2 Upper Paleozoic succession of Sverdrup Basin

Initiated by rifting in the Early Carboniferous, Sverdrup Basin rapidly expanded to reach 1000km in length and nearly 400km in width by the latest Carboniferous or earliest Permian (Beauchamp et al., 1989a). During this time, the basin was intracontinental in nature, with continental land masses existing to the north and south (Fig. 6). Only narrow straits allowed connections with the global ocean system, such that the basin was nearly landlocked during major sea-level lowstands (Beauchamp et al., 1987).

Sedimentological observations have shown that the late Paleozoic climate of Sverdrup Basin evolved from tropical sub-humid in the Early Carboniferous, to tropical arid/semi-arid in the Late Carboniferous and Early Permian, to temperate sub-humid in the middle Permian, to sub-polar/polar in the latest Permian (Beauchamp et al., 1989a). The nature of this climatic change is in accord with most plate tectonic reconstructions, which show that the Canadian High Arctic migrated from approximately 10°N in the Early Carboniferous, to 40-50°N or more in the Late Permian (Ziegler, 1988). The Upper Carboniferous succession of the Canyon Fiord Formation was deposited under the influence of a tropical arid/semi-arid climate, as evidenced by local marine evaporites, well developed caliche paleosols, and characteristic biotic elements in associated marine carbonates.

Beauchamp et al. (1989b) postulated that the upper Paleozoic succession of Sverdrup Basin consists of seven, transgressive-regressive sequences of second- and third-order periodicity (5Ma to 50Ma), and that the Canyon Fiord Formation, exposed essentially at the basin margin, encompasses Sequences 2 and 3 (Fig. 2). Basinward correlatives to the Canyon Fiord Formation include the Belcher Channel, Antoinette, Mount Bayley, Tanquary, and Nansen formations in the shelf area, and the Otto Fiord and Hare Fiord formations at the basin centre. The lower clastic member of the Canyon Fiord Formation, which is conformably overlain by the middle limestone member, was deposited during the transgressive phase of the second sequence of Beauchamp et al. (1989b), in a series of

Figure 6: Paleogeographic reconstruction of Arctic regions during late Paleozoic/early Mesozoic time. The seaways connecting Sverdrup Basin to the proto-arctic ocean were probably narrower during periods of low sea level (from Embry and Podruski, 1988).

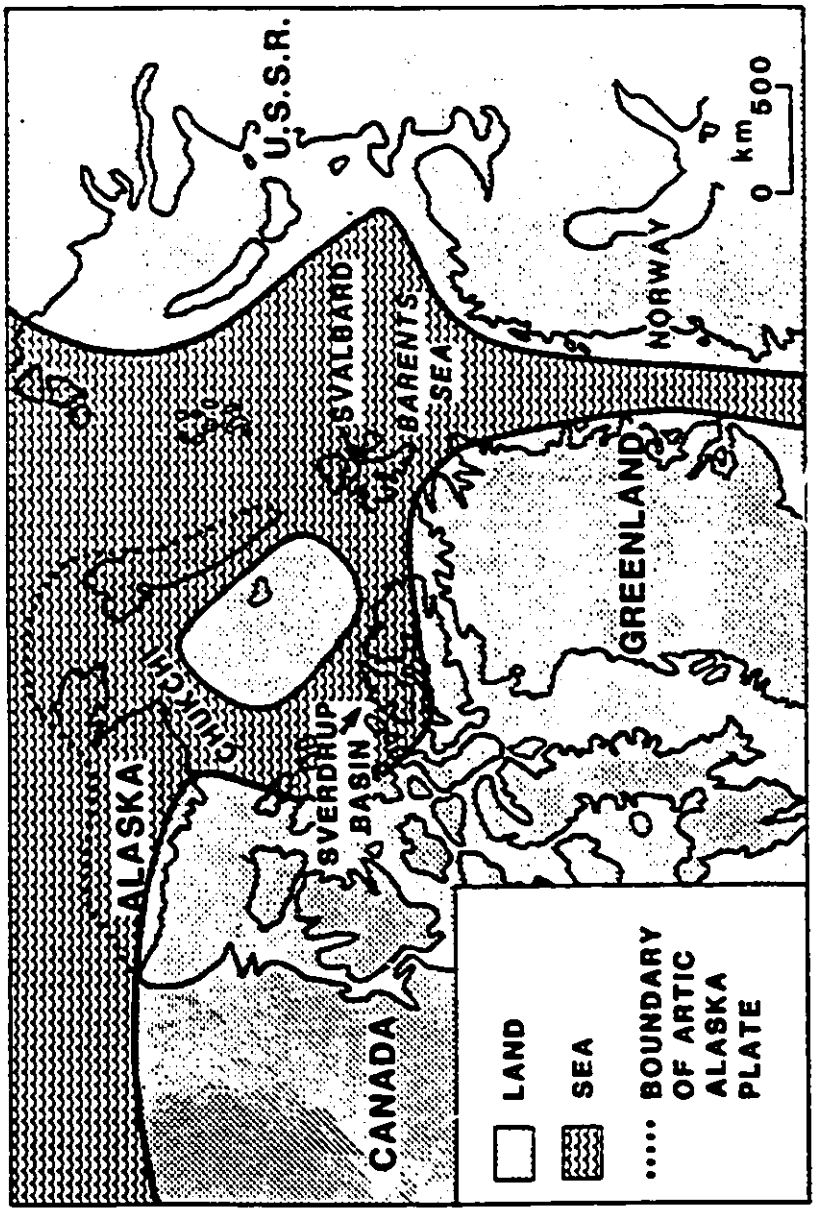
U.S.S.R.
ALASKA
SVERDRUP BASIN
SVALBARD
BARENTS SEA
NORWAY
GREENLAND
CANADA
0 km 600
LAND
SEA
BOUNDARY OF ARTIC ALASKA PLATE

subbasins at the basin margin (Thériault and Beauchamp, 1991). At the basin centre, a similar clastic unit is present and named the Borup Fiord Formation; it is by definition overlain by the Nansen or Otto Fiord formation (Thorsteinsson, 1974). Nassichuk and Davies (1980) and Beauchamp et al. (1989b) suggested that the basal clastic sediments of the Canyon Fiord and Borup Fiord formations may form a continuous and diachronous unit at the base of the second sequence, and extending from the basin margin to the basin centre (Fig. 2). However, the transition of one formation into the other has not yet been observed.

Based on biostratigraphic data, the lower clastic member of the Canyon Fiord Formation and the whole Borup Fiord Formation appear to represent two separate units. Lower Bashkirian to upper Moscovian fossils have been recovered from the basal Canyon Fiord Formation, whereas fossils from the Borup Fiord Formation indicate an early Serpukhovian age (Thorsteinsson, 1974). The older Borup Fiord Formation may therefore be part of a distinct sequence of Sverdrup Basin. This view is further supported by field evidence showing that an unconformity locally separates the Borup Fiord Formation from the overlying Nansen or Otto Fiord formation at the basin centre (Nassichuk and Davies, 1980). This unconformity, as observed by the author during the 1990 field season, cuts down into the Borup Fiord strata by as much as 200m or more at Girty Creek (northwestern Ellesmere Island). Biostratigraphic evidence shows that the basal Canyon Fiord and the Nansen formations are correlative (Thorsteinsson, 1974). The oldest unit of Sverdrup Basin, the Viséan Emma Fiord Formation, is present locally in both marginal and central areas of the basin. This unit is unconformably overlain by the Borup Fiord Formation in northwestern Ellesmere Island, and forms a distinct sequence that is older than the Borup Fiord sequence (Beauchamp et al., 1989b).

In summary, the three oldest sequences of Sverdrup Basin, based on field and biostratigraphic evidence, appear to be as follows: i) a first sequence represented by the Viséan Emma Fiord Formation, present locally in both marginal and central areas of the

basin; ii) a second sequence represented by the Serpukhovian Borup Fiord Formation, present essentially in central and northwestern marginal areas of the basin; and iii) a third sequence represented by the Upper Carboniferous Canyon Fiord and Antoinette formations at or near the basin margin, and by the Nansen, Otto Fiord, and Hare Fiord formations at the basin centre (Fig. 2).

1.5.3 Raanes Peninsula

Sverdrup Basin deposits are widespread and well exposed on Raanes Peninsula (Fig. 3). Triassic and younger units are predominant in the western, southern, and northern parts of the peninsula, whereas the eastern part consists mainly of Carboniferous and Permian units with subordinate Ordovician to Devonian units. These middle Paleozoic units are predominant in the area east of Trold Fiord.

On the basis of upper Paleozoic facies changes, Beauchamp (1987) established that the regional depositional strike was northwest-southeast on Raanes Peninsula during the latest Carboniferous and Permian. Major sequences consist mainly of shallow marine facies in the northeastern part of the peninsula, and of deep basinal facies in the southwestern part of the peninsula. This general depositional slope towards the southwest is nearly perpendicular to that observed elsewhere at the eastern and southeastern margin of Sverdrup Basin (northwest-sloping), suggesting that a major embayment existed in the vicinity of Raanes Peninsula during the late Paleozoic (Beauchamp, 1987). As demonstrated below, the general southwest-oriented depositional slope on Raanes Peninsula appears to have had less influence on sedimentation in the early to middle Late Carboniferous (basal Canyon Fiord time) than it did in latest Carboniferous and Permian time. Instead, facies distribution and dispersal patterns were controlled mainly by the superimposed local topography, resulting from the development of two subbasins on Raanes Peninsula.

The Canyon Fiord Formation is the oldest unit of Sverdrup Basin exposed on Raanes Peninsula, and hence it unconformably overlies deformed Ordovician to Devonian strata of the Franklinian Mobile Belt (Plate 1). The Lower Carboniferous Emma Fiord Formation, which locally underlies the Canyon Fiord Formation along the basin margin, is absent from Raanes Peninsula. The Canyon Fiord Formation is exposed within three distinct zones on Raanes Peninsula (Fig. 4): i) a narrow band, 65km long by less than 6km wide, situated on the western side of Trold Fiord; ii) a band 40km long by less than a few kilometres wide, located to the west of a north-south Tertiary fault, between Blind Fiord and Trold Fiord; and iii) an area east of the head of Trold Fiord, approximately 25km in length by less than 5km in width. The lower clastic member of the formation is exposed on the eastern edge of the two narrow bands between Blind Fiord and Trold Fiord. It also outcrops at one locality east of the head of Trold Fiord.

The geographic restriction of the Canyon Fiord Formation to a few narrow outcrop bands on Raanes Peninsula is the result of Tertiary deformation related to the Eurekan Orogeny. Eurekan structures are ubiquitous, including both compressional and extensional features showing mainly N-S orientations. Most prominent are two west-dipping faults called the Blind Fiord Fault and the Trold Fiord Fault, which extend north-south for several tens of kilometres on Raanes Peninsula (Fig. 3). These structures have been interpreted as oblique faults, each characterized by a minor component of eastward thrust motion and a major component of dextral strike-slip motion (Beauchamp, 1987). The strike-slip interpretation is based on the offset of both older mafic dykes and latest Carboniferous to Permian facies fronts, the magnitude of which was evaluated at 8km along the Blind Fiord Fault, and at 16km or more along the Trold Fiord Fault. Located on the west side of Trold Fiord, the Trold Fiord Fault has displaced the Canyon Fiord strata in such a way that they now outcrop as two adjacent bands of exposures. Because of this Tertiary displacement, the two bands of exposed Canyon Fiord strata do not reflect the relative position that they had at time of deposition in the Late Carboniferous. Partial restoration relocates the western

outcrop band and associated strata farther south by about twenty kilometres (Beauchamp, 1987), and farther west towards the basin centre by an unknown increment (Fig. 7). The steep dip of the fault, however, implies that relative displacement towards the east was not of great importance, perhaps no more than a few kilometres.

Figure 7: Map of Canyon Fiord exposure area after partial restoration along Trold Fiord Fault. Tertiary displacement is estimated at 20km dextral strike-slip motion and 3km thrust motion.

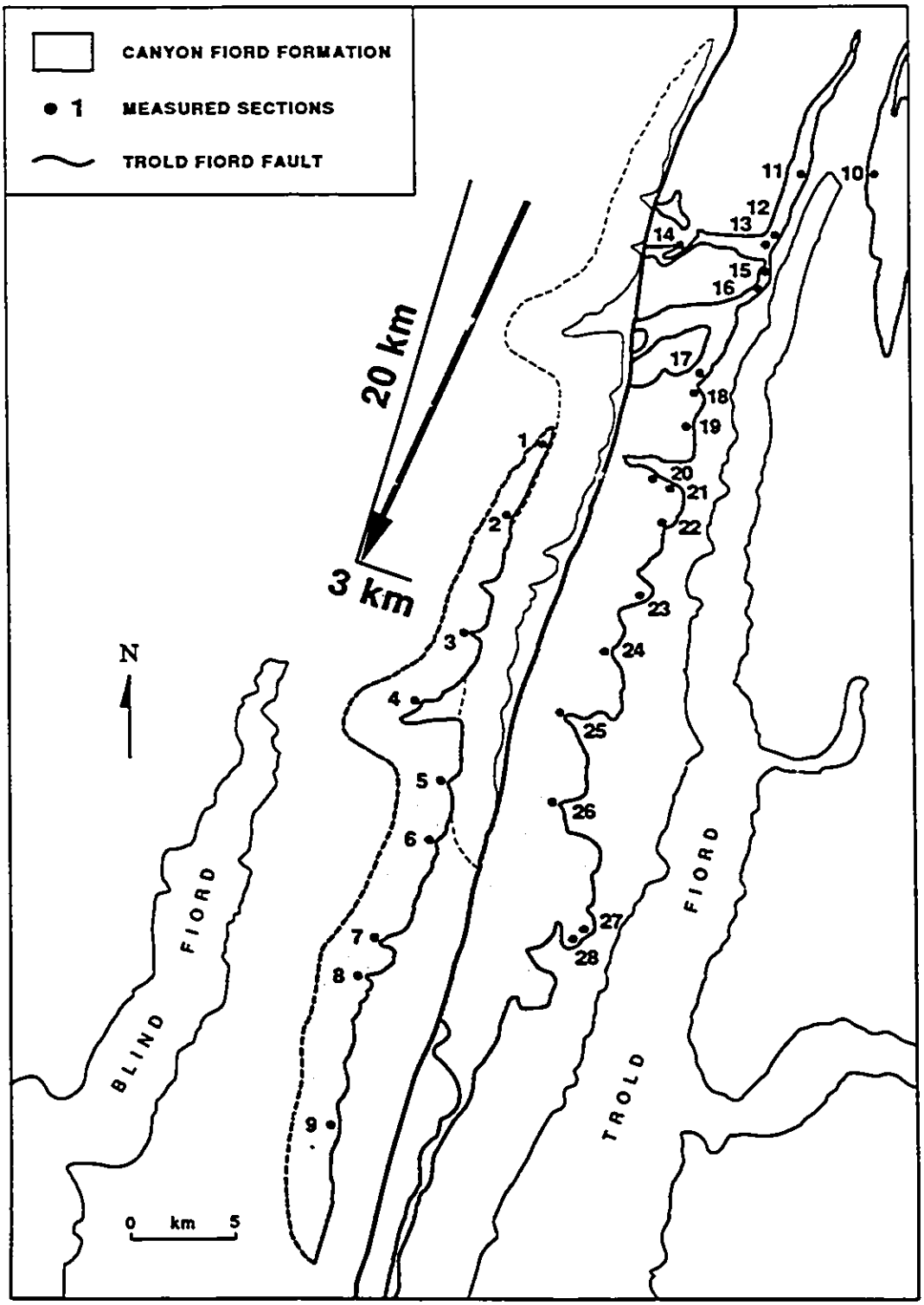
CANYON FIORD FORMATION
1 MEASURED SECTIONS
TROLD FIORD FAULT
20 km
3 km
N
BLIND FIORD
TROLD FIORD
0 km 5
1
2
3
4
5
6
7
8
9
10
11
12
13
14
15
16
17
18
19
20
21
22
23
24
25
26
27
28

CHAPTER 2: STRATIGRAPHY

The Canyon Fiord Formation reaches a maximum cumulative thickness of 1010m, at its type section in the Cañon Fiord area of west-central Ellesmere Island (Thériault and Beauchamp, 1991). The lower clastic member alone is 400m thick, and consists of 90m of conglomerate overlain by 310m of sandstone with minor conglomerate. On Raanes Peninsula, the basal part of the formation reaches 240m in thickness, and consists of five distinct facies assemblages. These are, in ascending stratigraphic order: i) a lower sandstone assemblage; ii) a conglomerate assemblage; iii) an upper sandstone assemblage; iv) an evaporite assemblage; and v) a limestone assemblage (base of the middle limestone member).

As will be discussed in Chapter 5, paleocurrents and facies relationships suggest that the two outcrop belts adjacent to the Trold Fiord Fault are related to two distinct Late Carboniferous subbasins, each with its distinct drainage system. For this reason, stratigraphic correlations will not be attempted across the outcrop belts, which are here termed the "Trold Fiord belt" and the "Blind Fiord belt". The isolated locality to the northeast of Trold Fiord is included in the Trold Fiord belt, since facies relationships between these two exposure areas are concordant with subregional paleogeographic interpretations presented below.

2.1 Trold Fiord Belt

All five facies assemblages are present in the Trold Fiord belt, the distribution and thicknesses of which are illustrated in Figures 8 and 9. The lower sandstone assemblage is locally exposed in the northern part of the belt (Sections 10, 11 and 16; Fig. 8 and 9), where it unconformably overlies either the Devonian Danish River Formation, or the Ordovician Cornwallis Group of the Franklinian Mobile Belt (Appendix 1). The lower

Figure 8: North-south cross-section at the eastern margin of the Trold Fiord belt. Datum represents a time-line, at the top of the conglomerate assemblage. Conodont biostratigraphic zones: A= lower C5b, B= C5a, C= C1 to P2, D= C4 (Beauchamp, 1987) to upper C5a (this study). Vertical exaggeration is approximately 65X.

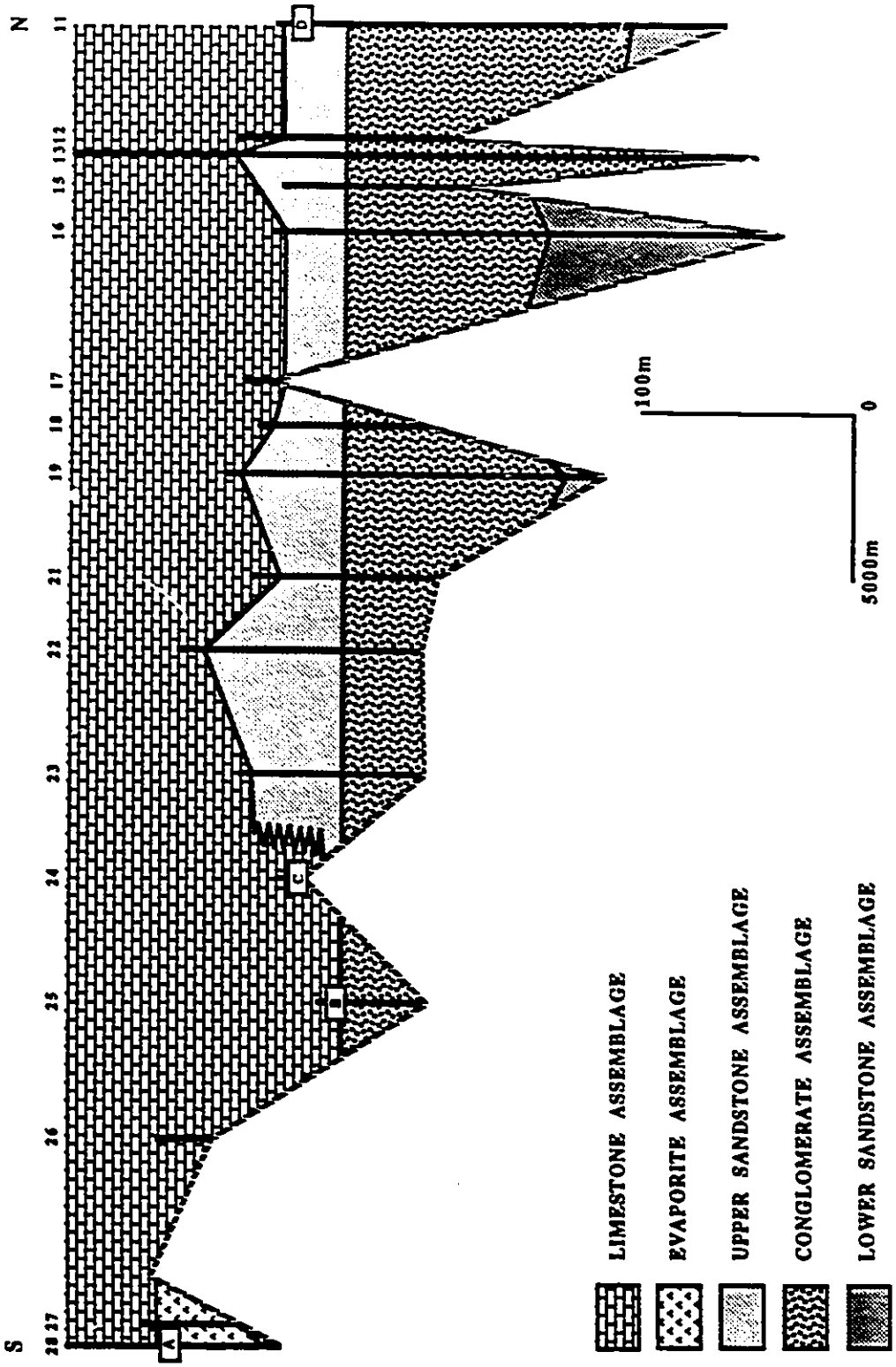
N
S
11
12
13
15
16
17
18
19
21
22
23
24
25
26
27
28
A
B
C
D
100m
0
5000m
LIMESTONE ASSEMBLAGE
EVAPORITE ASSEMBLAGE
UPPER SANDSTONE ASSEMBLAGE
CONGLOMERATE ASSEMBLAGE
LOWER SANDSTONE ASSEMBLAGE

Figure 9: East-west cross-section in the northernmost part of the Trold Fiord belt. Datum represents a time-line, at the top of the conglomerate assemblage. Conodont biostratigraphic zones: A= C4 (Beauchamp, 1987) to upper C5a (this study), B= C4 to C5a, C= upper C5a. Vertical exaggeration is approximately 7X.

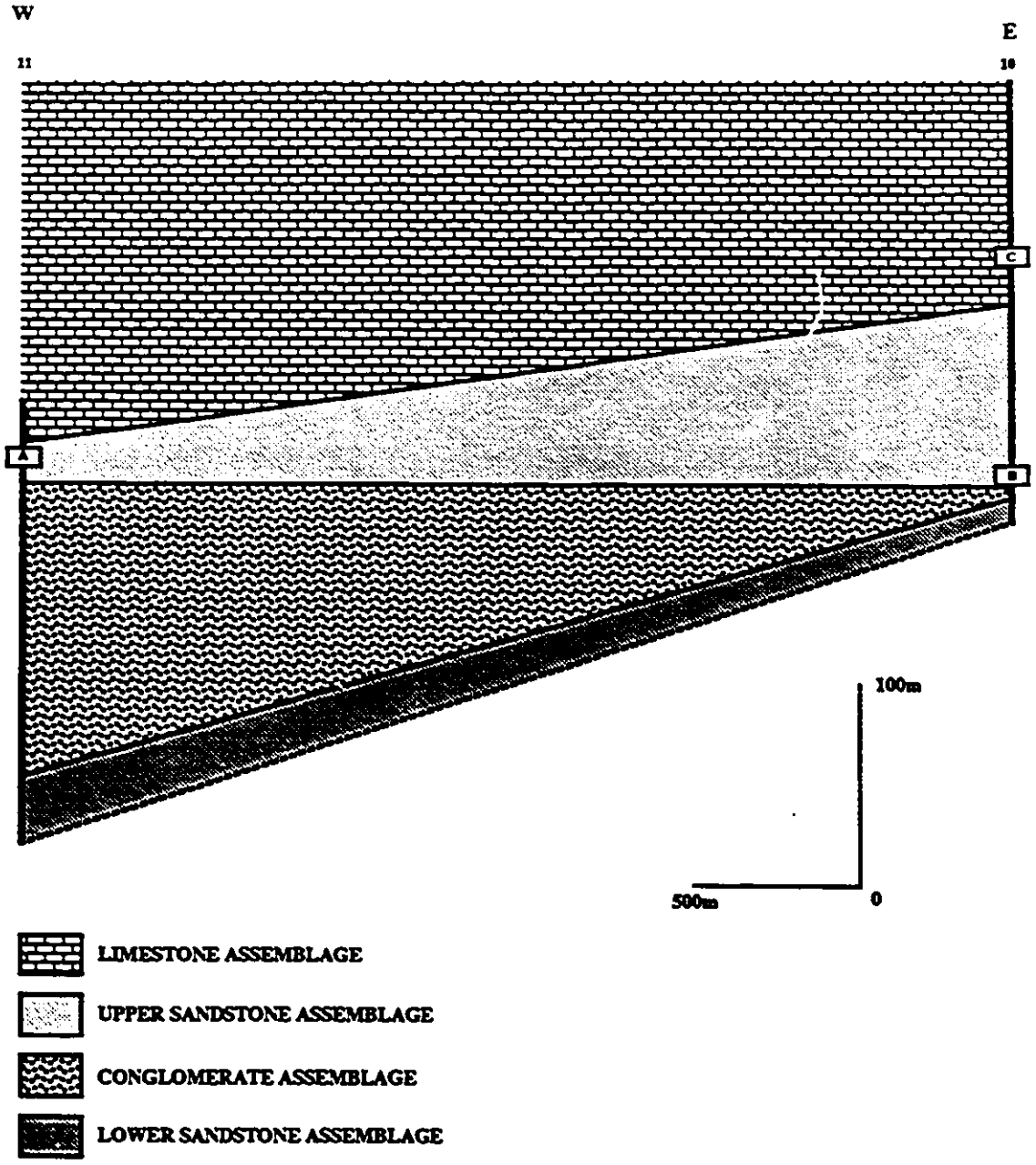
W
E
11
10
C
A
B
100m
500m
0
LIMESTONE ASSEMBLAGE
UPPER SANDSTONE ASSEMBLAGE
CONGLOMERATE ASSEMBLAGE
LOWER SANDSTONE ASSEMBLAGE

sandstone assemblage reaches a maximum thickness of 130m at Section 16. It is probably also present at the base of other sections in the Trold Fiord belt, where a recessive covered interval is present between the Franklinian basement and the conglomerate assemblage (Appendix 1, Sections 13 and 19).

The conglomerate assemblage is the most widespread and locally thickest unit in the Trold Fiord belt, reaching a maximum thickness of 175m at Section 13 (Appendix 1). It is exposed as a nearly continuous package segmented by three paleotopographic highs (Fig. 8). In general, the conglomerate assemblage increases in thickness from south to north, and either conformably overlies the lower sandstone assemblage, or rests with angular unconformity on the Devonian Danish River Formation, the Ordovician to Devonian Cape Phillips Formation, or the Ordovician Cornwallis Group (Appendix 1).

The upper sandstone assemblage is exposed in the central and northern parts of the Trold Fiord belt (Fig. 8, Sections 11 to 23), where it sharply overlies the conglomerate assemblage, and reaches 35m in thickness. The upper part of the upper sandstone assemblage is transitional with the base of the limestone assemblage, forming an interstratified package that is up to 55m thick. This interstratified package is included with the upper sandstone assemblage in Figure 8. The upper sandstone assemblage is locally absent in the north (Section 17), where a paleotopographic high is directly overlain by the limestone assemblage.

The evaporite assemblage occurs only at the southern limit of the Trold Fiord belt (Sections 27 and 28). It has a maximum thickness of 55m, and pinches out to the north and to the west within a distance of one kilometre. The southern and eastern extent of this assemblage cannot be determined because of the lack of exposure, as the strata are either eroded or concealed in the subsurface. The evaporite assemblage is sharply underlain by a thin edge of the conglomerate assemblage (Fig. 8), and is sharply overlain by the limestone assemblage.

The limestone assemblage in the northern part of the Trold Fiord belt is interstratified with the upper sandstone assemblage at its base, and grades upward into limestone-dominated lithologies. In the southern part of the Trold Fiord belt, the limestone assemblage overlies the conglomerate assemblage (Section 25), the evaporite assemblage (Sections 27 and 28), or the Cornwallis limestones of the Franklinian Mobile Belt (Sections 24 and 26). The boundary between the lower clastic member and the middle limestone member of the Canyon Fiord Formation is situated within the interstratified zone in northern Trold Fiord belt, at levels where limestones become predominant over sandstones, and at the base of the limestone assemblage in southern Trold Fiord belt.

Although the distribution of facies assemblages is well known from north to south, there is limited exposure to constrain it from east to west. Only a few deep canyons provide stratigraphic control in an E-W orientation. Similar to some of the N-S lateral transitions, the E-W facies changes exposed in these canyons are relatively sharp. At Section 14 for example, the limestone assemblage lies directly on Franklinian rocks whereas Section 13, located 4.5km to the east, comprises 220m of siliciclastic material (conglomerate and upper sandstone assemblages) below the basal limestone assemblage (Fig. 10). Sharp facies changes are also present in northern Trold Fiord (Fig. 9), an area where the lower sandstone and conglomerate assemblages (Section 11) pinch drastically towards the east (Section 10).

The three paleotopographic highs displayed in the Trold Fiord belt (Fig. 8, Sections 17, 24 and 26) either represent east-west oriented paleo-ridges separating local depositional areas in paleo-valleys, or correspond to small push-up blocks bounded by subsidiary transfer faults, of which the field expression has yet to be recognized. The influence of these pre-Canyon Fiord topographic highs on local sedimentation patterns seems to have been minimal, as paleocurrents from immediately adjacent depositional lows show no significant divergence from the average trend (Fig. 8, Sections 13 and 16; Appendix 1).

Figure 10: East-west cross-section in the northern part of the Trold Fiord belt. Datum corresponds to the inferred level of the C5b conodont zone. Conodont biostratigraphic zones: A= upper C5b, B= C4 (Beauchamp, 1987). Vertical exaggeration is approximately 8X.

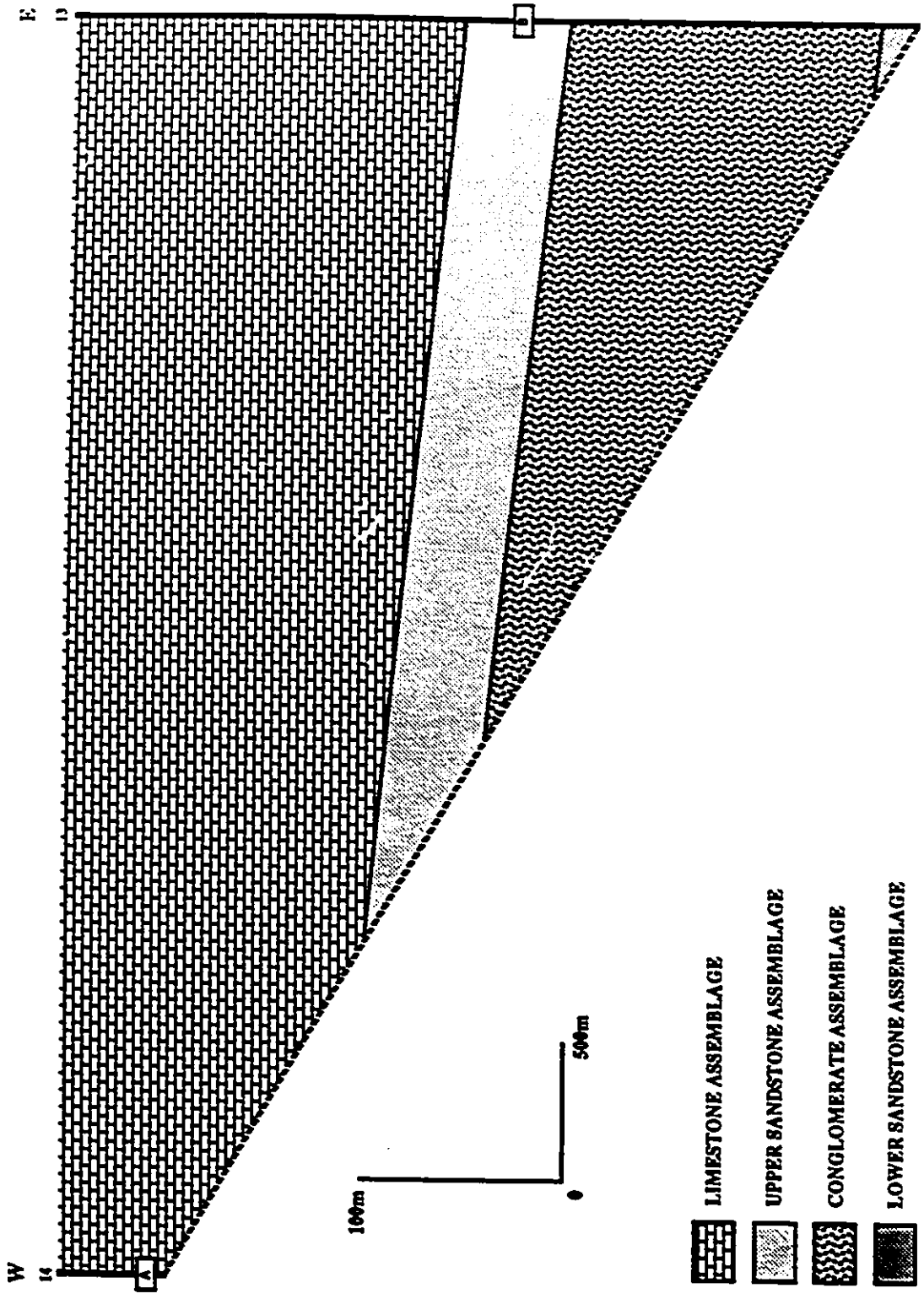
E
W
100m
500m
LIMESTONE ASSEMBLAGE
UPPER SANDSTONE ASSEMBLAGE
CONGLOMERATE ASSEMBLAGE
LOWER SANDSTONE ASSEMBLAGE

2.2 Blind Fiord Belt

The outcrop area located on the west side of the Trold Fiord Fault is referred to as the Blind Fiord belt, and forms a narrow band of exposures extending north-south for 40km. The conglomerate and limestone assemblages are the only units exposed within the Blind Fiord belt (Fig. 11). The lower sandstone may also be present in covered recessive intervals between the Franklinian basement and the conglomerate assemblage (Section 9).

The conglomerate assemblage is widespread and invariably underlain by folded strata of the Franklinian Mobile Belt (Cornwallis Group). The thickness of this assemblage is highly variable, reaching a maximum of 240m at Section 6 (Fig. 11). The conglomerate assemblage is overlain by a transitional interval up to 40m thick consisting of interstratified units of conglomerate and limestone. This interval, included in the limestone assemblage on Figure 11, is absent in the Trold Fiord belt, where the basal limestone assemblage is in contrast interstratified with the upper sandstone assemblage (Fig. 9). The boundary between the lower clastic member and the middle limestone member of the Canyon Fiord Formation throughout the Blind Fiord belt is situated within the transitional interval, at levels where limestones become predominant over conglomerates.

Lateral facies changes from east to west cannot be resolved in the Blind Fiord belt since exposures of the lower clastic member seldom extend for more than 500m in that direction. The geometry of the sedimentary package west of the Trold Fiord Fault therefore remains concealed in the subsurface.

2.3 Biostratigraphy

Stratigraphic correlations were partially based on conodont biostratigraphy, in relation to the work of Henderson (1988) who recognized seven distinct conodont zones in Sverdrup Basin for the Late Carboniferous time interval (Fig. 12). Eight samples have been

Figure 11: North-south cross-section at the eastern margin of the Blind Fiord belt. Datum represents a time-line, at the top of the conglomerate assemblage. Condont biostratigraphic zones: A= upper C5a. Vertical exaggeration is approximately 55X.

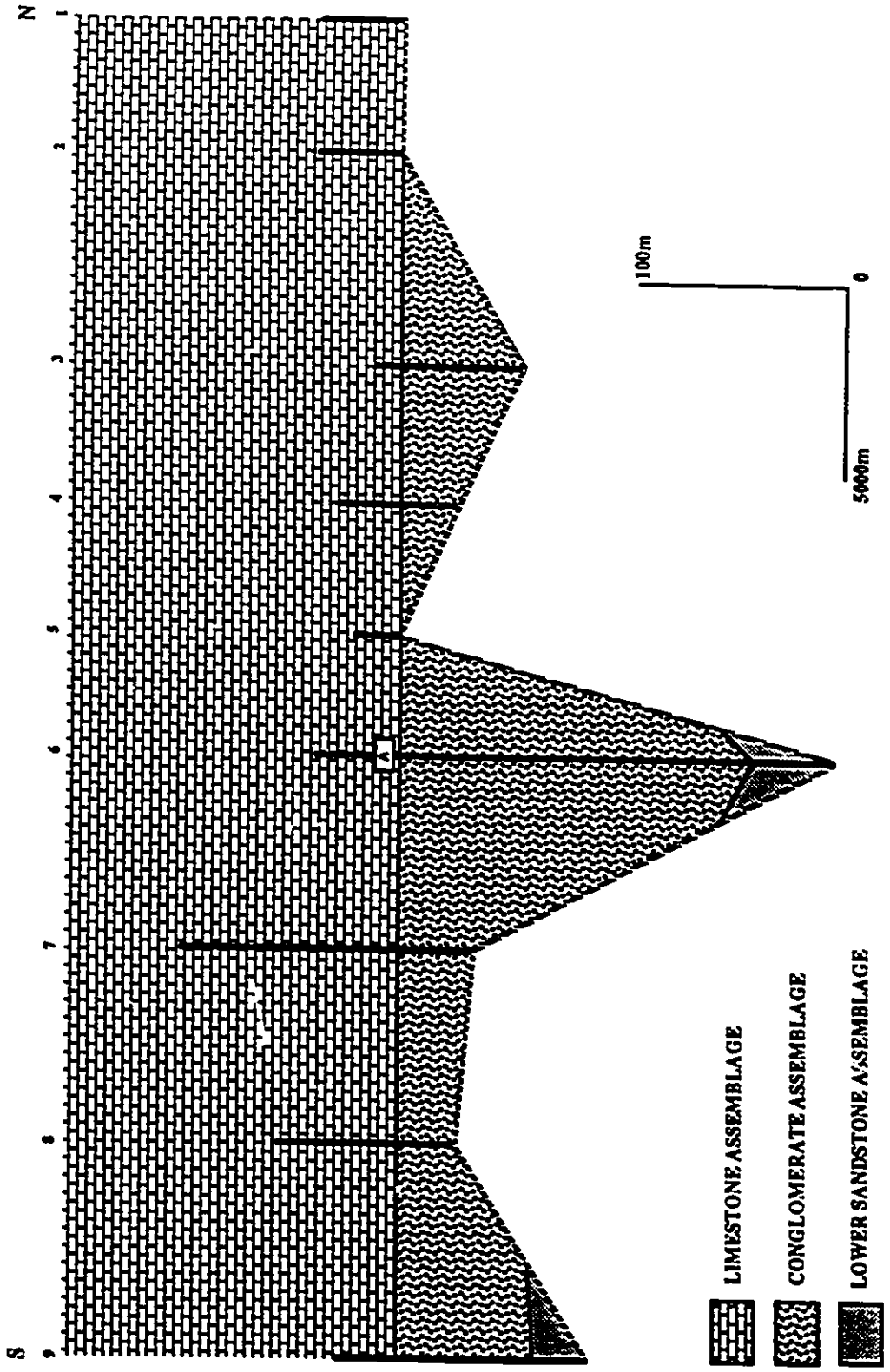
N
S
1
2
3
4
5
6
7
8
9
100m
0
5000m
LIMESTONE ASSEMBLAGE
CONGLOMERATE ASSEMBLAGE
LOWER SANDSTONE ASSEMBLAGE

Figure 12: Age ranges for conodont assemblages of Sverdrup Basin. Zones C4 to P9 are based on Henderson (1988) (from Beauchamp et al., 1989a).

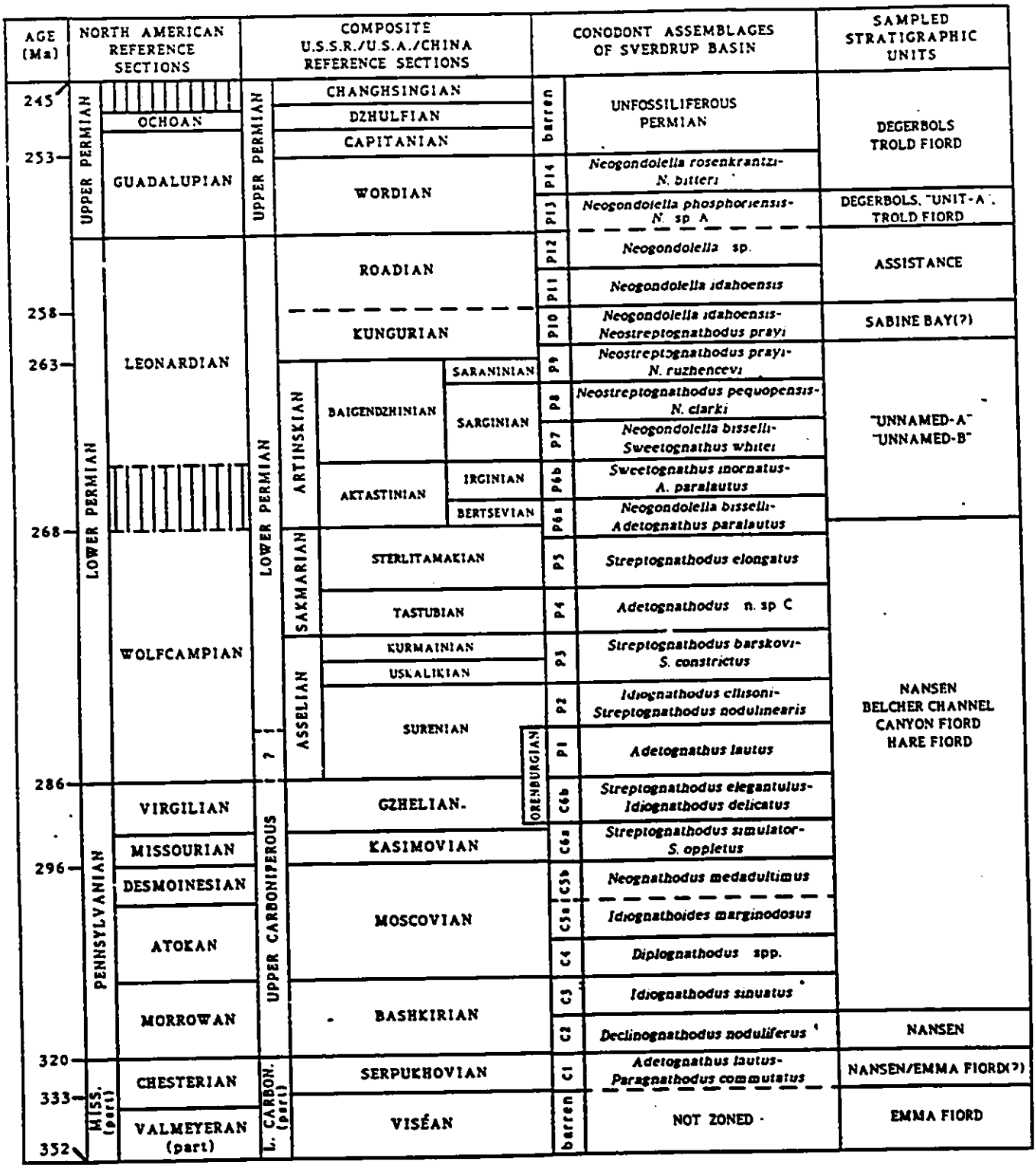
AGE (Ma)
NORTH AMERICAN REFERENCE SECTIONS
COMPOSITE U.S.S.R./U.S.A./CHINA REFERENCE SECTIONS
CONODONT ASSEMBLAGES OF SVERDRUP BASIN
SAMPLED STRATIGRAPHIC UNITS
245
253
258
263
268
286
296
320
333
352
UPPER PERMIAN
LOWER PERMIAN
PENNSYLVANIAN
MISS. (part)
OCHOAN
GUADALUPIAN
LEONARDIAN
WOLFCAMPIAN
VIRGILIAN
MISSOURIAN
DESMOINESIAN
ATOKAN
MORROWAN
CHESTERIAN
VALMEYERAN (part)
UPPER PERMIAN
LOWER PERMIAN
?
UPPER CARBONIFEROUS
L. CARBON. (part)
CHANGHSINGIAN
DZHULFIAN
CAPITANIAN
WORDIAN
ROADIAN
KUNGURIAN
ARTINSKIAN
SAKMARIAN
ASSELIAN
SARANINIAN
BAIGENDZHINIAN
SARGINIAN
AKTASTINIAN
IRGINIAN
BERTSEVIAN
STERLITAMAKIAN
TASTUBIAN
KURMAINIAN
USKALIKIAN
SURENIAN
ORENBURGIAN
GZHELIAN.
KASIMOVIAN
MOSCOVIAN
BASHKIRIAN
SERPUKHOVIAN
VISÉAN
barren
P14
P13
P12
P11
P10
P9
P8
P7
P6b
P6a
P5
P4
P3
P2
P1
C6b
C6a
C5b
C5a
C4
C3
C2
C1
barren
UNFOSSILIFEROUS PERMIAN
Neogondolella rosenkrantzi-N. bitteri
Neogondolella phosphoriensis-N. sp. A
Neogondolella sp.
Neogondolella idahoensis
Neogondolella idahoensis-Neostreptognathodus prayi
Neostreptognathodus prayi-N. ruzhencevi
Neostreptognathodus pequopensis-N. clarki
Neogondolella bisselli-Sweetognathus whitei
Sweetognathus inornatus-A. paralautus
Neogondolella bisselli-Adetognathus paralautus
Streptognathodus elongatus
Adetognathus n. sp C
Streptognathodus barskovi-S. constrictus
Idiognathodus ellisoni-Streptognathodus nodulinearis
Adetognathus lautus
Streptognathodus elegantulus-Idiognathodus delicatus
Streptognathodus simulator-S. oppletus
Neognathodus medadultimus
Idiognathoides marginodosus
Diplognathodus spp.
Idiognathodus sinuatus
Declinognathodus noduliferus
Adetognathus lautus-Paragnathodus commutatus
NOT ZONED
DEGERBOLS TROLD FIORD
DEGERBOLS, "UNIT-A", TROLD FIORD
ASSISTANCE
SABINE BAY(?)
"UNNAMED-A" "UNNAMED-B"
NANSEN BELCHER CHANNEL CANYON FIORD HARE FIORD
NANSEN
NANSEN/EMMA FIORD(?)
EMMA FIORD

productive in this study, ranging from zones C4 to C5b of Henderson (1988) and assigned to the Moscovian stage (Appendix 1 and 3). Five of these samples are from the basal part of the limestone assemblage, two are from the intercalated upper sandstone assemblage/ limestone assemblage interval, and one sample is from the upper part of the evaporite assemblage. Of the eight samples, only one is derived from the Blind Fiord outcrop belt.

Beauchamp (1987) clearly demonstrated that the depositional strike on Raanes Peninsula during latest Carboniferous and Permian time was oriented NW-SE, with deeper water facies occurring on the southwestern part of the peninsula. Marine conditions in Canyon Fiord time are therefore expected to have progressed from southwest to northeast, with older carbonates being found at southernmost localities in both the Blind Fiord and Trold Fiord belts. Diachronism from north to south at the base of the limestone assemblage, however, has not been recognized on the basis of conodont dating. As seen in Appendix 3, all samples corresponding to basal limestone intervals fall within the early to middle Moscovian age range. This narrow age range is not taken to indicate a lack of diachronism, but instead that marine transgression in a general southwest to northeast direction was relatively rapid, beyond the detectability of Henderson's (1988) conodont zones. For that matter, north-south correlations were predominantly based on lithostratigraphy, with the selected datum corresponding to the base of either the limestone assemblage in the southern part of the Trold Fiord belt and throughout the Blind Fiord belt, or the upper sandstone assemblage in the northern part of the Trold Fiord belt (Figs. 8 and 11). It is therefore assumed that the upper sandstone assemblage in the central and northern areas of the Trold Fiord belt is coeval with the basal limestone assemblage to the south. This relationship is supported by the sharp transition between the conglomerate assemblage and either the upper sandstone assemblage to the north, or the limestone assemblage to the south. These rapid vertical facies changes also suggest that the limestone and upper sandstone assemblages are both genetically related to a distinct episode of tectonic subsidence in the area (discussed in Chapter 5).

Although diachronism cannot be detected from south to north in the area, it is apparently displayed from east to west in the northern Trold Fiord belt (Fig. 10). Hence, conodonts recovered from the basal limestone assemblage at Section 13 are of zone upper C5a, whereas those at Section 14 are younger and belong to zone upper C5b (Fig. 12; Appendix 3). This diachronous relationship indicates that marine incursion towards the west during the middle Late Carboniferous was gradual in the area underlying the Trold Fiord belt. In contrast, it seems that marine incursion from south to north was relatively more rapid in the overall study area, suggesting that local topographic features (i.e. subbasins and associated highlands), superimposed upon the regional southwestward paleoslope, were more important in controlling depositional trends.

CHAPTER 3: SEDIMENTOLOGY

The basal part of the Canyon Fiord Formation on Raanes Peninsula comprises five distinct synrift assemblages: i) a lower sandstone assemblage, ii) a conglomerate assemblage, iii) an upper sandstone assemblage, iv) an evaporite assemblage; and v) a limestone assemblage.

3.1 Lower Sandstone Assemblage

The lower sandstone assemblage is exposed essentially in the Trold Fiord belt, at Sections 10, 11, and 16. (Figs. 8 and 9). Additional occurrences may also exist at the base of Sections 9, 13, and 19, where a relatively thick recessive interval is present between the Franklinian basement and the resistant conglomerate assemblage. The lower sandstone assemblage is composed of two distinct lithofacies: i) a heterogeneous sandstone/limestone lithofacies (90%); and ii) a stratified conglomerate lithofacies (10%). The stratified conglomerate lithofacies increases in relative abundance towards the top of the lower sandstone assemblage.

3.1.1 Heterogeneous sandstone/limestone lithofacies

This lithofacies consists of crudely-bedded sandstone units in which various proportions of calcium carbonate are present. The more terrigenous beds are medium to dark reddish-brown in colour, less than 1m thick, and parallel-laminated to ripple cross-laminated. Desiccation cracks are locally common on exposed bedding plane surfaces. These beds are composed chiefly of quartz grains (80%) and carbonate rock fragments (15%), with minor amounts of feldspar, chert, mica, pyrite, garnet, zircon, anhydrite and chlorite. Individual grains are subangular to angular, and average 50-200 microns in size (very coarse silt to very fine sand). The sorting is generally moderate. Matrix makes up approximately 50% of the rock, and consists mainly of fine-grained micrite. Hematization

is pervasive (~5%) throughout this micritic matrix and as grain coatings, giving the sediment its reddish-brown colouration. Several sandstone units are pebbly, with clasts composed mostly of fine-grained limestone derived from underlying Franklinian formations.

The more calcareous beds display a variety of internal features, including isolated calcite nodules surrounded by sandstone, coalesced nodules with minor sandstone, and $CaCO_3$-rich layers with massive, laminar, or pisolitic fabrics (Plates 2A, B, C, and 3A to 3D). Nodular and massive calcareous layers were most commonly observed, and occur as alternating units of variable thickness. The upward transition from the nodular to the massive fabric is gradual, whereas a sharp contact characterizes the opposite relationship. The laminar to pisolitic layers occur exclusively above massive units.

The isolated nodules occur in beds that average 20cm to 100cm in thickness. Individual carbonate nodules are greenish-grey/reddish brown (mottled), subspherical to irregular in shape, and range in size from less than 1cm to 15cm in diameter. They are composed of micrite with variable amounts of clay, and contain irregular to curvilinear, millimetre-sized sparite veins (Plate 3A). These veins often surround smaller nodules, forming a fabric commonly referred to as circum-granular cracking, which results from alternating shrinkage and expansion (Esteban and Klappa, 1983; Wright and Wilson, 1987). Layers of coalesced nodules are generally less than 1m thick, and contain features similar to those observed in isolated nodules (Plate 3B). Massive layers (20-100cm thick) are brownish-grey or mottled in colour, and are composed of abundant micrite and minor clay homogeneously distributed. Internal features include faint circum-granular cracking and sparite-filled fenestrae (Plate 3C). Laminar and pisolitic fabrics occur locally in close association, and form layers less than 20cm thick. The laminar fabric consists of relatively thin, slightly undulated to contorted laminae of pale greyish-brown micrite (Plate 3D). The pisolitic fabric is concentrated within discontinuous layers and small pockets, and consists

of closely-spaced pisoliths less than 5mm in size and composed of very thin concentric laminae of micrite (Plate 3D).

A distinct unit at the base of Section 11 is characterized by a 7m thick, dense nodular horizon overlain by a 1m thick massive to laminar/pisolitic horizon. The nodular horizon consists of coalesced nodules with abundant root casts that form a dense meshlike network. These root casts, less than 1cm in diameter, are composed of sparry calcite. The laminar/pisolitic intervals of the overlying horizon are composed of fine micrite laminae, with ubiquitous interstitial micro-detritus resembling phytoclastic plant material (Pedley,1990). Micrite coatings on pisolites and oncoids are locally discontinuous or asymmetric.

Microcodium is commonly present within the sandstone/limestone lithofacies, where it occurs as spherical to irregular clusters of submillimetre-sized calcite prisms. Inclusions of organic matter are common within individual prisms. *Microcodium* has been variably interpreted as algal, bacterial, or inorganic in origin, and more recently as calcified mycorrhizae, a symbiotic association between soil fungi and cortical cells of plant roots (Klappa, 1978). According to Beauchamp (pers. comm., 1990), the presence of plant roots and development of a soil, however, is not a prerequisite to the formation of *Microcodium*, a feature likely related to biodiagenetic bacteria-induced calcification of sediment in the vadose zone.

The heterogeneous sandstone/limestone lithofacies is interpreted as fluvial deposits laid down in the floodplain environment, based primarily on the fine-grained nature and reddish colour of the sediments, and on the presence of secondary limestone of apparent caliche origin. The internal characteristics of the different calcareous layers are similar to those of various caliches reported in the literature (Steel, 1974; Wright and Wilson, 1987). The upward increase in $CaCO_3$-content and concurrent variation from nodular to massive to laminar/pisolitic fabrics are also characteristic of most caliche profiles (Esteban and Klappa, 1983). Variations in composition and fabric are also indicative of a change in soil maturity.

Depending on the rates of floodplain aggradation, caliches either have little time to develop, in which case only immature nodular horizons are formed, or are developed at individual levels for an extended period of time, in the form of complete profiles with successive immature nodular, mature massive, and highly mature laminar/pisolitic horizons. Alternating mature and immature profiles were found locally in the heterogeneous sandstone/limestone lithofacies (Plate 2A). They were probably controlled by either channel avulsion, or minor episodes of tectonic rejuvenation along local rift structures.

The sandstone likely accumulated during seasonally humid periods, while the interstitial to interlayered caliches precipitated by evaporation during intervening periods of warm and dry weather. Alternating climatic conditions are highly favourable to the development of caliches, as indicated by the near restriction of Quaternary examples to semi-arid settings (Hubert, 1978). The seasonal fluctuations in humidity level lead to the meteoric dissolution of carbonate components in the upper part of the sediment column, and downward percolation of interstitial fluids during periods of intense rainfall. Subsequent precipitation of secondary calcium carbonate and reorganization into distinct caliche horizons occur during long periods of evaporation. Paleogeographic plate reconstructions position Sverdrup Basin in the tropical arid/semi-arid belt during the Late Carboniferous time interval (Ziegler, 1988). An *in situ* source of calcium carbonate would also have promoted the development of caliche. Limestone rock fragments derived from the Franklinian Mobile Belt formations likely provided sufficient calcium carbonate material to be dissolved and subsequently translocated down the profiles. $CaCO_3$ may have been also derived in part from eolian dust (Latmman, 1973).

The 8m thick unit at the base of Section 10, situated in the northeastern part of the Trold Fiord belt (Fig. 4), is interpreted as rhizolith-rich caliche and plant tufa that formed in a paludal environment. This environment may have been associated with adjacent lakes, the deposits of which could still be concealed in the subsurface, possibly to the east of the Trold Fiord belt.

3.1.2 Stratified conglomerate lithofacies

This lithofacies, accounting for 10% of the lower sandstone assemblage, consists of red-weathered, well-bedded tabular units of pebble conglomerate with minor sandstone interlayers (Plate 2D). These units range in thickness from 10cm to 80cm and are sharply bounded by layers of the heterogeneous sandstone/limestone lithofacies. The conglomerates are clast-supported, well-sorted, and usually normally-graded. Pebbles are less than 5cm in size and composed mostly of microcrystalline limestone. Matrix is a subordinate constituent and consists of calcareous mud, very fine quartz sand, and *Microcodium*. The interlayered sandstones are less than 10cm thick and ripple cross-laminated, locally forming discontinuous ripple trains. These interlayers either grade upward into a sandstone/limestone unit, or are sharply overlain by a pebble conglomerate bed.

The pebble conglomerate facies is interpreted as sheetflood deposits of floodplain origin, based on the tabular nature of individual units, the presence of normal grading (conglomerates) and cross-laminations (sandstone interlayers), and the lack of trough cross-bedding and channel structures. The conglomerates were deposited from overbank flooding of the main channels, either during seasonal storms or following minor tectonic pulses. Sedimentation rates were relatively rapid since caliche paleosols are absent, contrasting with their common occurrence within the interstratified sandstone/limestone lithofacies. Pedogenic activity was hindered by the high sedimentation rates and is not related to the difference in substrate, since caliches are common in similar coarse sediments of the overlying conglomerate assemblage.

3.1.3 Discussion

The occurrence of multistoried caliche profiles hosted in sandstone, along with minor sheetflood conglomerates, suggests that the lower sandstone assemblage was deposited in the floodplain environment of ephemeral, high sinuosity rivers. It has been

demonstrated that paleosols found in fluvial sequences are essentially restricted to the floodplain environment (Bown and Kraus, 1987; Kraus and Bown, 1986), an area characterized by short intervals of flood sedimentation and longer intervals of non-deposition during which soil-forming processes operate within surficial sediments. Paleosols are also more abundant and better developed away from active channel belts, in the distal floodplain environment (Bown and Kraus, 1987). The development of caliche in approximately 90% of the lower sandstone assemblage suggests that sedimentation proceeded mainly in the distal part of floodplains, with very limited influence of in-channel processes. The presence of sheetflood conglomerate interbeds in this distal setting probably indicates the proximity of elevated areas with sharp relief, resulting from rift-related extensional faulting. The orientation of the fluvial system that deposited the lower sandstone assemblage could not be determined from sedimentological observations, as most primary sedimentary structures have been obliterated by pedogenic processes.

The lower sandstone assemblage was also locally deposited in a paludal environment in the eastern part of the study area. Associated lacustrine deposits have not been found, but may be present farther east or elsewhere in the subsurface. The low energy fluvial and paludal facies characterizing the lower sandstone assemblage suggest conditions of internal drainage, and indicate that tectonic base-level change related to rifting at the margin of the Sverdrup Basin had not yet culminated. Greater relief and geomorphic disequilibrium was attained at a later stage, resulting in deposition of the much coarser-grained conglomerate assemblage.

3.2 Conglomerate Assemblage

The conglomerate assemblage is the most widespread and volumetrically important assemblage of the basal Canyon Fiord Formation (Figs. 8 to 11). The conglomerate assemblage is composed of three distinct lithofacies: i) stratified conglomerate (80%); ii)

massive conglomerate (10%); and iii) heterogeneous sandstone/limestone (10%). These lithofacies occur in random spatial distribution within the conglomerate assemblage.

3.2.1 Stratified conglomerate lithofacies

The stratified conglomerate lithofacies consists of red-weathered, stratified pebble to cobble conglomerate. Beds range in thickness from 5cm to 100cm, and are most commonly 30 to 40cm thick. Both sheetlike and lenticular units are present; individual sheets have sharp non-erosive bases and reach 75m or more in lateral extent, whereas lenticular units display erosive basal contacts with up to 2m of vertical relief, and locally persist laterally for a few tens of metres. Multistoried channels are locally present, and indicate occasional persistence of in-channel sedimentation. Channel pockets have also been found, and consist of isolated channel fills (up to 2m across by 1m in height) composed of well-sorted cobbles and boulders (Plate 4A). The conglomerates are crudely bedded and massive, with subordinate tabular or trough cross-bedded units. Individual cross-bed sets are up to 1m thick. Normally-graded beds are abundant (Plate 4B), most characterized by a well-sorted openwork base grading into a finer-grained, matrix-rich upper part (Plate 4C). The open framework intervals have been cemented by medium to coarse sparry calcite, and are commonly cross-bedded.

Clastic intrusions are locally common in the stratified conglomerate lithofacies. These structures consist of subvertical sandstone dykes that protrude the conglomerate host and reach 60cm in height and 10cm in width. Subhorizontal and oblique sandstone intrusions are also present. The clastic intrusions are interpreted as penecontemporaneous water escape structures, with liquefaction and fluidization of sediments possibly resulting from seismic disturbance related to displacement along Carboniferous faults. Ord et al. (1988) have demonstrated the close spatial and temporal relationship between soft-sediment deformation and extensional faults in the Lower Carboniferous Solway basin of Scotland.

The clastic intrusions could also be related to fluidization at time of deposition due to rapid sediment accumulation (Postma, 1983).

Several beds display an imbricated clast fabric from which paleocurrent directions were measured. Most imbricate clasts are characterized by an *a(t)b(i)* fabric, which consists of an a-axis oriented transverse to flow, and an imbricate b-axis dipping upstream (Harms et al., 1982). This type of imbrication is indicative of bedload transport by rolling, and has been observed in modern river deposits (Rust, 1972). Erosional groove casts are common on well exposed bed soles, and have also been measured for paleocurrent orientations. Their size (average of 20cm in width, 1-2m or more in length, 10cm of relief) and slightly sinuous nature suggest that they are gutter casts, an erosional structure possibly initiated by secondary currents (Whitaker, 1973). The paleocurrents measured from gutter casts and clast imbrications in the Trold Fiord belt indicate a consistent eastward to south-eastward paleoflow direction, whereas those recovered from a single locality in the Blind Fiord belt indicate a westward direction (Fig. 13). These patterns indicate that sedimentation was controlled by northerly-trending structures during the Late Carboniferous.

The stratified conglomerates are commonly clast-supported, and pebbly to cobbly with values of maximum particle size (MPS) ranging between 3cm and 30cm. Although MPS is generally taken to represent a statistical average of the 10 largest clasts within a bed (Nemec and Steel, 1984), the values in this study were obtained by visual estimate. Clasts are subangular to rounded, and composed mostly of silty/sandy microcrystalline limestone and dolostone. These extraclasts were derived from older Franklinian strata. Other clast types include reworked laminar caliche derived locally within the conglomerate assemblage.

Matrix is generally less than 50% in content, poorly sorted, and either sand- or mud-rich. Muddy matrices are reddish in colour and composed of hematized siliciclastic mud and micrite. Minor constituents include granules (compositionally identical to the pebbles and cobbles), silt- to sand-sized quartz, chert, and feldspar grains. Sandy matrices display a grey coloration and consist of carbonate granules and sand particles, as well as

Figure 13: Paleocurrent directions for the conglomerate assemblage. Measurements are from imbricate clasts (95%) and gutter casts (5%).

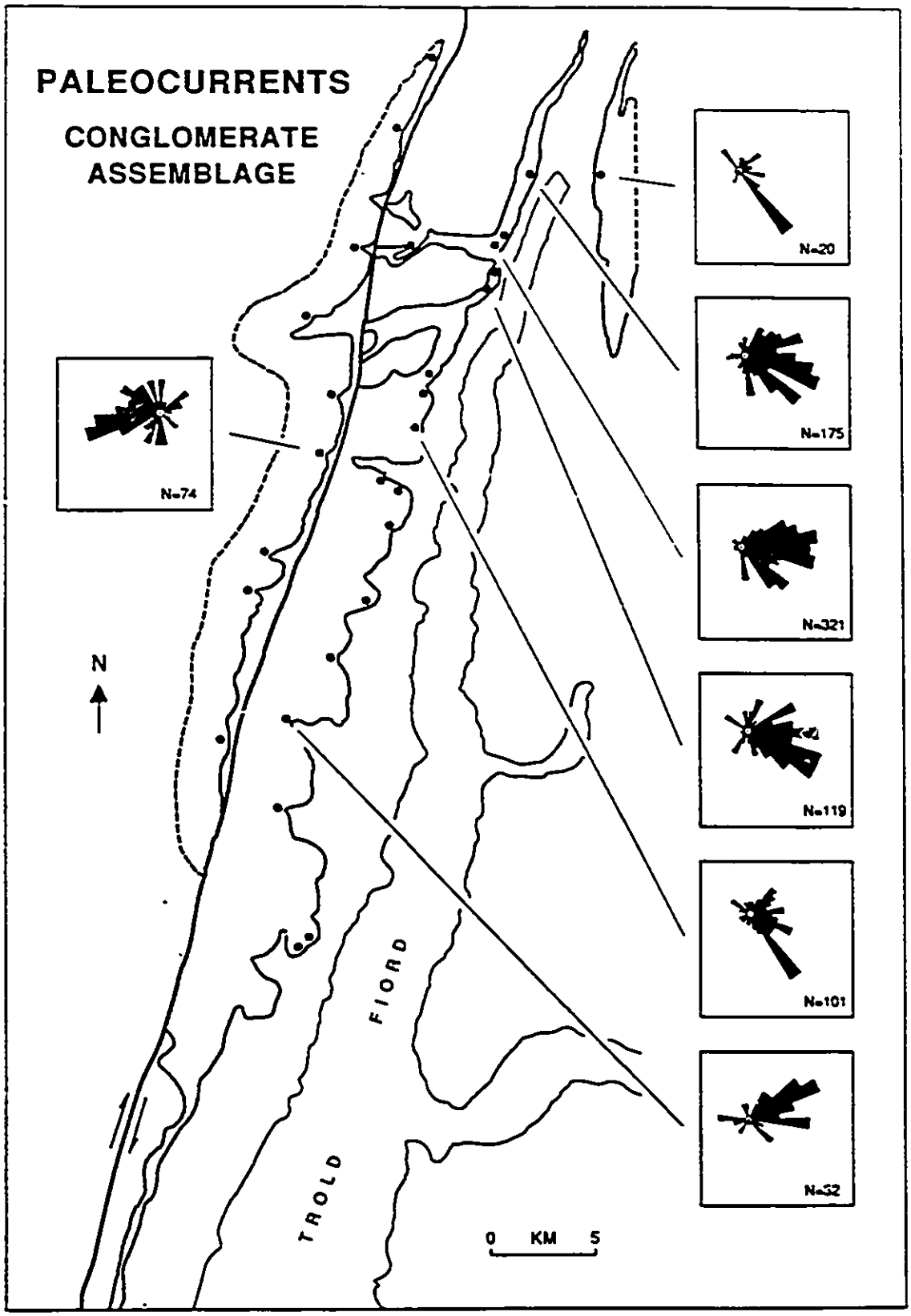
PALEOCURRENTS
CONGLOMERATE
ASSEMBLAGE
N=74
N=20
N=175
N=321
N=119
N=101
N=32
N
TROLD FIORD
0 KM 5

quartz sand and silt. Cement is composed exclusively of sparite, which occurs as openwork fabric and fracture infills, and as irregular patches.

Carbonate fabrics, comparable to those interpreted as caliches in the previous section, as well as alveolar textures, root structures, and *Microcodium,* are locally abundant and indicate pedogenic activity during periods of non-deposition. Caliche is relatively common and occurs in the massive and laminar variety. Massive caliche is restricted to the matrix of conglomerates, where it consists of structureless greyish micrite with minor detrital sand grains (Plate 5A). These "plugged" intervals reach approximately 30cm in thickness, and are often overlain by spectacular laminar caliche layers up to 15cm thick (Plates 4D and 5A to D). These layers are composed of finely laminated, pale beige to dark brownish-grey micrite. The laminar fabric consists of micrite laminae that are mainly subhorizontal and slightly undulated to contorted. Highly complex laminar fabrics are also present, and include caliche dikes (fracture-filling laminar caliche), micro-folds, micro-faults, overturned laminae, and internal breccias (Plate 5A to D). These various fabrics result from several alternating episodes of precipitation and dissolution with concurrent shrinkage and expansion. The massive and laminar caliches were occasionally found without any associated root structures or alveolar textures, suggesting that they may locally have a non-pedogenic origin. Non-pedogenic laminar caliche forms from the lateral enrichment in $CaCO_3$ of surficial water or groundwater flowing down topographic gradients, whereas pedogenic laminar caliche forms by *in situ* dissolution and gravitational percolation of fluids (Lattman, 1973; Ettensohn et al., 1988). The stratified conglomerate lithofacies is devoid of nodular caliches, contrasting with the lower sandstone assemblage in which this fabric is predominant. The difference is interpreted as being due to the control of substrate on fabric development. Sandstone hosts are relatively permeable and provide small nucleation sites around which nodules can grow progressively, whereas conglomerate hosts have their matrices rapidly cemented by massive caliche, after which laminar caliche can develop upon the impermeable "plugged" conglomerate.

In addition to caliche fabrics, alveolar textures are locally abundant within conglomerates matrices. The texture consists of sub-millimetre-sized tubular to irregular pores filled with cement and separated by interconnecting walls of micrite (Plate 6A, B). It has been interpreted as calcified entwined rhizoliths occurring in immature to mature caliche horizons (Wright and Wilson, 1987; Wright et al., 1988). A conventional root structure, consisting of a paired rhizolith and sparite-filled root cast, was found in close association with an alveolar texture (Plate 6C). The rhizolith is composed of thin concentric laminae of micrite encircling the cylindrical root cast. *Microcodium*, as in the lower sandstone assemblage, occurs locally in the form of irregular clusters of sub-millimetre-sized calcite prisms (Plate 6C, D). Its formation is probably related to calcification of organic-matter-rich sediments induced by micro-organisms (Beauchamp, pers. comm., 1990).

The stratified conglomerate lithofacies is interpreted as proximal streamflow deposits, probably of both sheetflood and stream-channel origin within the alluvial fan to proximal braided stream environment. The more sheetlike conglomerate units are of sheetflood origin, and accumulated from flood surges during which active channels spread out into broad sheets (Bull, 1977). The more lenticular conglomerate units are of stream-channel origin, and formed as cut-and-fill structures within the channels of active streams, with the bulk of their record also related to flood sedimentation.

3.2.2 Massive conglomerate lithofacies

This lithofacies makes up 10% of the conglomerate assemblage, and comprises two distinct types of deposits: 1) clast-supported cobble to boulder conglomerate (75%), and 2) matrix-supported pebble conglomerate (25%). Lateral or vertical stratigraphic transitions have not been observed between these two sublithofacies.

Clast-supported cobble to boulder conglomerates are red-weathered and occur as sheetlike units that are 1-2m thick on average. Individual beds are internally massive, ungraded, and have a high matrix content (Plate 7A, B). The fabric is poorly sorted with no

preferred clast orientation. Paleocurrent measurements were therefore not obtained. The clasts are of cobble to boulder, and have MPS values ranging from 20 to 35cm, with individual boulders reaching 60cm in diameter (Plate 7A). Most clasts are subspherical, have subrounded to subangular outlines, and are composed of microcrystalline limestone extraclasts with minor sandstone and caliche clasts. The matrix is unsorted, and consists of carbonate pebbles and granules, sand- to silt-sized quartz and feldspar grains, and hematized mud particles. Cement is locally present as sparry calcite or dolomite, and occurs either randomly within the matrix or as a fracture-filling product. Caliche, alveolar textures, root structures and *Microcodium* are locally present and display similar features to those described for the stratified conglomerate lithofacies.

The clast-supported cobble to boulder conglomerate sublithofacies is interpreted as subaerial debris flow deposits of alluvial fan origin, as evidenced by the massive and ungraded nature of beds, the abundance of an unsorted matrix, and the lack of clast fabric. These debris flows resulted from ephemeral discharge, as sediments produced by bedrock weathering in the source area were stored and subsequently tapped to the fan only during occasional floods (Bull, 1977).

The matrix-supported pebble conglomerate sublithofacies differs from the clast-supported sublithofacies by its mud-rich matrices, its bed thicknesses that rarely exceed 30cm, and its MPS values of 5cm or less (Plate 7C). Beds are also internally unsorted and ungraded. Individual clasts are subangular to angular, display no preferred orientation, and are composed mostly of microcrystalline limestone.

These matrix-supported conglomerates probably represent mudflow deposits that accumulated in the alluvial fan environment from ephemeral flash floods. They are randomly distributed within the succession, and show no close association with the coarser, clast-supported debris flow deposits.

3.2.3 Heterogeneous sandstone/limestone lithofacies

The heterogeneous sandstone/limestone lithofacies is overall red-weathered and composed of sandstone hosting variable proportions of nodular, massive, and laminar caliche. The lithofacies consists of 10cm to 200cm thick units occurring between thicker conglomerate intervals. These units display a regular vertical spacing on a 2m to 5m scale in relation to the conglomerate intervals, and are laterally extensive. Individual beds have poorly defined boundaries, and are internally massive as most primary sedimentary structures have been obliterated by pedogenesis. The sandstone intervals in which caliche is minor or absent are composed of clay, micrite, and silt- to sand-sized carbonate and quartz grains. Hematization of clay particles is pervasive. Root structures, alveolar textures, and *Microcodium* are common, especially in layers where caliche is conspicuous. The most common caliche fabric consists of isolated to locally coalesced nodules surrounded by more than 50% sandstone. More mature massive and laminar varieties are rare.

The heterogeneous sandstone/limestone lithofacies is interpreted as sheetflood deposits of alluvial fan to proximal braided stream origin that accumulated during periods when conglomerate sedimentation was halted. Their regular vertical spacing of 2m to 5m within the conglomerate assemblage suggests that these small-scale "cycles" were controlled by either channel avulsion or climate. Channel avulsion is preferred, however, based on the regularity and relatively constant thickness of the cycles, and also on the time factor that is required for the development of caliche within the sandstone intervals. Horizons of immature nodular caliches are reported to take between 100 and 5,000 years to develop (Leeder, 1975; Allen, 1986). Climatic cycles are typically longer in duration. A tectonic control is unlikely, as cycles of such origin are much thicker (Steel et al., 1977). Hence, the caliche-bearing sandstone intervals would represent long time spans during which conditions of low sedimentation rates or non-deposition prevailed, as gravel sedimentation was simultaneously occurring on an adjacent portion of the alluvial system.

Aggradation in this adjacent area would eventually result in the lateral shifting of the depositional locus, and recurrence of sedimentation above the calichified sediments.

The heterogeneous sandstone/limestone lithofacies of the conglomerate assemblage is distinguished from the lower sandstone assemblage by its thinner units and much more immature caliches. The lack of mature fabrics such as massive and laminar caliche indicate that sedimentation rates were greater for sandstones of the conglomerate assemblage.

3.2.4 Discussion

The conglomerate assemblage is interpreted as having been deposited in eastward-flowing (Trold Fiord belt) and westward-flowing (Blind Fiord belt) streams on alluvial fans and proximal braided streams. The distinct flow direction in each outcrop belt suggests their association with separate drainage basins, in which sedimentation was controlled by two N-S master faults of opposite dip. Each drainage basin was of local extent and characterized by ephemeral sedimentation, as evidenced by the presence of caliches within conglomerate and sandstone units.

The scarcity of debris flow deposits in the conglomerate assemblage may be due to one or more of the following: i) the Trold Fiord and Blind Fiord outcrop belts represent areas that were located beyond the proximal-middle reaches of the alluvial fan environment; ii) intrinsic factors, such as lack of mud at the source and substrate stabilization by caliche, inhibited the development of alluvial fans; and iii) the local tectonic setting did not favor the development of alluvial fans.

Proximal to middle alluvial fan environments were possibly not represented in the conglomerate assemblage. Studies on modern deposits and processes have established that the proximal reaches of alluvial fans in semi-arid settings are characterized mainly by debris flow deposits, with subordinate stream-channel and sieve deposits (Bull, 1977; Rust and Koster, 1984). In contrast, the distal fan reaches comprise sheetflood and stream-channel deposits that are related to streamflow processes. The mid-fan environment corresponds

approximately to the downfan extent of debris flows, and to the most proximal occurrence of sheetflood deposits. Since streamflow deposits are both widespread and volumetrically important in the conglomerate assemblage, deposition most likely proceeded in the distal alluvial fan environment. Also of importance is that alluvial fans in arid and semi-arid climates are relatively small, commonly less than a few kilometres across (Blissenbach, 1954; Hooke, 1967). The scarcity of debris flow deposits may therefore indicate that much of the conglomerate has been deposited in the adjacent braided stream environment, with most fans being located in areas that are more proximal than those where the conglomerate assemblage is presently exposed.

Debris flow processes could also have been partially inhibited by intrinsic factors. For instance, the source of mud required for debris flows to occur was probably minimal in the source area, as indicated by the limestone composition of nearly all detrital clasts and by the uncommon presence of mud-rich matrices. Stabilization by caliche, which is expected to have rapidly lithified surficial sediments, may have also inhibited debris flows. Non-pedogenic caliches are reported to occur on the steeper parts of alluvial fans from the evaporation of carbonate-rich fluids through lateral translocation in groundwater or surface runoff (Lattman, 1973).

The scarcity of debris flow deposits may also be related to the lack of alluvial fans in the area, themselves controlled by the local tectonic style in which the conglomerate assemblage was deposited. For instance, the development of half-graben subbasins has been shown to limit greatly the lateral extent of alluvial fans along major fault escarpments, as subbasin asymmetry hinders the progradation of fault-scarp sediments (Frostick and Reid, 1987; Frostick et al., 1988). It will be proposed in Chapter 5 that half-graben sedimentation did take place in the area during the Late Carboniferous, and may have been influencial in limiting alluvial fans and associated debris flow deposits.

The conglomerate assemblage is characterized by a few coarsening-upward sequences several tens of metres thick. These sequences are particularly evident at Section

6 (Appendix 1), where MPS values increase from 0m to 60m, and from 90m to 180m. Similar sequences are also present in the conglomerate assemblage at Section 11 (Appendix 1). Fining-upward and coarsening-upward megasequences in alluvial fan deposits have been widely reported (Steel et al., 1977; Heward, 1978; Elmore, 1984). The former are generally due to fan retrogradation resulting from backstepping of boundary faults or from periods of decreasing tectonic intensity, while the latter are related to fan progradation following tectonic rejuvenation (Steel and Wilson, 1975). The Devonian Hornelen Basin in Norway comprises a number of coarsening-upward megasequences around 100m thick, overprinted with smaller-scale sequences ranging from 10 to 25m (Steel et al, 1977). These cycles are interpreted as direct responses to tectonic base-level changes. Similarly, the two coarsening-upward sequences in the conglomerate assemblage may have resulted from minor tectonic pulses. It is difficult to determine if these two sequences are correlatable across the study area, since most localities lack MPS data or display no grain-size trends (Appendix 1). The inconsistency in cyclicity from section to section indicates that episodes of tectonic rejuvenation were relatively discrete, such that climatic changes and channel avulsion could have overprinted the cycles beyond recognition.

3.3 Upper Sandstone Assemblage

The upper sandstone assemblage is restricted to the Trold Fiord belt, and consists of two distinct lithofacies: i) stratified sandstone/pebbly sandstone (~50%), occurring at the base of the assemblage and in the northern Trold Fiord belt (Plate 8A); and ii) stratified sandstone/siltstone (~50%), usually found above the sandstone/pebbly sandstone lithofacies and in the southern part of the Trold Fiord belt (Appendix 1). The assemblage is commonly interbedded with units characteristic of the underlying conglomerate assemblage and of the overlying limestone assemblage.

3.3.1 Stratified sandstone/pebbly sandstone lithofacies

The stratified sandstone/pebbly sandstone lithofacies consists of randomly distributed interbeds of red-weathered sandstone, pebbly sandstone, and minor pebble/granule conglomerate. Beds are 30cm thick on average, and sheetlike or lenticular in shape. The pebbly sandstones and pebble conglomerates are commonly associated with channel structures, and exhibit erosional basal surfaces and sharp but non-erosive contacts with overlying sandstones (Plate 8B). They are normally-graded, and locally show an imbricated clast fabric. Sandstone and pebbly sandstones units are typically parallel laminated or tabular cross-bedded (Plate 8C, D, E), and rarely trough cross-bedded. Reactivation surfaces are relatively common, and result from erosion of the downflow parts of sand bars during lower stage of river flow (Allen, 1984). Paleocurrent measurements on primary current lineations, tabular cross-beds, current ripples, and pebble imbrications show that the lithofacies was deposited from southward-flowing streams (Fig. 14). In the northeastern part of the Trold Fiord belt, however, sedimentation appears to have proceeded in a westerly fashion (Fig. 14, Section 10).

The conglomerates are composed of variegated chert pebbles and granules within a sandy matrix that is texturally and compositionally identical to the sandstones described above. Chert clasts are subspherical to oblate, and rounded to well rounded. The sandstones are classified as quartz arenites, being composed of more than 90% monocrystalline quartz and lesser amounts of polycrystalline quartz (<5%), chert (<5%), potassium feldspar (trace), and hornblende (trace). The textural maturity is relatively high, as indicated by the very good sorting and subrounded to rounded grain outlines. The average grain size is approximately 600μm (coarse sand). Matrix is virtually absent, and grains are bounded by up to 15% poikilotopic calcite cement. Quartz overgrowths are ubiquitous, with original grain boundaries being outlined by hematite dust rims.

The sandstone/pebbly sandstone lithofacies was deposited in the braided stream environment, as suggested by the widespread occurrence of parallel stratification and

Figure 14: Paleocurrent directions for the upper sandstone assemblage. Measurements are from primary current lineations (85%), current ripples (10%), and imbricate pebbles (5%).

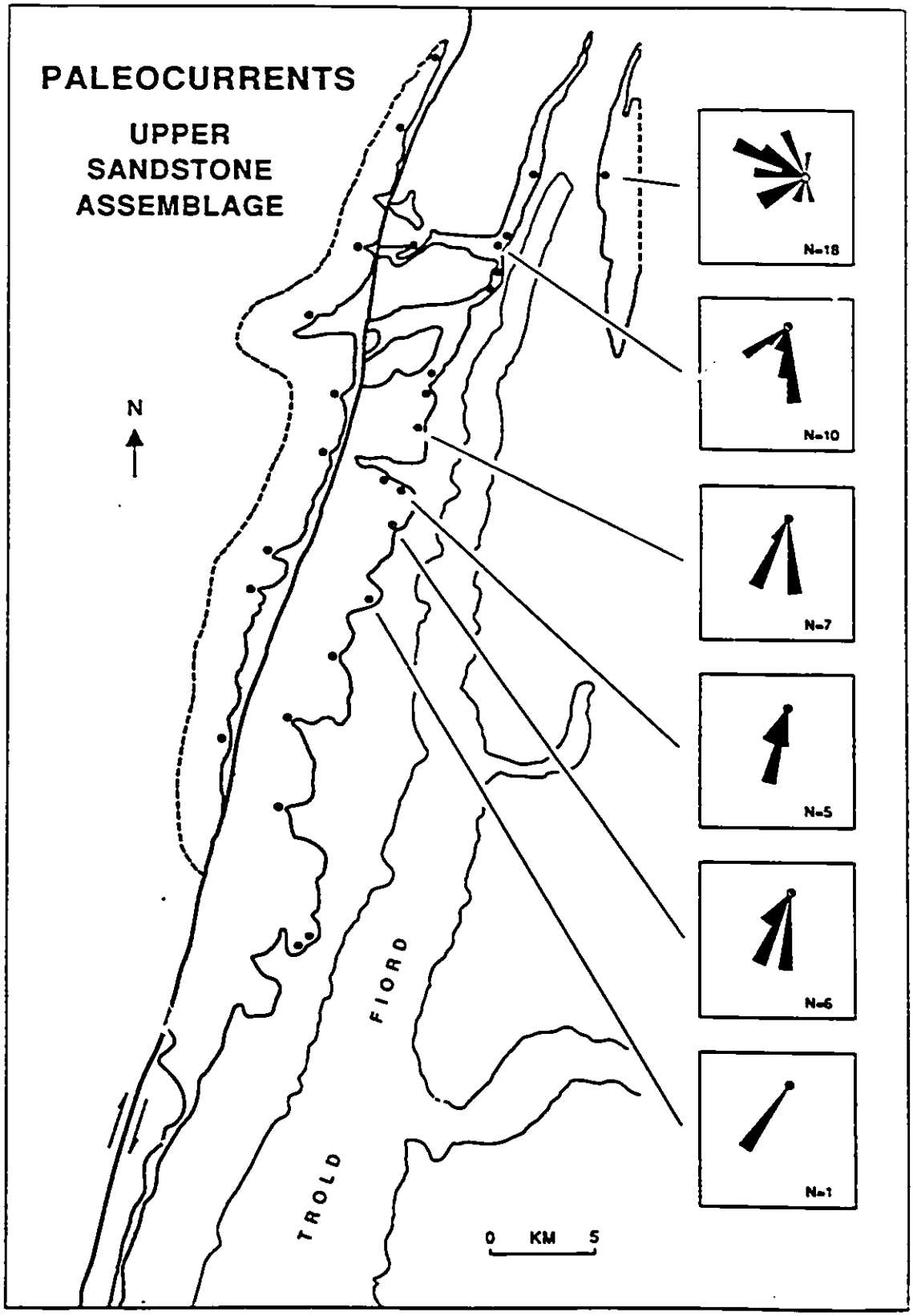
PALEOCURRENTS
UPPER
SANDSTONE
ASSEMBLAGE
N
N=18
N=10
N=7
N=5
N=6
N=1
TROLD
FIORD
0 KM 5

tabular crossbedding, and by the high textural and compositional maturity of the deposits (Miall, 1977; Cant, 1982; Walker and Cant, 1984). Of particular interest is the absence of caliches or any other soil-related features, indicating that sedimentation was little interrupted and proceeded at high rates, probably in perennial braided streams of subregional or regional extent.

3.3.2 Stratified sandstone/siltstone lithofacies

The sandstone/siltstone lithofacies consists of red-weathered medium sandstone to siltstone in which trough and tabular crossbedding, parallel laminations, trough ripples, and climbing ripples are common in several bed units (Plate 9A). Bed thicknesses may reach 1m, but are generally in the 5 to 10cm range. Other units are in contrast more massive, finer-grained, and include a wide range of textural and structural features, including: i) desiccation cracks, generally developed in siltstone with sandstone infilling (Plate 9B); ii) fossilized branches, found on bedding plane surfaces, measuring 5cm wide and 50cm long and displaying characteristic branching intersections (Plate 9B, C); iii) root structures, vertically-oriented and measuring up to 2cm in diameter and 10cm in length; iv) wind deflation structures, present as a network of sub-centimetre, irregularly-distributed, curved to discontinuous ridges; v) possible raindrop imprints; and vi) incipient nodular caliche. Trace fossils of the *Scoyenia* ichnofacies, reported to occur widely in floodplain sequences (Pemberton, 1988), are also present (Plate 9D). Tabular cross-beds, current ripples, primary current lineations and gutters casts were measured for paleocurrent orientations (Fig. 14). These orientations were similar to those obtained from the sandstone/pebbly sandstone lithofacies. The sandstone/siltstone lithofacies has a mineralogical composition identical to that of the sandstone/pebbly sandstone lithofacies.

The sandstone/siltsone lithofacies is commonly interbedded with marine limestone units characteristic of the limestone assemblage, and with subordinate unconsolidated terrigenous mud. The limestone interbeds are distributed at regular intervals within the

lithofacies, forming 5m to 15m thick cycles. An ideal cycle typically consists of up to 6m of sandstone/siltstone at the base, gradually overlain by 0.5m to 1.5m of limestone having a sandy basal part. The limestones are occasionally capped sharply by unconsolidated red mud less than 1m thick, interpreted as terra-rossa paleosols. These paleosols are usually overlain by units of the sandstone/siltstone lithofacies, and were developed during periods of relative low sea-level conditions. Terra-rossa paleosols result from the dissolution of limestone during subaerial exposure, and residual accumulation of insoluble material (James and Schenk, 1983).

The gradual upward transition from sandstone/siltstone to limestone suggests that the cycles are transgressive in nature, contrasting with the shallowing-upward "regressive" cycles widely reported in shelf successions. Cyclicity was most likely controlled by glacio-eustatic sea-level fluctuations. The predominance of transgressive deposits over regressive deposits has been reported for nearshore sequences and areas of coastal onlap controlled by glacio-eustasy (Vail et al., 1977; Beauchamp, 1987). It seems that tectonism was not an important factor in controlling cyclicity, since cycles do not exceed 15m in thickness. Furthermore, coarse terrigenous sediments are essentially absent. Delta-lobe switching is also an unlikely mechanism, as, under this scenario, fluvial sandstones would not be as widespread, and prograding deltaic sequences have not been identified.

The cyclicity displayed between the sandstone/siltstone lithofacies and the basal limestone assemblage indicates that the former was deposited in a coastal plain setting. The occurrence of fossilized roots and branches along with incipient caliche, absent from the sandstone/pebbly sandstone lithofacies, further indicates that vegetation was present in this paralic environment.

3.3.3 Discussion

The upper sandstone assemblage was deposited in braided stream and coastal plain environments. The braided stream deposits, which directly overly the conglomerate

assemblage, probably accumulated from perennial rivers of regional extent characterized by constant sedimentation rates. This nearly steady aggradation, punctuated by only short periods of non-deposition, is supported by the absence of interlayered fine-grained sediments and the scarcity of caliche. The time required for caliche to develop on sand bars was either insufficient, or immature profiles may have formed but were reworked by subsequent channel down-cutting.

The coastal plain deposits are interbedded with the limestone assemblage, and overlie either the braided stream deposits in the northern Trold Fiord belt, or the conglomerate assemblage in the southern part of this same belt (Fig. 8; Appendix 1). In contrast to the braided stream deposits, they were probably deposited in streams of relatively high sinuosity, as evidenced by the common presence of caliche and other soil-related structures. The relatively large size of roots and branches, as well as their widespread abundance, imply that plants successfully colonized the coastal plain area. Perhaps the water table in this paralic environment was higher then elsewhere, and provided the necessary soil humidity for vegetation to flourish.

Whereas the conglomerate assemblage was deposited from local and ephemeral fans/streams oriented perpendicular to the controlling master faults, the upper sandstone assemblage accumulated from regional and perennial streams that, in contrast, were oriented parallel to these master faults. The upper sandstone assemblage is therefore related to axial fluvial drainage, and this system was probably active even during the depositional history of the conglomerate assemblage, a time when it would have been located farther east beyond the extent of the Trold Fiord belt. For that matter, it is speculated that a similar axial fluvial system also existed in the Blind Fiord subbasin even though exposures are lacking. This system would have been remained west of the Blind Fiord belt area throughout its depositional history.

3.4 Evaporite Assemblage

The evaporite assemblage is exposed only in the southern Trold Fiord belt, at Sections 27 and 28 (Fig. 8; Appendix 1). It is subdivided into three distinct lithofacies, occurring in the following ascending stratigraphic order: i) mudstone/anhydrite lithofacies (40%); ii) anhydrite lithofacies (50%); and iii) limestone breccia lithofacies (10%). The vertical distribution of these lithofacies is illustrated in Plate 10A.

3.4.1 Mudstone/anhydrite lithofacies

This basal lithofacies is generally red-weathered and highly recessive, because of the presence of poorly consolidated to unconsolidated terrigenous mud units interpreted as possible pseudogley paleosols. Pseudogley is defined as "a densely packed, silty soil that is alternately waterlogged and rapidly dried out" (Bates and Jackson, 1987). These paleosol units, on fresh surfaces, are predominantly red with subordinate grey and brown interlayers, indicating periodic variations in redox conditions (Plate 10C). These colour variations resulted from the alternating conditions of waterlogging (below water table) and rapid drying (above water table). Pink anhydrite nodules scattered in the mud units are irregular in shape and average 10-15cm in size (Plate 10C).

The mudstone/anhydrite facies also contains distinct units of nodular anhydrite up to 7m thick. These units are more resistant than adjacent mud-rich units, and are characterized by pink to white anhydrite displaying a nodular texture. Minor limestones are also present, and consist of bituminous, non-fossiliferous, dark grey to black micrite with minor disseminated pyrite. These interlayers are less than 50cm thick and are typically massive to faintly laminated.

The mudstone/anhydrite deposits are interpreted as resulting from evaporative processes within a coastal playa, characterized by the periodic influx of floodplain mud and occasional inundation with marine water. The terrigenous mud was deposited at low sedimentation rates, allowing the development of pseudogley paleosols near the water

table. Nodules of anhydrite precipitated within the paleosols from interstitial brines filtered through the sediments, either by gravity percolation or evaporative drawback. Rare units of non-fossiliferous limestone and relatively pure nodular anhydrite resulted from precipitation following playa inundation due to marine invasion. Periodic marine influence within the enclosed or partially enclosed coastal playa was likely controlled by seasonal storms or high-order sea-level fluctuations. No shallowing-upward cycles have been identified, a feature characteristic of sabkha deposits (Kendall, 1984). Although marine influence is not a prerequisite for developing a sequence like that of the mudstone/anhydrite lithofacies, the overlying anhydrite facies is at least partially marine in origin, and therefore suggests a coastal setting.

3.4.2 Anhydrite lithofacies

Unlike the underlying red-weathered and recessive facies, the anhydrite lithofacies is invariably white to pale grey and exposed as relatively resistant intervals. It is dominated by nodular and nodular-bedded anhydrite, with subordinate bedded anhydrite and limestone interlayers (Plate 10D, E). The anhydrite nodules are up to 50cm in diameter and outlined by dark insoluble material displaced during growth, resulting in a well-defined chicken-wire texture (Plate 10D). Gypsum occurs along fractures and at nodule boundaries, suggesting it formed from recent nearsurface hydration of anhydrite (Plate 10D). Bedded anhydrite is common near the top of the evaporite assemblage, with individual layers being generally less than 5cm thick. Whereas the nodular and nodular-bedded fabrics probably resulted from the partial recrystallization of primary anhydrite, the bedded fabric represents original layering which escaped subsequent diagenetic recrystallization (Kendall, 1984).

The limestones in the anhydrite lithofacies, in contrast to those of the mudstone/anhydrite lithofacies, are fossiliferous. Four distinct biotic microfacies have been identified: i) an ostracod microfacies; ii) a fusulinacean/beresellid microfacies; iii) a

identified: i) an ostracod microfacies; ii) a fusulinacean/beresellid microfacies; iii) a fusulinacean microfacies; and iv) a bryozoan microfacies. As seen in Appendix 1 (Section 28), the base of the anhydrite lithofacies is represented by ostracod and fusulinacean/beresellid limestones, whereas the upper part comprises fusulinacean and bryozoan limestones.

The ostracod microfacies occurs in wackestones, and is composed mainly of carbonate mud with ostracod valves, some of which have been flattened due to compaction (Plate 11A). Encrusting foraminifers (apterrinellids) are locally common, along with minor calcispheres. The matrix consists of dark micrite relatively rich in organic matter (a few percent) and minor disseminated pyrite.

The three other microfacies have a relatively well diversified biota. The fusulinacean/beresellid microfacies consists of packstones dominated by fusulinid foraminifers, beresellid algae, and encrusting foraminifers, together with common to minor bryozoans, brachiopods, echinoderms, small foraminifers, ungdarellid algae, trilobites, and ostracods (Plate 11B). The fusulinacean microfacies is characterized by wackestones and packstones comprising abundant fusulinid foraminifers, echinoderms, and brachiopods, with subordinate bryozoans, small forams, ungdarellid and beresellid algae, trilobites, and ostracods (Plate 11C). The bryozoan microfacies consists of wackestones composed almost exclusively of bryozoans, brachiopods, and echinoderms.

The presence of fossiliferous wackestone/packstone and lack of terrigenous mudstone within the anhydrite lithofacies suggest that deposition occurred in the marine environment, probably in a hypersaline lagoon. The bryozoan/fusulinacean limestone interlayer in the upper part of the anhydrite lithofacies (Appendix 1, Section 28) indicates that open marine conditions periodically existed, during which barriers or spits protecting and restricting the hypersaline lagoon were rapidly submerged by a relative rise in sea-level.

3.4.3 Limestone breccia lithofacies

A 3m thick breccia caps the evaporite assemblage. It is composed of limestone, chert, and anhydrite clasts set in a microcrystalline carbonate matrix (Plate 11D). Individual clasts are angular to very angular and less than 2cm in size. Limestone clasts are composed mostly of mudstone and wackestone. Chert clasts are of diagenetic origin and replace some of the anhydrite clasts, exhibiting local ghost structures of coarse anhydrite crystals. The matrix consists of laminated to non-laminated micrite and microspar, along with minor detrital quartz silt. Microspar is common in silt-rich laminae, and resulted from the neomorphic recrystallization of micrite. The breccia is overall highly porous, characterized by both euhedral pores resulting from the dissolution of some of the anhydrite clasts, and irregular interparticle pores. The high interparticular porosity combined with the absence of allochthonous clasts suggest that the breccia resulted from the dissolution and *in situ* collapse of uppermost evaporite beds, and is unlikely of tectonic origin. Collapsing was probably due to post-depositional dissolution and concurrent compaction from the weight of overlying limestone units. Isotopic analyses performed on the carbonate matrix (see Chapter 4) suggest that this event may have occurred as late as the middle Tertiary, during the Eurekan Orogeny. Similar collapse breccias have been documented elsewhere, with some units attaining several tens of metres in thickness (Lauritzen, 1981).

3.4.4 Discussion

In addition to sedimentological observations, the carbonates and sulphates of the evaporite assemblage were also analyzed to determine its stable isotope composition. The results are presented and interpreted in Chapter 4.

Based on both sedimentological and geochemical evidence, it appears that sediments of the evaporite assemblage precipitated from sea water, and accumulated in a coastal playa that evolved into a hypersaline lagoon; the succession is therefore transgressive in nature. The base of the evaporite assemblage (mudstone/anhydrite

lithofacies) accumulated in a coastal playa, characterized by floodplain sedimentation, paleosol development, and growth of anhydrite nodules from interstitial brines. This playa was periodically infilled with marine water, from which layers of anhydrite and non-fossiliferous limestone were precipitated. The evaporite layers were precipitated during lowstand intervals, with hypersaline conditions being achieved from poor circulation and evaporation. With progressive submergence, marine conditions became prevalent and the coastal playa sediments were succeeded by hypersaline lagoon sediments. Hence, the dominant fluvial, pedogenic, and surficial diagenetic processes were replaced by subaqueous precipitation of sulphates and carbonates, at or near the sediment/water interface. Connections to the adjacent sea were no longer ephemeral, and marine conditions became virtually uninterrupted by continental processes. With continuing marine transgression and concurrent increase in water depth, rates of evaporation dropped and limestones became predominant. The collapse breccia marks the end of evaporite sedimentation, and is overlain by the limestone assemblage. At this time, the coastal salina and hypersaline lagoon had evolved into an open shelf environment, and the bar spits or barrier islands were permanently submerged.

Thorsteinsson (1974) suggested that the evaporite assemblage of the Canyon Fiord Formation may represent a local extension at the basin margin of the Otto Fiord Formation, a unit thought to be restricted essentially to the central areas of Sverdrup Basin (Fig. 2). However, conodonts of early late Moscovian age have been recovered from the upper part of the evaporite assemblage (Appendix 3), indicating that this assemblage is not part of a diachronous unit that includes the basin centre Otto Fiord Formation, dated as Bashkirian to early Moscovian (Thorsteinsson, 1974). The paleogeographic setting of the basal Canyon Fiord Formation in the study area (north-south-oriented subbasins), and apparent pinching of the evaporite assemblage to the northeast and to the west also suggest that the assemblage represents an isolated deposit at the margin of the basin.

3.5 Limestone Assemblage

The basal part of the middle limestone member of the Canyon Fiord Formation is referred to in this study as the limestone assemblage. It is related to a basin-wide marine transgression in Late Carboniferous time (Beauchamp et al., 1989b) that gradually encroached on and submerged the entire study area. Five biotic microfacies have been identified at the base of the limestone assemblage, and were named according to their dominant constituents. They are: i) the encrusting foraminiferal microfacies; ii) the dasycladacean microfacies; iii) the fusulinacean-beresellid microfacies; iv) the bioclastic microfacies; and v) the fusulinacean microfacies. The relative abundance of biotic components present in each microfacies is shown in Figure 15. The microfacies present in the lowermost beds of the limestone assemblage was compared for each locality of the study area, and shows no particular geographic trend (Fig. 16). The bioclastic microfacies commonly is closely associated with well segregated beds of pebbly grainstones. These pebbly beds are described below with the bioclastic microfacies.

3.5.1 Encrusting foraminiferal microfacies

The encrusting foraminiferal microfacies consists of packstone and wackestone, of which the main constituents are encrusting foraminifers (mainly apterrinellid), small benthic foraminifers (mostly globivalvulinid), and red algae (Plate 12A, B). Subordinate biotic elements include bryozoans, crinoids, brachiopods, and ostracods. This microfacies has a relatively well diversified biota showing some degree of marine restriction (Fig. 15). Deposition occurred either in shallow lagoons or estuaries, with the restricted nature of the biota being promoted by hypersaline or brackish conditions, and/or by poor circulation.

3.5.2 Dasycladacean microfacies

The dasycladacean microfacies occurs only at one locality in the study area (Appendix 1, Section 19). It consists of grainstones to packstones dominated by

Figure 15: Relative abundance of biotic elements in microfacies of the limestone assemblage.

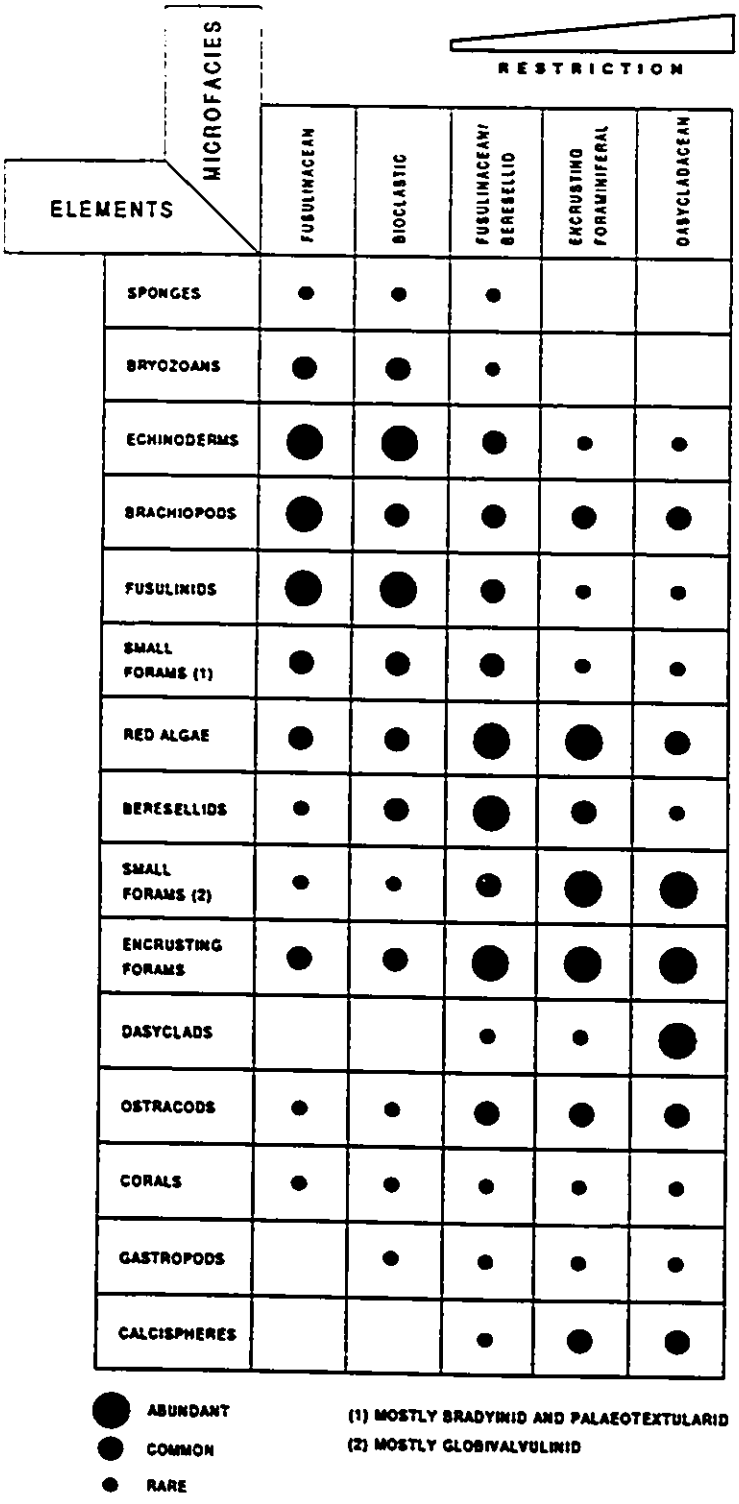
MICROFACIES
ELEMENTS
RESTRICTION
FUSULINACEAN
BIOCLASTIC
FUSULINACEAN/ BERESELLID
ENCRUSTING FORAMINIFERAL
DASYCLADACEAN
SPONGES
BRYOZOANS
ECHINODERMS
BRACHIOPODS
FUSULINIDS
SMALL FORAMS (1)
RED ALGAE
BERESELLIDS
SMALL FORAMS (2)
ENCRUSTING FORAMS
DASYCLADS
OSTRACODS
CORALS
GASTROPODS
CALCISPHERES
ABUNDANT
COMMON
RARE
(1) MOSTLY BRADYINID AND PALAEOTEXTULARID
(2) MOSTLY GLOBIVALVULINID

Figure 16: Map showing the geographic distribution of microfacies in the basal limestone assemblage at several localities in the study area.

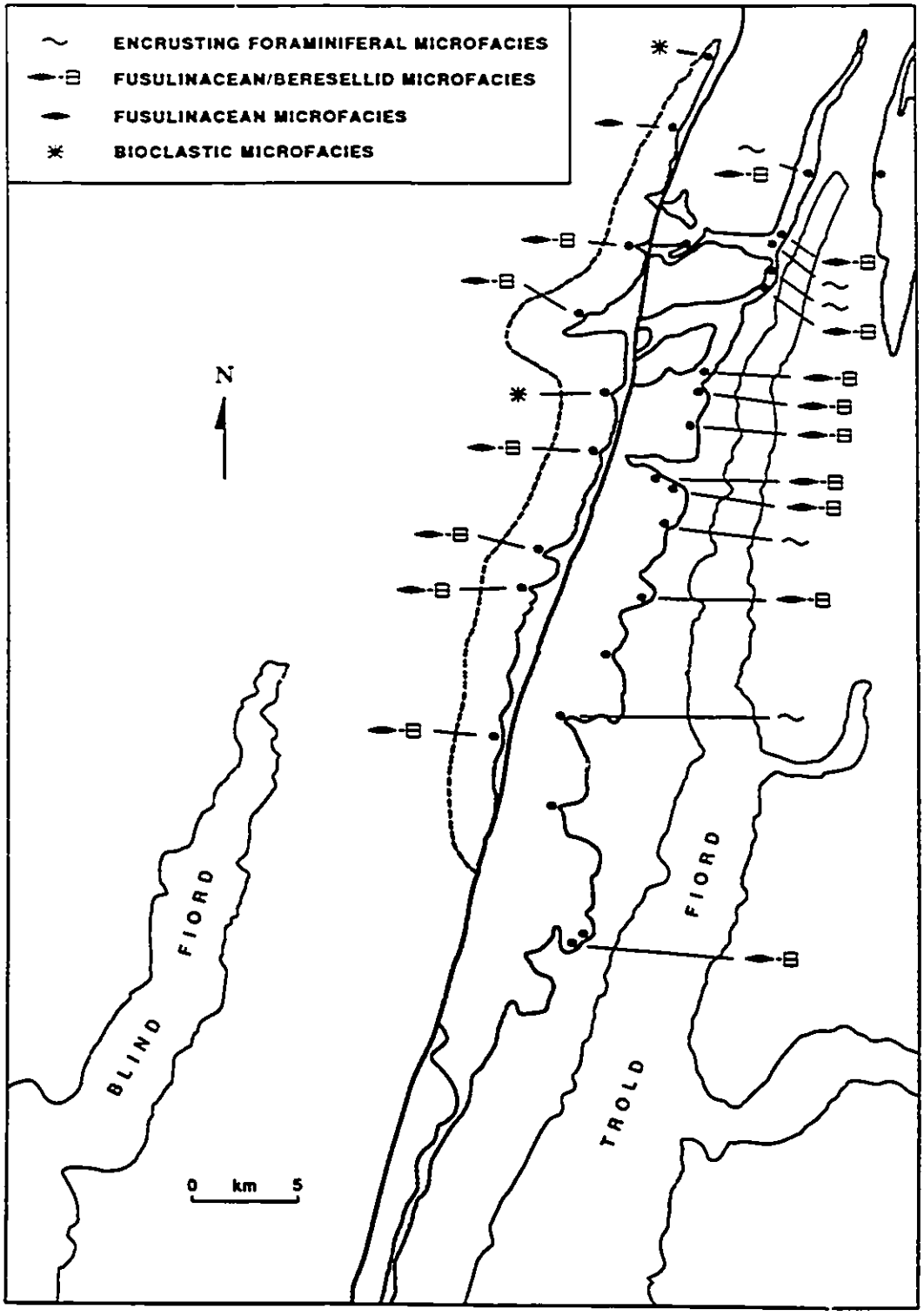
ENCRUSTING FORAMINIFERAL MICROFACIES
FUSULINACEAN/BERESELLID MICROFACIES
FUSULINACEAN MICROFACIES
BIOCLASTIC MICROFACIES
N
BLIND FIORD
TROLD FIORD
0 km 5

dasycladacean green algae, and both encrusting (apterrinellid) and small benthic (globivalvulinid) foraminifers (Plate 12C, D). Other common constituents include brachiopods, red algae, and ostracods (Fig. 15). Shallow lagoons or estuaries were most likely the depositional environments, with still a fair amount of restriction (Fig. 15) implied by the rare occurrence of certain fossil groups (fusulinids, brachiopods, bryozoans, sponge spicules) that are common in the more open marine limestones of the Canyon Fiord Formation (Beauchamp, 1987).

3.5.3 Bioclastic microfacies

The bioclastic microfacies consists of grainstones composed of several groups of algae and foraminifers (mostly fusulinids), along with common bryozoans, echinoderms, brachiopods, gastropods, limestone and caliche extraclasts, and reworked *Microcodium* fragments (Plate 13A, B; Fig. 15). These carbonate grains are fine to coarse sand in size, and are associated with detrital quartz silt and sand. The bioclastic microfacies was deposited in a high energy shallow marine environment, possibly as beaches or sand shoals. Pebbly grainstones interlayers found locally within the bioclastic grainstones are medium grey, well stratified, well sorted, clast- to matrix-supported, and less than 1m thick. They are composed mainly of rounded limestone pebbles (extraclasts) set in a bioclastic limestone matrix (Plate 13C, D). These pebbly grainstone interlayers were likely deposited in the beach or fan-delta environment.

3.5.4 Fusulinacean/beresellid microfacies

The fusulinacean/beresellid microfacies is the most widespread in the study area (Fig. 16). It consists of well diversified grainstones, packstones, and boundstones dominated by fusulinacean foraminifers, beresellid green algae, ungdarellid red algae, and encrusting foraminifers (Plate 14A, B). Brachiopods, crinoids, ostracods, and small benthic foraminifers are relatively common (Fig. 15). The grainstones were deposited above wave base, possibly as sand shoals, whereas the packstones probably accumulated

in an open marine environment below wave base. The boundstones correspond to stabilized algal thickets and/or meadows composed of beresellid algae, encrusting foraminifers, and encrusting ungdarellid red algae. The abundance of beresellids (green algae) in these thickets and/or meadows suggests relatively low water depth, probably in a protected environment behind sand shoals.

3.5.5 Fusulinacean microfacies

The fusulinacean microfacies is present locally at the base of the limestone assemblage (Fig. 16). It consists of packstone and wackestone composed mostly of echinoderms, brachiopods, and fusulinids (Plate 14C, D). Less common constituents include bryozoans, small benthic foraminifers, red algae, and encrusting foraminifers (Fig. 15). These limestones accumulated below wave base in an open shelf environment. Although rare at the base of the limestone assemblage, this facies is more abundant up-section (Appendix 1; Section 13). This suggests that the study area evolved from a protected coastal environment to an open shelf environment.

3.5.6 Discussion

The basal limestone assemblage was deposited in relatively well protected nearshore environments. These restricted environments, controlled mainly by topographic relief in the area, resulted in the deposition of the encrusting foraminiferal, the dasycladacean, and the fusulinacean/beresellid microfacies (Figs. 15 and 16). The bioclastic facies was also deposited locally in less restricted, and more agitated nearshore environments. With rising sea-level, the partially restricted basal limestones were gradually succeeded by more open marine facies, including the fusulinacean and bryozoan microfacies (Fig. 15; Appendix 1, Section 13). Stabilized algal thickets and/or meadows are believed to have been locally present. Where hydrodynamic conditions were high, reworking of carbonate debris resulted in deposition of the bioclastic microfacies (calcarenites), probably in the nearshore environment as beaches and/or bars. Of interest is the absence of ooids in all facies of the

basal limestone assemblage, even though they are abundant in younger carbonates of the middle limestone member (Beauchamp, 1987). This suggests insufficient agitation for ooid formation during deposition of the basal limestone assemblage (except bioclastic microfacies), and suggests a relatively well protected and restricted marine environment.

As illustrated in Figure 11, the base of the limestone assemblage in the Blind Fiord belt is interbedded with units of the conglomerate assemblage. These conglomerate units appear to be of fan-delta origin, as they are mainly grey-weathered and contain fossiliferous matrices. Additional evidence supporting this depositional environment, however, has not been observed. The interlayering of conglomerates and limestones was probably controlled by both sea-level fluctuations and seasonal flood events. The conglomerate units are limited to a few tens of metres or less above the base of the limestone assemblage, indicating that the area underlying the Blind Fiord belt became rapidly submerged by the sea.

CHAPTER 4: STABLE ISOTOPE GEOCHEMISTRY

Stable isotope ratios were determined on samples of limestone and evaporite at Section 28. The general purpose was to verify if stable isotopes could support the sedimentological interpretations for the evaporite assemblage. The basal mudstone/ anhydrite lithofacies of this assemblage is believed to have been deposited within a coastal playa, whereas the overlying anhydrite lithofacies was deposited within a salina or hypersaline lagoon.

4.1 Sample Descriptions

Nineteen limestone (calcite) samples and eighteen evaporite (gypsum and anhydrite) samples were analysed for carbon and oxygen isotopes, and for sulphur isotopes, respectively. Based on petrographic and field observations, the limestones have been subdivided into four groups: collapse-breccia limestone (CBL), conglomerate-hosted caliche (CHC), non-fossiliferous limestone (NFL), and fossiliferous limestone (FL); and the evaporites into two groups: nodular gypsum (NG), and nodular to bedded anhydrite (NBA).

The CBL samples were collected in the uppermost part of the evaporite assemblage, and consist of a matrix of non-fossiliferous lime mudstone between clasts of anhydrite, chert, and limestone. This matrix is either laminated or non-laminated, and comprises various proportions of micrite, microspar, and detrital quartz sand. Microspar is neomorphic in origin after micrite.

The CHC samples are from the conglomerate assemblage underlying the evaporite assemblage at Section 28. These samples consist of a pedogenic matrix of laminar and massive caliches within fluvial, clast-supported conglomerates. This caliche matrix is composed of dark micrite with minor detrital quartz and limestone fragments.

The NFL samples represent interlayered limestone within the evaporite assemblage. They are composed of dark micrite with minor microspar and disseminated pyrite, and up to a few percent of organic matter.

The FL samples were collected mainly from the anhydrite facies of the evaporite assemblage. A sample of the overlying limestone assemblage was also analyzed for comparison. The FL samples consist of beresellid algae, brachiopod, echinoderm, and fusulinid wackestones and packstones. The matrix is composed of micrite, with up to 25% neomorphic microspar, 1-2% organic matter, and minor pyrite.

The NG and NBA samples are from the two facies of the evaporite assemblage. The NG samples are white to pale pink, and occur either in distinct weathered intervals or as an alteration product coating anhydrite nodules and lining fractures. This restricted mode of occurrence for gypsum suggests that hydration of anhydrite could be a relatively recent phenomenon. The NBA samples are white to pale grey and occur in nodular-mosaic, nodular-bedded, and well-bedded fabrics.

4.2 Results

All isotopic analyses were done on the least altered portions of whole-rock samples. Isotopic ratios are expressed as ∂-values (‰) relative to PDB (C, O) and CDT (S) standards. The isotope values for each sample are listed in Appendix 4, together with respective stratigraphic levels and a brief lithological description. $\partial^{18}O$ and $\partial^{13}C$ values of limestone samples are plotted on Figure 17. The range of isotope ratios for each group is as follows: from -16.0 to -12.7‰ in $\partial^{18}O$, and from -1.6 to -0.5‰ in $\partial^{13}C$ for CBL; from -4.5 to -2.9‰ in $\partial^{18}O$, and from -7.8 to -5.6‰ in $\partial^{13}C$ for CHC; from -6.3 to -3.8‰ in $\partial^{18}O$, and from -1.9 to +1.4‰ in $\partial^{13}C$ for NFL; from -4.9 to -3.5‰ in $\partial^{18}O$, and from +1.9 to +3.0‰ in $\partial^{13}C$ for FL. The $\partial^{34}S$ values of sulphate samples have the following range: from +15.9 to +16.0‰ for NG, and from +14.9 to +16.2‰ for NBA.

Figure 17: Cross plot of $\partial^{13}C$ and $\partial^{18}O$ relative to PDB for the different limestone groups at Section 28. Meteoric and marine cement zones (M. Savard, pers. comm., 1990) are from Late Carboniferous calcite cements of Sverdrup Basin.

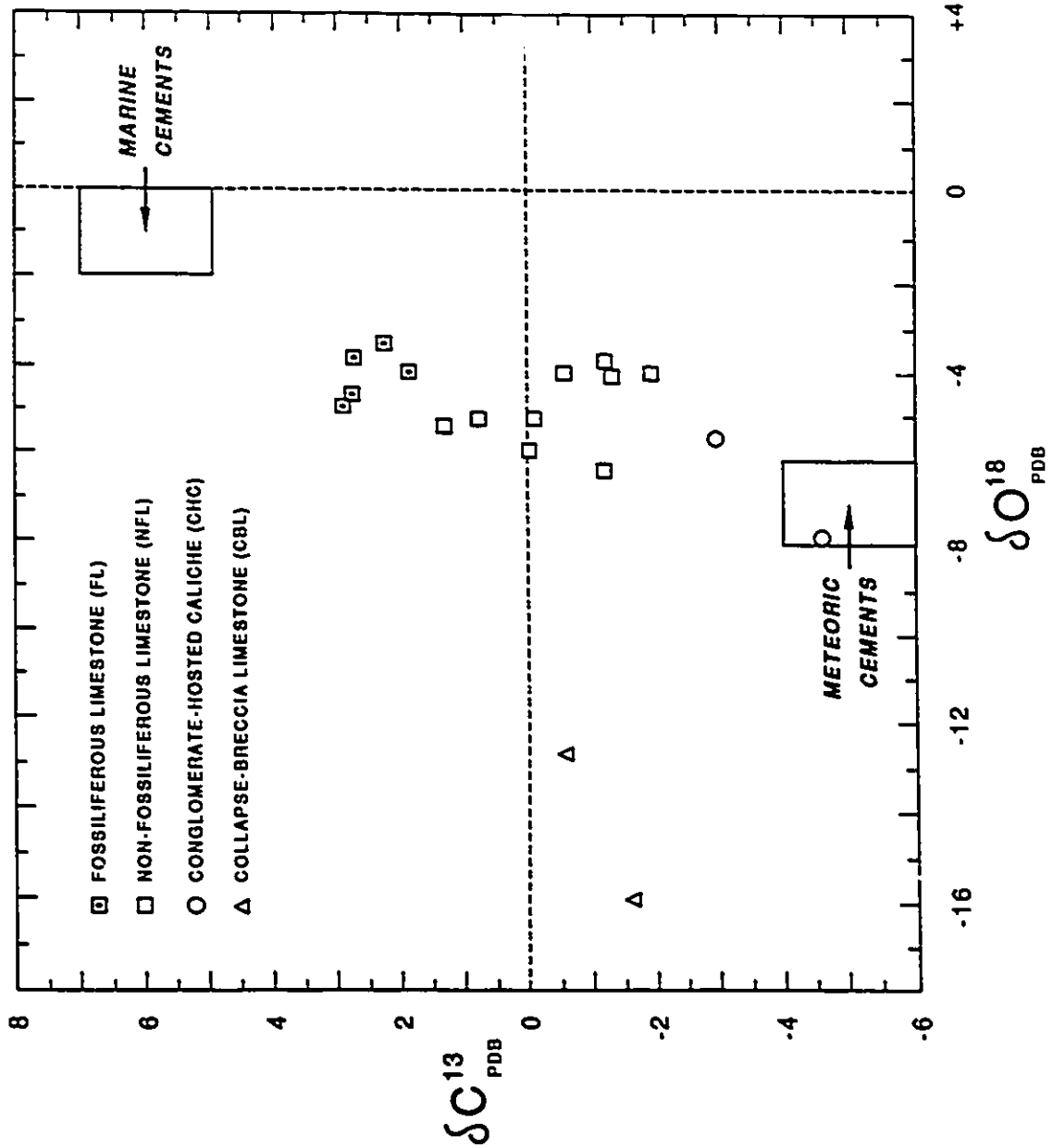
FOSSILIFEROUS LIMESTONE (FL)
NON-FOSSILIFEROUS LIMESTONE (NFL)
CONGLOMERATE-HOSTED CALICHE (CHC)
COLLAPSE-BRECCIA LIMESTONE (CBL)
MARINE CEMENTS
METEORIC CEMENTS
δC13 PDB
δO18 PDB
8
6
4
2
0
-2
-4
-6
+4
0
-4
-8
-12
-16

Of particular interest is the stratigraphic trend displayed in $\partial^{13}C$ ratios of limestone samples and in $\partial^{34}S$ ratios of evaporite samples within the evaporite assemblage (Figs. 18 and 19 respectively). An overall upward-enriching trend in $\partial^{13}C$ is present, with values ranging from -1.9 to -1.1‰ for the basal mudstone/anhydrite lithofacies and from -1.1 to +3.0‰ (excluding CBL that show a probable diagenetic overprint) for the overlying anhydrite lithofacies. An overall upward-depleting trend in $\partial^{34}S$ is also observed, with values ranging from +15.9 to +16.2‰ for the mudstone/anhydrite lithofacies, and from +14.9 to +15.7‰ (excluding NG) for the anhydrite lithofacies.

4.3 Discussion

4.3.1. Carbon and Oxygen

It had long been accepted that $\partial^{13}C_{PDB}$ ratios for marine carbonates range within 0 ±3-5‰, and that there is no significant trend with geologic time (Craig, 1953; Galimov et al., 1975). Veizer et al. (1980), however, demonstrated more recently that secular variations in $\partial^{13}C$ likely occurred during the late Proterozoic and Phanerozoic. In the Late Carboniferous, a time when $\partial^{13}C$ values were relatively high, Veizer et al. (1986) have shown that the average $\partial^{13}C$ of unaltered marine carbonates ranges from +2‰ to +3.5‰. These values reflect the average isotopic composition of sea water on a global scale.

On a more regional scale, it is also documented that sea water in isolated or closed basins can undergo significant enrichment in ^{13}C as a result of either extensive evaporation (Stiller et al., 1985), or preferential removal of ^{12}C by organic matter (Schidlowski et al., 1976). Non-altered shallow water limestones from the Upper Carboniferous of Sverdrup Basin, which was partially isolated from the paleo-Pacific ocean at that time, were analyzed for $\partial^{13}C$ by Beauchamp et al. (1987). Their values range from +4‰ to +7‰, and are enriched in ^{13}C relative to global sea water of the same age (ranges between +2.0‰ and +3.5‰). Beauchamp et al. (1987) interpreted this ^{13}C enrichment as resulting mostly from

Figure 18: Stratigraphic trend in $\partial^{13}C$ relative to PDB for limestone samples at Section 28.

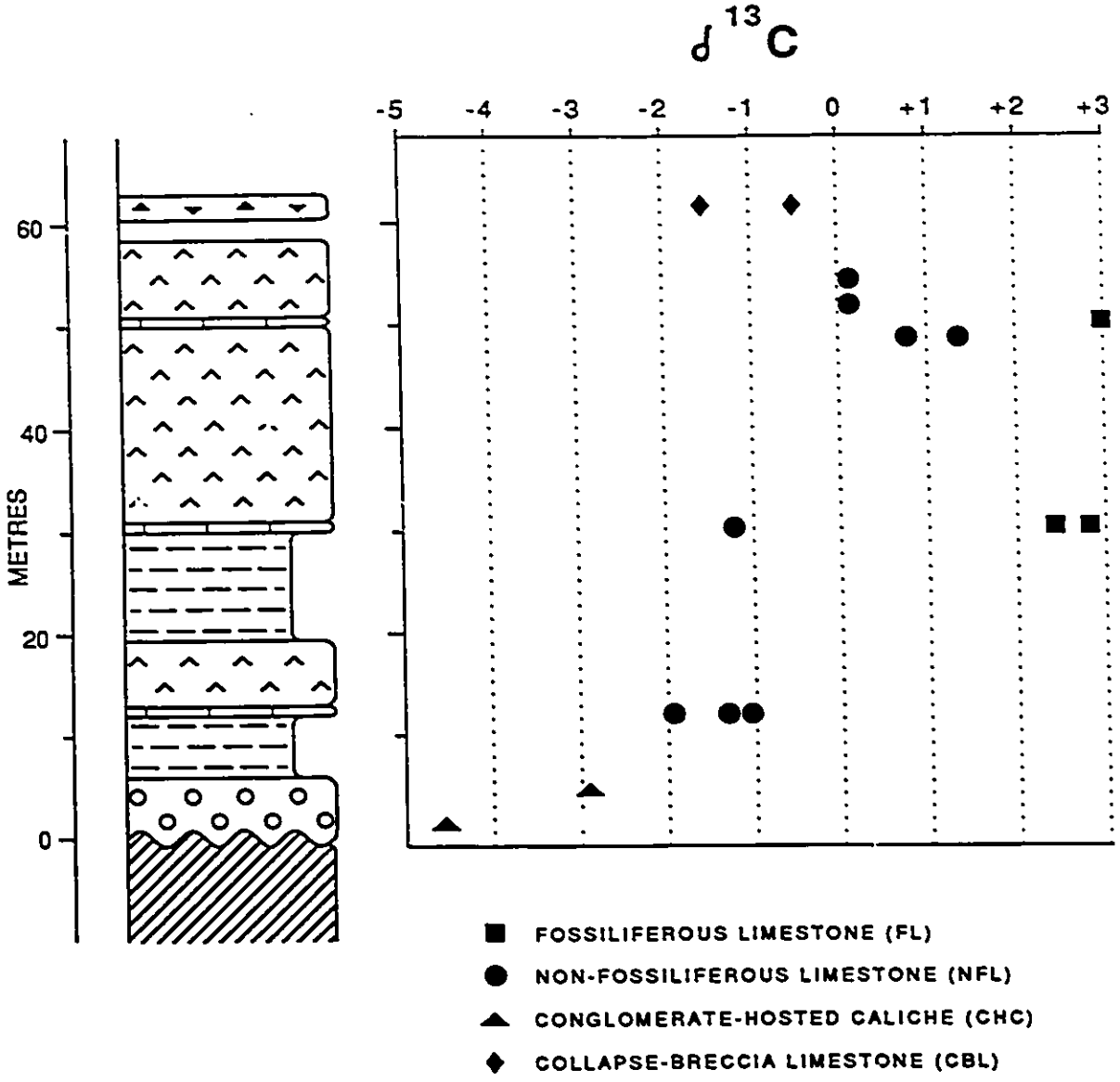
δ 13C
-5
-4
-3
-2
-1
0
+1
+2
+3
METRES
60
40
20
0
FOSSILIFEROUS LIMESTONE (FL)
NON-FOSSILIFEROUS LIMESTONE (NFL)
CONGLOMERATE-HOSTED CALICHE (CHC)
COLLAPSE-BRECCIA LIMESTONE (CBL)

Figure 19: Stratigraphic trend in $\partial^{34}S$ relative to CDT for sulphate samples at Section 28.

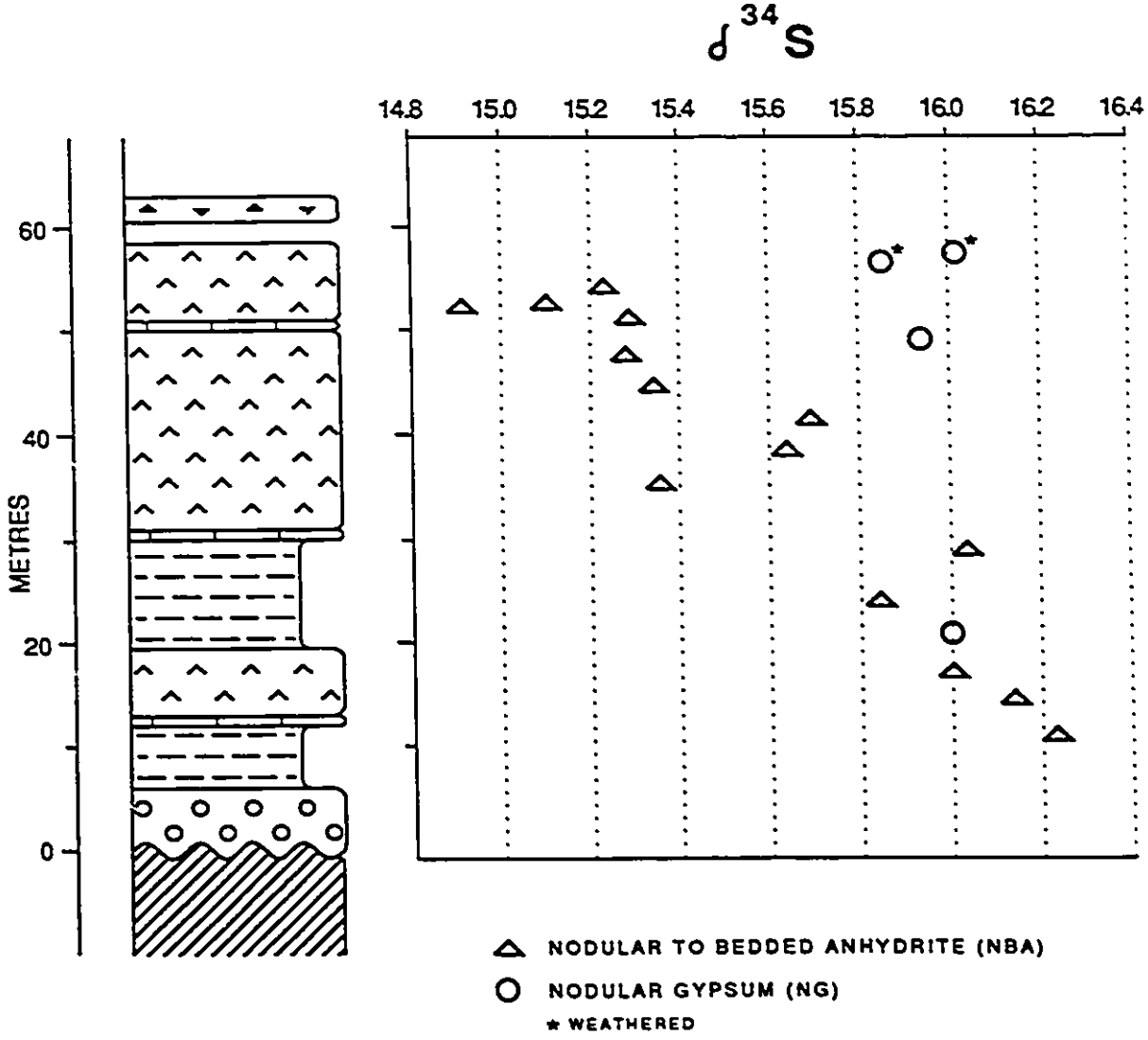
δ 34S
14.8
15.0
15.2
15.4
15.6
15.8
16.0
16.2
16.4
METRES
60
40
20
0
NODULAR TO BEDDED ANHYDRITE (NBA)
NODULAR GYPSUM (NG)
★ WEATHERED

preferential uptake of ^{12}C by organic matter in the deeper part of the basin, and concurrent ^{13}C enrichment of dissolved carbonates in shallow water. It was also suggested that evaporation was partially responsible for the depletion from middle Carboniferous to Early Permian time, as evidenced by the presence of deep basinal (Otto Fiord Formation) and basin marginal (evaporite assemblage of this study; Mount Bayley Formation) evaporites. In addition, Beauchamp et al. (1987) analyzed meteoric-influenced limestones, which were found to be depleted in both ^{13}C and ^{18}O relative to Upper Carboniferous isotopic seawater values. This depletion was explained by diagenetic overprint, with dissolution and recrystallization occurring in the presence of meteoric water. Recent work by Martine Savard (pers. comm., 1990) on marine and meteoric cements confirmed the values obtained by Beauchamp et al. (1987). The $\partial^{13}C$ values for marine cements average +6‰, whereas those for the meteoric cements cluster around -5‰ (Fig. 17).

The $\partial^{18}O$ of ocean water has been shown, through the analyses of ancient marine cherts and limestones, to decrease in value with increasing geologic age (Veizer and Hoefs, 1976). This secular change is still highly debated, as many workers claim that the trend reflects progressive diagenetic evolution (Hoefs, 1987). Nevertheless, Veizer et al. (1986) suggested that the $\partial^{18}O$ composition of Late Carboniferous marine water ranged from 0‰ to -3‰. Savard (pers. comm.) reports that $\partial^{18}O$ for marine and meteoric cements from Sverdrup Basin cluster around -1‰ and -7‰ respectively (Fig. 17).

The $\partial^{13}C$ and $\partial^{18}O$ values for fossiliferous limestones (FL) and non-fossiliferous limestones (NFL) of the present study are both depleted with respect to the marine values of Sverdrup Basin (Fig. 17) reported by Beauchamp et al. (1987) and Savard (pers. comm.). This depletion reflects in part that whole rocks were analyzed instead of individual cement zones. Beauchamp et al. (1987) showed that whole rock isotope ratios of non-altered shallow water limestones devoid of organic matter are only slightly depleted relative to values from isolated cements. The depletion in ^{13}C of FL and NFL is therefore interpreted as resulting from the presence of organic matter within the analyzed samples. It

is well known that bacterial degradation of organic matter releases ^{12}C-enriched CO_2 that may be incorporated into diagenetic calcite, which in turn would lower whole rock $\partial^{13}C$. Organic matter, which preferentially incorporates ^{12}C during its formation, has an average $\partial^{13}C$ of -24‰ (Hudson, 1977).

A stratigraphically upward-increasing trend in $\partial^{13}C$ values of FL and NFL is also displayed in Figures 17 and 18. This trend may have been controlled partially by the interaction of fluids with organic matter, although petrographic observations have unfortunately revealed little or no variation in organic matter content between samples. The upward-increasing isotopic ratios could also be a result of meteoric diagenesis in the lower part of the section, as the ratios for FL, NFL, and CHC vary in the direction of the meteoric water pole of Savard (pers. comm.). However, this contention is supported only by the observation of localized neomorphic microspar in thin section, with no apparent trend of abundance. The upward-increasing isotopic ratios are thought to reflect mainly a shift in primary water composition, such that the observed trend in depletion would indicate precipitation from brackish water for the basal part of the evaporite assemblage, and from more saline marine water for the upper part of the assemblage. Although a hypersaline environment was necessarily required for precipitation of the evaporites interlayered with FL and NFL, it is possible that the more basal NFL resulted from ephemeral episodes of lacustrine or brackish conditions. Carbonates of lacustrine origin have been reported elsewhere in Sverdrup Basin (e.g. Emma Fiord Formation; Davies and Nassichuk, 1988). Alternating evaporitic and lacustrine facies have also been observed in the lower Upper Carboniferous succession of the Buckingham O-68 well (B. Beauchamp, pers. comm., 1990), drilled in the western Arctic.

The caliche samples in the conglomerate assemblage (CHC) display $\partial^{13}C$ and $\partial^{18}O$ ratios that are only slightly lighter than the lowermost NFL samples (Fig. 17). These ratios are similar to those obtained by Savard (pers. comm.) for meteoric cements, and support the caliche interpretation for CHC. In addition, the two CHC samples are depleted by

4.5‰ and 7‰ relative to the $\partial^{18}O$ of Savard (pers. comm.) from marine cements. Analyses of recent fresh water in the Mediterranean area have shown an average depletion of 5.0 to 7.0‰ in $\partial^{18}O$ with respect to sea water (Longinelli, 1979).

The CBL samples are strongly depleted relative to Late Carboniferous sea water with $\partial^{18}O$ values of -16.0 and -12.7‰, indicating that they were diagenetically altered. This is in agreement with sedimentological observations, in that they are collapse-breccias. Dissolution of uppermost evaporite layers and concurrent collapse of overlying limestones are believed to have been synchronous and closely tied to the isotopic alteration of these limestones. The strong depletion in ^{18}O of CBL cannot be related to a temperature increase associated with burial, since regional organic matter maturation indicate that the rocks lying at the exposed margin of Sverdrup Basin were never deeply buried (Utting et al., 1989). Also, the ^{18}O depletion cannot reflect a late Paleozoic meteoric overprint because meteoric water in equatorial paleogeographic settings is not strongly depleted in ^{18}O. The ^{18}O depletion may have resulted, however, from either alteration by shallow hydrothermal fluids, or from the introduction of cold meteoric fluids in the nearsurface environment. Direct evidence for a hydrothermal origin is lacking, but warm fluids would have easily promoted the dissolution of uppermost sulphates and concurrent brecciation. The introduction of cold meteoric fluids is suggested by indirect evidence. In assuming meteoric water diagenesis, the northern part of North America had to have drifted from its sub-tropical position in the late Paleozoic into much colder sub-Arctic or Arctic latitudes. Interestingly, this paleogeographic positioning was probably in effect by the middle Tertiary, a time when cold meteoric fluids could have easily travelled down fracture systems resulting from faulting related to tectonic uplift during the Eurekan Orogeny. The two CBL values are slightly enriched in both ^{13}C and ^{18}O with respect to arctic/subarctic meteoric water (approximately $\partial^{18}O$ -22‰ and $\partial^{13}C$ -5‰ at 15°C for latitude 70-80°: Anderson and Arthur, 1983; Savard, pers. comm.), probably as a result of the combined presence of primary micrite and secondary microspar in whole rock samples. To assess this

interpretation, analysis of carbonate veins cross-cutting middle Tertiary and older strata is required for comparison with the $\partial^{18}O$ values of CBL.

4.3.2 Sulphur

The secular curve of sulphur in marine sulphates, unlike that of carbon and oxygen in marine carbonates, is now accepted by most authors as reflecting global fluctuations in the isotopic composition of sea water through geologic time. The $\partial^{34}S$ of sea water for middle Late Carboniferous time ranges from approximately +13 to +18‰, with a mean of +14.5-15.0‰ (Claypool et al., 1980). NG and NBA $\partial^{34}S$ range from 14.9 to 16.2‰, indicating that these sulphates were derived from normal Late Carboniferous sea water. Even anhydrite nodules scattered within the paleosol of the mudstone/anhydrite facies (Appendix 4) have a seawater isotopic signature, indicating that interstitial fluids were introduced by marine storms, intrasediment seawater recharge, and/or during periods of high sea-level conditions. Similarly, Davies and Krouse (1975) reported $\partial^{34}S$ ratios ranging from +13.9 to +18.0‰ for evaporites of the Otto Fiord Formation, an Upper Carboniferous unit of marine origin at the centre of Sverdrup Basin. Continental water is commonly 6-7‰ lighter in $\partial^{34}S$ than contemporaneous sea water (cf. Rouse and Sherif, 1980), and is dependent on the isotopic composition of shales or evaporites being dissolved upstream or from a hot spring source (Holser and Kaplan, 1966; Stemmerik et al., 1988).

Although ratios fall within the isotopic range of sea water, there is a notable upward-depleting trend in NBA $\partial^{34}S$ ratios from the base to the top of the evaporite assemblage (Fig. 19). The lighter $\partial^{34}S$ ratios in the upper part of the assemblage may have resulted from the progressive depletion in ^{34}S of the sulphate reservoir as a result of sulphate precipitation. This possibility, however, is unlikely because the restricted basin was replenished several times throughout its history, as indicated by the interfingered fossiliferous limestones. The upward decrease in $\partial^{34}S$ ratios is most likely related to

bacterial-sulphate reduction in the depositional environment at the base of the evaporite assemblage, and its progressive decline upward. This process involves the biological fractionation of sulphur isotopes whereby ^{32}S is preferentially incorporated into sulphide phases, incidently increasing the $\partial^{34}S$ of dissolved sulphates (Holser and Kaplan, 1966; Longinelli, 1979). Bacterial-sulphate reduction is believed to be especially significant in restricted basins (Fritz et al., 1988). Since the isotopic trend parallels a depositional trend from nonmarine to increasingly marine conditions, bacterial-sulphate reduction near the base of the evaporite assemblage was probably closely related to pedogenic processes, as indicated by the ubiquitous reddish to brownish pseudogley paleosols. In addition, bacterial-sulphate reduction may have become progressively less important during evaporite deposition due to increasing sedimentation rates. The trend is therefore interpreted as representing isotopic relocation from bacterial-sulphate reduction during pedogenesis in the basal part of the evaporite assemblage (mudstone/anhydrite lithofacies), and increasingly better preservation of the true marine signature towards the top.

4.4 Conclusions

The isotopic signatures of carbonates and sulphates within the evaporite assemblage support the sedimentological evidence; together, they lead to the following conclusions:

1) The $\partial^{18}O$ and $\partial^{13}C$ ratios for NF and NFL samples, as well as the $\partial^{34}S$ ratios for NG and NBA samples, indicate that the carbonates and sulphates in both the mudstone/anhydrite and the anhydrite facies were precipitated from Late Carboniferous sea water.
2) The marine isotopic signature recorded by carbonates and sulphates from the paleosol-dominated mudstone/anhydrite facies indicates that these phases precipitated from sea water, either during periods of high sea-level conditions following marine storms, or by intrasediment seawater recharge. Freshwater

input in the form of rain, continental runoff, or intrasediment recharge may have been occasionally important. The mudstone/anhydrite facies does not appear to have been deposited in a fully continental playa, but in a coastal playa experiencing periodic marine influence.

3) The trends of upward-enriching $\partial^{13}C$ and upward-depleting $\partial^{34}S$ isotopic ratios support the sedimentological interpretations that the evaporite assemblage gradually evolved from a restricted coastal playa environment, characterized by pedogenic activity and possible brackish water conditions, to a more open marine environment with isotopic composition reflecting more closely that of Late Carboniferous sea water.

CHAPTER 5: TECTONO-SEDIMENTARY ANALYSIS

5.1 Introduction

The basal Canyon Fiord Formation is genetically related to an active period of continental rifting at the margin of Sverdrup Basin. Five distinct facies assemblages accumulated during this period on Raanes Peninsula:

1) A lower sandstone assemblage, deposited in the floodplain environment of high sinuosity streams, and locally in a paludal environment
2) A conglomerate assemblage, deposited in an alluvial fan to proximal braided stream environment
3) An upper sandstone assemblage, deposited in braided stream and coastal plain environments
4) An evaporite assemblage, deposited in a local coastal playa and hypersaline lagoon
5) A limestone assemblage, deposited in restricted to relatively open, shallow marine environments.

These assemblages are exposed within two outcrop belts, each associated with a distinct Upper Carboniferous subbasin. The Trold Fiord belt hosts a sedimentary succession that was deposited within a subbasin here called the Trold Fiord Depression, whereas the Blind Fiord belt hosts a sedimentary succession deposited within a subbasin here called the Blind Fiord Depression (Fig. 20). The presence of two subbasins is interpreted on the basis of: i) distinct sedimentary successions: the upper sandstone and evaporite assemblages are absent from the Blind Fiord belt; ii) different paleocurrent directions: measurements from the conglomerate assemblage show eastward paleoflows in the Trold Fiord Belt, and westward paleoflows in the Blind Fiord belt; iii) lack of

Figure 20: Late Carboniferous paleotectonic elements in the Trold Fiord/Blind Fiord area of Raanes Peninsula. Heavy lines represent suggested arrangement of master listric faults. Dashed lines represent approximate outline of each half-graben depression. Positioning of Blind Fiord Depression is after partial restoration along Trold Fiord Fault (as in Fig. 7).

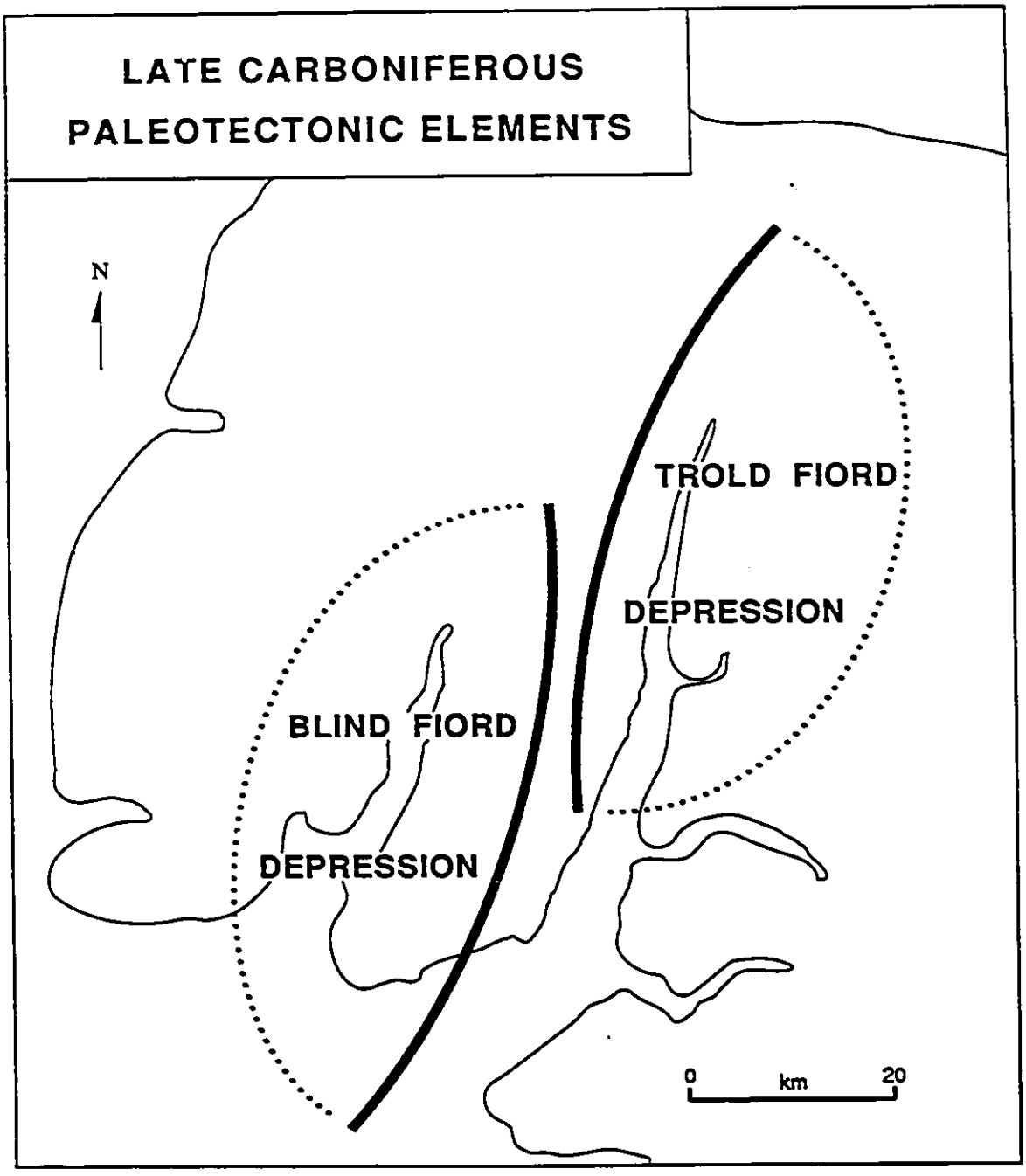
LATE CARBONIFEROUS
PALEOTECTONIC ELEMENTS
N
TROLD FIORD
DEPRESSION
BLIND FIORD
DEPRESSION
0
km
20

stratigraphic continuity in an east-west direction: after partial restoration along the Trold Fiord Fault, paleotopographic highs and sections with a thick clastic succession do not correlate well from one outcrop belt to the other (Figs. 7, 8, and 11); and iv) Tertiary faults separating the two outcrop belts: one or more of these faults are probably reactivated Carboniferous structures, especially those oriented roughly parallel or perpendicular to the inferred subbasin axes (NNE-SSW). Unfortunately, the geometrical arrangement of these faults is such that disposition of the two subbasins in relation to possible reactivated structures could not be established. The position of the Blind Fiord and Trold Fiord depressions and associated master listric faults shown in Figure 20 is therefore conceptual, and is not related to the actual location and orientation of Tertiary structures. As demonstrated in the final part of this chapter, the two subbasins were probably formed by lateral dip-slip extension, and represent asymmetric half-grabens of opposite polarity.

5.2 Paleogeographic History

The characteristics of each facies assemblage as well as their respective spatial distribution suggest that the paleogeographic history of the basal Canyon Fiord Formation, within both the Trold Fiord Depression and the Blind Fiord Depression, was controlled by two successive tectono-sedimentary episodes. The first tectono-sedimentary episode (TSE-1) affected mainly the depositional history of the lower sandstone and conglomerate assemblages. The second tectono-sedimentary (TSE-2) episode affected mainly the depositional history of the upper sandstone, the evaporite, and the limestone assemblages.

5.2.1 Tectono-sedimentary episode #1 (TSE-1)

The Canyon Fiord/Franklinian Mobile Belt unconformity marks the end of a long period of erosion following the Late Devonian Ellesmerian Orogeny, and the beginning of a long period of nearly continuous sedimentation in marginal areas of Sverdrup Basin. Such shifting from a highly erosional to a highly depositional regime will take place only if

significant base-level drop occurs, in the form of either tectonic subsidence or glacio-eustatic sea-level rise (Bull, 1977). In the present synrift context and since marine deposits are not predominant at the base of the Canyon Fiord Formation, the episode of base-level drop that initiated Canyon Fiord sedimentation on Raanes Peninsula is interpreted as being of tectonic origin. This episode is called TSE-1, and led to the deposition of first the lower sandstone assemblage, in a floodplain environment, and then the conglomerate assemblage, in an alluvial fan to proximal braided stream environment. The coarsening-upward megasequence displayed by these assemblages is probably a result of progressive increase in topographic relief and fault-controlled subsidence rates.

Early TSE-1 (late Bashkirian ?): The onset of TSE-1 resulted in the deposition of the lower sandstone assemblage (Figs. 21 and 27). Although exposures are restricted to the northern Trold Fiord belt, covered intervals present at the bases of several sections throughout both belts suggest that this assemblage was more widespread in the area (Appendix 1).

The lower sandstone assemblage accumulated predominantly in the floodplain environment during ephemeral flood discharge, and also locally in lakes and associated paludal environments. Sedimentation rates were relatively low, as indicated by ubiquitous caliche deposits, suggesting that base-level drop had not yet created a strong topographic gradient along local fault scarps. The rivers were probably flowing away from the margins of each subbasin toward its axial region, such that drainage was internal with no inter-basinal connections. Internal drainage is a common feature of isolated fault-bounded depressions in the Basin and Range Province of southwestern USA, which are also often characterized by basin marginal rivers and axial playa lakes (Leeder and Gawthorpe, 1987).

Because of the scarcity of primary sedimentary structures due to extensive caliche development, paleocurrent directions have not been measured for the lower sandstone assemblage. However, the confinement of exposures to two relatively narrow E-W

Figure 21: Conceptual paleogeographic map of the Blind Fiord/Trold Fiord area during Early TSE-1 (Late Bashkirian?). Brown= fluvial drainage area; Blue= lakes; Grey= inter-basinal highlands. Map is after partial restoration along Trold Fiord Fault (as in Fig. 7).

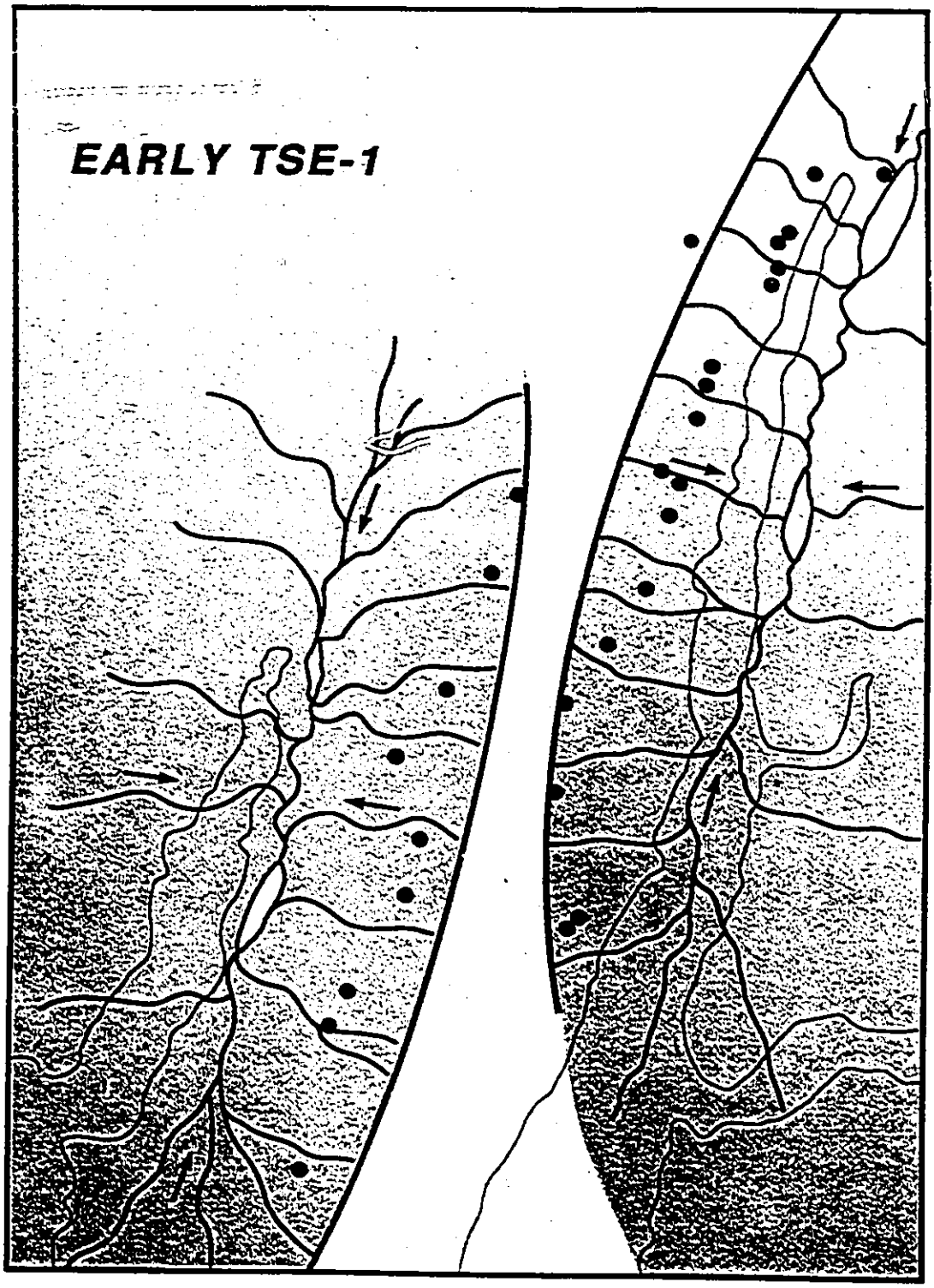
EARLY TSE-1

paleovalleys flanked by paleotopographic highs in the northern Trold Fiord belt (Fig. 8) suggests that the rivers had an east-west orientation in that area. An eastward-flowing direction is favoured, because paleocurrents of the overlying conglomerate assemblage in the northern Trold Fiord belt are in this direction: both assemblages were likely derived from the immediately adjacent footwall block to the west. The axial region of the Trold Fiord Depression would have therefore been east of the Trold Fiord belt, an interpretation further suggested by the presence of tufas of probable paludal origin at Section 10. The localized distribution of the lower sandstone assemblage also suggests that the two outcrop belts were in basin marginal areas, where subsidence was minor and sediments were bypassed to more axial areas.

Late TSE-1 (early Moscovian ?): Although the contact between the lower sandstone assemblage and the conglomerate assemblage is poorly exposed, the former generally coarsens-upward and grades into the latter (Appendix 1, Sections 11 and 16). This relationship suggests that both assemblages are genetically associated to TSE-1, and form a coarsening-upward megasequence. During Late TSE-1, the conglomerate assemblage gradually prograded above the lower sandstone assemblage as topographic relief was increased through progressive base-level drop (Figs. 22 and 27).

The conglomerate assemblage accumulated in the distal alluvial fan to proximal braided stream environment, with sedimentation occurring predominantly during episodic flood events. Pedogenic caliche development was greatly diminished during Late TSE-1 as a result of more rapid sedimentation. Eastward to southeastward paleoflow orientations were obtained throughout the Trold Fiord belt, indicating that highlands acting as a source of coarse sediments were present to the west and northwest of the Trold Fiord Depression (Fig. 13). An east-southeast flow direction is further supported by the apparent provenance of sediments in this belt. In the southern and central Trold Fiord belt, the conglomerate assemblage overlies limestones of the Cornwallis Group, whereas farther north, the

Figure 22: Conceptual paleogeographic map of the Blind Fiord/Trold Fiord area during Late TSE-1 (Early Moscovian?). Light brown= fluvial drainage area; Dark brown= alluvial fans; Grey= inter-basinal highlands. Map is after partial restoration along Trold Fiord Fault (as in Fig. 7).

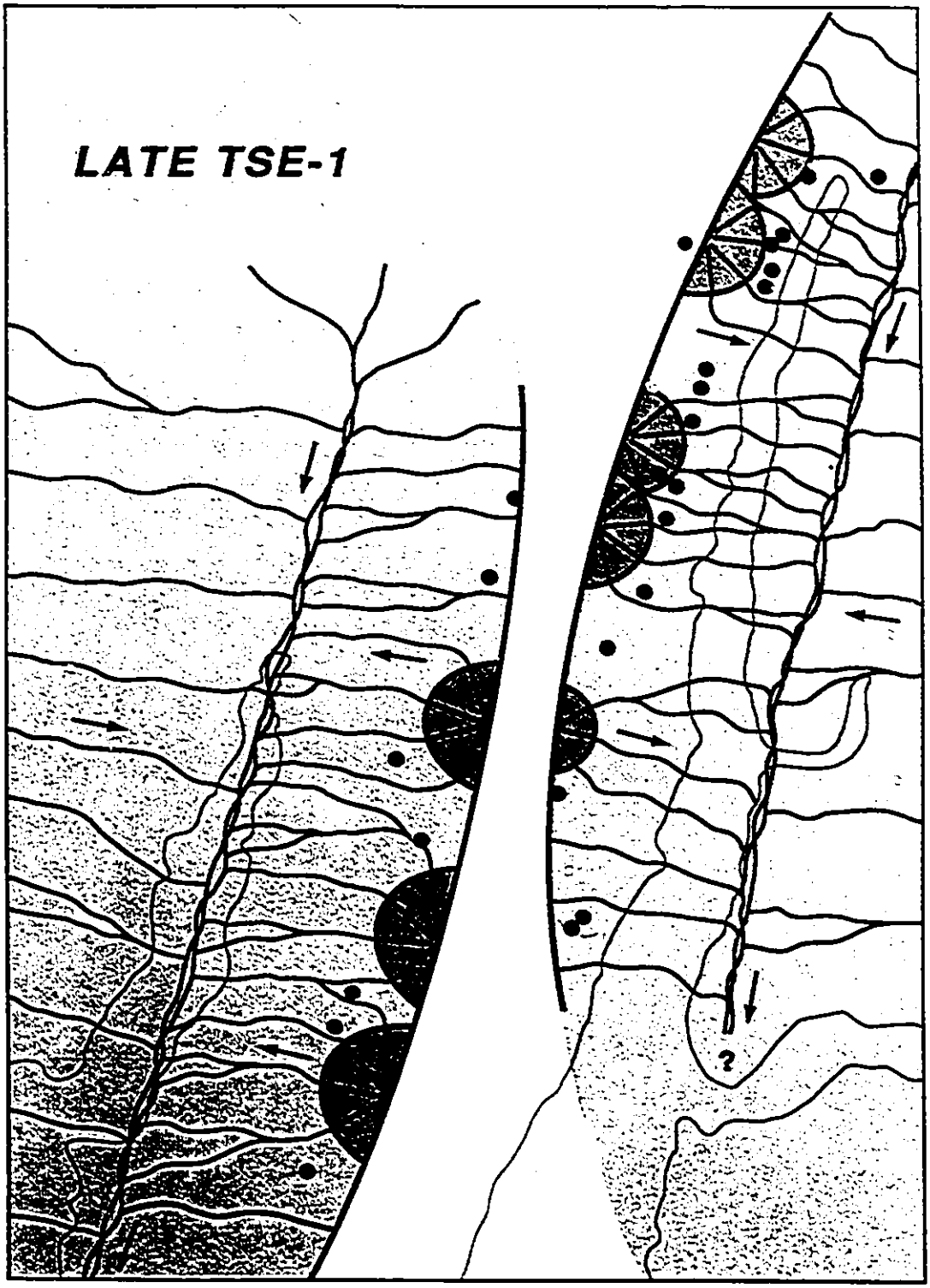
LATE TSE-1
?

uppermost strata of the Franklinian Mobile Belt consist of Cape Phillips shales and Danish River siltstones and sandstones (Appendix 1). Despite this lateral variation in basement composition, conglomerates throughout the Trold Fiord belt are predominantly composed of Cornwallis Group limestone clasts, suggesting the widespread N-S exposure of this source to the west during Late TSE-1. Direct evidence is provided in the northeastern part of the Trold Fiord belt, an area where the conglomerates directly overlie Danish River clastics, but also where the required source of Cornwallis Group limestone is exposed farther west as an inlier (Fig. 10, Section 14). This inlier is interpreted as a Carboniferous paleotopographic high, since it is directly overlain by upper Moscovian strata of the limestone assemblage (upper C5b conodont zone), and probably represents an exposed remnant of the north-south topographic highlands from which sediments of the conglomerate assemblage were shed eastward. In contrast to the paleocurrents measured in the Trold Fiord belt, those from the Blind Fiord belt display opposite westward orientations (Fig. 13). These contrasting paleocurrent directions are supporting evidence for the presence of two subbasins in the area, whereby the Trold Fiord conglomerates would have been derived from the east-facing fault scarp of the Trold Fiord Depression, and the Blind Fiord conglomerates from the west-facing fault scarp of the Blind Fiord Depression (Fig. 20).

The transverse alluvial fans and proximal braided streams probably flowed into axial braided stream systems in the axial area of each subbasin. Poor outcrop control in an E-W orientation is such, however, that the Late TSE-1 deposits of these two axial systems are still concealed in the subsurface. Both axial rivers were of subregional or regional importance, and flowed southward to southwestward into the Sverdrup sea as they were possibly controlled in part by the regional, southwestward depositional slope inferred by Beauchamp (1987).

5.2.2 Tectono-sedimentary episode #2 (TSE-2)

Deposition of the upper sandstone, the evaporite, and the limestone assemblages was controlled by a second episode of base-level drop in the area (TSE-2). Whereas TSE-1 involved chiefly local to regional tectonic subsidence, TSE-2 may have been a result of both tectonic subsidence and global sea-level rise. Ross and Ross (1988) have shown that a global marine transgression affected all shallow marine successions during the middle Carboniferous. This global transgression, interpreted on the basis of coastal onlaps and temperature trends from Ca/Mg ratios in stable cratonic sequences, could be of either tectono-eustatic or glacio-eustatic origin. The middle Moscovian (middle Late Carboniferous) age of the lowermost marine limestones of the Canyon Fiord Formation indicates that deposition was probably controlled at least in part by the worldwide transgressive event. It is unlikely that this global rise in sea level was in itself sufficient to modify the depositional history on Raanes Peninsula as sharply as that shown by stratigraphic relationships. Of relevance is the scarcity of conglomerate interbeds within the upper sandstone or limestone assemblages, as well as the absence of a fining-upward megasequence in the upper part of the conglomerate assemblage; these observations are inconsistent with the gradual facies transitions that usually accompany coastal sequences of global transgressive origin (i.e. Steel and Worsley, 1984). It is therefore suggested that deposition of the upper sandstone, the evaporite, and the limestone assemblages was mainly controlled by an episode of base-level drop related to tectonic rejuvenation along local extensional structures, and overprinting the global marine transgression.

Based on a number of recent and ancient examples of cyclic tectonic successions, Blair and Bilodeau (1988) postulated that fine-grained deposits should be considered as indicators of renewed tectonic activity in continental successions, instead of coarse-grained sediments. They argued that the rate of response to tectonic base-level drop is faster in low-gradient fluvial, lacustrine, or marine settings than it is in high-gradient fluvial environments such as alluvial fans. Fine-grained sediments are therefore expected to

accumulate at the base of tectonically-formed depressions immediately following base-level drop, whereas coarse sediments should gradually predominate the sequence only at a later stage (Blair, 1987; Blair and Bilodeau, 1988; Bowman, 1988). In view of the Blair and Bilodeau (1988) concept, the onset of TSE-2 led to the deposition of the upper sandstone assemblage, in a relatively low gradient fluvial environment, and to the deposition of the evaporite and limestone assemblages in marine environments, and not to renewed alluvial fan or proximal braided stream sedimentation of coarse-grained and transverse clastic facies. In fact, progradation of coarse clastics, expected at a later stage in TSE-2, was only minor in both subbasins. It is thought that these sediments were inhibited by the ongoing incursion of the sea within the subbasins, resulting in the backstepping of transverse fluvial facies while marine carbonate production was rapidly established. Because the underlying lower sandstone and conglomerate assemblages of TSE-1 were related likely to a common fluvial system, the concept of Blair and Bilodeau (1988) was not applicable, and this tectono-sedimentary episode was instead interpreted in terms of progressive increase in topographic relief and rates of tectonic subsidence.

Earliest TSE-2 (middle / late middle Moscovian): The second tectono-sedimentary episode to affect the marginal Sverdrup Basin deposits on Raanes Peninsula first resulted in the deposition of the limestone assemblage throughout the Blind Fiord belt, the upper sandstone assemblage in the northern Trold Fiord belt, and the limestone assemblage in the south-central Trold Fiord belt (Figs. 23 and 27). The absence of the upper sandstone assemblage from the Blind Fiord belt indicates that the axial fluvial system that probably existed in the Blind Fiord Depression during Late TSE-1 did not prograde laterally (to the east) onto the basin marginal alluvial fans and proximal braided streams with the onset of TSE-2. Instead, marine conditions were rapidly established throughout much of the Blind Fiord Depression, and the conglomerate assemblage was succeeded by the limestone assemblage (Fig. 11). Marine incursion also affected the southern part of the Trold Fiord

Figure 23: Conceptual paleogeographic map of the Blind Fiord/Trold Fiord area during Earliest TSE-2 (middle / late middle Moscovian). Light brown= fluvial drainage area; Dark brown= alluvial fans; Blue= Sverdrup sea; Grey= inter-basinal highlands. Less elevated accommodation zone between the two depressions is partially submerged. Map is after partial restoration along Trold Fiord Fault (as in Fig. 7).

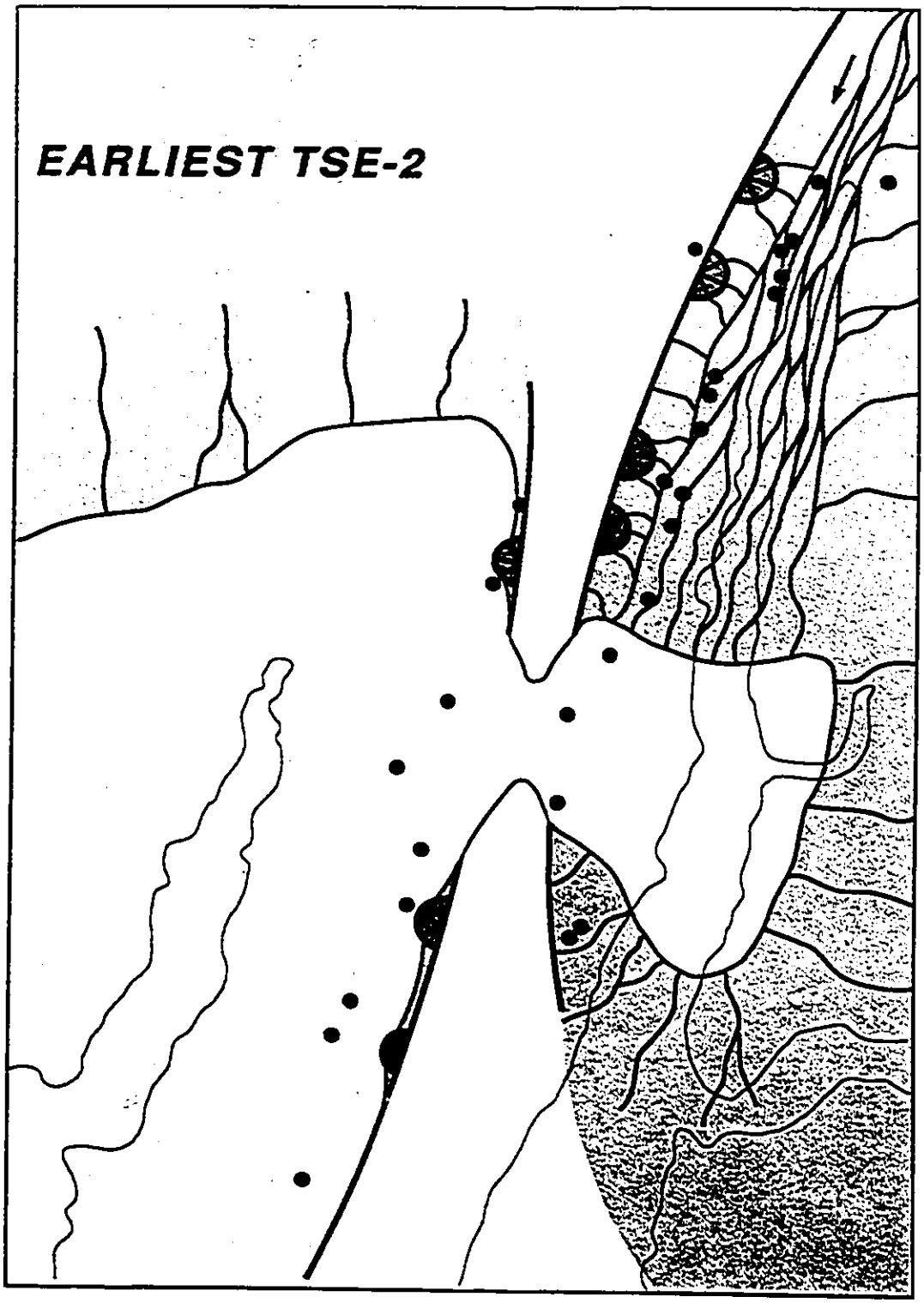
EARLIEST TSE-2

Depression during Earliest TSE-2, since the limestone assemblage overlies either the conglomerate assemblage or the Franklinian Mobile Belt basement in that area (Fig. 8).

The base of the limestone assemblage yielded conodonts of middle and late middle Moscovian age in both the Blind Fiord Depression (Appendix 3, Section 6) and the south-central Trold Fiord Depression (Appendix 3, Section 25). The southern part of the Trold Fiord Depression was not submerged during Earliest TSE-2, since conodonts recovered from a limestone bed within the evaporite assemblage at Section 28 are early late Moscovian in age (Appendix 3). This interpretation implies that the sea invaded the Trold Fiord Depression from the west by submerging the accommodation zone between the two subbasins, instead of directly from the south. Topographic relief at the accommodation zone was probably never significant, since the conglomerate assemblage reaches a maximum thickness of only 55m in that area (Appendix 1, Sections 1 to 5, and 23 to 26; Fig. 7). The basal limestone assemblage accumulated in restricted to relatively open, shallow marine environments (Fig. 16). Gravel deposition in fan-deltas or on beaches also occurred episodically, as evidenced by the presence of conglomerate units (Appendix 1).

In the northern part of the Trold Fiord Depression during Earliest TSE-2, the axial fluvial system responded rapidly to tectonic base-level drop, and sediments of the upper sandstone assemblage prograded westward above those of the conglomerate assemblage. This lateral progradation must have been relatively rapid, since only a few conglomerate beds are found above the basal strata of the upper sandstone assemblage. The upper sandstone assemblage accumulated in southward-flowing streams of mainly braided stream origin in the northern Trold Fiord belt (Appendix 1, Sections 11, 13, 16, and 18), and of mostly coastal plain origin in the southern part of this same belt (Sections 20 to 23). The braided stream to coastal plain transition indicates that the Late Carboniferous transgression first affected the topographically-lower southern part of the Trold Fiord Depression. The westward paleocurrent direction obtained from Section 10 (located in the northeastern part

of the Trold Fiord belt) possibly indicates sedimentation on the eastern flank of the Trold Fiord Depression (Fig. 14).

The upper sandstone assemblage is characterized by the absence of caliches, and by high textural and compositional maturity, indicating that the axial river system was perennial and fed by a relatively distant source. This source was most probably exposed in the vicinity of the Bay Fiord high, a subregional paleotopographic high in the Bay Fiord area and located 35km north of Trold Fiord. The Bay Fiord high controlled sedimentation patterns on Raanes Peninsula from the Late Carboniferous through the Early Triassic (Beauchamp, 1987; J.R. Devaney, pers. comm., 1989).

Early TSE-2 (middle / early late Moscovian): Marine incursion was rapid across the study area during the middle Moscovian, such that sediments of the upper sandstone assemblage in the northern to central Trold Fiord belt were rapidly succeeded by those of the limestone assemblage (Figs. 24 and 27). Conodonts recovered from the basal limestones in the northern Trold Fiord belt, like those of Earliest TSE-2 farther south, yielded a middle Moscovian age (Appendix 3, Sections 10 and 11). This age indicates that the transgression was rapid from south to north in the Trold Fiord Depression, and that both subbasins were rapidly submerged soon after the onset of TSE-2. Marine submergence also proceeded southward within the Trold Fiord Depression, resulting in the deposition of the evaporite assemblage exposed in the southernmost part of the Trold Fiord belt. The coastal playa to hypersaline lagoon environment of the evaporite assemblage indicates that barrier islands or bar spits prevented full connection of this area with the adjacent sea.

Late TSE-2 (latest Moscovian): With ongoing transgression, open marine conditions were gradually established within both subbasins, and succeeded the initial coastal environments (Figs. 25 and 27). Vertical facies transitions (Appendix 1, Section 13) in the Trold Fiord belt clearly demonstrate this deepening-upward trend, with encrusting-foraminiferal,

Figure 24: Conceptual paleogeographic map of the Blind Fiord/Trold Fiord area during Early TSE-2 (middle / early late Moscovian). Brown= fluvial drainage area; Blue= Sverdrup sea; Pink= coastal playa/hypersaline lagoon; Grey= inter-basinal highlands, and barrier bars or islands. Map is after partial restoration along Trold Fiord Fault (as in Fig. 7).

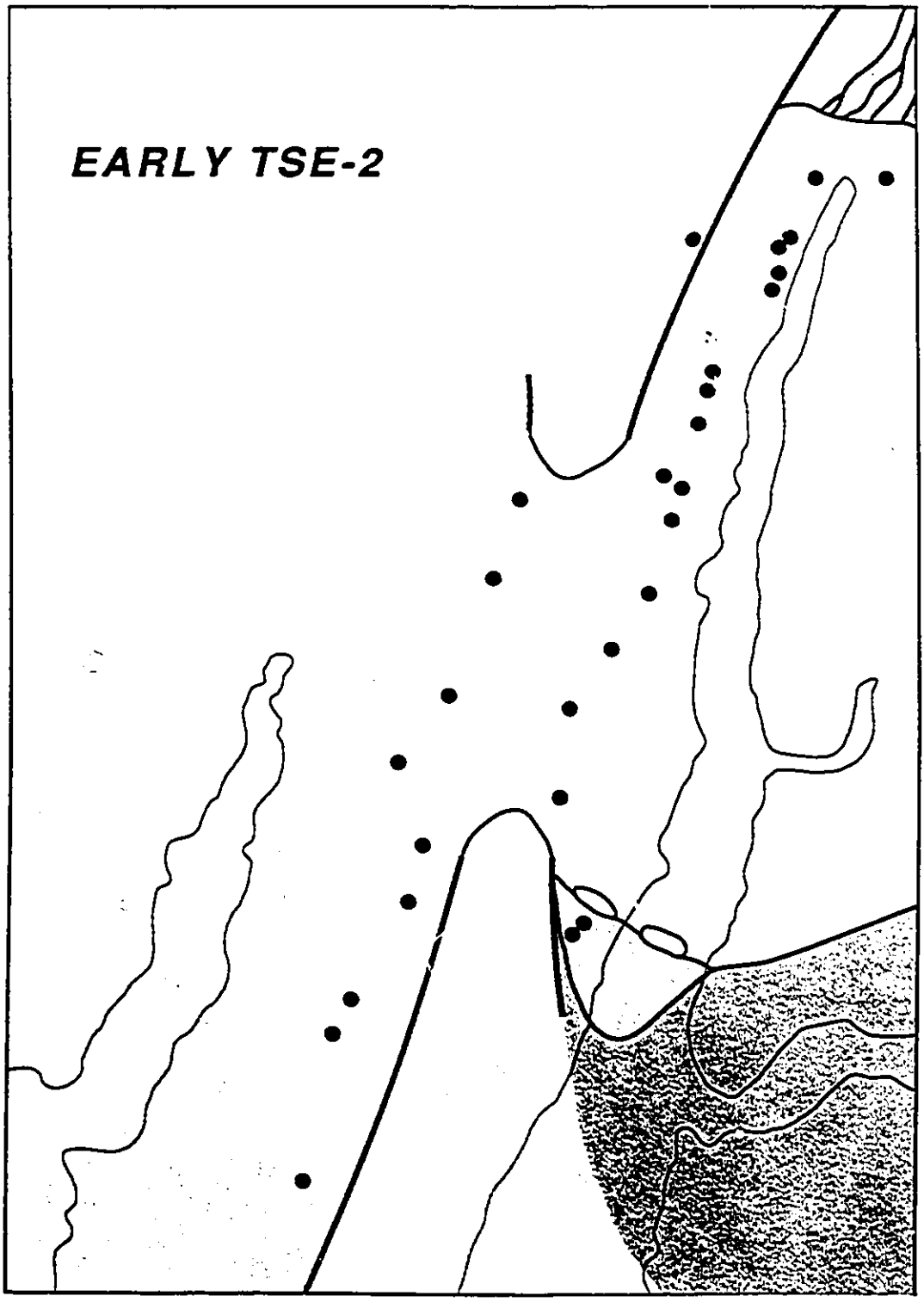
EARLY TSE-2

Figure 25: Conceptual paleogeographic map of the Blind Fiord/Trold Fiord area during Late TSE-2 (latest Moscovian). Brown= fluvial drainage area; Blue= Sverdrup sea; Grey= islands. Map is after partial restoration (as in Fig. 7).

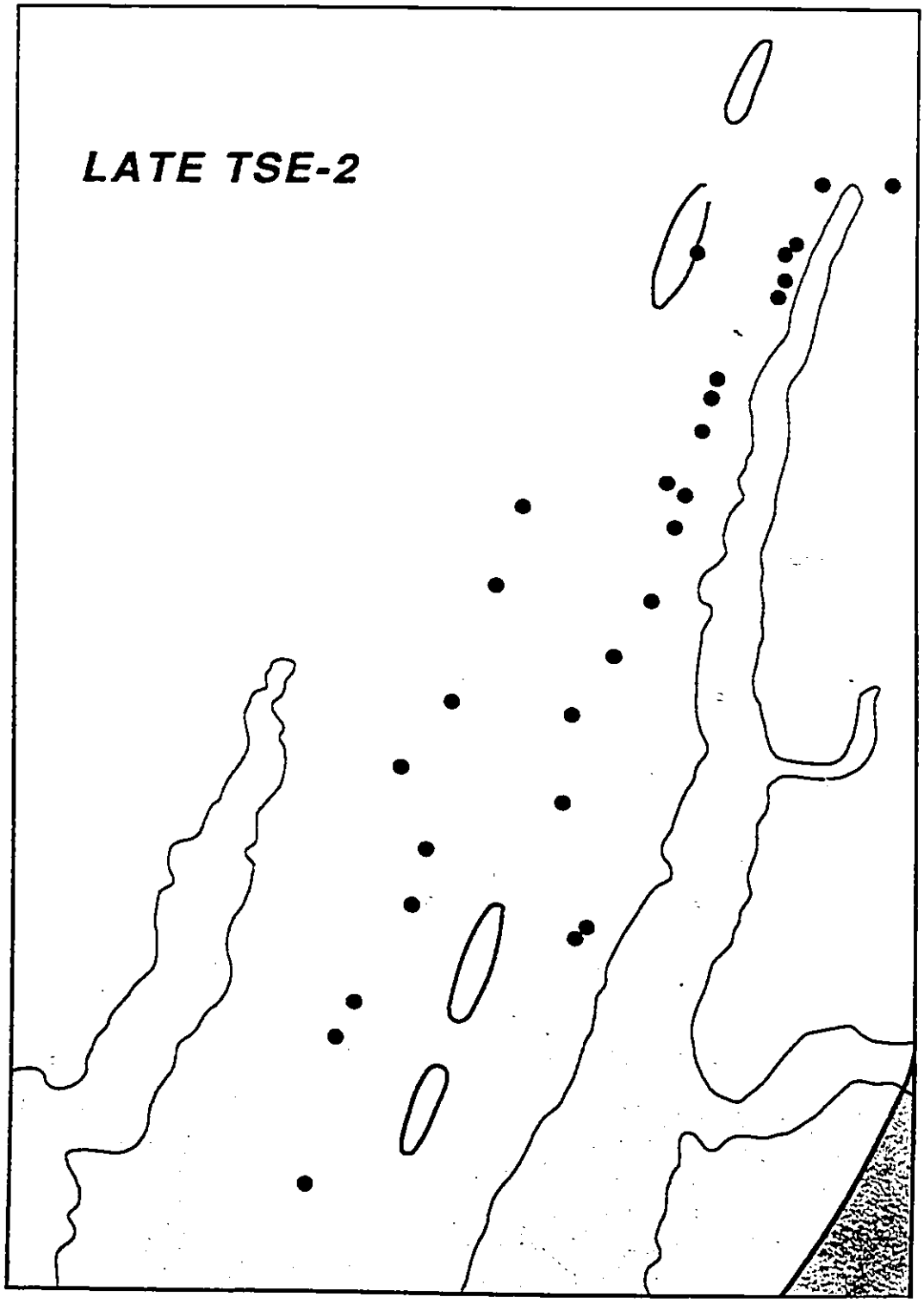
LATE TSE-2

beresellid, and fusulinacean/beresellid facies at the base being overlain by more open and deeper water fusulinacean, bryozoan, and spicular microfacies. The entire study area was then gradually submerged, with the remaining tectonic highlands terminating their continental history as a series of islands (Fig. 25). Section 14, in the northwestern part of the Trold Fiord belt, was submerged at this time during the latest Moscovian (Appendix 3), suggesting its position on the footwall block of the Trold Fiord Depression.

Sedimentation within the Trold Fiord and Blind Fiord depressions probably continued during much of the depositional history of the middle limestone member, and perhaps longer. This interpretation is based on the unusually thin nature of the TSE-1/TSE-2 succession, which is no more than 300m, in comparison to the thickness of extensional subbasin fills, which are commonly 2000-3000m (Anderson et al., 1983). The sedimentary succession of the Weatherall Depression of Melville Island, a typical half-graben subbasin at the southern margin of Sverdrup Basin, appears to be more than 2100m on the basis of seismic profiles (Harrison and Riediger, in press). Other tectono-sedimentary episodes (TSE-3, TSE-4, etc.) are therefore expected to have affected the sedimentary succession of the two subbasins.

5.2.3 Summary

The Trold Fiord and Blind Fiord depressions evolved from:

1) Continental subbasins with interior drainage during Early TSE-1 (late Bashkirian ?)
2) Continental subbasins with local fault-scarp and regional axial drainage during Late TSE-1 (early Moscovian ?)
3) Continental/marine subbasins with local fault-scarp and regional axial drainage in the central to northern Trold Fiord Depression, and nearshore shallow marine processes in the southern Trold Fiord Depression and

throughout the Blind Fiord Depression, during Earliest TSE-2 (middle / late middle Moscovian)

4) Marine subbasins with nearshore shallow marine processes, and local coastal playa to hypersaline lagoon processes in the southern Trold Fiord Depression, during Early TSE-2 (middle / early late Moscovian)
5) Marine subbasins with coastal to open marine processes during Late TSE-2 (latest Moscovian), and probably during TSE-3, TSE-4, etc. (latest Carboniferous to Early Permian ?).

5.3 Regional Implications

Results from this study, and from work by Harrison and Riediger (in press) and Thériault and Beauchamp (1991), indicate that the margin of Sverdrup Basin was segmented into a number of smaller subbasins during the Late Carboniferous. One of these subbasins, at the southern margin of Sverdrup Basin on northeastern Melville Island (Weatherall Depression; Fig. 1, Locality 10), shows field and seismic characteristics of an asymmetric, classical half-graben, with its master listric fault dipping cratonward (Harrison and Riediger, in press). Another subbasin, at the eastern margin of Sverdrup Basin on west-central Ellesmere Island (Hamilton-Fosheim subbasin) and situated immediately north of the present study area (Fig. 1, Localities 5 and 6), was identified on the basis of sediment dispersal patterns, distinct facies assemblages, and stratigraphic configuration (Thériault and Beauchamp, 1991). The sedimentary succession of this subbasin, however, is exposed only as a narrow north-south oriented belt, such that the overall basin geometry could not be assessed. Like the Hamilton-Fosheim subbasin, the Trold Fiord and Blind Fiord depressions of the present study are exposed essentially as narrow outcrop belts that limits the understanding of E-W facies relationships, and incidentally of the overall geometry of the sedimentary package. Facies distribution and paleocurrent directions

recovered in the northern Trold Fiord belt, however, provide local evidence for a possible half-graben geometry for the Trold Fiord Depression.

The marginal succession of the Trold Fiord Depression is represented by the conglomerate assemblage, deposited in proximal eastward-flowing rivers in the western part of the subbasin (Fig. 13), and possibly also by the upper sandstone assemblage in northeastern Trold Fiord belt (Section 10, Fig. 4), an area where sandstones accumulated from eastward-flowing rivers (Fig. 14). These facies distribution and dispersal patterns suggest lateral asymmetry within a half-graben, controlled by a footwall scarp to the west, and a hanging wall ramp face to the east (Fig. 26). Exposures on the inferred eastern margin of the Trold Fiord Depression are restricted to Section 10. Although the geometry of a subbasin should not be interpreted from the characteristics of marginal sediments alone, facies distribution and dispersal patterns of the Trold Fiord Depression compare well with those of the Weatherall Depression (Harrison and Riediger, in press), and suggest that both are asymmetric half-grabens. Because E-W facies relationships are lacking in the Blind Fiord belt, the geometry of the Blind Fiord Depression will remain equivocal until seismic studies resume in the area.

Modern rift zones such as the East African Rift system, not unlike the Late Carboniferous marginal areas of Sverdrup Basin, are typically subdivided into a number of small subbasins, most of which displaying a half-graben geometry (Baker, 1986; Rosendahl et al., 1986; Williams and Chapman, 1986; Colletta et al., 1988; Strecker et al., 1990). The acquisition of unequivocal seismic data over the last two decades has further demontrated the ubiquitous presence of these half-grabens in ancient rift settings (Bally et al., 1981; Anderson et al., 1983; Gibbs, 1987; Frostick et al., 1988), to the extent that this structure is now considered to be the dominant feature of all tectonic environments characterized by pure extension. Series of half-grabens have been found to alternate in polarity of asymmetry along strike (Rosendahl et al., 1986; Colletta et al., 1988; Dunkelman et al., 1988; Hamblin, 1989), with adjacent subbasins being separated by

Figure 26: Schematic E-W profile views showing Bashkirian? to Moscovian tectono-sedimentary evolution of the Trold Fiord Depression.

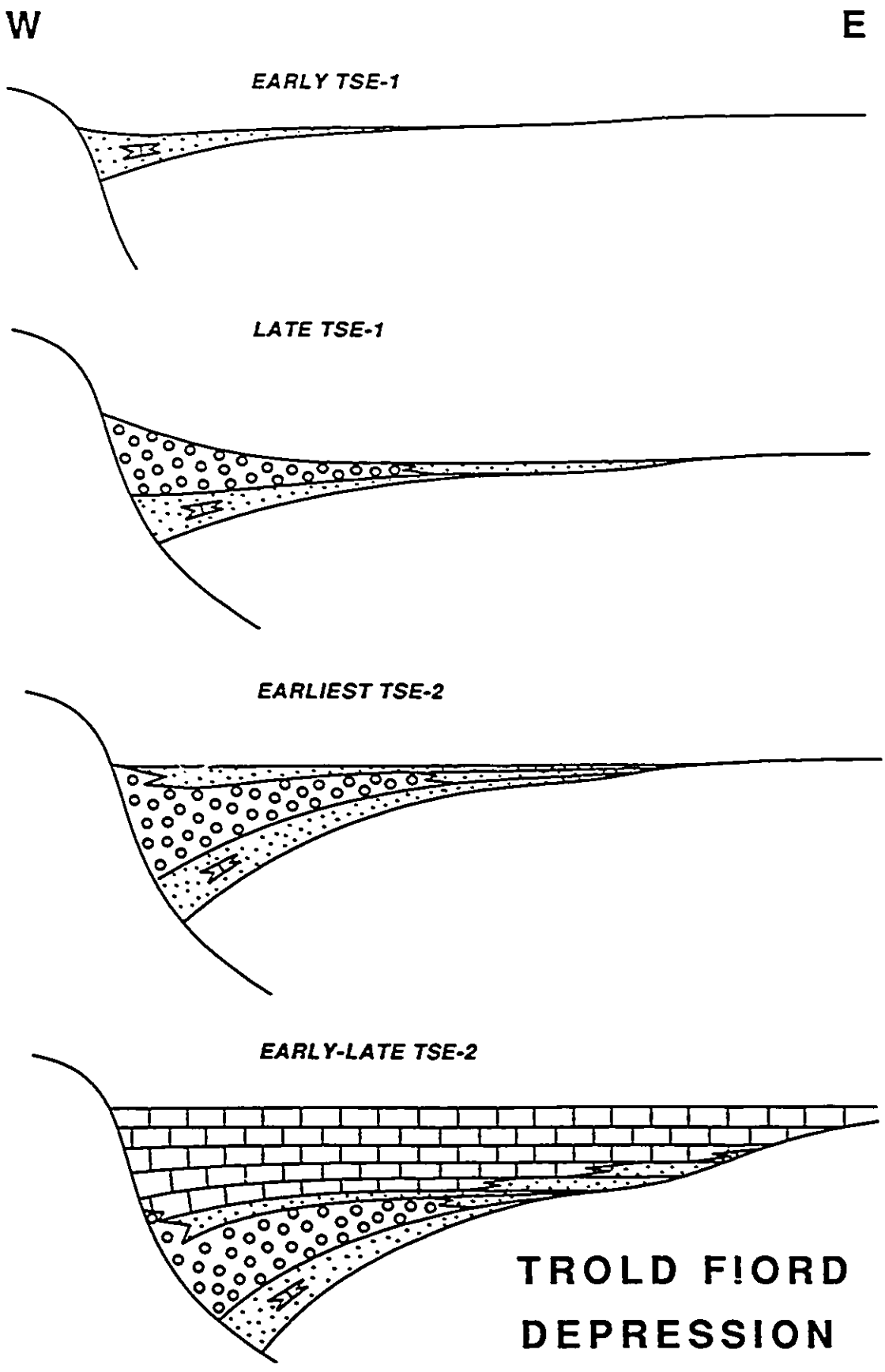
W
E
EARLY TSE-1
LATE TSE-1
EARLIEST TSE-2
EARLY-LATE TSE-2
TROLD FIORD
DEPRESSION

positive areas where transfer or accommodation faulting is common (Frostick and Reid, 1987). The area underlying Lake Tanganyika in the East African Rift, for example, is segmented into nine half-grabens that all alternate in polarity along strike (Fig. 27). On Raanes Peninsula, similar alternation in polarity is suggested by paleocurrents and facies distribution, with the Blind Fiord Depression in the southwest representing a "down-to-the-basin" (master fault dipping basinward) half-graben, and the Blind Fiord Depression in the northeast representing a "down-to-the-craton" (master fault dipping cratonward) half-graben (Fig. 20).

The characteristics of basin-marginal facies in the Trold Fiord Depression and apparent alternation in subbasin polarity suggest that Late Carboniferous sedimentation on Raanes Peninsula, and perhaps along much of the margin of Sverdrup Basin, occurred within asymmetric half-grabens. These half-grabens were first infilled with essentially continental sediments (lower sandstone, conglomerate, and upper sandstone assemblages of the Canyon Fiord Formation). During that time, marine sedimentation was already established in more axial areas of Sverdrup Basin (i.e. Nansen and Otto Fiord formations, Fig. 2). With ongoing fault-controlled subsidence, the sea gradually invaded marginal areas, and the half-grabens were infilled with predominantly marine sediments (evaporite and limestone assemblages of the Canyon Fiord Formation, and probably younger marginal strata). The unusually thin continental infill characterizing the Blind Fiord and Trold Fiord depressions is mainly related to the nearly pericratonic position of Sverdrup Basin and proximity of the paleo-Arctic ocean. Connections with the global ocean system were therefore formed shortly after the onset of rifting, causing marine submergence of axial, then marginal areas of Sverdrup Basin.

Figure 27: Map of main structural elements along Lake Tanganyika, East African Rift system. Note that fault segments alternate in polarity along strike (from Hamblin, 1989).

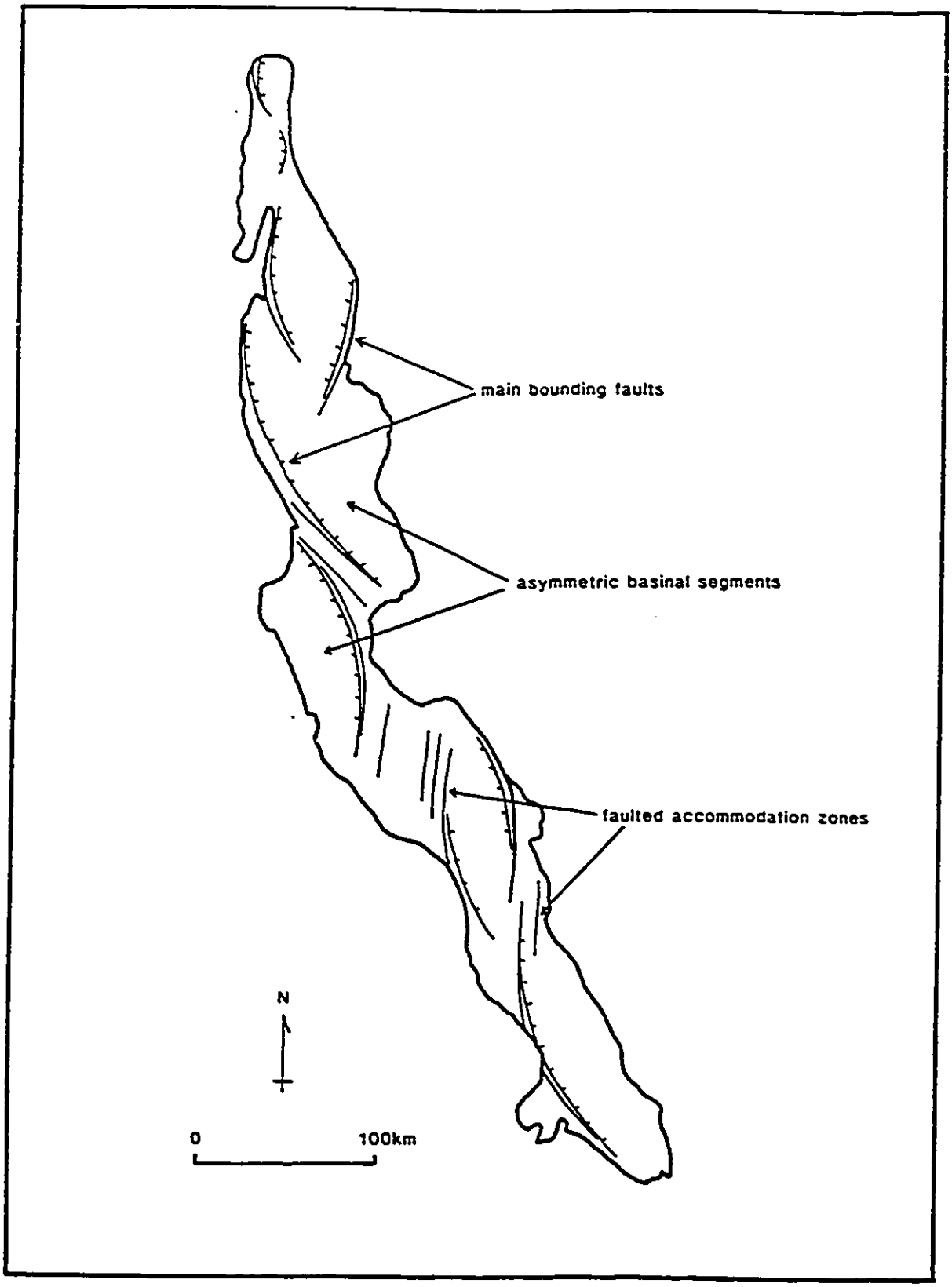
main bounding faults
asymmetric basinal segments
faulted accommodation zones
N
0
100km

5.4 Paleoclimate

Paleotectonic plate reconstructions for the late Paleozoic show that the northern tip of North America migrated northward from approximately 5-10^{0}N to more than 50^{0}N of the paleoequator during the Early Carboniferous to Late Permian time interval (Ziegler, 1988). This northward migration implies that the climate in Sverdrup Basin, which is polar and arid at the present time, gradually shifted from warm humid/sub-humid to warm arid/semi-arid to temperate/cool sub-humid and to possibly subpolar during the late Paleozoic. This climatic evolution is reflected by various features present in both the continental and marine successions of the basin. The Lower Carboniferous Emma Fiord Formation comprises coal-bearing strata and palynomorphs indicating that a warm subhumid climate existed at the time of deposition (Davies and Nassichuk, 1988). The continental succession of the Upper Carboniferous to Lower Permian Canyon Fiord Formation is deep reddish in colour and hosts abundant caliche paleosol profiles, reflecting a warm arid/semi-arid climate. This time interval is also represented by marine evaporites of the Otto Fiord, Canyon Fiord and Mount Bayley formations, also indicating relatively dry climatic conditions. The middle Permian Sabine Bay Formation contains yellowish to dark brownish gley paleosols and numerous coal layers hosted in white fluvial sandstones that reflect a subhumid climate. The Upper Permian succession is indicative of a cool, possibly subpolar climate, as the marine succession of the Trold Fiord Formation contains glauconitic sandstones and dropstone-bearing shales, and the uppermost Permian shelf succession of the Degerböls Formation consists almost exclusively of white spicular chert (Beauchamp et al., 1989b). In addition to the above features, a gradual drop in temperature is reflected by the change in the nature and diversity of biotic and abiotic limestone assemblages during the late Paleozoic history of Sverdrup Basin (Beauchamp, 1987).

The Upper Carboniferous (Bashkirian? to Moscovian) lower clastic member of the Canyon Fiord Formation displays several features that indicate deposition in a warm arid/semi-arid climate. These features are: i) caliche paleosols; ii) continental red beds; iii) coastal evaporites; and iv) beresellid-rich limestones. Indirect evidence is also given by the lack of coal deposits in the basal Canyon Fiord Formation, and their common occurrence in the older Emma Fiord Formation and younger Sabine Bay Formation.

Caliche paleosols display a wide spectrum of fabrics, including incipient nodular, nodular, massive, laminar, pisolitic, and brecciated varieties. The presence of numerous well-developed and mature caliche profiles within the lower sandstone assemblage, in particular, suggests that climatic conditions were not only suitable for their development but likely optimal. Such conditions are present in warm semi-arid areas like the southern United States, West Indies, Spain, Algeria, Syria, South Africa, Lebanon, and western Australia, where extensive occurrences of Quaternary caliches have been documented (Durand, 1963; Harrison, 1977; Watts, 1977; Hubert, 1978; Mann and Horwitz, 1979; Hay and Wiggins, 1980; Coniglio and Harrison, 1983; Jones, 1988). Warm semi-arid regions are characterized by annual precipitation in the 250-500mm range, as well as potential evaporation in excess of 1 000mm per year (Ettensohn et al., 1988). This net moisture deficit is critical, as caliches are precipitated during extended periods of evaporation. Arid conditions, with annual evaporation exceeding 3 000mm (Mann and Horwitz, 1979), are less favourable since seasonal rainfall is required to dissolve sufficient calcium carbonate in the host sediment for pedogenic translocation. Similarly, equatorial climates are not conducive to the formation of caliche, since abundant rainfall and minimal evaporation promotes the continuous leaching of calcium carbonate.

The deep reddish coloration of the Canyon Fiord fluvial sandstones and conglomerates indicates that deposition proceeded under oxidizing conditions. Although such continental red beds commonly are associated with other features indicative of relatively dry climatic conditions, they are also known to form in humid tropical climates

(Turner, 1980). In the present case, the occurrence of red beds is supportive of an arid/semi-arid climate, since caliches and evaporites are also present in the succession.

The evaporite assemblage of the Canyon Fiord Formation was necessarily formed under climatic conditions in which evaporation exceeded precipitation. Interestingly, the distribution of modern evaporite deposits is restricted to between 10^0 and 40^0 north and south of the equator (Kendall, 1984), corresponding roughly to the zone occupied by the tropical arid and semi-arid climatic belts where net evaporation occurs (Bartholomew, 1958). Ancient deposits, however, are shown to have formed in areas closer to the paleo-poles during periods of low sea level, such as in late Paleozoic time when the global continental mass was overall emergent. The temporal association of the evaporite assemblage with caliche deposits nevertheless suggests that sedimentation proceeded under semi-arid climatic conditions.

The predominance of the beresellid-fusulinacean facies within the limestone assemblage also points to a relatively dry climate. Beauchamp (1987) postulated that the restricted beresellid-rich facies of Upper Carboniferous limestones was likely equivalent to the modern "chloralgal" association, which is found essentially in warm hypersaline sea water. If this is the case, the ubiquitous presence of beresellid algae and common lack of faunal diversity within the basal limestone assemblage would also be indicative of warm and dry conditions during Late Carboniferous time.

CONCLUSIONS

The basal Canyon Fiord Formation was deposited in a series of subbasins at the margin of Sverdrup Basin, where rift-related subsidence occurred in the Late Carboniferous. Five syntectonic facies assemblages are present on Raanes Peninsula:

1) A lower sandstone assemblage, deposited in the floodplain environment of high sinuosity streams, and locally in a paludal environment
2) A conglomerate assemblage, deposited in an alluvial fan to proximal braided stream environment
3) An upper sandstone assemblage, deposited in braided stream and coastal plain environments
4) An evaporite assemblage, deposited in a local coastal playa and hypersaline lagoon
5) A limestone assemblage, deposited in restricted to relatively open, shallow marine environments.

These facies assemblages accumulated within two half-graben subbasins of opposite polarity: i) the Trold Fiord Depression, on northeastern Raanes Peninsula; and ii) the Blind Fiord Depression, on southwestern Raanes Peninsula. Basin-fill characteristics indicate that continental sedimentation was rapidly succeeded by marine sedimentation, and that two tectono-sedimentary episodes took place. In response to these tectono-sedimentary episodes, the paleogeography within the Trold Fiord and Blind Fiord depressions evolved as follows:

1) Continental half-grabens with interior drainage during Early TSE-1 (late Bashkirian ?)
2) Continental half-grabens with local fault-scarp and regional axial drainage during Late TSE-1 (early Moscovian ?)

3) Continental/marine half-grabens with local fault-scarp and regional axial drainage in the central to northern Trold Fiord Depression, and nearshore shallow marine processes in the southern Trold Fiord Depression and throughout the Blind Fiord Depression, during Earliest TSE-2 (middle / late middle Moscovian)
4) Marine half-grabens with nearshore shallow marine processes, and local coastal playa to hypersaline lagoon processes in the southern Trold Fiord Depression, during Early TSE-2 (middle / early late Moscovian)
5) Marine half-grabens with coastal to open marine processes during Late TSE-2 (latest Moscovian), and probably during TSE-3, TSE-4, etc. (latest Carboniferous to EarlyPermian ?).

REFERENCES

Allen, J.R.L.
1984: Sedimentary Structures: their character and physical basis; Developments in Sedimentology, vol. 30, Elsevier, New York.

1986: Pedogenic calcretes in the Old Red Sandstone facies (Late Silurian-Early Carboniferous) of the Anglo-Welsh area, southern Britain; *in* Wright, V.P. (ed.); Paleosols: their recognition and interpretation; Princeton University Press, New Jersey, p. 58-86.

Anderson, R.E., Zoback, M.L., and Thompson, G.A.
1983: Implications of selected subsurface data on the structural form and evolution of some basins in the northern Basin and Range province, Nevada and Utah; Geological Society of America Bulletin, vol. 94, p. 1055-1072.

Anderson, T.F. and Arthur, M.A.
1983: Stable isotopes of oxygen and carbon and their application to sedimentologic and paleoenvironmental problems; *in* Stable Isotopes in Sedimentary Geology, Society of Economic Paleontologists and Mineralogists, Short Course No. 10, Dallas, 1983, p. 1-1 to 1-151.

Aydin, A. and Nur, A.
1982: Evolution of pull-apart basins and their scale independence; Tectonics, vol. 1, p. 91-105.

Baker, B.H.
1986: Tectonism and volcanism of the southern Kenya Rift Valley and its influence on rift sedimentation; *in* Frostick, L.E., Renaut, R.W., Reid, I., and Tiercelin, J.J. (eds.); Sedimentation in the African Rifts, Geological Society of America Special Publication No. 25, p. 45-57.

Bally, A.W., Bernoulli, D., Davies, G.A., and Montadert, L.
1981: Listric normal faults; Oceanologica Acta, Proceedings of the 26th International Geological Congress, Geology of continental margins symposium, Paris, 1980, p. 87-101.

Bartholomew, J.
1958: The Times Atlas of the World - Mid-Century Edition, vol. 1, The Times Publishing Company Ltd., London, Plate 3.

Bates, R.L. and Jackson, J.A.
1987: Glossary of Geology, Third Edition; American Geological Institute, Virginia.

Beauchamp, B.
1987: Stratigraphy and facies analysis of the Upper Carboniferous to Lower Permian Canyon Fiord, Belcher Channel and Nansen formations, southwestern Ellesmere Island; Ph.D. thesis, University of Calgary, June 1987, 370 p.

Beauchamp, B., Harrison, J.C., and Henderson, C.M.
1989a: Upper Paleozoic stratigraphy and basin analysis of the Sverdrup Basin, Canadian Arctic Archipelago: Part 1, time frame and tectonic evolution; *in* Current Research, Part G, Geological Survey of Canada, Paper 89-1G, p. 105-113.

1989b: Upper Paleozoic stratigraphy and basin analysis of the Sverdrup Basin, Canadian Arctic Archipelago: Part 2, transgressive-regressive sequences; *in* Current Research, Part G, Geological Survey of Canada, Paper 89-1G, p. 115-124.

Beauchamp, B., Oldershaw, A.E., and Krouse, H.R.
1987: Upper Carboniferous to Upper Permian ^{13}C-enriched primary carbonates in the Sverdrup Basin, Canadian Arctic: comparisons to coeval western North American ocean margins; Chemical Geology, vol. 65, p. 391-413.

Blair, T.C.
1987: Tectonic and hydrologic controls on cyclic alluvial fan, fluvial, and lacustrine rift-basin sedimentation, Jurassic-lowermost Cretaceous Todos Santos Formation, Chiapas, Mexico; Journal of Sedimentary Petrology, vol. 57, p. 845-862.

Blair, T.C. and Bilodeau, W.L.
1988: Development of tectonic cyclothems in rift, pull-apart, and foreland basins: sedimentary response to episodic tectonism; Geology, vol. 16, p. 517-520.

Blissenbach, E.
1954: Geology of alluvial fans in semiarid regions; Geological Society of America Bulletin, vol. 65, p. 175-190.

Bowman, D.
1988: The declining but non-rejuvenating base level - the Lisan Lake, the Dead Sea area, Israel; Earth Surface Processes and Landforms, vol. 13, p. 239-249.

Bown, T.M. and Kraus, M.J.
1987: Integration of channel and floodplain suites, I. Developmental sequence and lateral relations of alluvial paleosols; Journal of Sedimentary Petrology, vol. 57, p. 587-601.

Bull, W.B.
1977: The alluvial-fan environment; Progress in Physical Geography, vol. 1, p. 222-270.

Cabrera, L., Roca, E., and Santanach, P.
1988: Basin formation at the end of a strike-slip fault: the Cerdanya Basin (eastern Pyrenees); Journal of the Geological Society, London, vol. 145, p. 261-268.

Cameron, B.I.
1989: Petrochemistry and origin of altered Permian basalts in the Sverdrup Basin, Arctic Canada. M.Sc. thesis, Dalhousie University, September 1989, 392 p.

Cant, D.J.
1982: Fluvial facies models and their application; *in* Scholle, P.A. and Spearing, D. (eds.); Sandstone Depositional Environments, The American Association of Petroleum Geologists, Memoir 31, p. 115-137.

Christie-Blick, N. and Biddle, K.T.
1985: Deformation and basin formation along strike-slip faults; in Biddle, K.T. and Christie-Blick, N. (eds.); Strike-Slip Deformation, Basin Formation, and Sedimentation, Society of Economic Paleontologists and Mineralogists, Special Publication No. 37, p. 1-34.

Claypool, G.E., Holser, W.T., Kaplan, I.R., Sakai, H., and Zak, I.
1980: The age curves of sulfur and oxygen isotopes in marine sulfate and their mutual interpretation; Chemical Geology, vol. 28, p. 199-260.

Colletta, B., Le Quellec, P., Letouzey, J., and Moretti, I.
1988: Longitudinal evolution of the Suez rift structure (Egypt); Tectonophysics, vol. 153, p. 221-233.

Coniglio, M. and Harrison, R.S.
1983: Holocene and Pleistocene caliche from Big Pine Key, Florida; Bulletin of Canadian Petroleum Geology, vol. 31, p. 3-13.

Craig, H.
1953: The geochemistry of the stable isotopes of carbon. Geochimica et Cosmochimica Acta, vol. 3, p. 53-92.

Davies, G.R. and Krouse, H.R.
1975: Sulphur isotope distribution in Paleozoic sulphate evaporites, Canadian Arctic Archipelago; Geological Survey of Canada, Paper 75-1, Part B, p. 221-225.

Davies, G.R. and Nassichuk, W.W.
1988: An Early Carboniferous (Viséan) lacustrine oil shale in Canadian Arctic Archipelago; The American Association of Petroleum Geologists Bulletin, vol. 72, p. 8-20.

Davies, G.R. and Nassichuk, W.W.
1990: Carboniferous to Permian geology of the Sverdrup Basin, Canadian Arctic Archipelago. Volume of Decade of North American Geology.

Dawes, P.R. and Christie, R.L.
1982: History of exploration and geology in the Nares Strait region; *in* Dawes, P.R. and Kerr, J.W. (eds.); Nares Strait and the drift of Greenland: a conflict in plate tectonics, Meddelelser Om Grønland, Geoscience No. 8, p. 19-36.

Devaney, J.R. and Fyles, J.G.
1988: Sedimentology and stratigraphy of the Beaufort Formation, Prince Patrick Island, N.W.T. (abstract); Geological Association of Canada/Mineralogical Association of Canada/Canadian Society of Petroleum Geologists, Joint Annual Meeting, St. John's 1988, Program with Abstracts, p. A31.

Dunkelman, T.J., Karson, J.A., and Rosendahl, B.R.
1988: Structural style of the Turkana Rift, Kenya; Geology, vol. 16, p. 258-261.

Durand, J.-H.
1963: Les croûtes calcaires et gypseuses en Algérie: formation et âge; Bulletin de la Société Géologique de France, vol. 7, p. 959-968.

Elmore, R.D.
1984: The Copper Harbour Conglomerate: a late Precambrian fining-upward alluvial fan sequence in northern Michigan; Geological Society of America Bulletin, vol. 95, p. 610-617.

Embry, A.F.
1988: Triassic sea-level changes: evidence from the Canadian Arctic Archipelago; *in* Sea-Level Changes - An Integrated Approach, Society of Economic Paleontologists and Mineralogists, Special Publication No. 42.

Embry, A.F. and Podruski, J.A.
1988: Third-order depositional sequences of the Mesozoic succession of Sverdrup Basin; *in* James, D.P. and Leckie, D.A. (eds.); Sequences, Stratigraphy, Sedimentology: Surface and Subsurface, Canadian Society of Petroleum Geologists, Memoir 15, p. 73-84.

Esteban, M. and Klappa, C.F.
1983: Subaerial exposure environment; *in* Scholle, P. A., Bebout, D.G., and Moore, C.H. (eds.); Carbonate Depositional Environments, The American Association of Petroleum Geologists, Memoir 33, p. 1-95.

Ettensohn, F.R., Dever Jr., G.R., and Grow, J.S.
1988: A paleosol interpretation for profiles exhibiting subaerial exposure "crusts" from the Mississippian of the Appalachian Basin; *in* Reinhardt, J. and Sigleo, W.R. (eds.); Paleosols and Weathering Through Geologic Time: Principles and Applications, Geological Society of America, Special Paper No. 216, p. 49-79.

Fitton, J.G.
1983: Active versus passive continental rifting: evidence from the West African rift system; Tectonophysics, vol. 94, p. 473-481.

Fortier, Y.O. et al.
1963: Geology of the north-central part of the Arctic Archipelago, Northwest Territories (Operation Franklin); Geological Survey of Canada, Memoir 320.

Frisch, T.
1983: Reconnaissance geology of the Precambrian shield of Ellesmere Island, Devon and Coburg islands, Arctic Archipelago: a preliminary account; Geological Survey of Canada, Paper 82-10, 11 p.

Fritz, P., Lapcevic, P.A., Miles, M., Krape, S.K., Lawson, D.E., and O'Shea, K.J.
1988: Stable isotopes in sulphate minerals from the Salina formation in southwestern Ontario; Canadian Journal of Earth Sciences, vol. 25, p. 195-205.

Frostick, L.E. and Reid, I.
1987: Tectonic control of desert sediments in rift basins ancient and modern; in Frostick, L.E. and Reid, I. (eds.); Desert Sediments: Ancient and Modern, Geological Society of America, Special Publication No. 35, p. 53-68.

Frostick, L., Reid, I., Jarvis, J., and Eardley, H.
1988: Triassic sediments of the Inner Moray Firth, Scotland: early rift deposits; Journal of the Geological Society, London, vol. 145, p. 235-248.

Fyles, J.G.
1990: Beaufort Formation (Late Tertiary) as seen from Prince Patrick Island, Arctic Canada. Arctic, vol. 43, p. 393-403.

Galimov, E.M., Migdisov, A.A., and Ronov, A.B.
1975: Variation in the isotopic composition of carbonate and organic carbon in sedimentary rocks during Earth's history; Geochemistry International, vol. 12, p. 1-19.

Gibbs, A.
1987: Development of extension and mixed-mode sedimentary basins; *in* Coward, M.P., Dewey, J.F., and Hancock, P.L. (eds.); Continental Extensional Tectonics, Geological Society of America, Special Publication No. 28, p. 19-33.

Gloppen, T.G. and Steel, R.J.
1981: The deposits, internal structure and geometry in six alluvial fan - fan delta bodies (Devonian-Norway): a study in the significance of bedding sequence in conglomerates; *in* Ethridge, F.G. and Flores, R.M. (eds.); Recent and Ancient Nonmarine Depositional Environments, Models for Exploration, Society of Economic Paleontologists and Mineralogists, Special Publication No. 31, p. 49-69.

Grove, A.T.
1986: Geomorphology of the African Rift System; *in* Frostick, L.E. (ed.); Sedimentation in the African Rifts, Geological Society of America Special Publication No. 25, p. 9-16.

Hamblin, A.P.
1989: Sedimentology, tectonic control and resource potential of the Upper Devonian - Lower Carboniferous Horton Group, Cape Breton Island, Nova Scotia; Ph.D. thesis, University of Ottawa, 300 p.

Harker, P. and Thorsteinsson, R.
1960: Permian rocks and faunas of Grinnell Peninsula, Arctic Archipelago; Geological Survey of Canada, Bulletin 309, 89 p.

Harms, J.C., Southard, J.B., and Walker, R.G.
1982: Structures and Sequences in Clastic Rocks; Society of Economic Paleontologists and Mineralogists, Short Course No. 9, Calgary, 1982.

Harrison, J.C. and Riediger, C.L.
in press: The Upper Carboniferous and Lower Permian Canyon Fiord Formation, Melville Island; *in* Geological Reports, Melville Island, R.L. Christie (ed.); Geological Survey of Canada, Paper.

Harrison, J.C., Riediger, C.L., and Brent, T.
1988: Late Paleozoic extension and associated sedimentation at the southern margin of the Sverdrup Basin (abstract); Geological Association of Canada/Mineralogical Association of Canada, Joint Annual Meeting, St. John's, 1988, Program with Abstracts, vol. 13, p. A53.

Harrison, R.S.
1977: Caliche profiles; indication of near-surface subaerial diagenesis, Barbados, West Indies; Bulletin of Canadian Petroleum Geology, vol. 25, p. 123-173.

Hay, R.L. and Wiggins, B.
1980: Pellets, ooids, sepiolite and silica in three calcretes of the southwestern United States; Sedimentology, vol. 27, p. 559-576.

Henderson, C.M.
1988: Conodont paleontology and biostratigraphy of the Upper Carboniferous to Lower Permian Canyon Fiord, Belcher Channel, Nansen, an unnamed, and van Hauen formations, Canadian Arctic Archipelago; Unpublished Ph.D. Thesis, University of Calgary, Calgary, Alberta, 287 pp.

Heward, A.P.
1978: Alluvial fan and lacustrine sediments from the Stephanian A and B (La Magdalena, Cinera-Matallana and Sabero) coalfields, northern Spain; Sedimentology, vol. 25, p. 451-488.

Hoefs, J.
1987: Stable Isotope Geochemistry; Springer-Verlag, New York, 241 p.

Holser, W.T. and Kaplan, I.R.
1966: Isotope geochemistry of sedimentary sulfates; Chemical Geology, vol. 1, p. 93-135.

Hooke, R.B.
1967: Processes on arid-region alluvial fans; Journal of Geology, vol. 75, p. 438-460.

Hubert, J.F.
1978: Paleosol caliche in the New Haven Arkose, Newark Group, Connecticut; Palaeogeography, Palaeoclimatology, Palaeoecology, vol. 24, p. 151-168.

Hudson, J.D.
1977: Stable isotopes and limestone lithification; Journal of the Geological Society of London, vol. 133, p. 637-660.

James, N.P. and Schenk, P.E.
1983: Field Guide to Pleistocene and Modern Carbonates of Bermuda; Bermuda Biological Station for Research, Special Publication No. 25.

Jones, B.
1988: The influence of plants and micro-organisms on diagenesis in caliche: example from the Pleistocene Ironshore Formation on Cayman Brac, British West Indies; Bulletin of Canadian Petroleum Geology, vol. 36, p. 191-201.

Jowett, E.C. and Jarvis, G.T.
1984: Formation of foreland rifts; Sedimentary Geology, vol. 40, p. 51-72.

Kendall, A.C.
1984: Evaporites; *in* Walker, R.G. (ed.); Facies Models, Second Edition, Geoscience Canada, Reprint Series No. 1, p. 259-296.

Kerr, J.W.
1981: Evolution of the Canadian Arctic islands: a transition between the Atlantic and Arctic oceans; *in* Nairn, A.E.M., Churkin, M. Jr., and Stehli, F.G. (eds.); The Ocean Basins and Margins, Volume 5: The Arctic Ocean, Plenum Press, New York, 199 p.

1982: History and implications of the Nares Strait conflict; *in* Dawes, P.R. and Kerr, J.W. (eds.); Nares Strait and the drift of Greenland: a conflict in plate tectonics, Meddelelser Om Grønland, Geoscience No. 8, p. 37-49.

Klappa, C.F.
1978: Biolithogenesis of *Microcodium*: elucidation; Sedimentology, vol. 25, p. 489-522.

Kraus, M.J. and Bown, T.M.
1986: Paleosols and time resolution in alluvial stratigraphy; *in* Wright, V.P. (ed.); Paleosols: their recognition and interpretation; Princeton University Press, New Jersey, p. 180-207.

Lattman, L.H.
1973: Calcium carbonate cementation of alluvial fans in southern Nevada; Geological Society of America Bulletin, vol. 84, p. 3013-3028.

Lauritzen, Ø.
1981: Investigation of Carboniferous and Permian sediments in Svalbard; Norsk Polarinst. Skr., vol. 176, 44 p.

Leeder, M.R.
1975: Pedogenic carbonates and flood sediment accretion rates: a quantitative model for alluvial arid-zone lithofacies; Geological Magazine, vol. 112, p. 257-270.

Leeder, M.R. and Gawthorpe, R.L.
1987: Sedimentary models for extensional tilt-block/half-graben basins; *in* Coward, M.P., Dewey, J.F., and Hancock, P.L. (ed.); Continental Extensional Tectonics, Geological Society of America Special Publication No. 28, p. 139-152.

Longinelli, A.
1979: Isotope geochemistry of some Messinian evaporites: paleoenvironmental implications; Palaeogeography, Palaeoclimatology, Palaeoecology, vol. 29, p. 95-123.

Mann, A.W. and Horwitz, R.C.
1979: Groundwater calcrete deposits in Australia: some observations from Western Australia; Journal of the Geological Society of Australia, vol. 26, p. 293-303.

Mann, P., Hempton, M.R., Bradley, D.C., and Burke, K.
1983: Development of pull-apart basins; Journal of Geology, vol. 91, p. 529-554.

Manspeizer, W.
1985: The Dead Sea rift: impact of climate and tectonism on Pleistocene and Holocene sedimentation; *in* Biddle, K.T. and Christie-Blick, N. (eds.); Strike-Slip Deformation, Basin Formation, and Sedimentation, Society of Economic Paleontologists and Mineralogists, Special Publication No. 37, p. 143-158.

Mayr, U.
in press: Upper Devonian to Permian stratigraphy of northeastern Ellesmere Island, Canadian Arctic Archipelago; Geological Survey of Canada, Bulletin.

McLaren, D.J.
1963: Goose Fiord to Bjorne Peninsula; *in* Geological Survey of Canada, Memoir 320, p. 310-338.

McLaughlin, R.J. and Nilsen, T.H.
1982: Neogene non-marine sedimentation and tectonics in small pull-apart basins of the San Andreas fault system, Sonora County, California; Sedimentology, vol. 29, p. 865-876.

Miall, A.D.
1977: A review of the braided-river depositional environment; Earth Science Reviews, vol. 13, p. 1-62.

1981: Alluvial sedimentary basins: tectonic setting and basin architecture; *in* Miall, A.D. (ed.); Sedimentation and Tectonics in Alluvial Basins, Geological Association of Canada, Paper No. 23, p. 1-33.

1983: The Nares Strait problem: a re-evaluation of the geological evidence in terms of a diffuse oblique-slip plate boundary between Greenland and the Canadian Arctic islands; Tectonophysics, vol. 100, p. 227-239.

1986: Effects of Caledonian tectonism in Arctic Canada; Geology, vol. 14, p. 904-907.

Morgan, P. and Baker, B.H.
1983: Introduction - Processes of continental rifting; Tectonophysics, vol. 94, p. 1-10.

Nassichuk, W.W.
1965: Pennsylvanian and Permian rocks in the Parry Islands Group, Canadian Arctic Archipelago; Geological Survey of Canada, Paper 65-1, p. 9-12.

1975a: Carboniferous ammonoids and stratigraphy in the Canadian Arctic Archipelago; Geological Survey of Canada; Bulletin 237, 240 pp.

1975b: The stratigraphic significance of Permian ammonoids on Ellesmere Island; Geological Survey of Canada, Paper 75-1C, p. 267-277.

Nassichuk, W.W. and Davies, G.R.
1975: The Permian Belcher Channel Formation at Grinnell Peninsula, Devon Island; *in* Report of Activities, Part C, Geological Survey of Canada.

1980: Stratigraphy and sedimentation of the Otto Fiord Formation; Geological Survey of Canada, Bulletin 286.

Nassichuk, W.W. and Wilde, G.L.
1977: Permian Fusulinaceans and stratigraphy at Blind Fiord, southwestern Ellesmere Island; Geological Survey of Canada, Bulletin 268.

Nemec, W. and Steel, R.J.
1984: Alluvial and coastal conglomerates: their significant features and some comments on gravelly mass-flow deposits; *in* Koster, E.H. and Steel, R.J. (eds.); Sedimentology of Gravels and Conglomerates, Canadian Society of Petroleum Geologists, Memoir 10, p. 1-32.

Ord, D.M., Clemmey, H., and Leeder, M.R.
1988: Interaction between faulting and sedimentation during Dinantian extension of the Solway basin, SW Scotland; Journal of the Geological Society, London, vol. 145, p. 249-259.

Pemberton, G.
1988: Trace Fossil Concepts, Canadian Society of Petroleum Geologists, Short Course *in* Sequences, Stratigraphy, Sedimentology: Surface and Subsurface Conference, 1988.

Postma, G.
1983: Water escape structures in the context of a depositional model of a mass flow dominated conglomeratic fan-delta (Abrioja Formation, Pliocene, Almeria Basin, SE Spain); Sedimentology, vol. 30, p. 91-103.

Reading, H.G.
1980: Characteristics and recognition of strike-slip fault systems; *in* Ballance, P.F. and Reading, H.G. (eds.); Sedimentation in Oblique-Slip Mobile Zones, International Association of Sedimentologists, Special Publication No. 4, p. 7-26.

Rosendahl, B.R., Reynolds, D.J., Lorber, P.M., Burgess, C.F., McGill, J., Scott, D., Lambiase, J.J., and Derksen, S.J.
1986: Structural expressions of rifting: lessons from Lake Tanganyika, Africa; *in* Frostick, L.E., Renaut, R.W., Reid, I., and Tiercelin, J.J. (eds.); Sedimentation in the African Rifts, Geological Society of America Special Publication No. 25, p. 29-43.

Ross, C.A. and Ross, J.R.
1988: Late Paleozoic transgressive-regressive deposition; in Sea-Level Changes - An Integrated Approach, Society for Economic Paleontologists and Mineralogists, Special Publication No. 42, p. 227-247.

Rouse, J.E. and Sherif, N.
1980: Major evaporite deposits from groundwater remobilized salts; Nature, vol. 285, p. 409-412.

Rust, B.R.
1972: Structure and process in a braided river; Sedimentology, vol. 18, p. 221-245.

1984: Coarse Alluvial Deposits; *in* Walker, R.G. (ed.); Facies Models, Second Edition, Geoscience Canada, Reprint Series 1, p. 53-69.

Schei, P.
1903: Summary of geological results (Second Norwegian North Polar Expedition in the Fram, 1898-1902); Geographical Journal, vol. 22, p. 56-65.

Schidlowski, M., Eichmann, R., and Junge, C.E.
1976: Carbon isotope geochemistry of the Precambrian Lomagundi carbonate province, Rhodesia; Geochimica et Cosmochimica Acta, vol. 40, p. 449-455.

Steel, R.J.
1974: New Red Sandstone floodplain and piedmont sedimentation in the Hebridean Province, Scotland; Journal of Sedimentary Petrology, vol. 44, p. 336-357.

Steel, R.J. and Gloppen, T.G.
1980: Late Caledonian (Devonian) basin formation, western Norway: signs of strike-slip tectonics during infilling; *in* Ballance, P.F. and Reading, H.G. (eds.); Sedimentation in Oblique-Slip Mobile Zones, International Association of Sedimentologists, Special Publication No. 4, p. 79-103.

Steel, R.J., Maehle, S., Nilsen, H, Røe, S.L. and Spinnangr, A.
1977: Coarsening-upward cycles in the alluvium of Hornelen Basin (Devonian) Norway: sedimentary response to tectonic events; Geological Society of America Bulletin, vol. 88, p. 1124-1134.

Steel, R.J. and Wilson, A.C.
1975: Sedimentation and tectonism (?Permo-Triassic) on the margin of the North Minch Basin, Lewis; Journal of the Geological Society of London, vol. 131, p. 183-202.

Steel, R.J. and Worsley, D.
1984: Svalbard's post-Caledonian strata - an atlas of sedimentational patterns and palaeogeographic evolution; *in* Graham and Trotman (eds.): Petroleum Geology of the North European Margin, Norwegian Petroleum Society, p. 109-135.

Stemmerik, L., Rouse, J.E., and Spiro, B.
1988: S-isotope studies of shallow water, laminated gypsum and associated evaporites, Upper Permian, East Greenland; Sedimentary Geology, vol. 58, p. 37-46.

Stephenson, R.A., Embry, A.F., Nakiboglu, S.M., and Hastaoglu, M.A.
1987: Rift-initiated Permian to Early Cretaceous subsidence of the Sverdrup Basin; *in* Beaumont, C. and Tankard, A.J. (eds.): Sedimentary Basins and Basin-Forming Mechanisms, Canadian Society of Petroleum Geologists, Memoir 12, p. 213-231.

Stiller, M., Rousnick, J.S., and Shasha, S.
1985: Extreme carbon-isotope enrichments in evaporating brines. Nature, vol. 316, p. 434-435.

Strecker, M.R., Blisniuk, P.M., and Eisbacher, G.H.
1990: Rotation of extension direction in the central Kenya Rift; Geology, vol. 18, p. 299-302.

Sverdrup, O.
1904: New Land: four years in the Arctic regions; Longmas, New York.

Thériault, P. and Beauchamp, B.
1991: Preliminary interpretation of the depositional history and tectonic significance of the Carboniferous to Permian Canyon Fiord Formation, west-central Ellesmere Island, Arctic Archipelago; in Current Research, Part B, Geological Survey of Canada, Paper 91-1B, p. 93-103.

Thorsteinsson, R.
1974: Carboniferous and Permian stratigraphy of Axel Heiberg Island and western Ellesmere Island, Canadian Arctic Archipelago; Geological Survey of Canada, Bulletin 224.

Thorsteinsson, R. and Tozer, E.T.
1970: Geology of the Arctic Archipelago; *in* Douglas, R.J.W. (ed.); Geology and Economic Minerals of Canada, Geological Survey of Canada, Economic Geology Report No. 1, p. 548-590.

Tozer, E.T.
1963: Blind Fiord; *in* Geological Survey of Canada, Memoir 320, p. 380-386.

Trettin, H.P.
1969: Geology of Ordovician to Pennsylvanian rocks, M'Clintock Inlet, north coast of Ellesmere Island, Canadian Arctic Archipelago; Geological Survey of Canada, Bulletin 183, 93 p.

1989: The Arctic Islands; *in* A.W. Bally and A.R. Palmer (ed.); The Geology of North America - An overview, Boulder, Colorado, Geological Society of America, The Geology of North America, Volume A, p. 349-370.

Troelsen, J.C.
1950: Contributions to the geology of northwest Greenland, Ellesmere Island and Axel Heiberg Island; Meddelelser Om Grønland, vol. 7, p. 1-85.

1952: Geological investigations in Ellesmere Island, 1952; Arctic, vol. 5, p. 199-210.

Turcotte, D.L. and Emerman, S.H.
1983: Mechanisms of active and passive rifting; Tectonophysics, vol. 94, p. 39-50.

Turner, P.
1980: Continental Red Beds, Developments in Sedimentology No 29, Elsevier Scientific Publishing Company.

Utting, J., Jachowicz, M., and Jachowicz, A.
1989: Palynology of the Lower Carboniferous Emma Fiord Formation of Devon, Axel Heiberg, and Ellesmere islands, Canadian Arctic Archipelago; *in* Canadian Contributions to Paleontology, Geological Survey of Canada, Bulletin.

Vail, P.R., Mitchum, R.M., Todd, R.G., and Widmier, J.M.
1977: Seismic stratigraphy and global sea level changes from seismic stratigraphy; *in* Payton, C.E. (ed.); Stratigraphic Interpretation of Seismic Data, American Association of Petroleum Geologists, Memoir 26, p. 49-212.

Veizer, J., Fritz, P., and Jones, B.
1986: Geochemistry of brachiopods: Oxygen and carbon isotopic records of Paleozoic oceans; Geochimica et Cosmochimica Acta, vol. 50, p. 1679-1696.

Veizer, J. and Hoefs, J.
1976: The nature of O^{18}/O^{16} and C^{13}/C^{12} secular trends in sedimentary carbonate rocks; Geochimica et Cosmochimica Acta, vol. 40, p. 1387-1395.

Veizer, J., Holser, W.T., and Wilgus, C.K.
1980: Correlation of C^{13}/C^{12} and $^{34}S/^{32}S$ secular variations; Geochimica et Cosmochimica Acta, vol. 44, p. 579-587.

Walker, R.G. and Cant, D.J.
1984: Sandy fluvial systems; *in* Walker, R.G. (ed.); Facies Models, Second Edition, Geoscience Canada, Reprint Series 1, p. 71-89.

Watts, N.L.
1977: Pseudo-anticlines and other structures in some calcretes of Botswana and South Africa; Earth Surface Processes, vol. 2, p. 63-74.

Whitaker, J.H. McD.
1973: Nor. Geol. Tidsskr., 53, p. 403-417.

Williams, L.A.J. and Chapman, G.R.
1986: Relationships between major structures, salic volcanism and sedimentation in the Kenya Rift from the equator northwards to Lake Turkana; *in* Frostick, L.E., Renaut, R.W., Reid, I., and Tiercelin, J.J. (eds.); Sedimentation in the African Rifts, Geological Society of America Special Publication No. 25, p. 59-74.

Wright, V.P., Platt, N.H., and Wimbledon, W.A.
1988: Biogenic laminar calcretes: evidence of calcified root-mat horizons in paleosols; Sedimentology, vol. 35, p. 603-620.

Wright, V.P. and Wilson, R.C.L.
1987: A terra rossa-like paleosol complex from the Upper Jurassic of Portugal; Sedimentology, vol. 34, p. 259-273.

Zak, I. and Freund, R.
1981: Asymmetry and basin migration in the Dead Sea rift; *in* Freund, R. and Garfunkel, Z. (eds.); The Dead Sea Rift, Tectonophysics, vol. 80, p. 27-38.

Ziegler, P.A.
1988: Evolution of the Arctic - North Atlantic and the Western Tethys; American Association of Petroleum Geologists, vol. 43, 198 p.

PLATE 1

Exposures of the basal Canyon Fiord Formation

A. Cliff exposure of the basal Canyon Fiord Formation overlying with angular unconformity the Devonian Danish River Formation (sandstone, siltstone, shale) of the Franklinian Mobile Belt. The conglomerate assemblage (CA), the upper sandstone assemblage (USA), and the limestone assemblage (LA) of the basal Canyon Fiord Formation are present. Black arrow denotes unconformity (Section 13; northern Trold Fiord belt). Stratigraphic thickness of CA and USA on photograph is approximately 200m.

B. Cliff exposure of Ordovician-Devonian Cape Phillips shales and limestones overlain with angular unconformity by the conglomerate assemblage (CA), a transitional interval of the upper sandstone and limestone assemblages (TR), and the limestone assemblage (LA) (between sections 18 and 19; central Trold Fiord belt). Stratigraphic thickness of CA and TR on photograph is approximately 125m.

C. Cliff exposure of the conglomerate assemblage (CA) overlain by a recessive and snow covered interval comprising intercalated units of the upper sandstone and limestone assemblages. Canyon Fiord Formation unconformably overlies well-stratified limestones of the Ordovician Cornwallis Group (Section 22; central Trold Fiord belt). CA is 40m thick.

D. Field photograph of the angular unconformity (white arrows) between the limestone assemblage of the Canyon Fiord Formation and underlying Cornwallis limestones of the Franklinian Mobile Belt (Section 5; Blind Fiord belt). Hammer is 25cm long (left of top arrow).

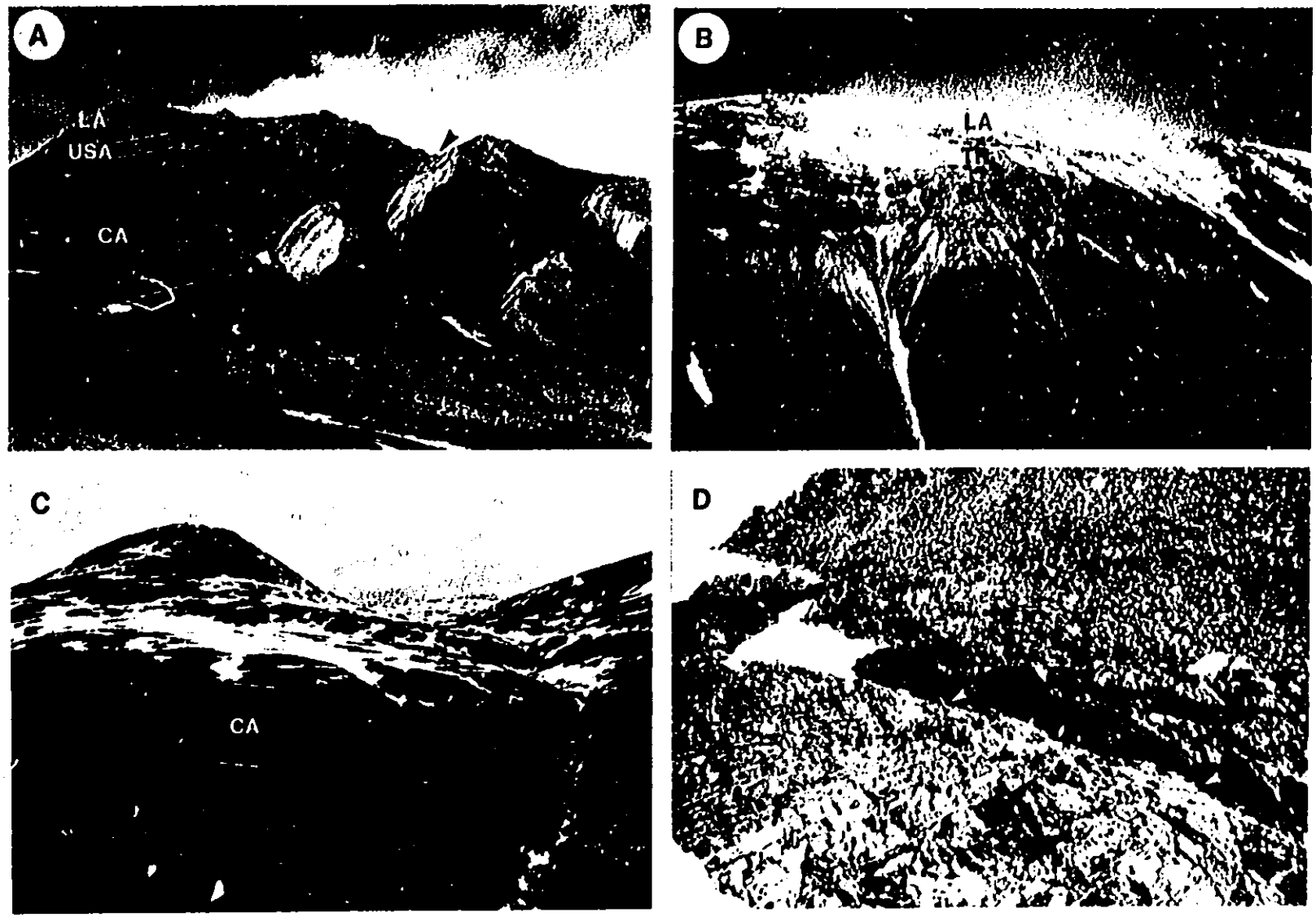
A
LA
USA
CA
B
LA
TD
C
CA
D

PLATE 2

Lower sandstone assemblage

A. Alternating layers of massive (resistant, light-coloured) and nodular (less resistant, darker-coloured) caliche. Lower part of the section is dominated by massive caliche (M), and the upper part by nodular caliche (N) (Section 11; northern Trold Fiord belt).

B. Section view of a thick horizon of plant tufa and rhizolith-rich nodular caliche. Interstitial sandstone is minor due to displacement from progressive growth of calcium carbonate (Section 10; northeastern Trold Fiord belt). Hammer is 25cm long.

C. Section view of massive caliche overlain sharply by sandstone-hosted nodular caliche. Increase in the size of nodules up-section reflects an upward increase in the maturity level within a single soil profile. Massive horizon in lower part of photograph represents the mature top of an underlying profile (Section 11; northern Trold Fiord belt). Hammer is 25cm long.

D. Section view of pebble conglomerate unit with discontinuous lenses of parallel laminated to ripple cross-laminated sandstone (white arrows) (Section 16; central Trold Fiord belt).

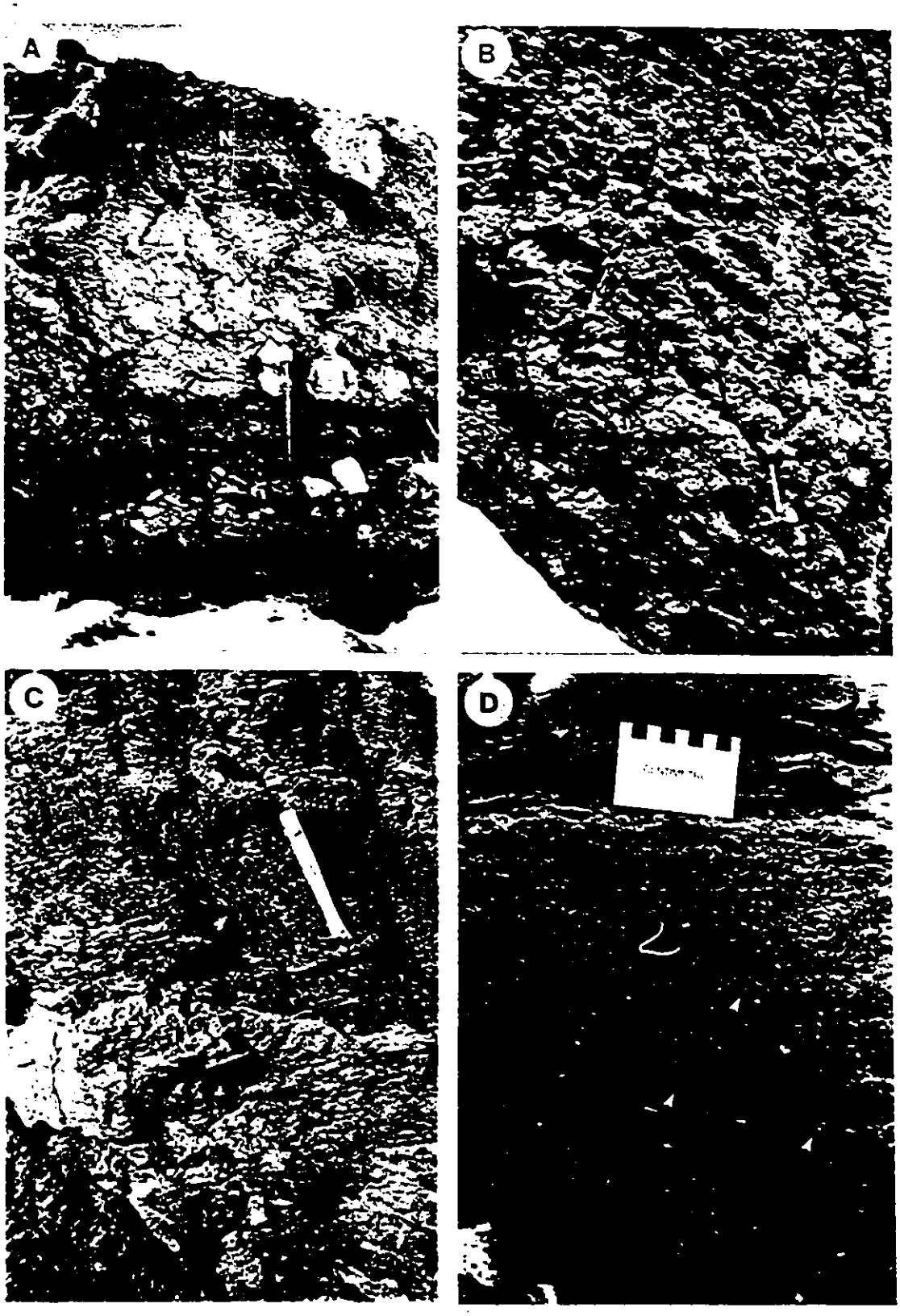
A
B
C
D

PLATE 3

Lower sandstone assemblage

A. Polished slab of an individual caliche nodule displaying mottled appearance. Note circum-granular cracking (CC) and local agglomeration of smaller internal nodules (No) (Section 16; northern Trold Fiord belt). Scale bar is 1cm.

B. Polished slab of mottled nodular-massive caliche. Calcite veins are pedogenic in origin and represent circum-granular cracking (white arrows) (Section 10, northeastern Trold Fiord belt). Scale bar is 1cm.

C. Polished slab of massive caliche showing diffuse circum-granular cracking (CC) and spar-filled fenestrae (Fe) (Section 16; northern Trold Fiord belt). Scale bar is 1cm.

D. Polished slab of laminar and pisolitic caliche. Laminar fabric (L) consists of sub-horizontal undulose to contorted fine laminae of micrite. Pisolitic fabric (P) occurs within isolated pockets and is composed of concentric accumulations of fine micrite laminae (Section 10; northeastern Trold Fiord belt). Scale bar is 1cm.

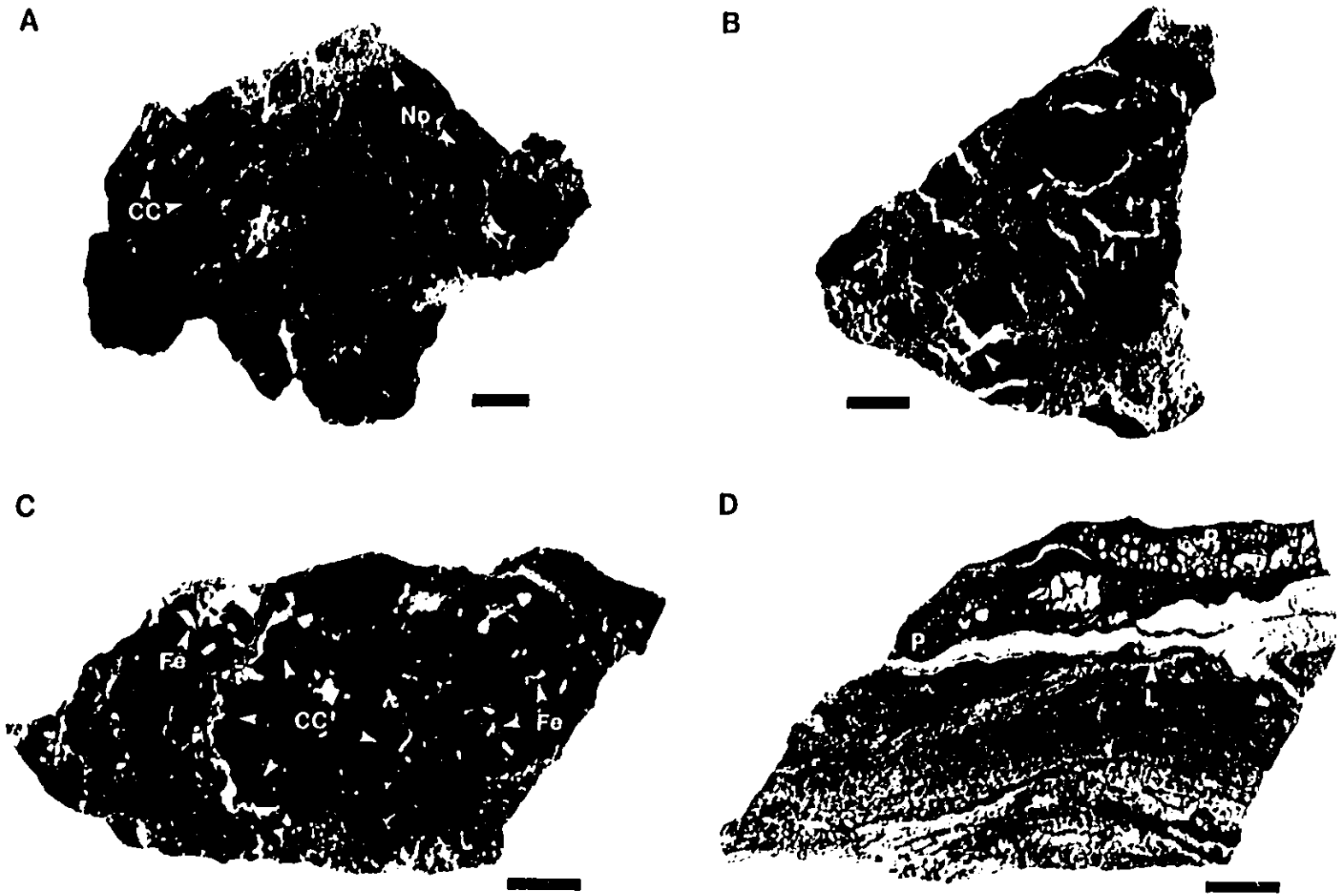
A
No
CC
B
C
Fe
CC
Fe
D
P
L

PLATE 4

Conglomerate assemblage

A. Section view of clast-supported pebble to cobble conglomerate displaying normal grading (Section 11; northern Blind Fiord belt). Hammer is 25cm long.

B. Section view of clast-supported pebble conglomerate with normally-graded beds. Basal part of beds shows spar-filled open framework; top of beds is composed of well-sorted fine pebbles and granules with minor interstitial sparry calcite (Section 6; central Blind Fiord belt). Lens cap is 6cm wide.

C. Oblique view of a scour pocket filled with well-sorted cobbles and boulders (Section 6; central Blind Fiord belt). Hammer is 25cm long.

D. Section view of massive caliche in clast-supported pebble conglomerate capped by finely-laminated laminar caliche (Section 9; southern Blind Fiord belt).

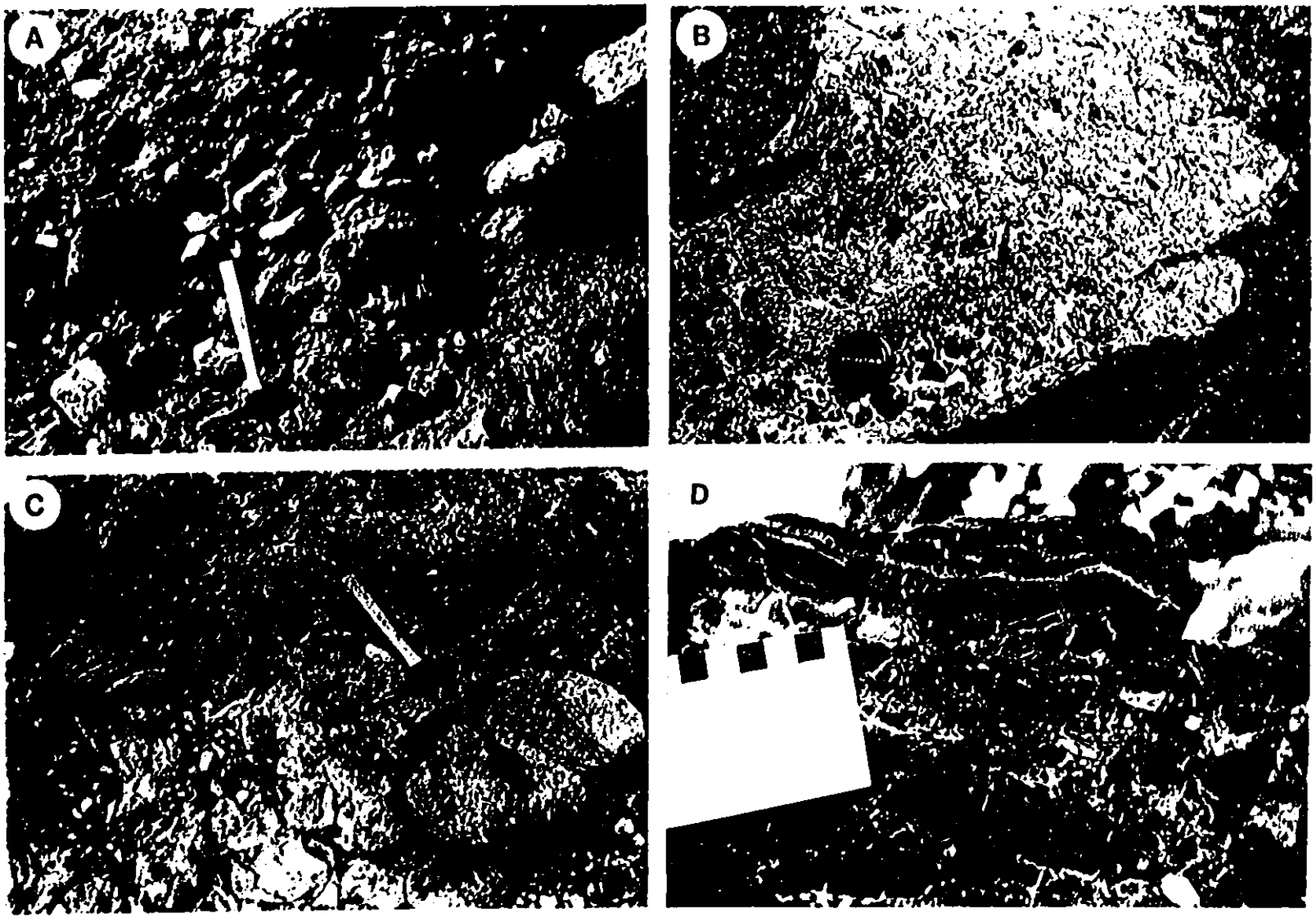
A
B
C
D

PLATE 5

Conglomerate assemblage

A. Polished slab of massive caliche hosted in pebble conglomerate that is capped with laminar caliche. Note that lowermost set (pale grey) of laminated micrite is discontinuous and sharply bounded at its top by a dissolution micro-unconformity (MU) (Section 3; northern Blind Fiord belt). Scale bar is 1cm.

B. Polished slab of laminar caliche containing a sub-vertical caliche dike (CD) filled with dark laminated micrite. Note left-lateral motion along plane of caliche dike, and also the well defined dissolution micro-unconformity (MU) in the upper part (Section 9; southern Blind Fiord belt). Scale bar is 1cm.

C. Polished slab of highly deformed laminar caliche. Micrite laminae are undulated, contorted, micro-folded (MFo), micro-faulted (MFa), and cross-cut by a caliche dike (CD) (Section 9; southern Blind Fiord belt). Scale bar is 1cm.

D. Polished slab of interlayered massive (light-coloured) and laminar caliche (dark-coloured). Sample is overall brecciated, with deformational features including micro-faulting (MFa) and possible root pedoturbation (PD). White cement is blocky sparite (Section 19; central Trold Fiord belt). Scale bar is 1cm.

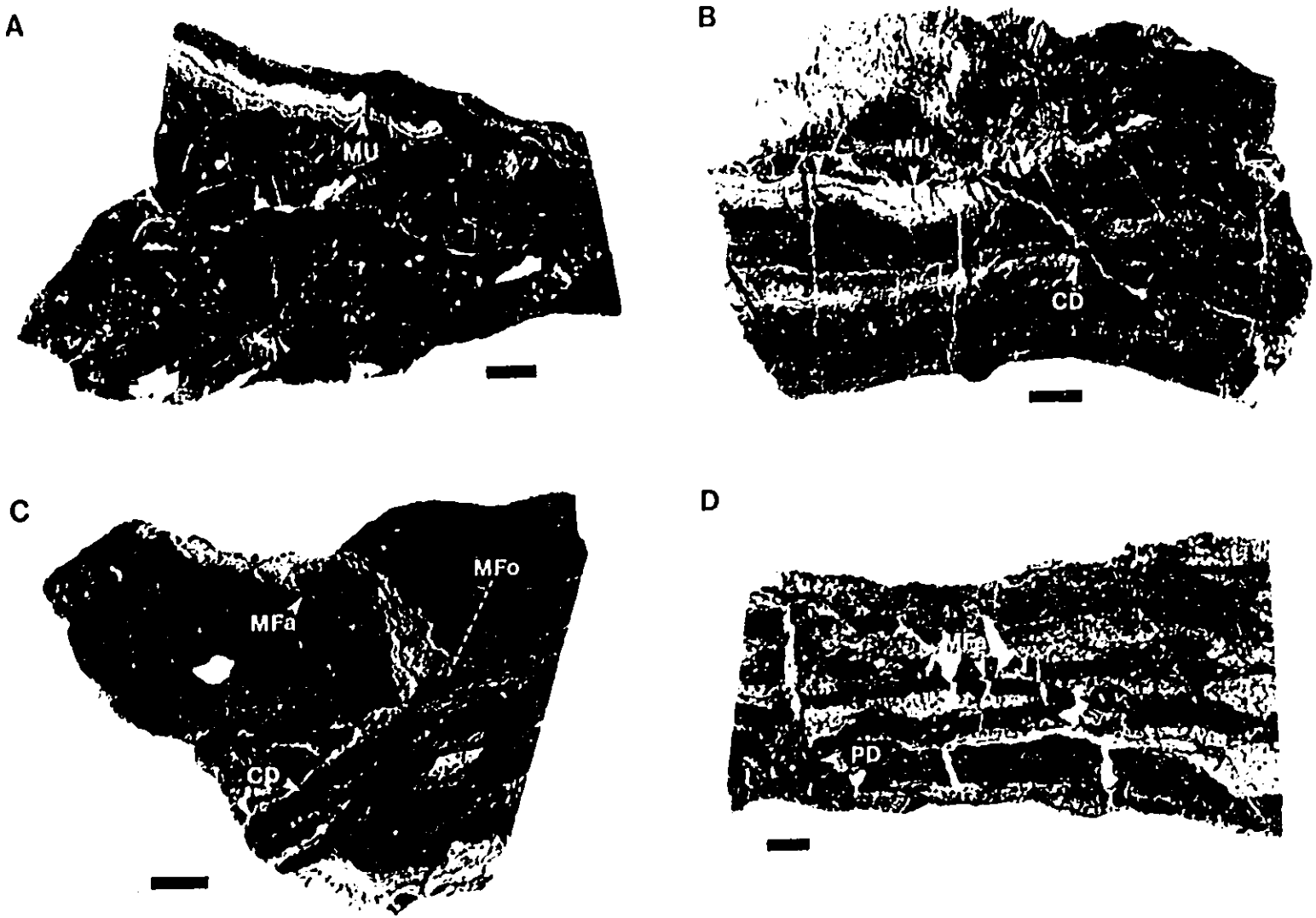
A
MU
B
MU
CD
C
MFo
MFa
CP
D
MFp
PD

PLATE 6

Conglomerate assemblage

A. Photomicrograph of an alveolar texture displaying complex tubular forms infilled with sparite, and surrounded by dark micrite. Host is silty massive caliche (Section 15; northern Trold Fiord belt). Scale bar is 1mm.

B. Photomicrograph of an alveolar texture displaying spar-filled chambers separated by thin micritic walls. Note laminar caliche fabric (L) in the upper part (Section 6; central Blind Fiord belt). Scale bar is 1mm.

C. Photomicrograph of a rhizolith consisting of a central root mould (RM) filled with sparite, surrounded by a micritic rhizocretion (Rz). Possible alveolar texture (AT) around and near rhizolith. *Microcodium* (M) is also present (Section 6; central Blind Fiord belt). Scale bar is 0.5m.

D. Photomicrograph of *Microcodium* occurring as subrounded to sub-hexagonal calcite prisms with organic matter inclusions. Prisms are either isolated, or coalesced in the form of irregular rosettes (Section 6; central Blind Fiord belt). Scale bar is 0.2mm.

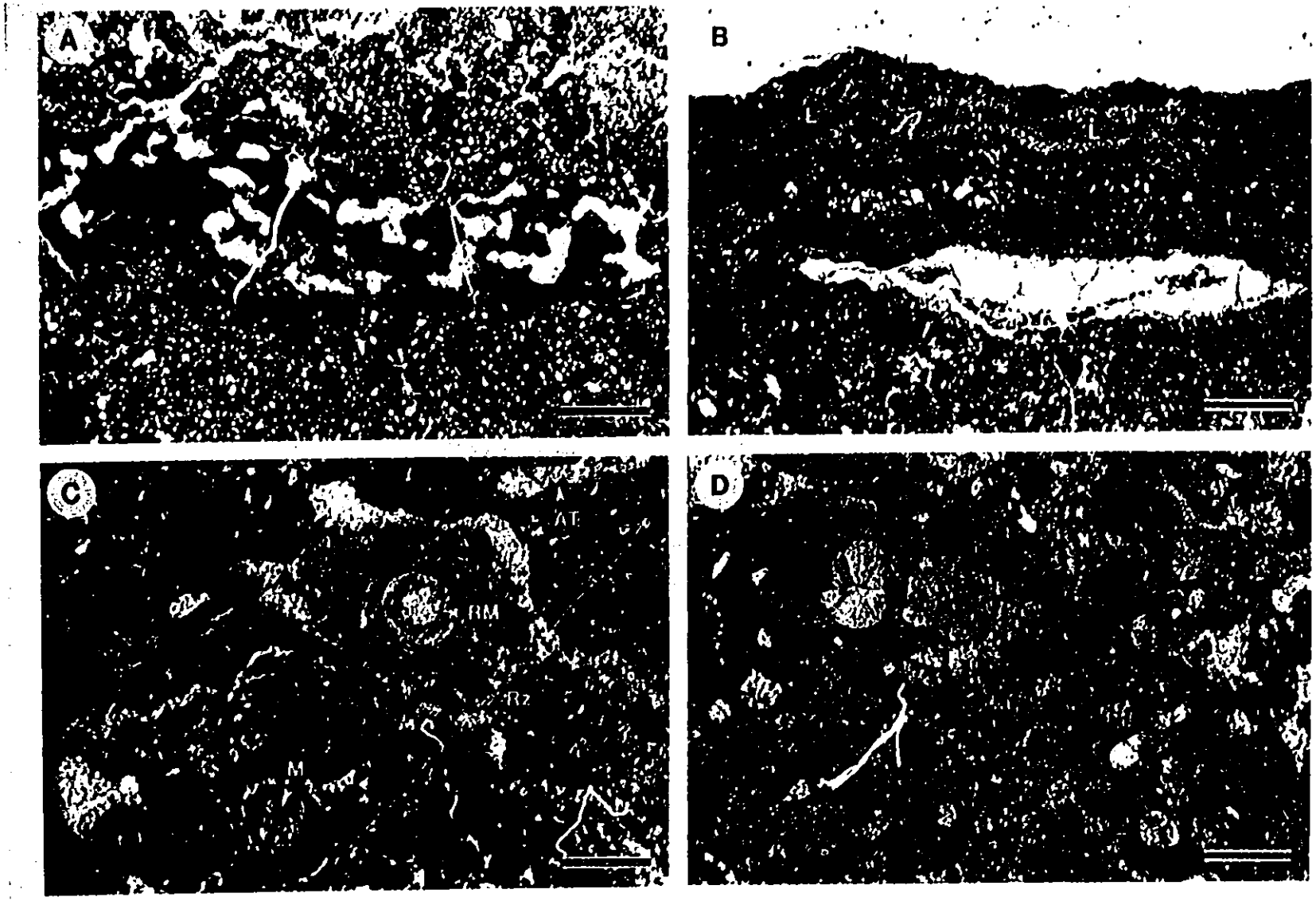
A
B
L
L
C
AT
BM
Rz
M
D

PLATE 7

Conglomerate assemblage

A. Section view of clast-supported cobble/boulder conglomerate displaying massive, ungraded, and unsorted internal features (Section 22; central Trold Fiord belt). Scale card is in centimetres.

B. Section view of clast- to matrix-supported cobbly conglomerate that is massive, ungraded, unsorted, and has a high content of sand/mud matrix (Section 11; northern Trold Fiord belt). Hammer is 25cm long.

C. Section view of matrix-supported pebbly conglomerate with massive texture and unorganized fabric. Note angular/subangular nature of clasts. Bedding plane is inclined at approximately 45^0 towards the left of photograph (Section 3; northern Blind Fiord belt). Lens cap is 6cm wide.

D. Section view of a sandstone interval within the conglomerate assemblage hosting nodular to nodular-massive caliche (Section 11; northern Trold Fiord belt). Hammer is 25cm long.

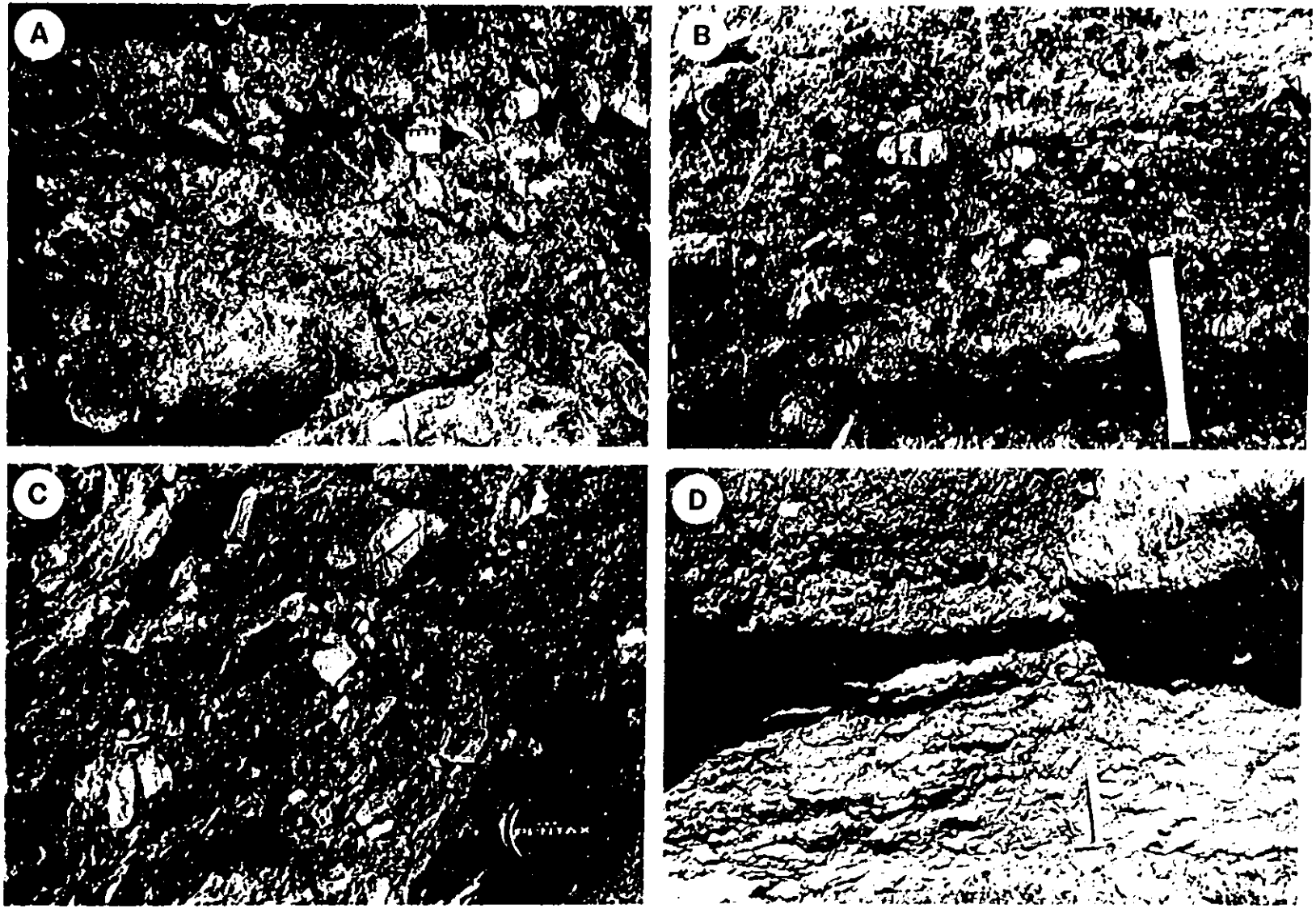
A
B
C
D

PLATE 8

Upper sandstone assemblage

A. Pebbly sandstone/sandstone lithofacies (lower resistant unit) successively overlain by a thin unit of the sandstone/siltstone lithofacies and by the limestone assemblage (Section 13; northern Trold Fiord belt). Well exposed knob of pebbly sandstone/sandstone lithofacies (K) is 18m thick.

B. Section view of large channel structure filled with pebble conglomerate and pebbly sandstone (Section 13; northern Trold Fiord belt). Hammer is 25cm long.

C. Section view of low angle tabular cross-bedded sandstone sharply overlain by pebble conglomerate (Section 13; northern Trold Fiord). Lens cap is 6cm wide.

D. Cliff exposure showing parallel-laminated to low angle cross-bedded sandstone and pebbly sandstone (Section 13; northern Trold Fiord belt). Hammer is 25cm long.

E. Section view of tabular cross-bed sets and normal grading (white arrow) in interlayered sandstone and pebbly sandstone (Section 13; northern Trold Fiord belt). Lens cap is 6cm wide.

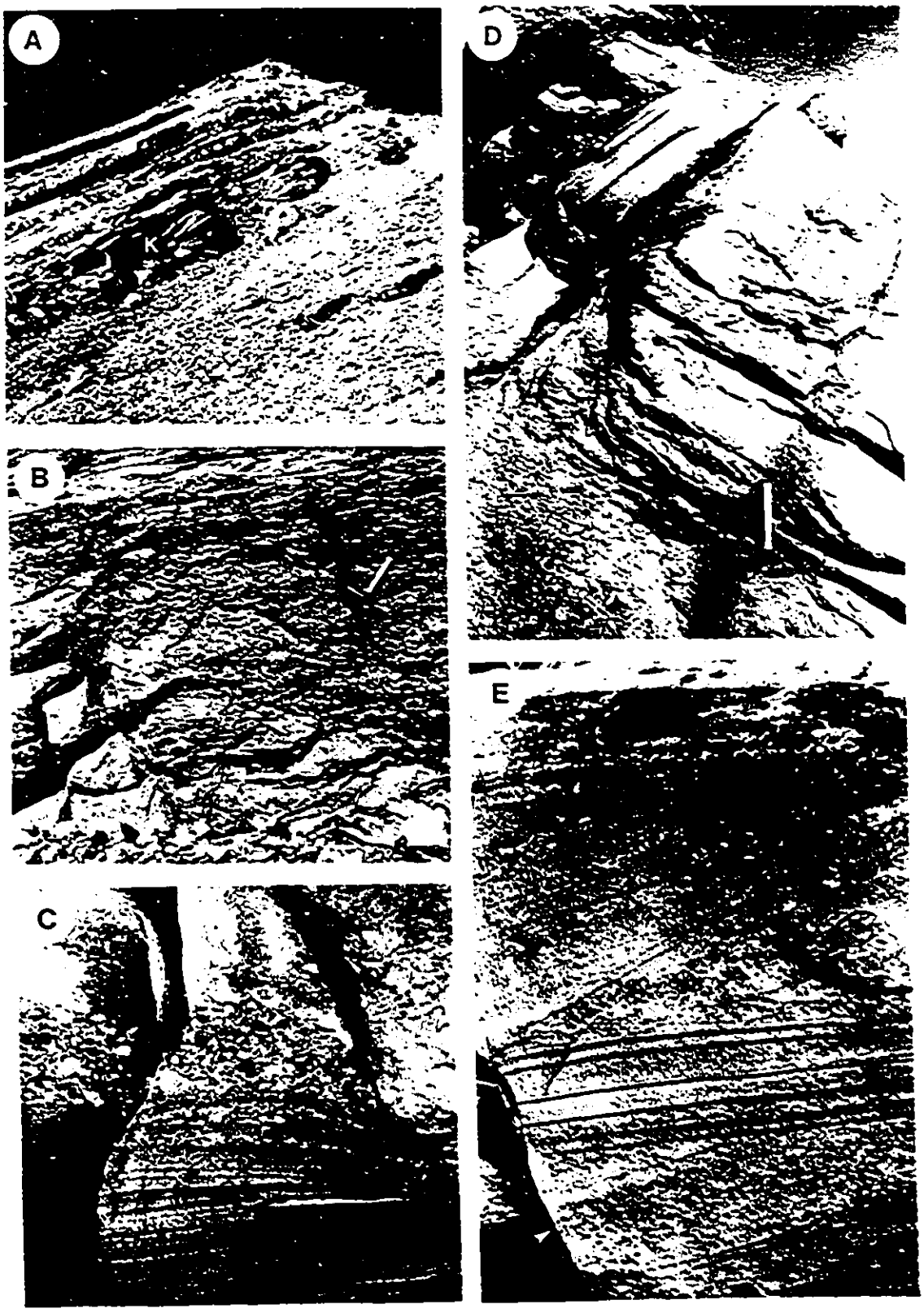
A
K
B
C
D
E

PLATE 9

Upper sandstone assemblage

A. Section view of thin- to medium-bedded sandstone/siltstone showing parallel bedding and low-angle tabular cross-bedding (Section 10; northeastern Trold Fiord belt). Hammer is 25cm long.

B. Bedding plane view of desiccation cracks in siltstone with sandstone infill. Note fossilized branch (white arrows) more than 25cm in length (Section 10; northeastern Trold Fiord belt). Lens cap is 6cm wide.

C. Loose block showing large fossilized branch or trunk in sandstone host (Section 10; northeastern Trold Fiord belt).

D. Loose block showing dense arrangment of *Scoyenia* trace fossils in sandstone (Section 10; northeastern Trold Fiord belt).

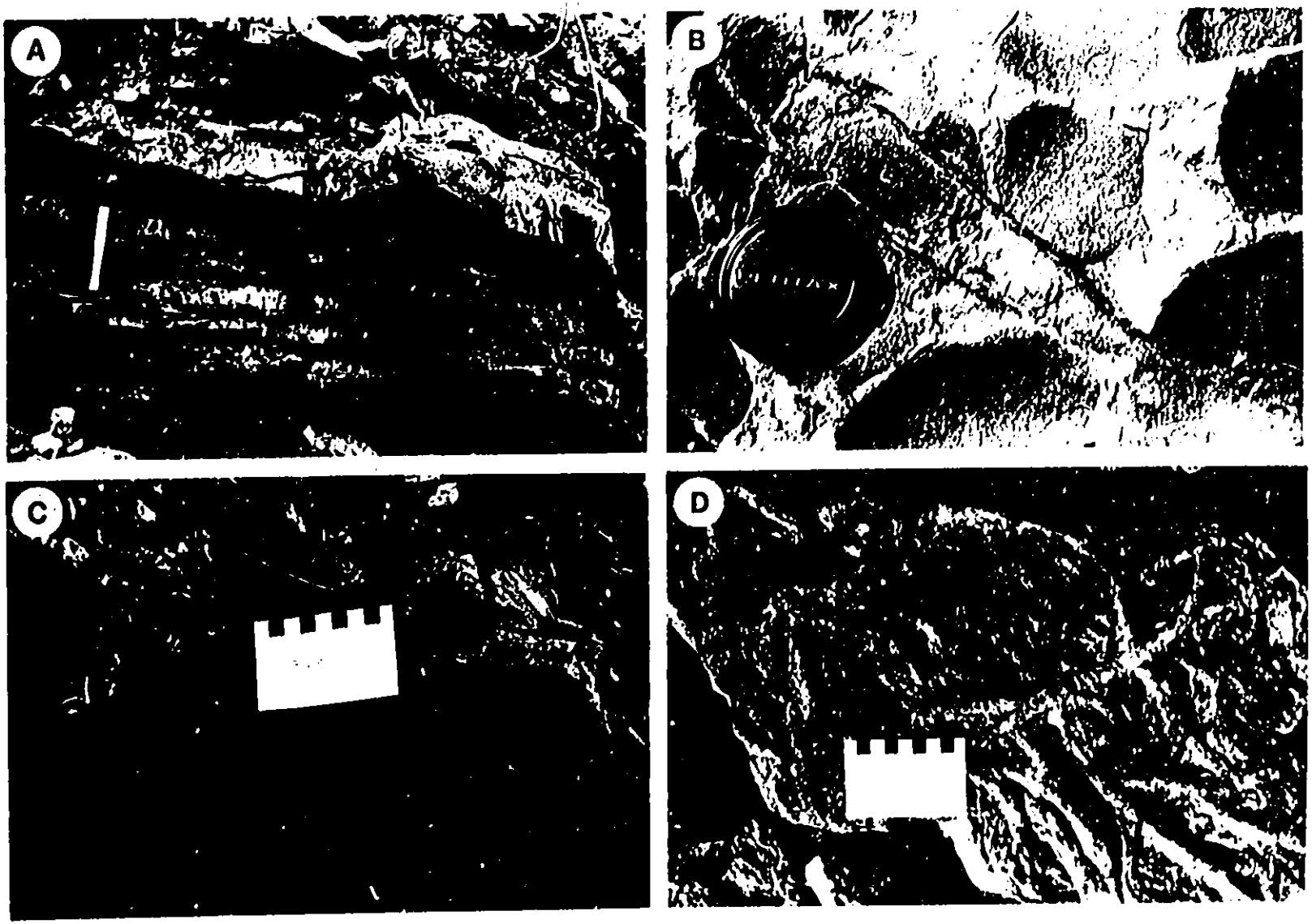
A
B
C
D

PLATE 10

Evaporite assemblage

A. Cliff view towards west of the local evaporite assemblage at Section 28. The mudstone/anhydrite lithofacies (M/An) and anhydrite lithofacies (An) are overlying a thin unit of the conglomerate assemblage (CAs). This basal Canyon Fiord succession overlies with angular unconformity the Franklinian "basement". Note laterally continuous dark limestone layer (white arrow) near the top of the anhydrite lithofacies (Section 28; southern Trold Fiord belt). Evaporite assemblage (M/An and An) at section 28 is 57m thick.

B. Cliff view towards north of the evaporite assemblage exposed at sections 27 and 28. Darker mudstone/anhydrite lithofacies in the lower part of the assemblage is actually deep reddish-brown in color. The assemblage decreases in thickness from 57m at Section 28 to 33 m at Section 27 (southern Trold Fiord). People for scale at base of section 28.

C. Close-up view of the mudstone/anhydrite lithofacies showing unconsolidated mudstone interpreted as pseudogley paleosol (section view). Note color contrast (dark = reddish-brown; lighter = yellowish brown) of paleosol and presence of evaporite nodules (N) of probable early diagenetic origin (Section 28; southern Trold Fiord belt). Scale card is in centimetres.

D. Close-up view of the anhydrite lithofacies displaying nodular "chicken-wire" texture (Section view). Gypsum (Gp) probably resulting from recent hydration occurs along fractures (Section 28; southern Trold Fiord belt).

E. Section view of a fossiliferous limestone interbed at the base of the anhydrite lithofacies. The predominant biotic elements are ostracods, beresellid green algae and fusulinacean foraminifers (Section 28; southern Trold Fiord belt). Hammer is 25cm long.

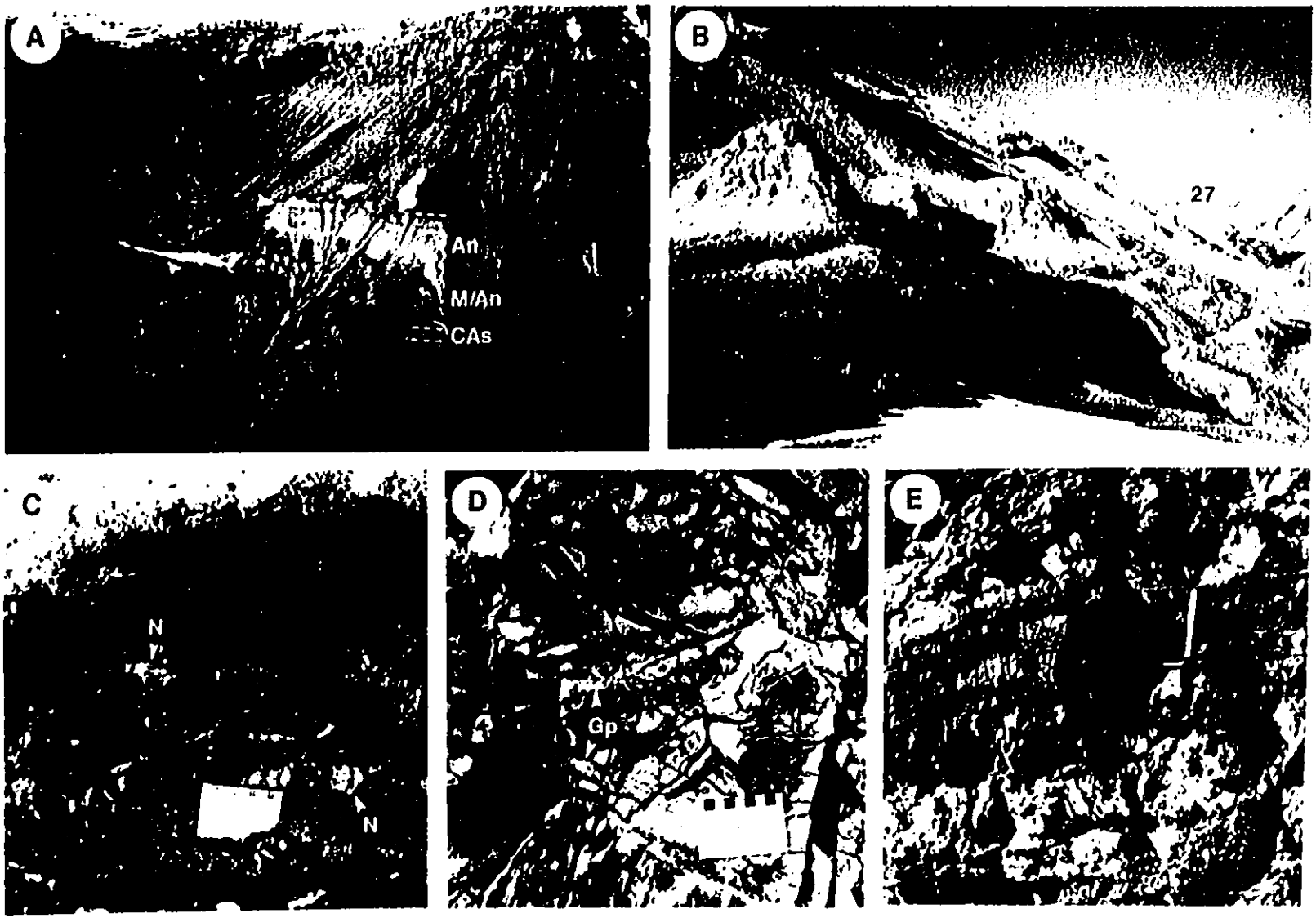
A
An
M/An
CAs
B
27
C
N
N
D
Gp
E

PLATE 11

Evaporite assemblage

A. Photomicrograph of ostracod microfacies in wackestone. Biotic elements consist mainly of well-preserved to compacted ostracod shells (Os) and of small encrusting foraminifers (EF) (Section 28; southern Trold Fiord belt). Scale bar is 0.5mm.

B. Photomicrograph of fusulinacean-beresellid microfacies in grainstone/packstone. Fusulinacean foraminifers (Fu), beresellid green algae (Be), and ungdarellid red algae (Un) are the most common constituents (Section 28; southern Trold Fiord belt). Scale bar is 0.5mm.

C. Photomicrograph of fusulinacean microfacies in wackestone. Fusulinacean foraminifers (Fu), echinoderms (Ec), and brachiopods (Bp) are common (Section 28; southern Trold Fiord belt). Scale bar is 1mm.

D. Polished slab of limestone breccia lithofacies, interpreted as a dissolution collapse breccia. Clasts are angular, composed of limestone (Lm), gypsum (Gp), and chert, and are supported by a carbonate matrix. The breccia is also relatively porous (P = pore) (Section 28; southern Trold Fiord belt). Scale bar is 2cm.

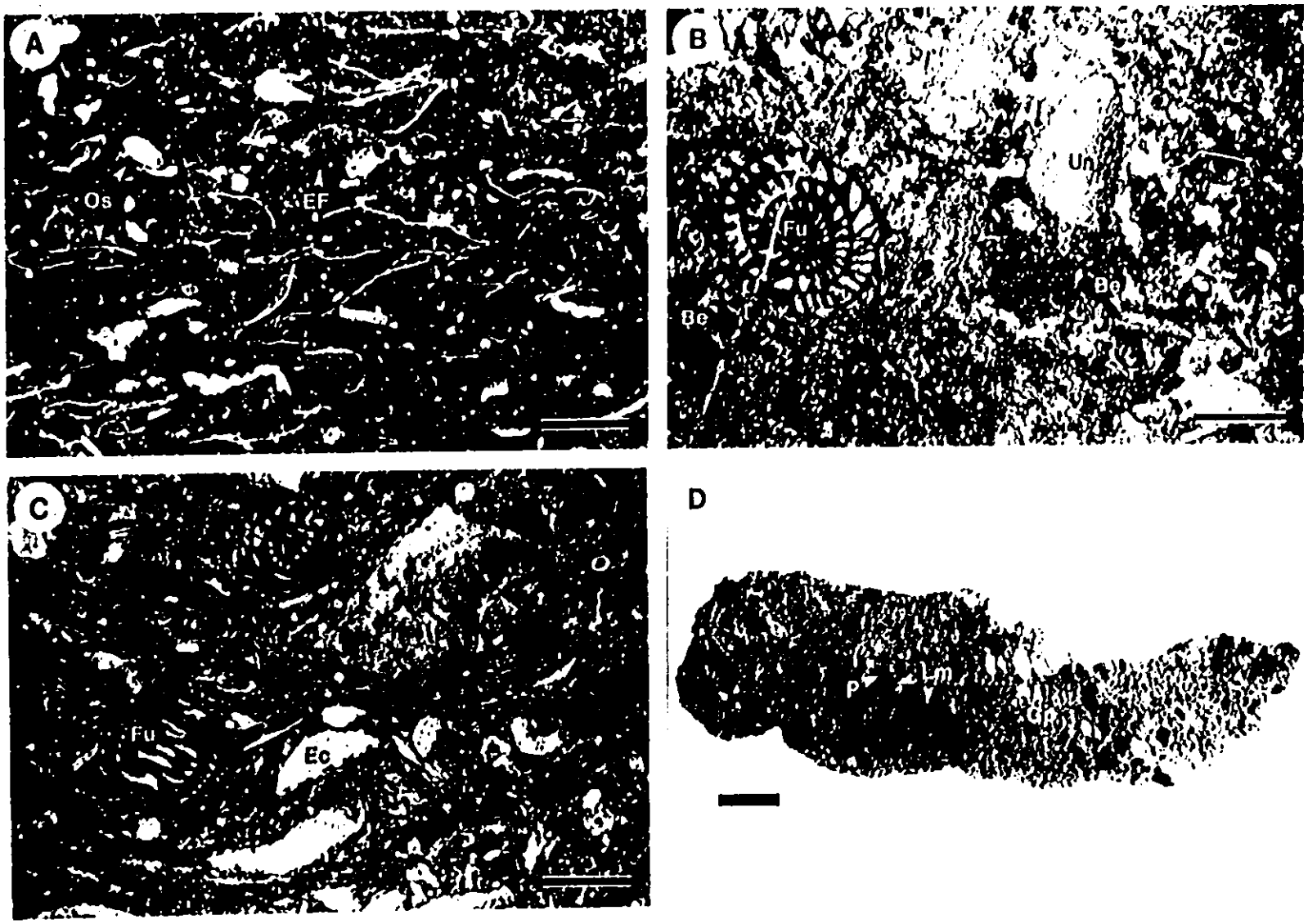
A
Os
EF
B
Un
Fu
Be
Be
C
Fu
Ec
D
P
Lm

PLATE 12

Limestone assemblage

A. Photomicrograph of encrusting foraminiferal microfacies in packstone/grainstone. Apterinellid encrusting foraminifers (EF) are abundant, along with common brachiopods (Bp), ostracods and calcispheres (Section 25; southern Trold Fiord belt). Scale bar is 0.5mm.

B. Photomicrograph of encrusting foraminiferal microfacies in packstone/grainstone. Abundant encrusting foraminifers (EF) and common ostracods (Os) are represented (Section 12; northern Trold Fiord belt). Scale bar is 0.5mm.

C. Photomicrograph of dasycladacean microfacies in grainstone. Dasycladacean green algae (Da) and globivalvulinid foraminifers (black arrows) are abundant, along with common encrusting foraminifers and ostracods (Section 22; central Trold Fiord belt). Scale bar is 1mm.

D. Photomicrograph of dasycladacean microfacies in grainstone. Dasycladacean green algae (Da), globivalvulinid foraminifers ((black arrows), ostracods (Os) and encrusting foraminifers are the most common biotic elements (Section 22; central West Trold Fiord). Scale bar is 0.5mm.

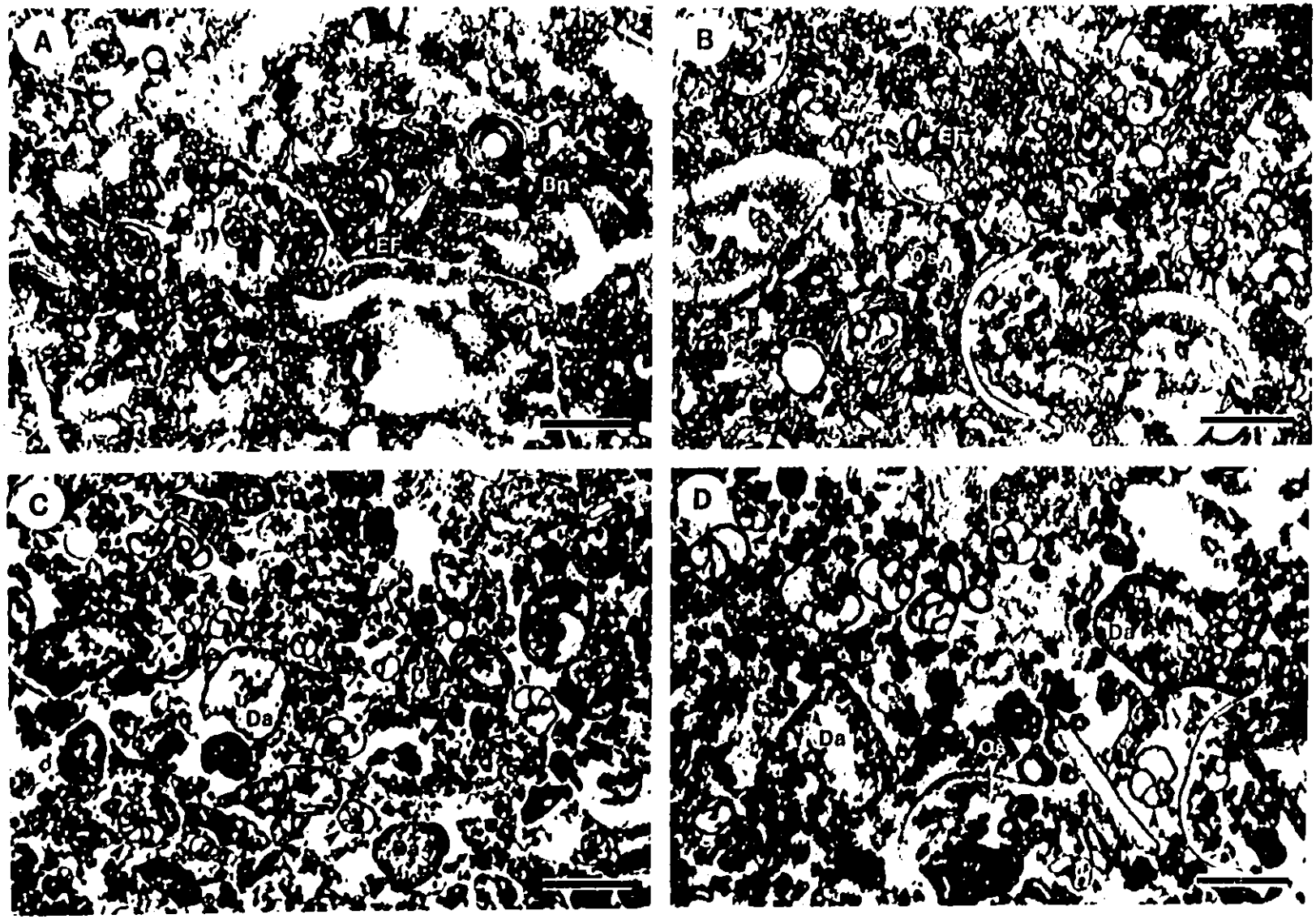
A
Bn
EF
B
EF
C
Da
D
D
Da
Ob

PLATE 13

Limestone assemblage

A. Photomicrograph of bioclastic microfacies in grainstone. A variety of framework grains are present, including common fusulinacean (Fu), echinoderms, brachiopods, bryozoans, ungdarellid and stachein red algae, beresellid green algae, encrusting (EF) and small benthic foraminifers, reworked *Microcodium* fragments (M) and limestone extraclasts (Section 7; southern Blind Fiord belt). Scale bar is 1mm.

B. Photomicrograph of bioclastic microfacies in silty grainstone. Fusulinacean foraminifers, ungdarellid red algae, ostracods, a gastropod (G) and a tetrataxid foraminifer (Te) are represented (Section 6; central Blind Fiord belt). Scale bar is 1mm.

C. Section view of interlayered pebble conglomerate and bioclastic grainstone. Conglomerate matrix consists of bioclastic grainstone (Section 5; central Blind Fiord belt). Lens cap is 6cm wide.

D. Polished slab of pebble conglomerate with bioclastic grainstone matrix. Larger components include limestone extraclasts (Ex), as well as rugose coral (Co) and echinoderm (Ec) fragments (Section 5; central Blind Fiord belt). Scale bar is 1cm.

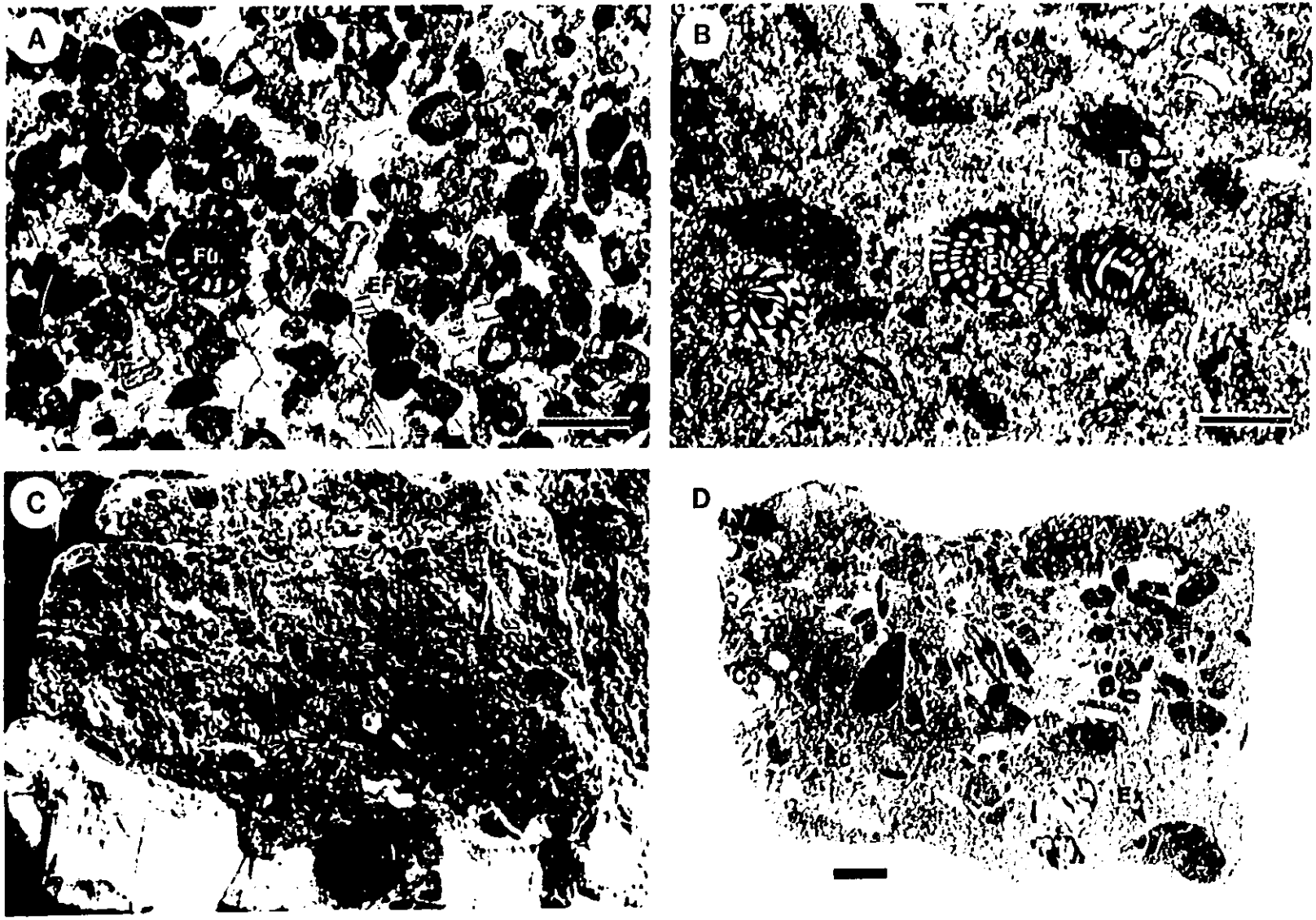
A
FU
EF
B
To
C
D
E

PLATE 14

Limestone assemblage

A. Photomicrograph of fusulinacean-beresellid microfacies in grainstone/packstone. Beresellid green algae (Be), fusulinacean foraminifers, small benthic foraminifers (including bradyinids (Bd)), encrusting foraminifers, and ungdarellid red algae (Un) are the most common framework elements (Section 10; northeastern Trold Fiord belt). Scale bar is 1mm.

B. Photomicrograph of fusulinacean-beresellid microfacies in grainstone/packstone. Beresellid algae are abundant (white arrows), along with fusulinacean (Fu), encrusting, and small benthic foraminifers, ungdareliid algae, ostracods and calcispheres (Section 7; southern Trold Fiord belt). Scale bar is 0.5mm.

C. Photomicrograph of fusulinacean microfacies in wackestone. Fusulinids, echinoderms (Ec) and brachiopods are abundant, along with common bryozoans, small benthic and encrusting foraminifers, and ungdarellid algae (Section 8; southern Blind Fiord belt). Scale bar is 2mm.

D. Photomicrograph of fusulinacean microfacies in wackestone. Fusulinids are associated with echinoderms (Ec) and ungdarellid algae (Un) (Section 8; southern Blind Fiord belt). Scale bar is 1mm.

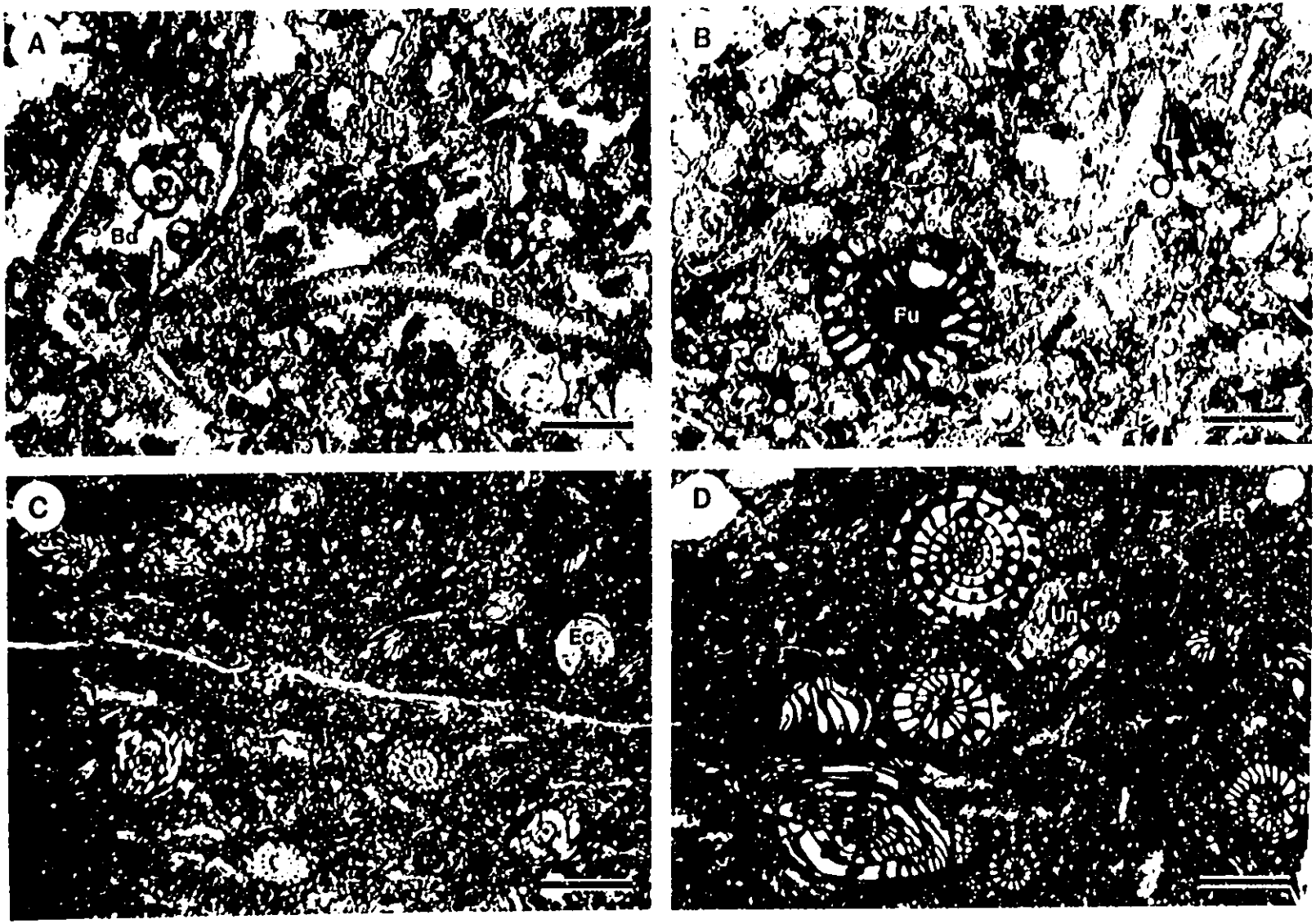
A
Bd
B
Fu
C
Ec
D
Un
Ec

APPENDIX 1: STRATIGRAPHIC SECTIONS

Schematic representation of measured sections. Conodont zones are based on Henderson (1988). Data for the 230m to 450m interval at Section 13 is from Beauchamp (1987). Paleocurrents show mean orientations for selected beds. MPS= maximum particle size, an average of the ten largest clasts from selected beds. Units less than 1m thick are not illustrated. Exposed facies boundaries are represented by solid lines; covered facies boundaries are represented by dashed lines. Symbols for lithologies, fossil groups, facies assemblages, and interpretation are listed in the following page.

CARBONATE FACIES

FOSSIL MICROFACIES

- SPICULITIC
- BRYOZOAN
- FUSULINACEAN
- BIOCLASTIC
- FUSULINACEAN/BERESELLID
- BERESELLID
- DASYCLADACEAN
- ENCRUSTING FORAMINIFERAL
- OSTRACOD

OTHERS

- OOID
- CALICHE
- PLANT TUFA

LITHOLOGIES

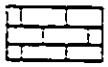
LIMESTONE

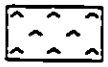
EVAPORITE

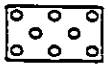
CONGLOMERATE

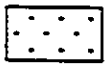
SANDSTONE


MUDSTONE

FACIES ASSEMBLAGES

LSA: LOWER SANDSTONE ASSEMBLAGE

CA: CONGLOMERATE ASSEMBLAGE

USA: UPPER SANDSTONE ASSEMBLAGE

EA: EVAPORITE ASSEMBLAGE

LA: LIMESTONE ASSEMBLAGE

INTERPRETATIONS

FP: FLOODPLAIN

PA PALUDAL

AF-BS: ALLUVIAL FAN / BRAIDED STREAM

FD: FAN-DELTA

BS: BRAIDED STREAM

CP: COASTAL PLAIN

PL: COASTAL PLAYA

HL: HYPERSALINE LAGOON

E-L: ESTUARINE / LAGOON

NS: HIGH ENERGY NEARSHORE

OM: OPEN MARINE

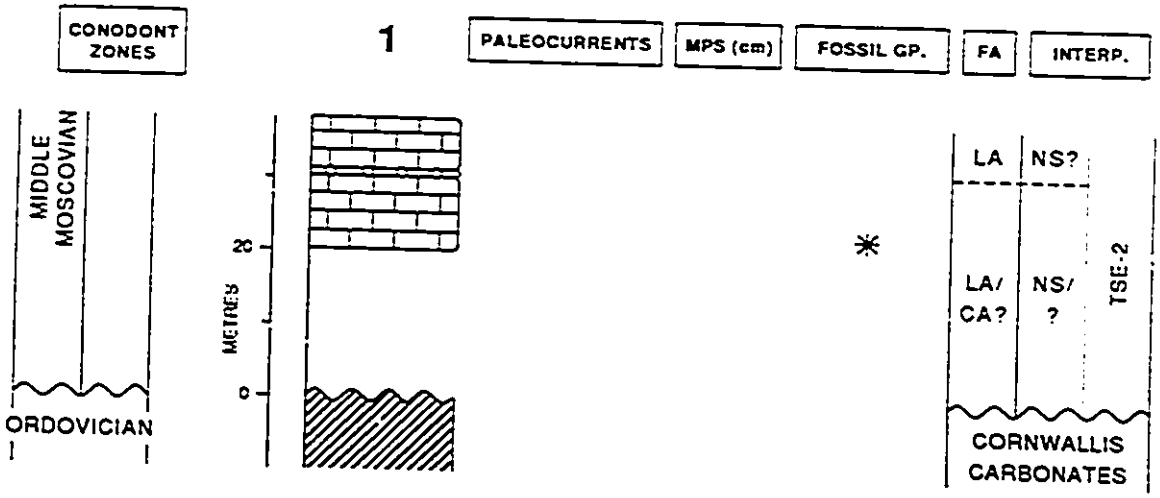
CONODONT ZONES
1
PALEOCURRENTS
MPS (cm)
FOSSIL GP.
FA
INTERP.
MIDDLE MOSCOVIAN
ORDOVICIAN
METRES
20
0
LA
NS?
LA/ CA?
NS/ ?
TSE-2
CORNWALLIS CARBONATES

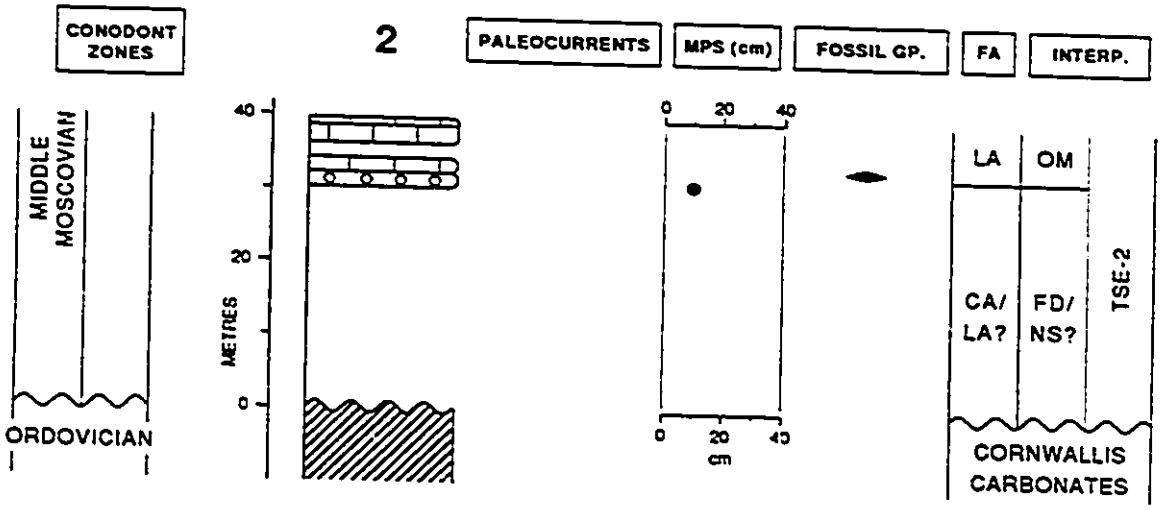
CONODONT ZONES
2
PALEOCURRENTS
MPS (cm)
FOSSIL GP.
FA
INTERP.
MIDDLE MOSCOVIAN
ORDOVICIAN
METRES
40
20
0
0
20
40
cm
LA
OM
CA/ LA?
FD/ NS?
TSE-2
CORNWALLIS CARBONATES

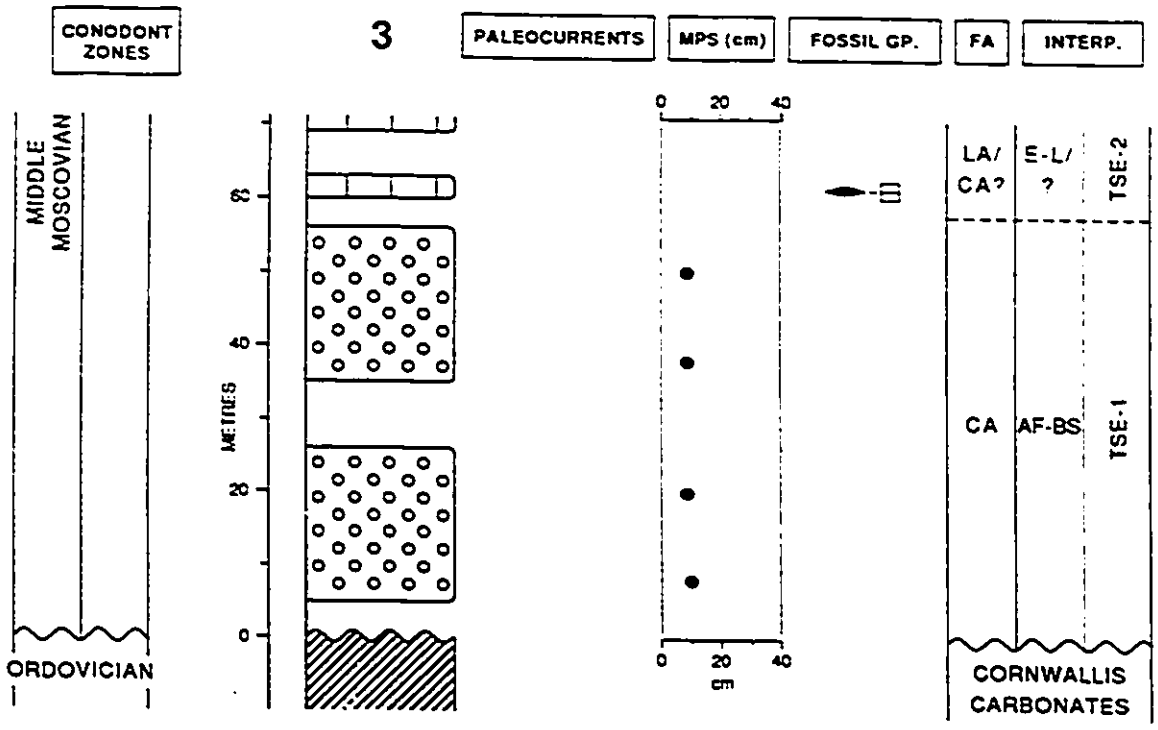
CONODONT ZONES
3
PALEOCURRENTS
MPS (cm)
FOSSIL GP.
FA
INTERP.
MIDDLE MOSCOVIAN
ORDOVICIAN
METRES
0
20
40
cm
LA/ CA?
E-L/ ?
TSE-2
CA
AF-BS
TSE-1
CORNWALLIS CARBONATES

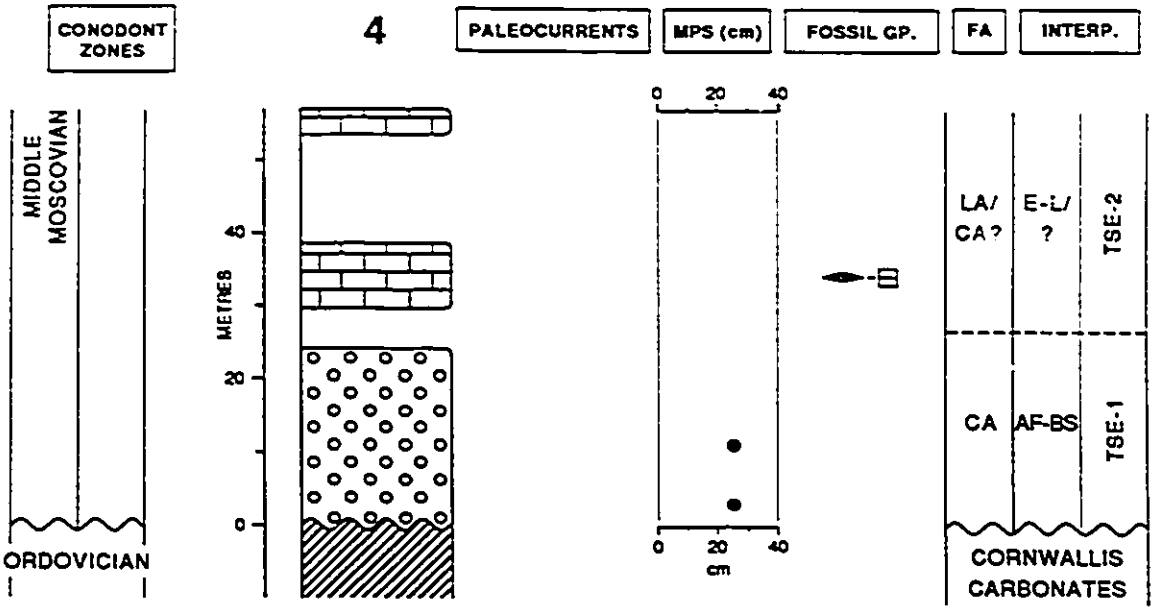
CONODONT ZONES
4
PALEOCURRENTS
MPS (cm)
FOSSIL GP.
FA
INTERP.
MIDDLE MOSCOVIAN
ORDOVICIAN
METRES
0
20
40
cm
LA/ CA?
E-L/ ?
TSE-2
CA
AF-BS
TSE-1
CORNWALLIS CARBONATES

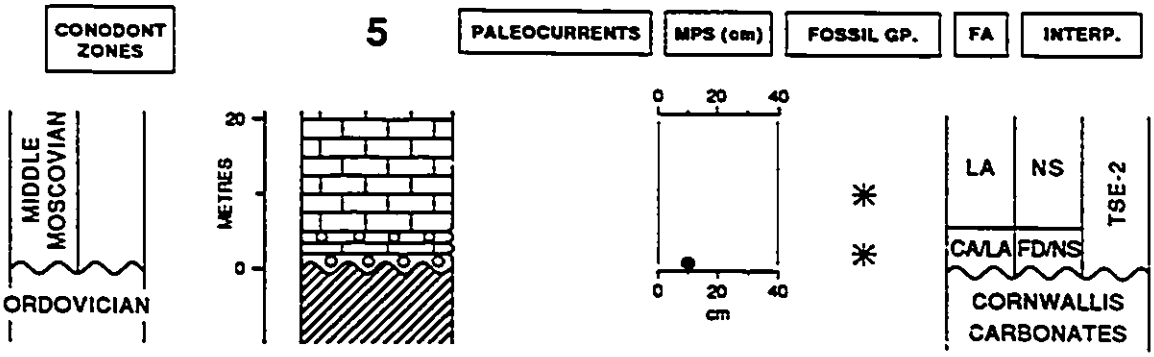
CONODONT ZONES
5
PALEOCURRENTS
MPS (cm)
FOSSIL GP.
FA
INTERP.
MIDDLE MOSCOVIAN
ORDOVICIAN
METRES
0
20
40
cm
LA
NS
TSE-2
CA/LA
FD/NS
CORNWALLIS CARBONATES

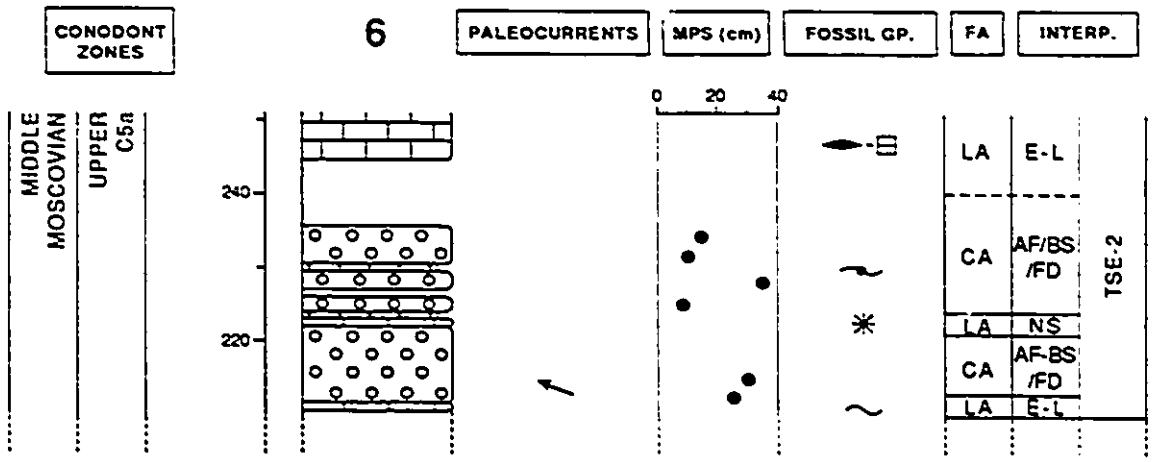
CONODONT ZONES
6
PALEOCURRENTS
MPS (cm)
FOSSIL GP.
FA
INTERP.
MIDDLE MOSCOVIAN
UPPER
C5a
240
220
0
20
40
LA
E-L
CA
AF/BS /FD
LA
NS
CA
AF-BS /FD
LA
E-L
TSE-2

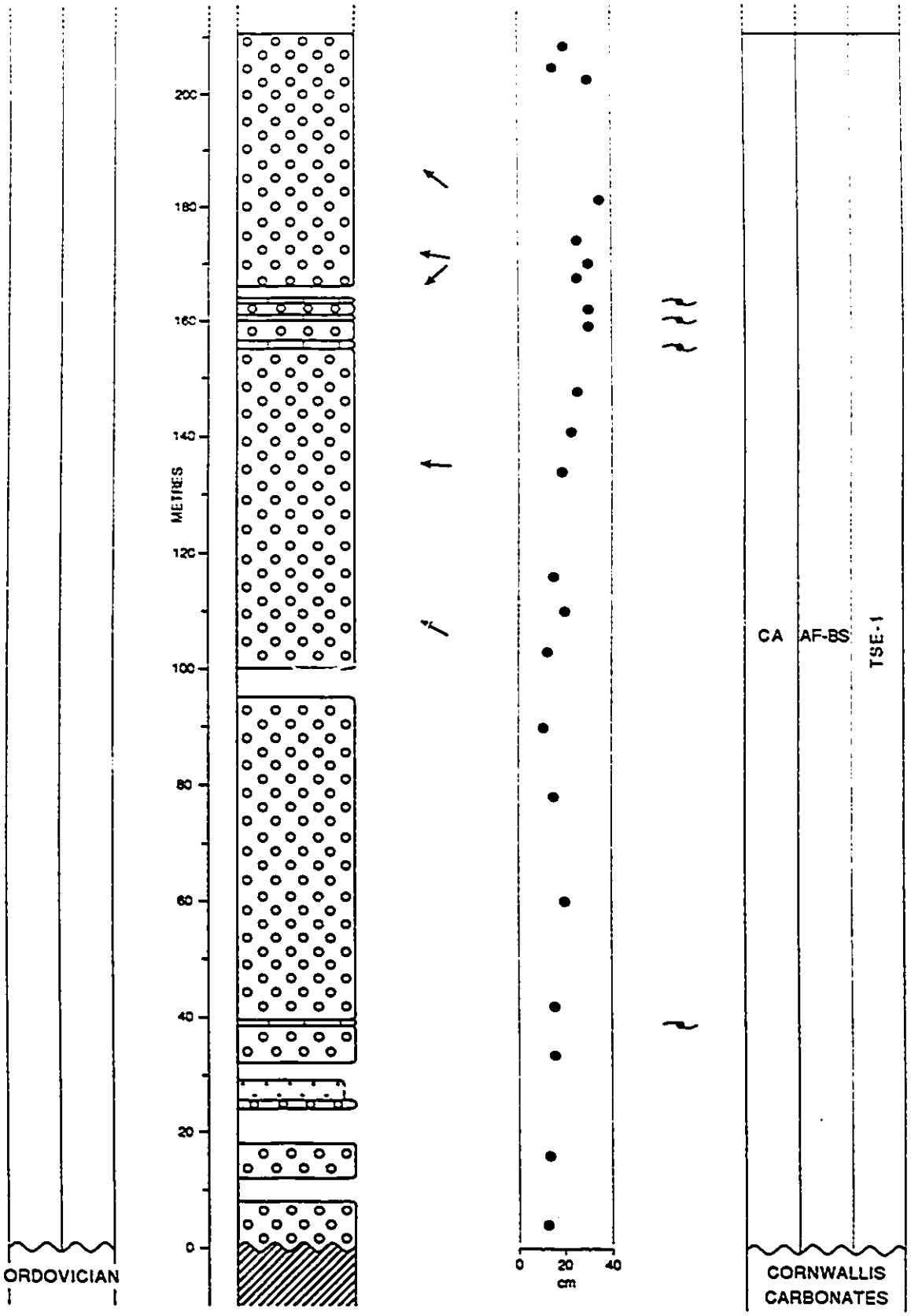
ORDOVICIAN
METRES
0
20
40
60
80
100
120
140
160
180
200
0
20
40
cm
CA
AF-BS
TSE-1
CORNWALLIS
CARBONATES

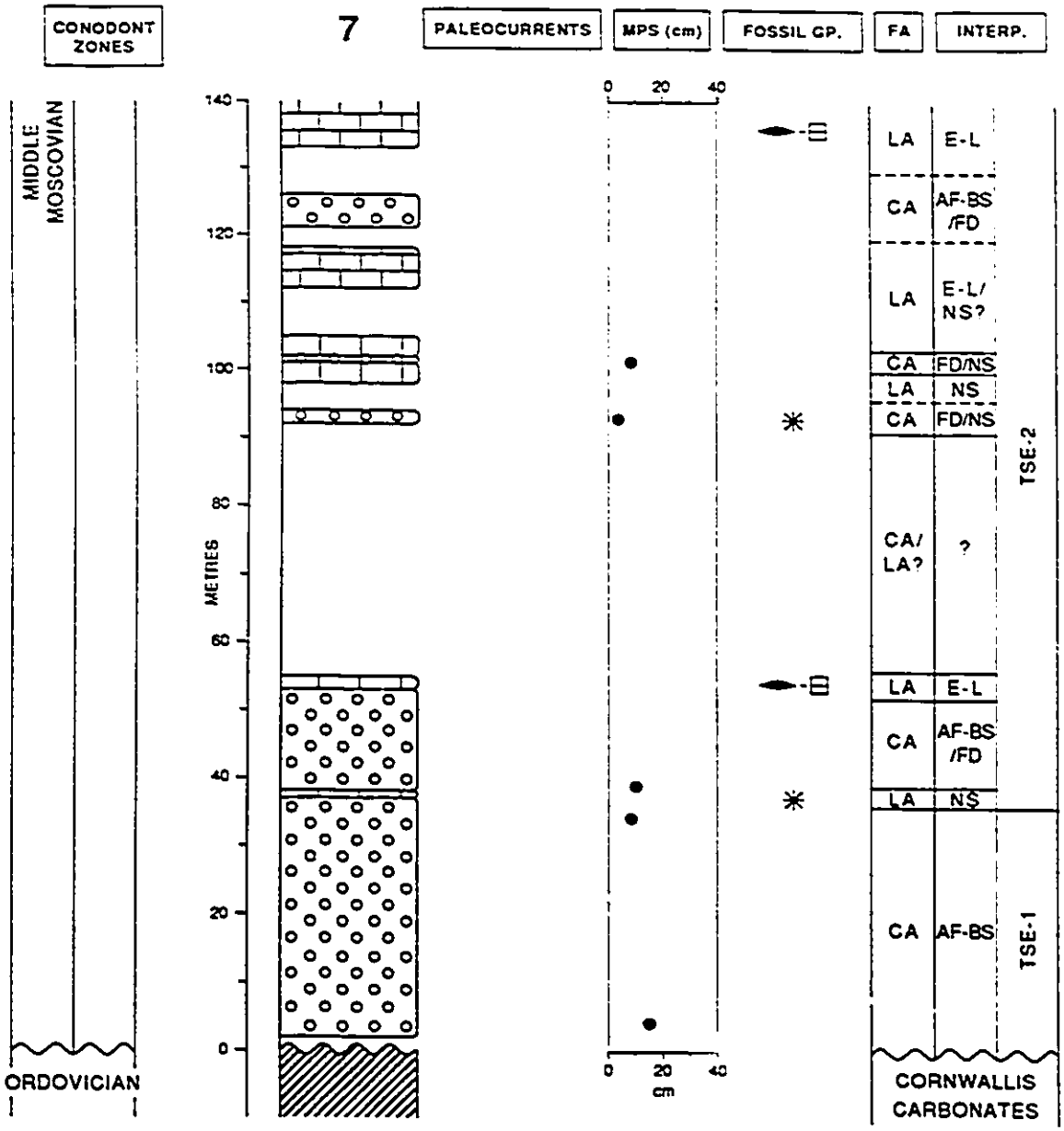
CONODONT ZONES
7
PALEOCURRENTS
MPS (cm)
FOSSIL GP.
FA
INTERP.
MIDDLE MOSCOVIAN
ORDOVICIAN
METRES
0
20
40
60
80
100
120
140
0
20
40
cm
LA
E-L
CA
AF-BS /FD
LA
E-L/ NS?
CA
FD/NS
LA
NS
CA
FD/NS
CA/ LA?
?
LA
E-L
CA
AF-BS /FD
LA
NS
CA
AF-BS
TSE-2
TSE-1
CORNWALLIS CARBONATES

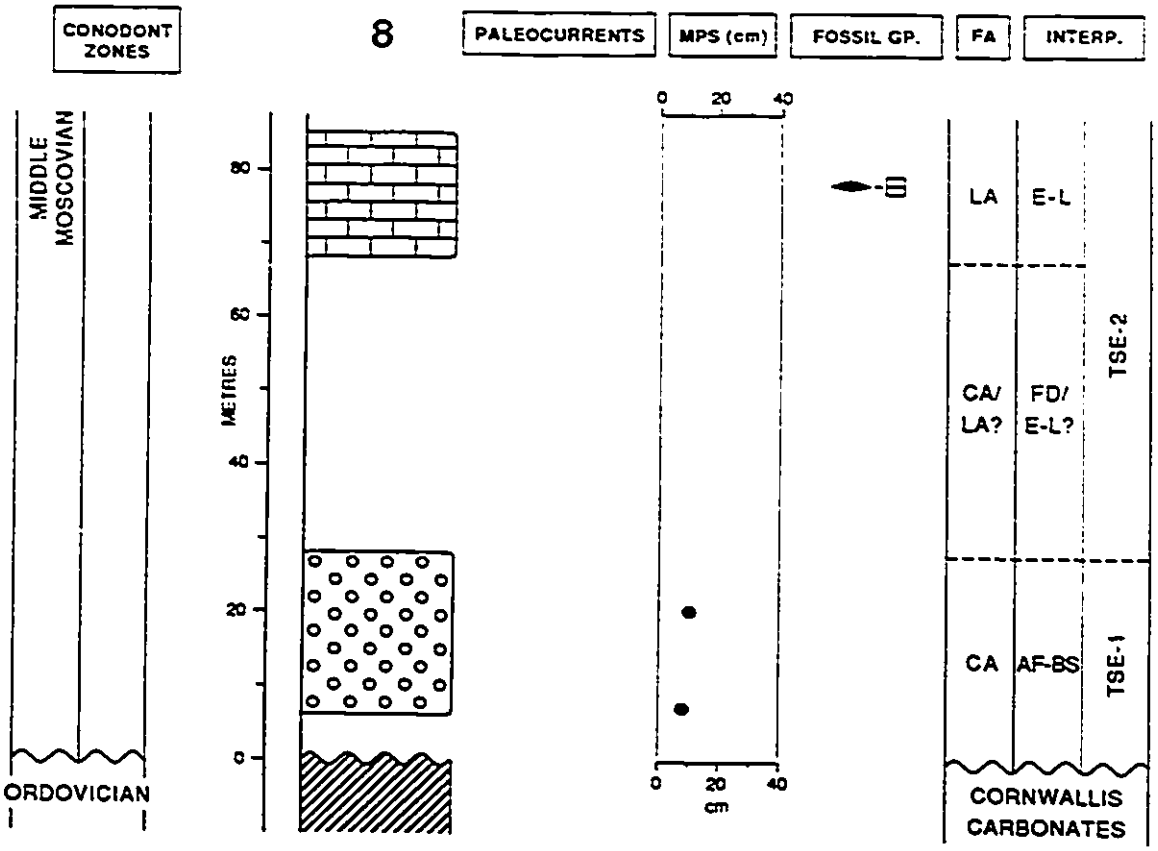
CONODONT ZONES
8
PALEOCURRENTS
MPS (cm)
FOSSIL GP.
FA
INTERP.
MIDDLE MOSCOVIAN
ORDOVICIAN
METRES
0
20
40
60
80
0
20
40
cm
LA
E-L
CA/ LA?
FD/ E-L?
CA
AF-BS
TSE-2
TSE-1
CORNWALLIS CARBONATES

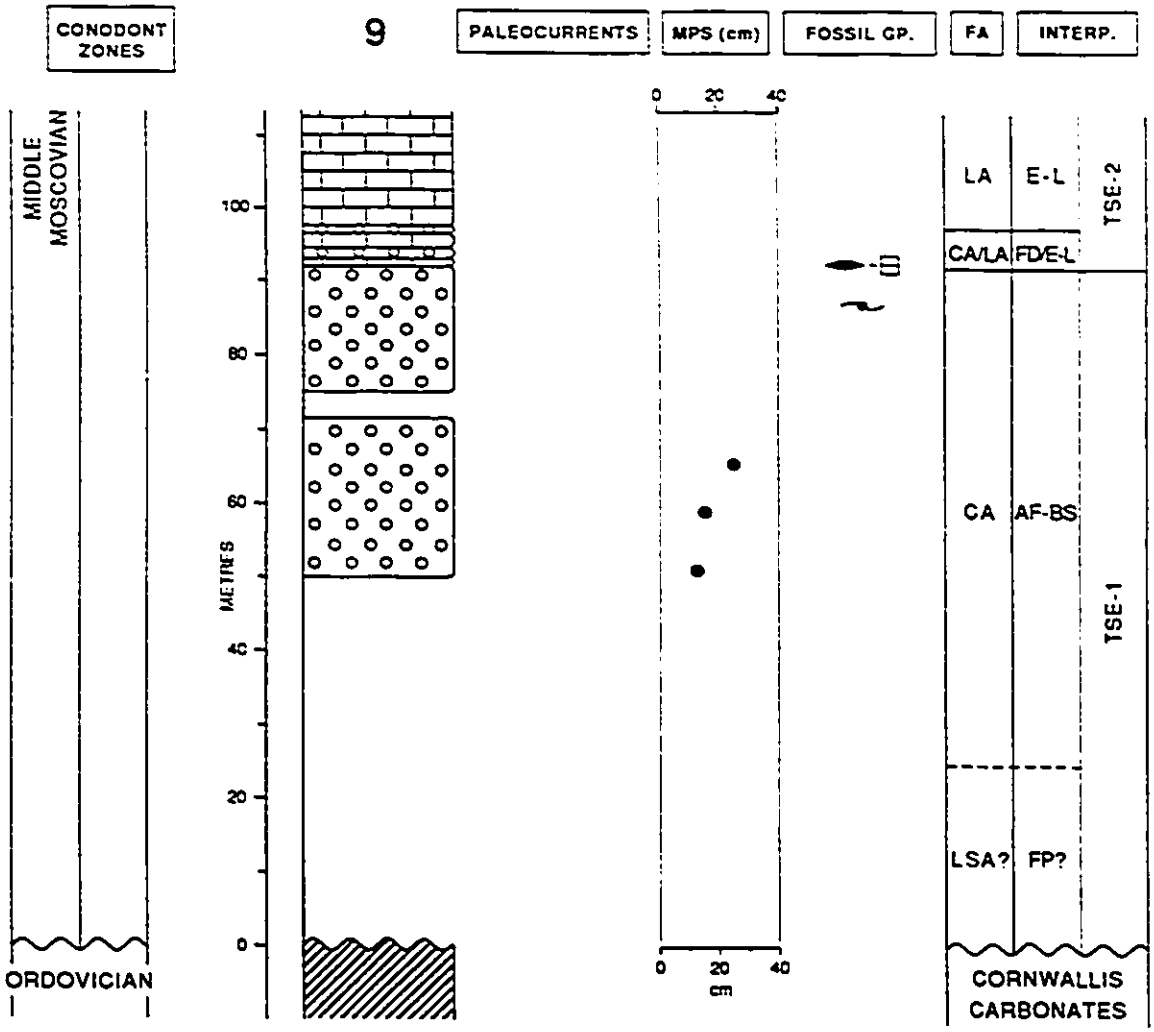
CONODONT ZONES
9
PALEOCURRENTS
MPS (cm)
FOSSIL GP.
FA
INTERP.
MIDDLE MOSCOVIAN
ORDOVICIAN
METRES
0
20
40
60
80
100
cm
LA
E-L
CA/LA
FD/E-L
CA
AF-BS
LSA?
FP?
TSE-2
TSE-1
CORNWALLIS CARBONATES

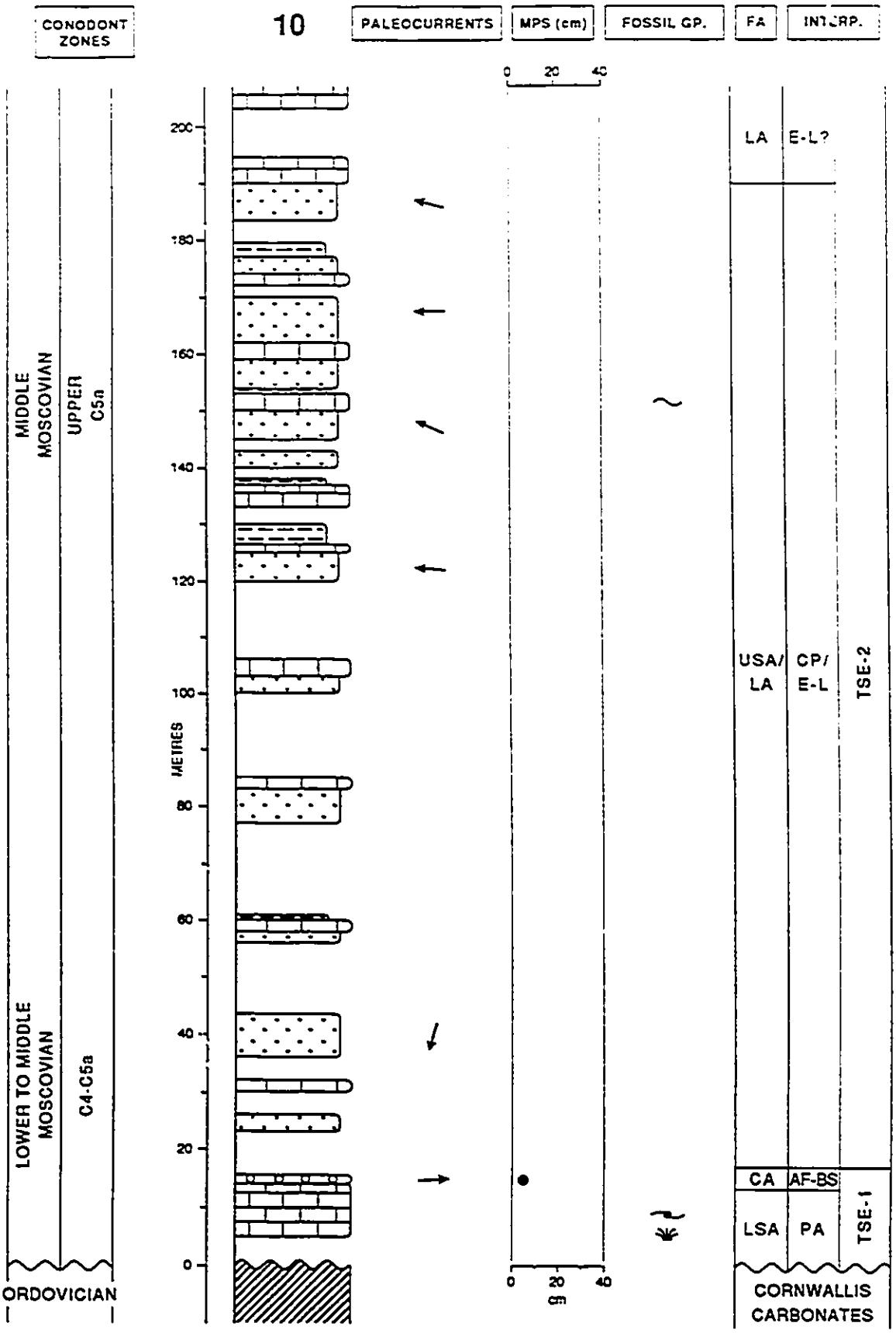
CONODONT ZONES
10
PALEOCURRENTS
MPS (cm)
FOSSIL GP.
FA
INTERP.
MIDDLE MOSCOVIAN
UPPER
C5a
LOWER TO MIDDLE MOSCOVIAN
C4-C5a
ORDOVICIAN
METRES
200
180
160
140
120
100
80
60
40
20
0
0
20
40
mm
LA
E-L?
USA/ LA
CP/ E-L
TSE-2
CA
AF-BS
LSA
PA
TSE-1
CORNWALLIS CARBONATES

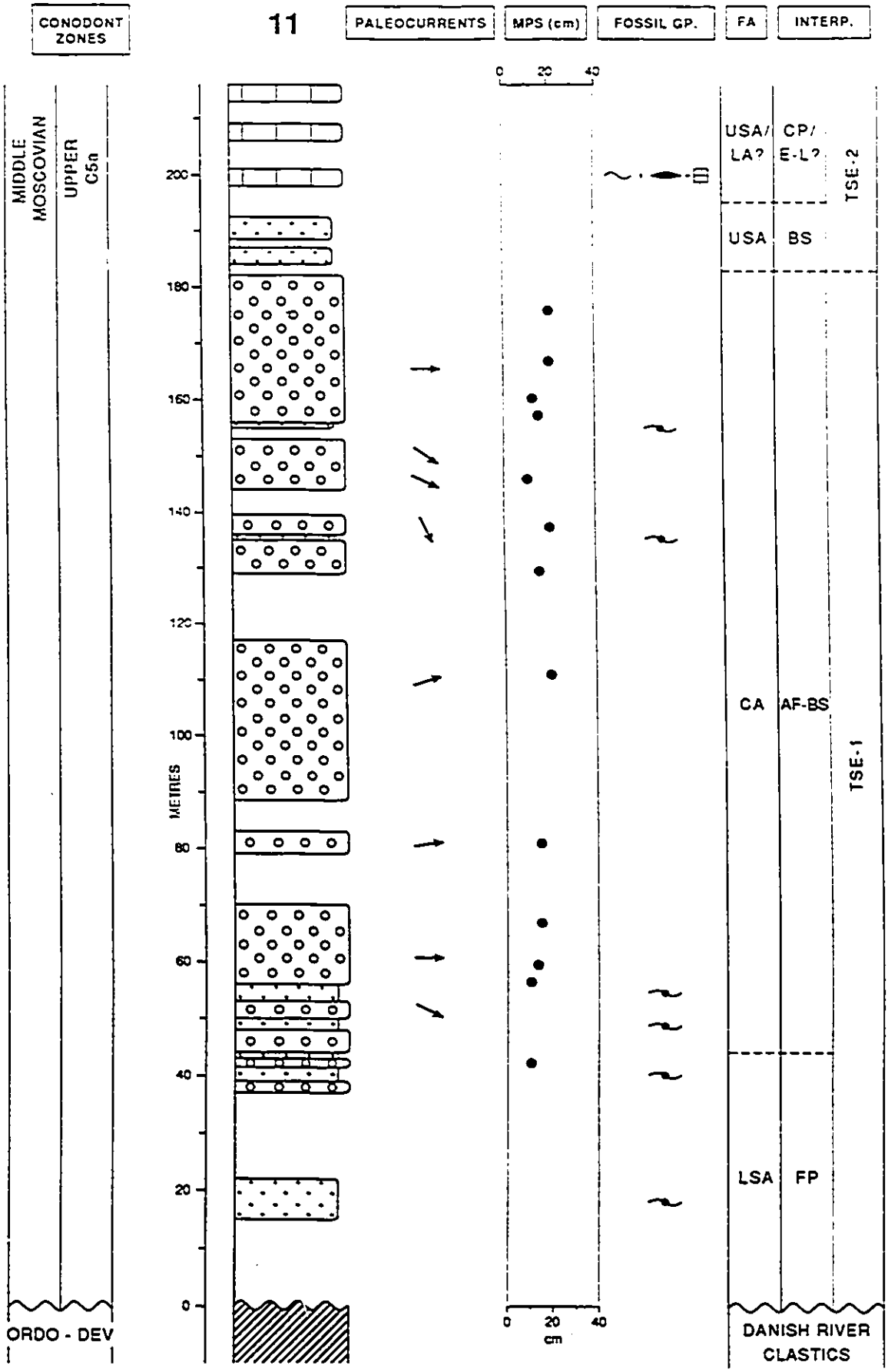
CONODONT ZONES
11
PALEOCURRENTS
MPS (cm)
FOSSIL GP.
FA
INTERP.
MIDDLE MOSCOVIAN
UPPER C5n
METRES
0
20
40
60
80
100
120
140
160
180
200
0
20
40
cm
USA/ LA?
CP/ E-L?
TSE-2
USA
BS
CA
AF-BS
TSE-1
LSA
FP
ORDO - DEV
DANISH RIVER CLASTICS

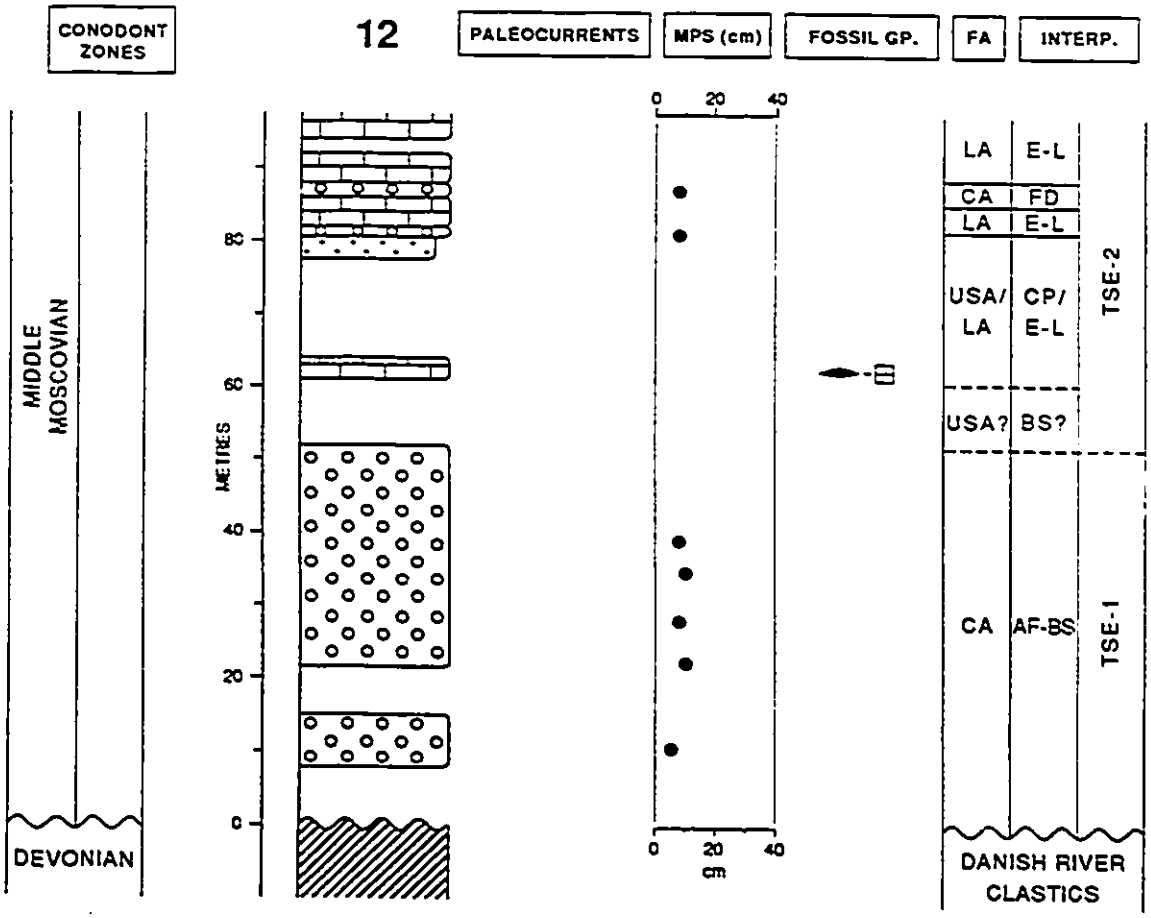
CONODONT ZONES
12
PALEOCURRENTS
MPS (cm)
FOSSIL GP.
FA
INTERP.
MIDDLE MOSCOVIAN
DEVONIAN
METRES
0
20
40
60
80
0
20
40
cm
LA
E-L
CA
FD
LA
E-L
USA/ LA
CP/ E-L
TSE-2
USA?
BS?
CA
AF-BS
TSE-1
DANISH RIVER CLASTICS

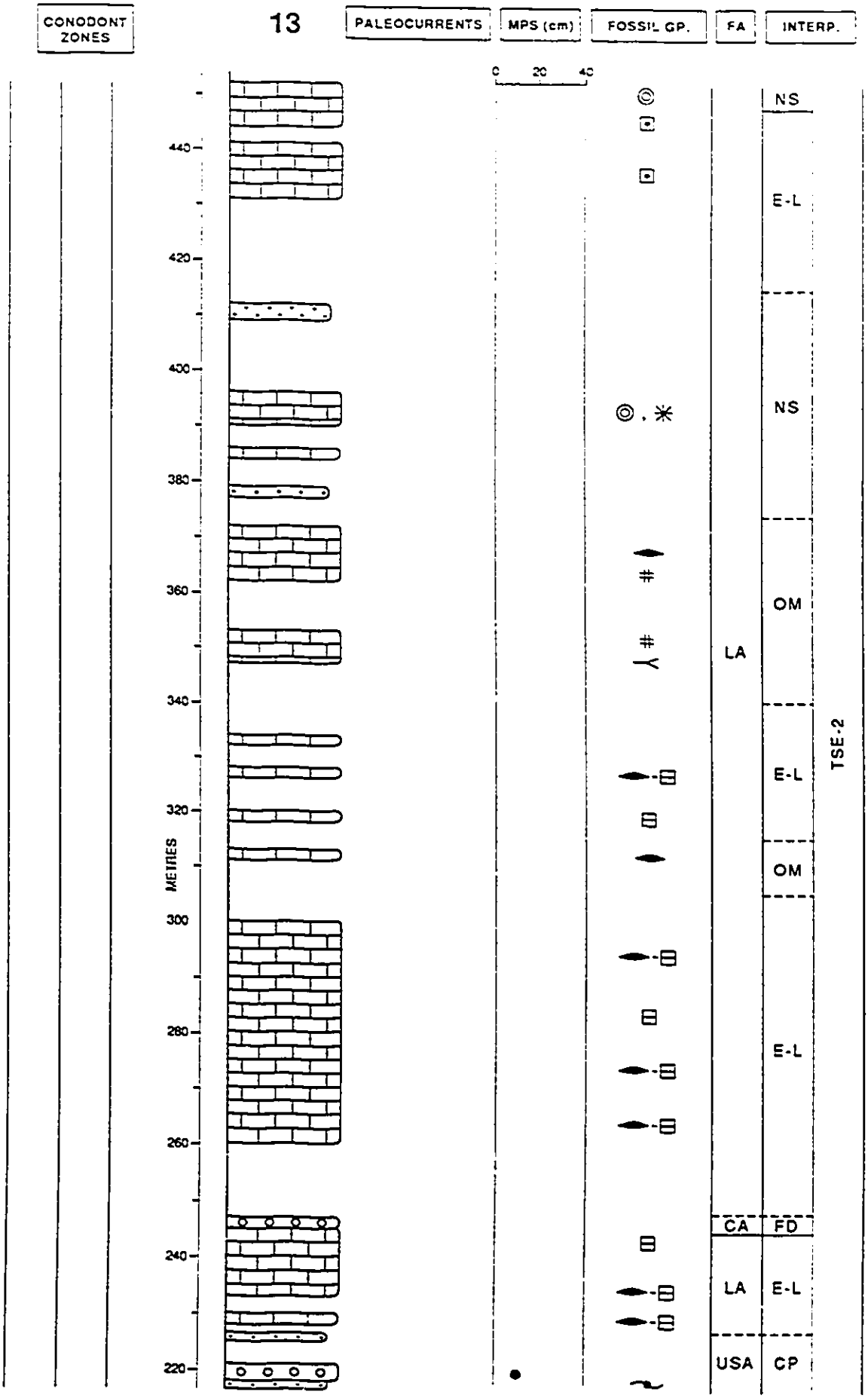
CONODONT ZONES
13
PALEOCURRENTS
MPS (cm)
0
20
40
FOSSIL GP.
FA
INTERP.
METRES
440
420
400
380
360
340
320
300
280
260
240
220
NS
E-L
NS
OM
LA
E-L
OM
E-L
TSE-2
CA
FD
LA
E-L
USA
CP

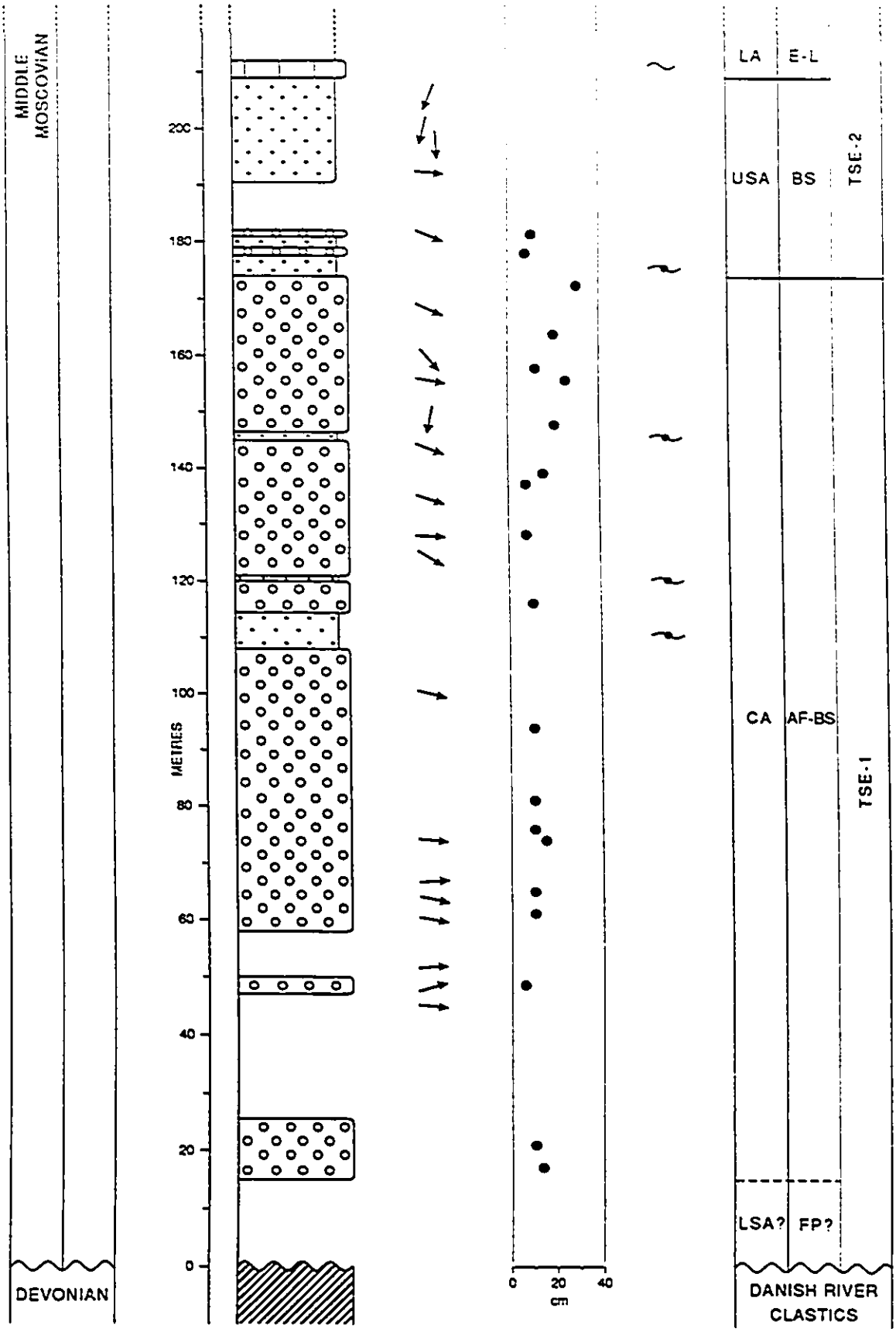
MIDDLE MOSCOVIAN
DEVONIAN
METRES
0
20
40
60
80
100
120
140
160
180
200
0
20
40
GR
LA
E-L
USA
BS
TSE-2
CA
AF-BS
TSE-1
LSA?
FP?
DANISH RIVER CLASTICS

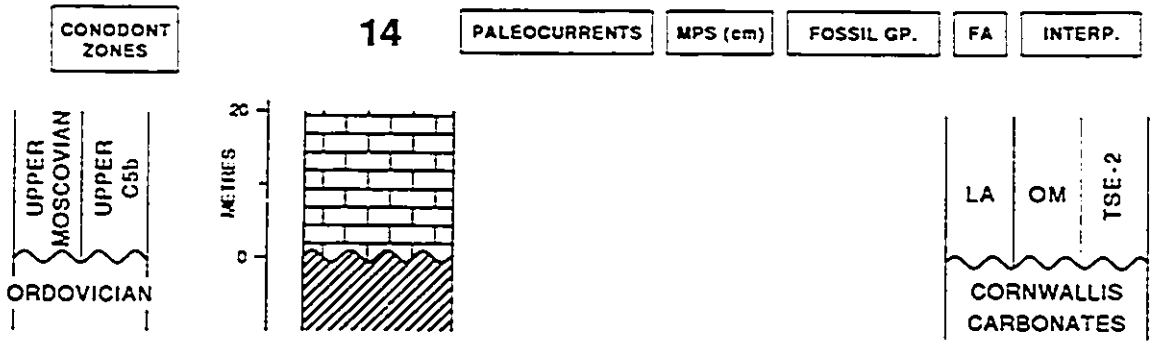
CONODONT ZONES
14
PALEOCURRENTS
MPS (cm)
FOSSIL GP.
FA
INTERP.
UPPER MOSCOVIAN
UPPER C5b
ORDOVICIAN
METRES
20
0
LA
OM
TSE-2
CORNWALLIS CARBONATES

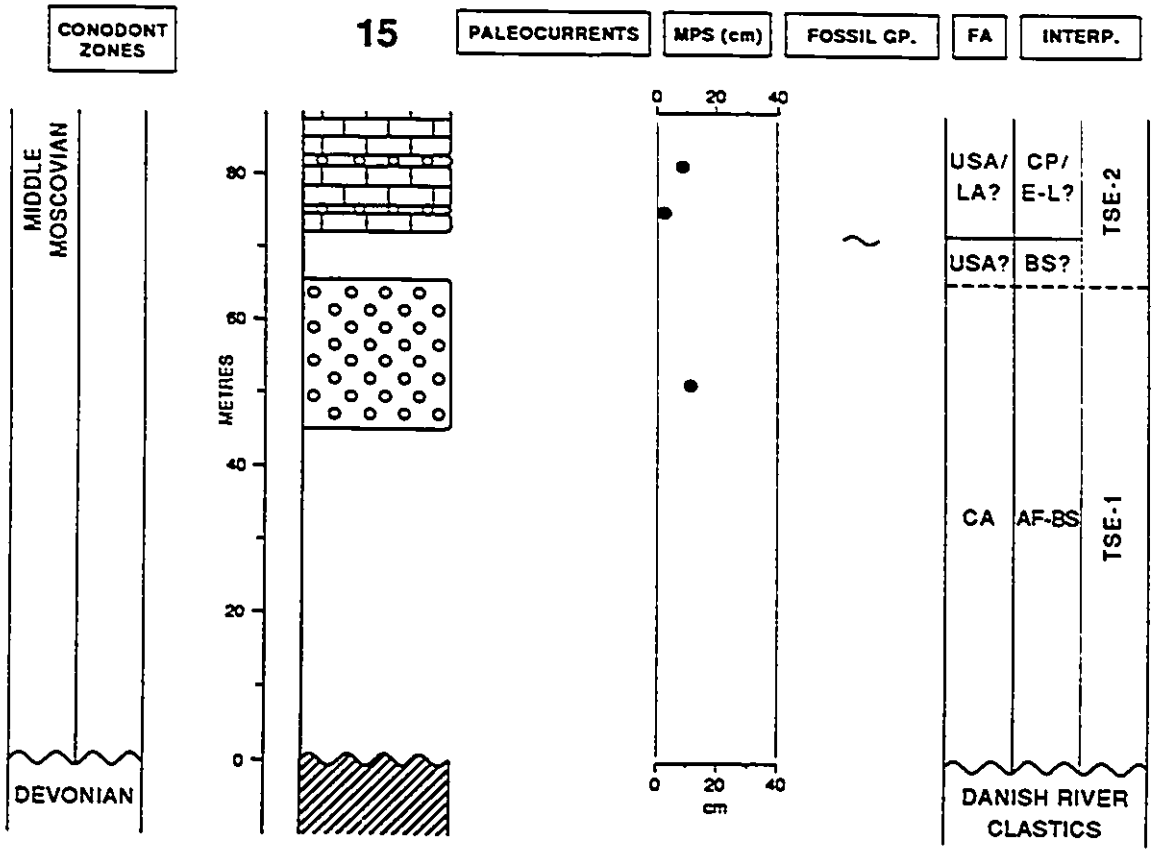
CONODONT ZONES
15
PALEOCURRENTS
MPS (cm)
FOSSIL GP.
FA
INTERP.
MIDDLE MOSCOVIAN
DEVONIAN
METRES
80
60
40
20
0
0
20
40
cm
USA/ LA?
CP/ E-L?
TSE-2
USA?
BS?
CA
AF-BS
TSE-1
DANISH RIVER CLASTICS

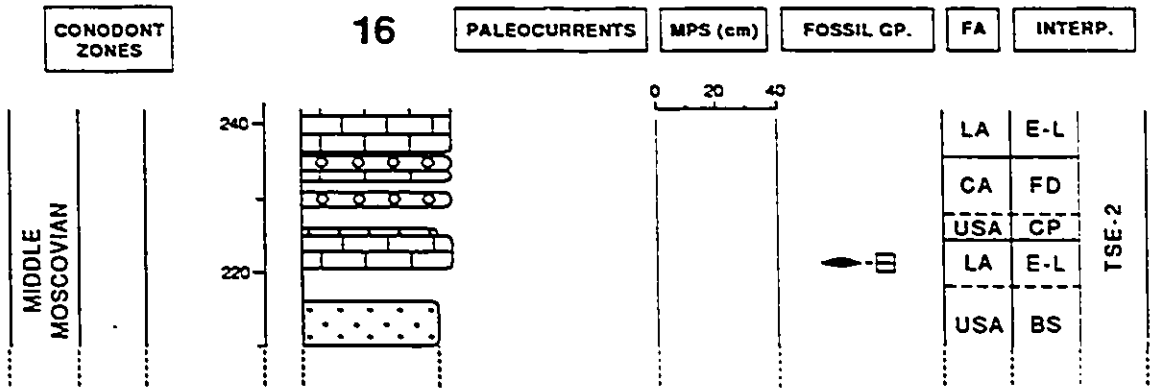
CONODONT ZONES
16
PALEOCURRENTS
MPS (cm)
FOSSIL GP.
FA
INTERP.
MIDDLE MOSCOVIAN
240
220
0
20
40
LA
E-L
CA
FD
USA
CP
LA
E-L
USA
BS
TSE-2

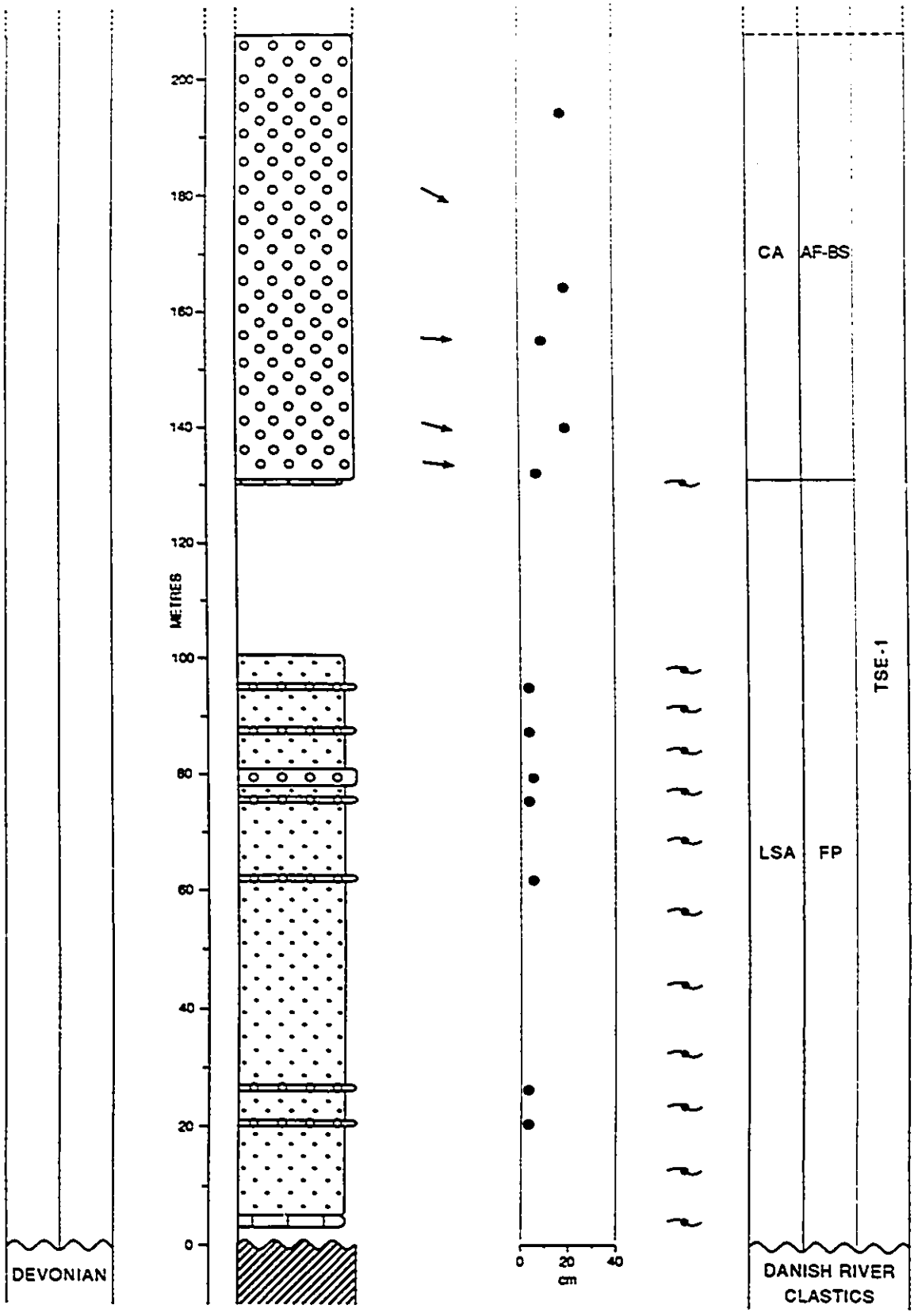
DEVONIAN
METRES
200
180
160
140
120
100
80
60
40
20
0
0
20
40
cm
CA
AF-BS
LSA
FP
TSE-1
DANISH RIVER
CLASTICS

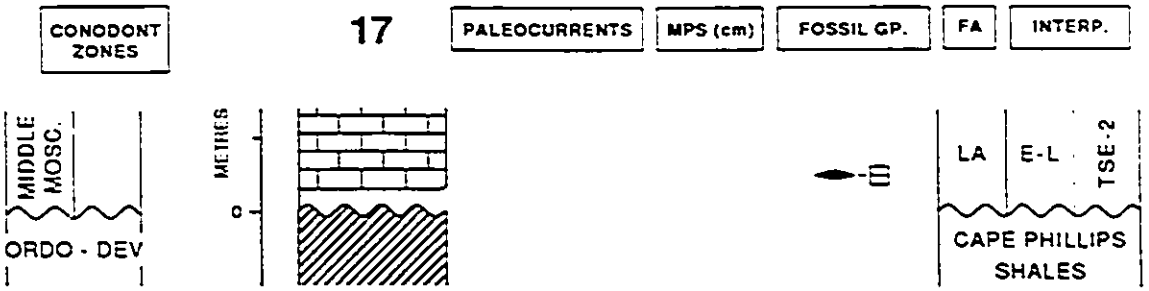
CONODONT ZONES
17
PALEOCURRENTS
MPS (cm)
FOSSIL GP.
FA
INTERP.
MIDDLE MOSC.
ORDO - DEV
METRES
0
LA
E-L
TSE-2
CAPE PHILLIPS SHALES

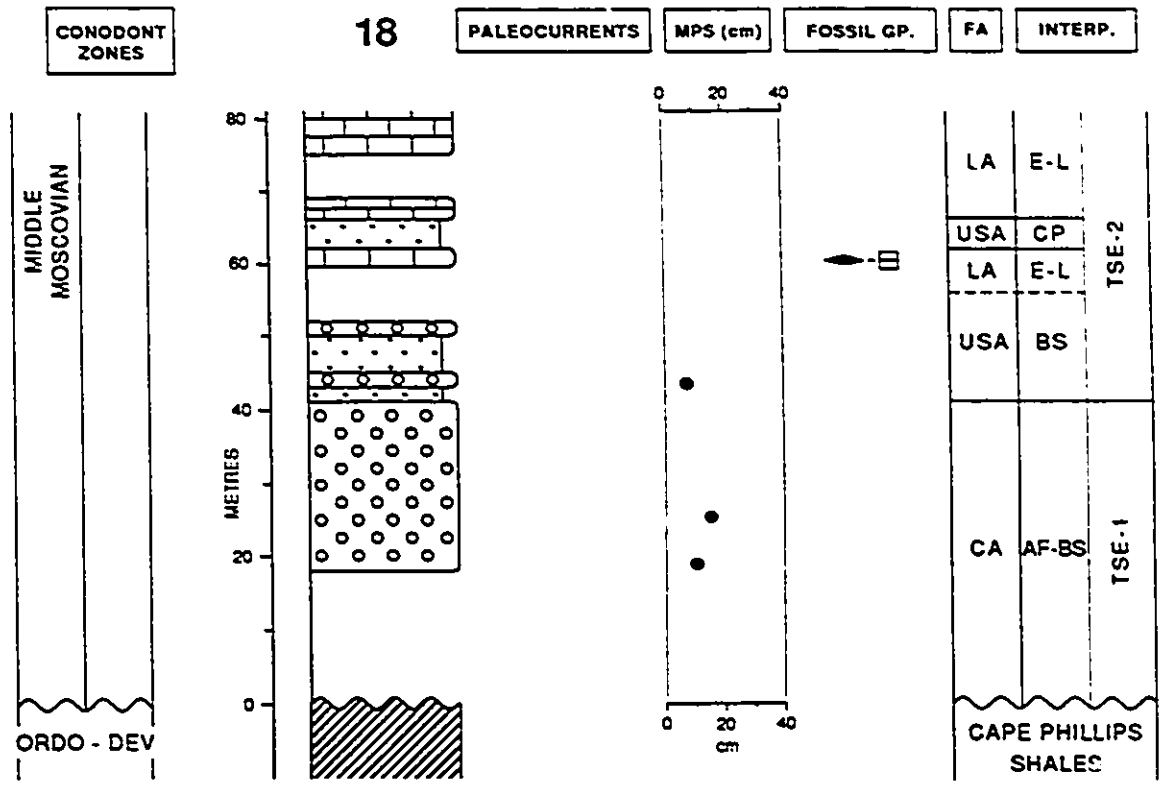
CONODONT ZONES
18
PALEOCURRENTS
MPS (cm)
FOSSIL GP.
FA
INTERP.
MIDDLE MOSCOVIAN
ORDO - DEV
METRES
80
60
40
20
0
0
20
40
cm
LA
E-L
USA
CP
LA
E-L
USA
BS
CA
AF-BS
TSE-2
TSE-1
CAPE PHILLIPS SHALES

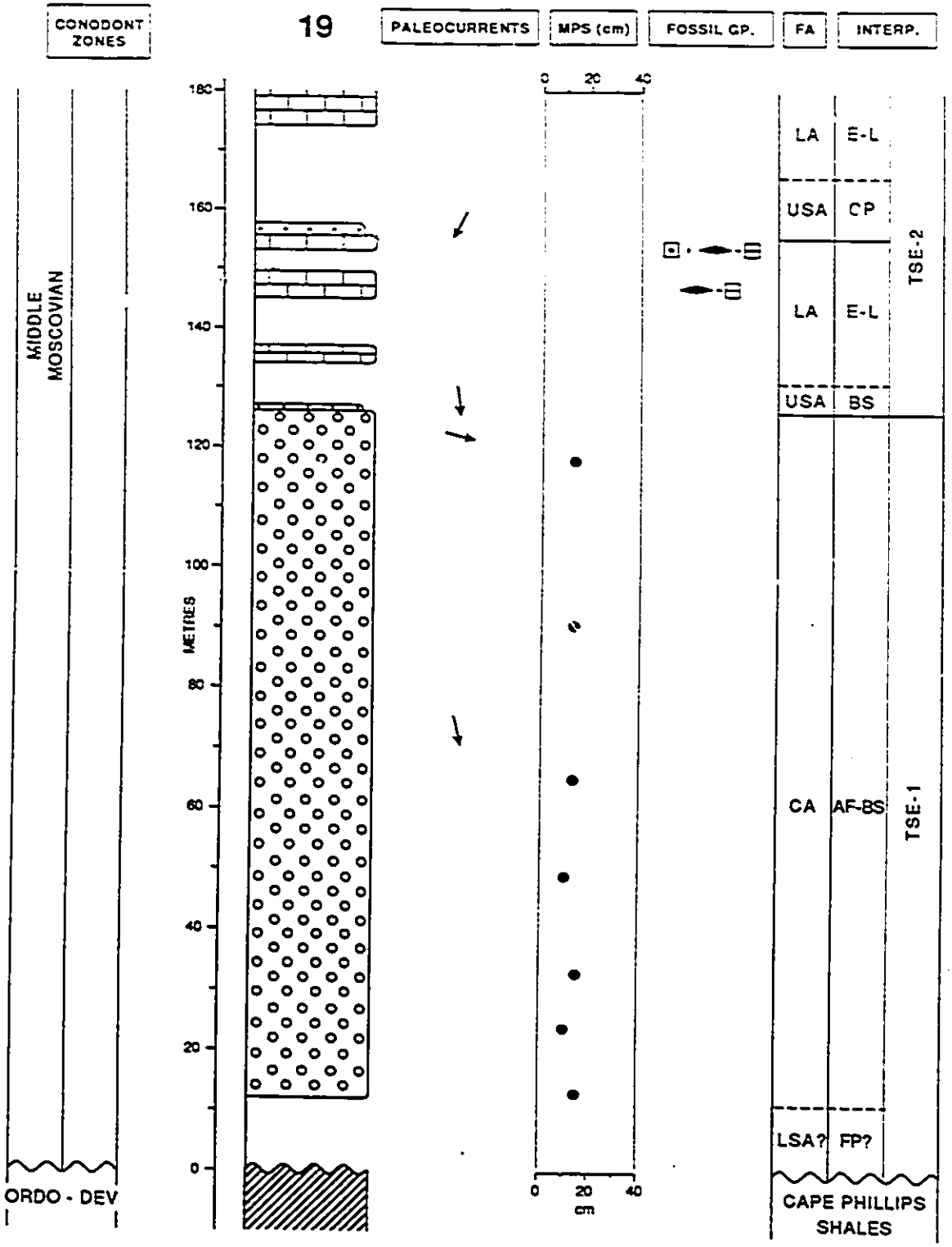
CONODONT ZONES
19
PALEOCURRENTS
MPS (cm)
FOSSIL GP.
FA
INTERP.
MIDDLE MOSCOVIAN
ORDO - DEV
METRES
180
160
140
120
100
80
60
40
20
0
0
20
40
cm
LA
E-L
USA
CP
LA
E-L
USA
BS
CA
AF-BS
LSA?
FP?
TSE-2
TSE-1
CAPE PHILLIPS SHALES

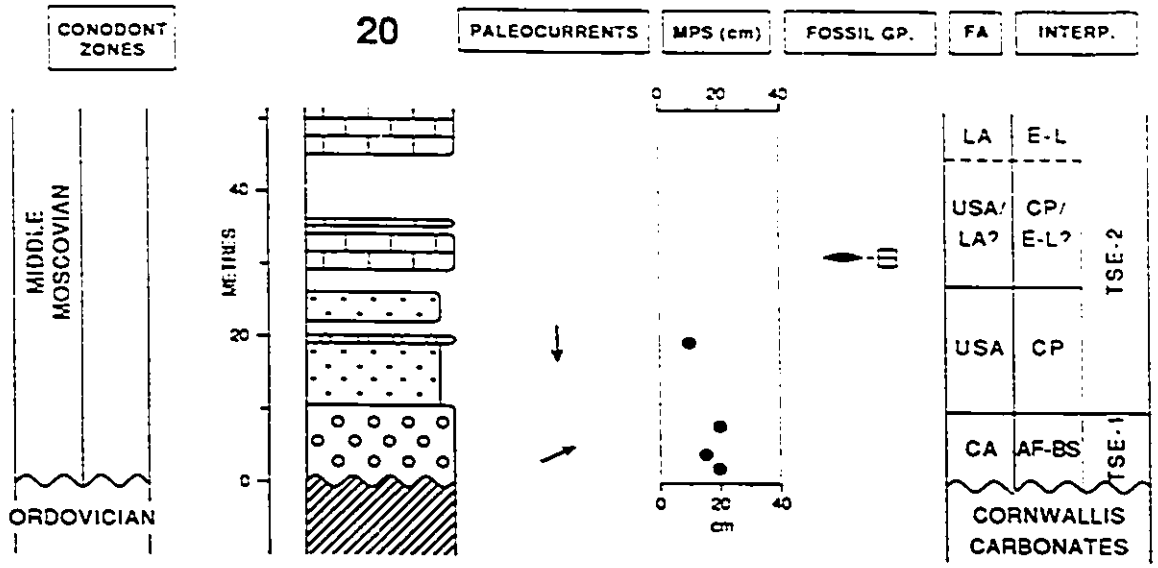
CONODONT ZONES
20
PALEOCURRENTS
MPS (cm)
FOSSIL GP.
FA
INTERP.
MIDDLE MOSCOVIAN
ORDOVICIAN
METRES
0
20
40
cm
LA
E-L
USA/ LA?
CP/ E-L?
USA
CP
CA
AF-BS
TSE-2
TSE-1
CORNWALLIS CARBONATES

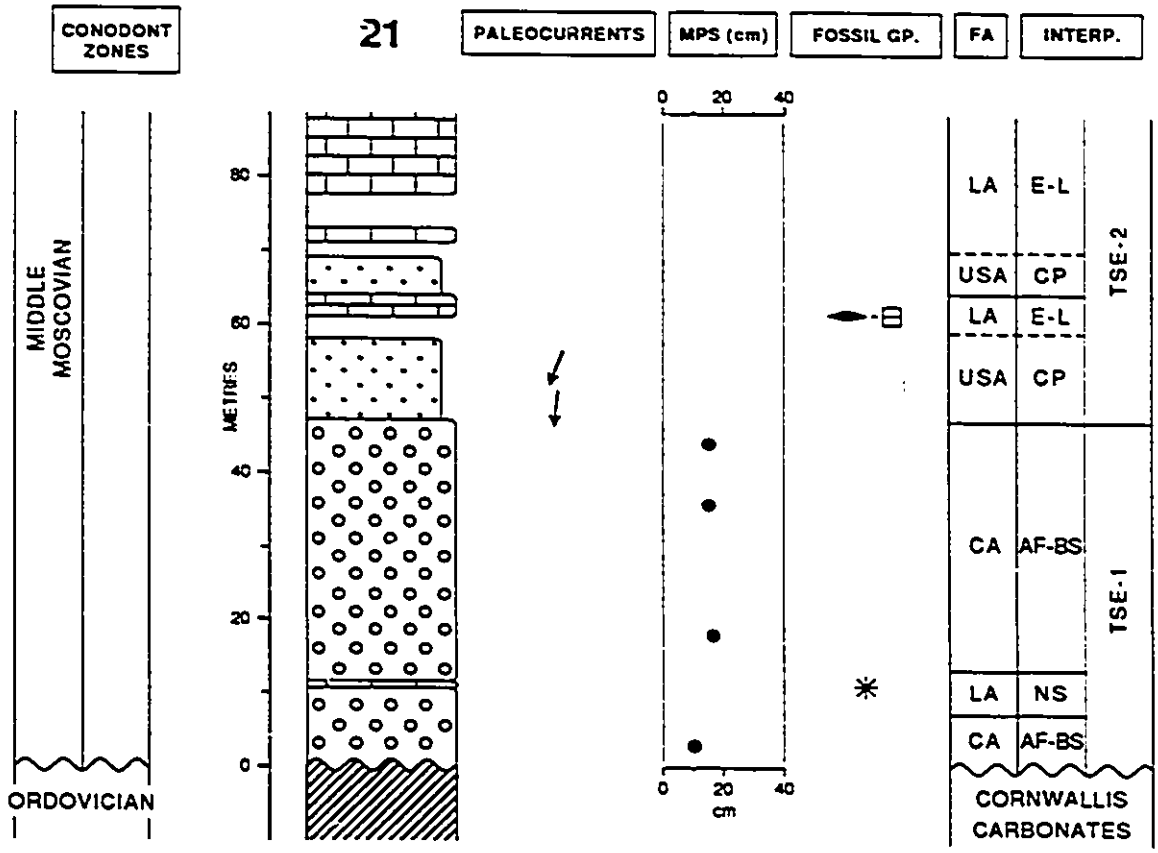
CONODONT ZONES
21
PALEOCURRENTS
MPS (cm)
FOSSIL GP.
FA
INTERP.
MIDDLE MOSCOVIAN
ORDOVICIAN
METRES
0
20
40
60
80
cm
LA
E-L
USA
CP
LA
E-L
USA
CP
CA
AF-BS
LA
NS
CA
AF-BS
TSE-2
TSE-1
CORNWALLIS CARBONATES

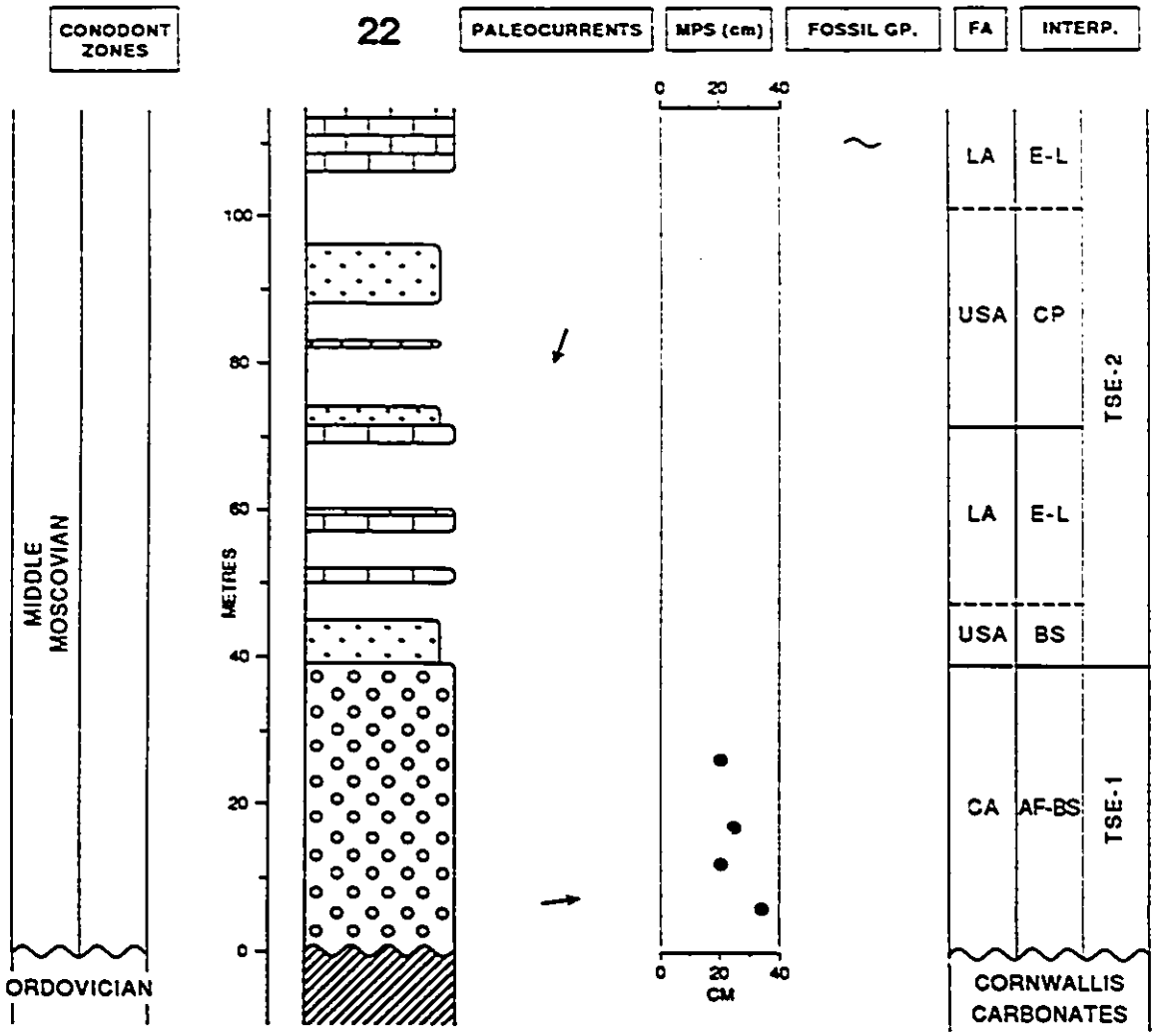
CONODONT ZONES
22
PALEOCURRENTS
MPS (cm)
FOSSIL GP.
FA
INTERP.
MIDDLE MOSCOVIAN
ORDOVICIAN
METRES
0
20
40
60
80
100
0
20
40
CM
LA
E-L
USA
CP
LA
E-L
USA
BS
CA
AF-BS
TSE-2
TSE-1
CORNWALLIS CARBONATES

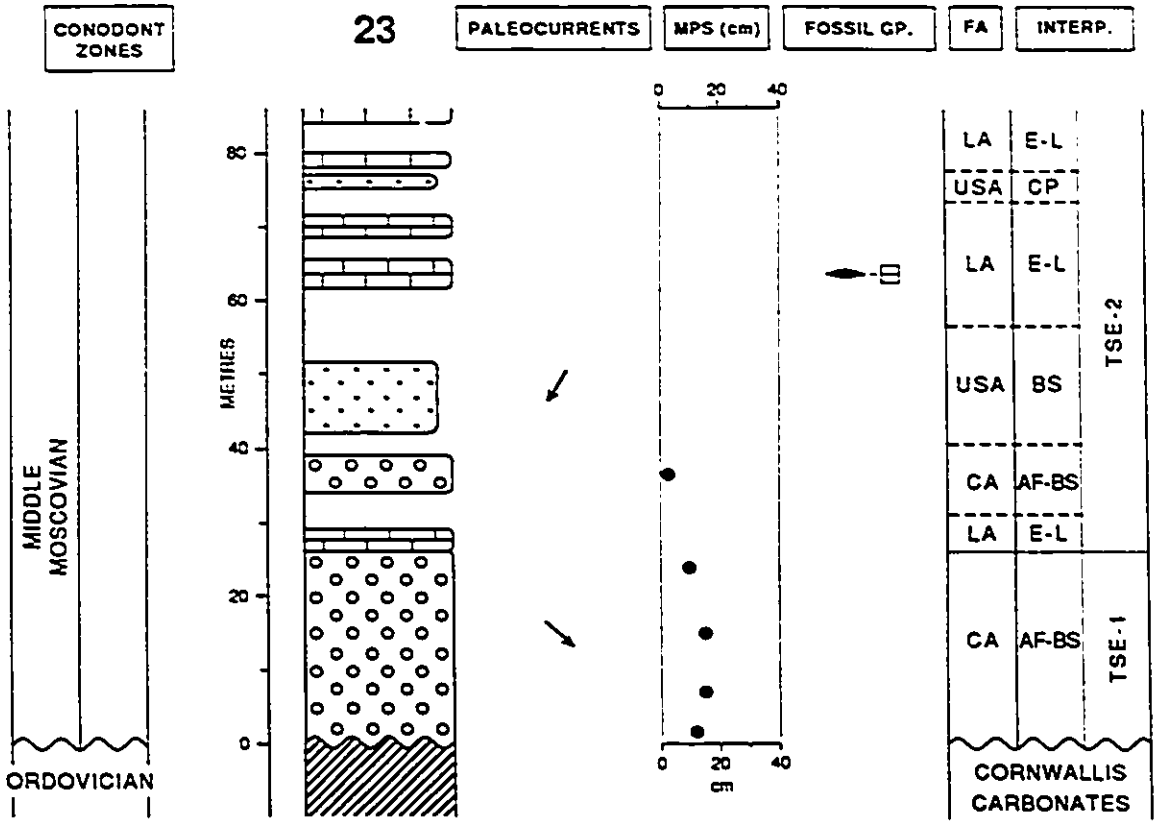
CONODONT ZONES
23
PALEOCURRENTS
MPS (cm)
FOSSIL GP.
FA
INTERP.
MIDDLE MOSCOVIAN
ORDOVICIAN
METRES
0
20
40
60
80
cm
LA
E-L
USA
CP
LA
E-L
USA
BS
CA
AF-BS
LA
E-L
CA
AF-BS
TSE-2
TSE-1
CORNWALLIS CARBONATES

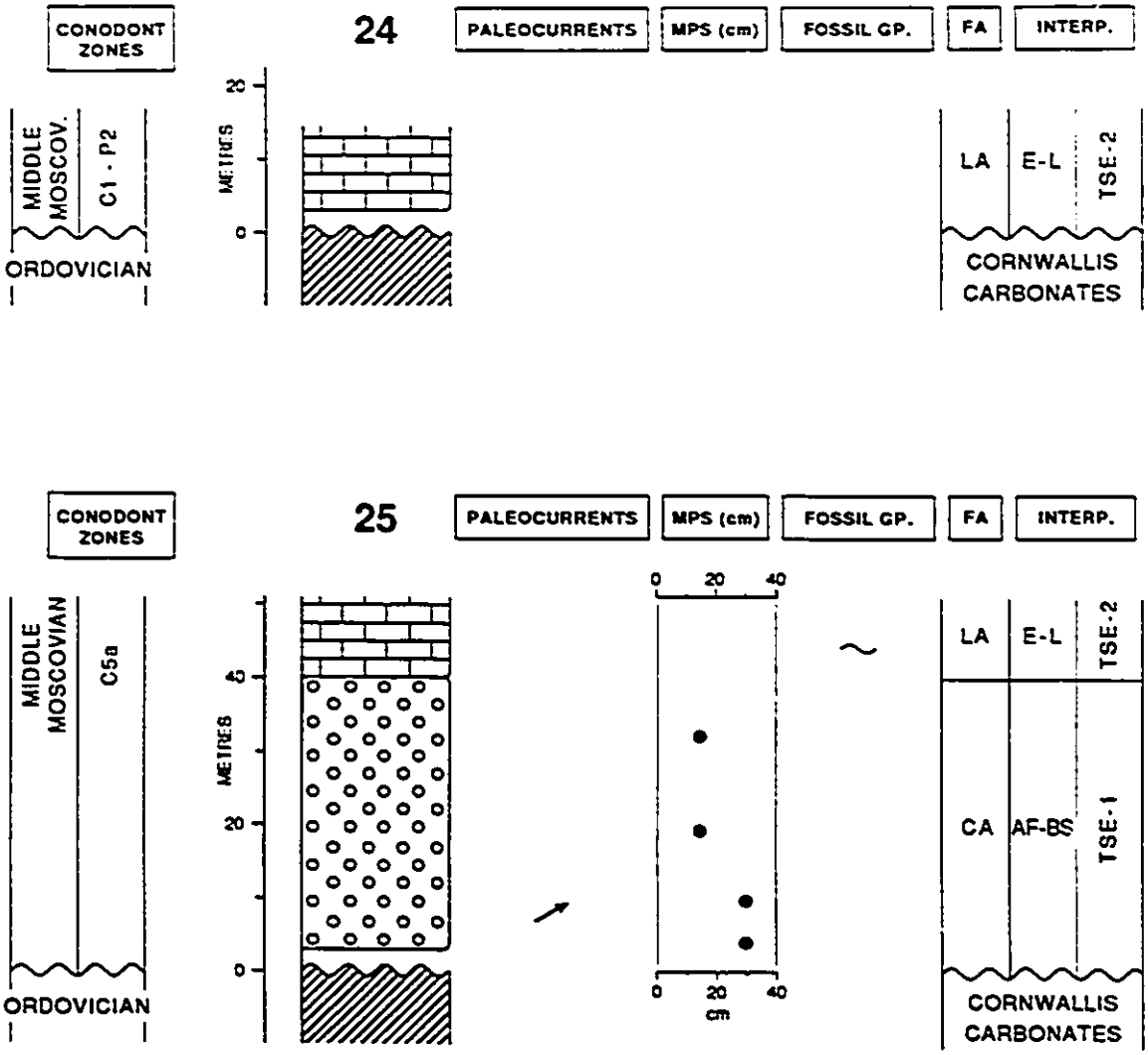
CONODONT ZONES
24
PALEOCURRENTS
MPS (cm)
FOSSIL GP.
FA
INTERP.
MIDDLE MOSCOV.
C1 - P2
ORDOVICIAN
METRES
20
0
LA
E-L
TSE-2
CORNWALLIS CARBONATES
CONODONT ZONES
25
PALEOCURRENTS
MPS (cm)
FOSSIL GP.
FA
INTERP.
MIDDLE MOSCOVIAN
C5a
ORDOVICIAN
METRES
40
20
0
0
20
40
cm
LA
E-L
TSE-2
CA
AF-BS
TSE-1
CORNWALLIS CARBONATES

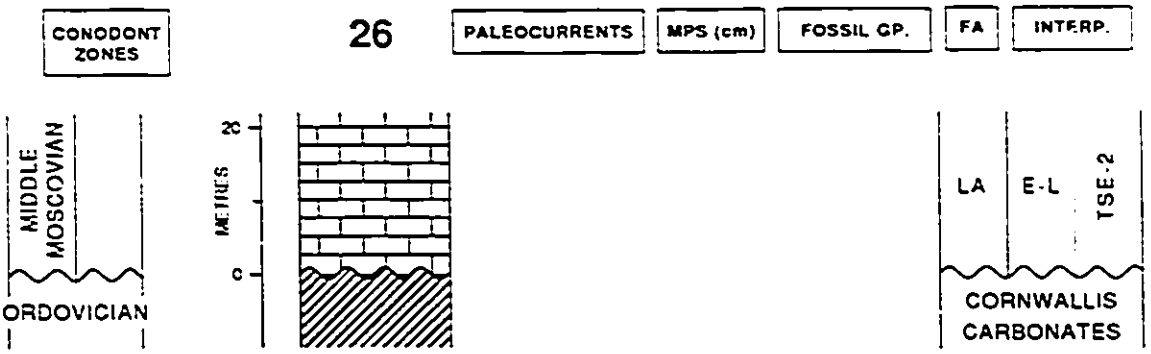
CONODONT ZONES
26
PALEOCURRENTS
MPS (cm)
FOSSIL GP.
FA
INTERP.
MIDDLE MOSCOVIAN
ORDOVICIAN
METRES
20
0
LA
E-L
TSE-2
CORNWALLIS CARBONATES

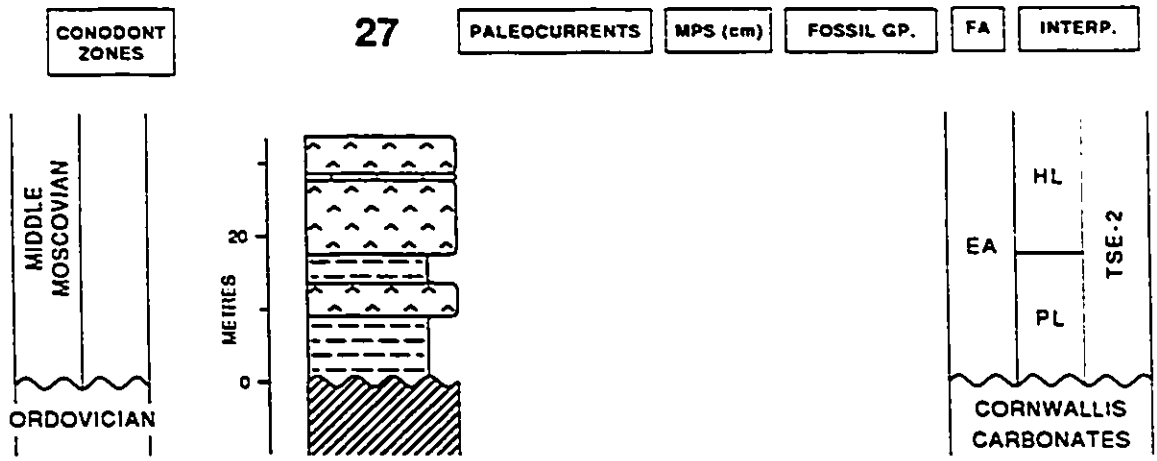
CONODONT ZONES
27
PALEOCURRENTS
MPS (cm)
FOSSIL GP.
FA
INTERP.
MIDDLE MOSCOVIAN
ORDOVICIAN
METRES
20
0
HL
EA
PL
TSE-2
CORNWALLIS CARBONATES

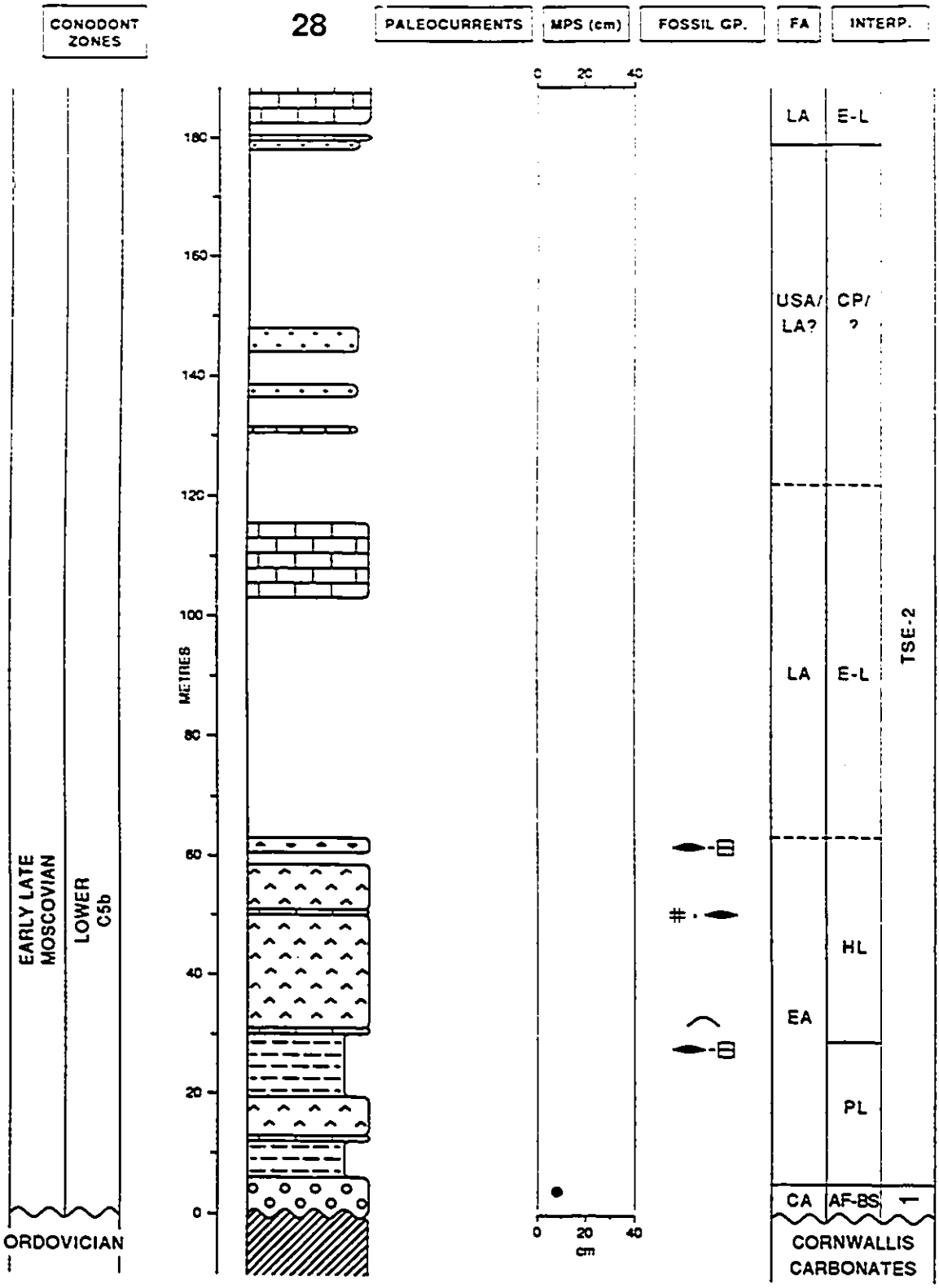
28
CONODONT ZONES
PALEOCURRENTS
MPS (cm)
FOSSIL GP.
FA
INTERP.
METRES
0
20
40
180
160
140
120
100
80
60
40
20
0
LA
E-L
USA/ LA?
CP/ ?
LA
E-L
HL
EA
PL
CA
AF-BS
1
TSE-2
EARLY LATE MOSCOVIAN
LOWER C5b
ORDOVICIAN
CORNWALLIS CARBONATES
cm

APPENDIX 2: SECTION LOCALITIES

Localities of measured sections on Raanes Peninsula. See Thorsteinsson (1974), Map 1300A, for complete geologic and topographic features.

Section	Latitude	Longitude
1	78^0 38' N	84^0 53' W
2	78^0 37' N	84^0 57' W
3	78^0 34' N	85^0 02' W
4	78^0 33' N	85^0 10' W
5	78^0 31' N	85^0 07' W
6	78^0 29' N	85^0 07' W
7	78^0 27' N	85^0 16' W
8	78^0 25' N	85^0 18' W
9	78^0 21' N	85^0 20' W
10	78^0 36' N	84^0 33' W
11	78^0 36' N	84^0 38' W
12	78^0 34' N	84^0 45' W
13	78^0 34' N	84^0 45' W
14	78^0 35' N	84^0 59' W
15	78^0 34' N	84^0 45' W
16	78^0 33' N	84^0 47' W
17	78^0 31' N	84^0 55' W
18	78^0 30' N	84^0 55' W
19	78^0 29' N	84^0 56' W
20	78^0 28' N	84^0 58' W
21	78^0 28' N	84^0 58' W
22	78^0 27' N	84^0 58' W
23	78^0 25' N	85^0 03' W
24	78^0 23' N	85^0 05' W
25	78^0 22' N	85^0 13' W
26	78^0 19' N	85^0 13' W
27	78^0 16' N	85^0 13' W
28	78^0 16' N	85^0 13' W

APPENDIX 3: CONODONT SAMPLES

Locality, facies assemblage, stratigraphic level, conodont zone, and age of samples processed for conodont identification. Conodont zones and ages were determined by Dr. Charles Henderson at the University of Calgary.

	C-184540	C-184547	C-184548	C-184549
Locality	6	10	10	11
Assemblage	basal LA	LA/USA	LA/USA	basal LA
Strat. Level (m)	248	32	152	200
Zone	Upper C5A	C4-C5a	Upper C5a	Upper C5a
Age (Moscovian)	middle	early-mid.	late middle	late middle

	C-184553	C-184570	C-184572	C-184580
Locality	14	24	25	28
Assemblage	LA	LA	basal LA	upper EA
Strat. Level (m)	2	2	42	50
Zone	upper C5b	C1 to P2	C5a	lower C5b
Age (Moscovian)	latest	(Carb/Perm)	middle	early late

APPENDIX 4: STABLE ISOTOPE SAMPLES

Facies assemblage, stratigraphic level, description, and isotopic ratios (C, O, S) of limestone and evaporite samples collected at Section 28. Analyses were done by Dr. Roy Krouse at the University of Calgary.

Sample #	Assemblage	Lev.(m)	Description	$\partial^{13}C$	$\partial^{18}O$	$\partial^{34}S$
C-184576	CA	2.0	M caliche (CHC)	-4.54	-7.78	—
C-184848	CA	6.0	M caliche (CHC)*	-2.88	-5.55	—
C-184502	EA (M/An)	12.0	Black mudstone (NFL)	-1.14	-3.80	—
C-184577	EA (M/An)	12.0	Black mudstone (NFL)	-1.26	-4.15	—
C-184591	EA (M/An)	12.0	Black mudstone (NFL)	-1.87	-4.07	—
C-184592	EA (M/An)	12.3	NB gypsum (NG)	—	—	16.22
C-184593	EA (M/An)	15.0	NB gypsum (NG)	—	—	16.17
C-184594	EA (M/An)	18.0	NB gypsum (NG)	—	—	15.99
C-184595	EA (M/An)	21.0	N gypsum (NG)	—	—	16.02
C-184596	EA (M/An)	24.0	N anhydrite (NBA)	—	—	15.83
C-184506	EA (M/An)	30.0	NM anhydrite (NBA)	—	—	16.07
C-184845	EA (An)	30.2	Black wackestone (FL)	+2.30	-3.49	—
C-184573	EA (An)	30.5	Black wackestone (FL)	+2.77	-3.82	—
C-184581	EA (An)	30.5	Black mudstone (NFL)	-0.51	-4.10	—
C-184597	EA (An)	36.0	NB anhydrite (NBA)	—	—	15.34
C-184598	EA (An)	36.1	Black mudstone (NFL)	-1.12	-6.32	—
C-184599	EA (An)	39.0	NB anhydrite (NBA)	—	—	15.63
C-184600	EA (An)	42.0	NB anhydrite (NBA)	—	—	15.70
C-184751	EA (An)	45.0	NM anhydrite (NBA)	—	—	15.33
C-184752	EA (An)	48.0	NB anhydrite (NBA)	—	—	15.27
C-184753	EA (An)	49.0	Black mudstone (NFL)	+1.36	-5.35	—
C-184754	EA (An)	49.2	N gypsum (NG)	—	—	15.93
C-184755	EA (An)	49.3	Black mudstone (NFL)	+0.83	-5.16	—
C-184756	EA (An)	50.5	Black wackestone (FL)	+2.95	-4.94	—
C-184504	EA (An)	50.5	Black wackestone (FL)	+2.80	-4.66	—
C-184757	EA (An)	51.0	NB gypsum (NG)	—	—	15.28
C-184758	EA (An)	51.5	Gyps. mudstone (NFL)	+0.04	-5.86	—
C-184759	EA (An)	52.5	Gyps. mudstone (NFL)	-0.04	-5.16	14.92
C-184760	EA (An)	53.0	B anhydrite (NBA)	—	—	15.10
C-184761	EA (An)	54.5	NB anhydrite (NBA)	—	—	15.23
C-184762	EA (An)	57.0	Gypsum (NG)*	—	—	15.85
C-184763	EA (An)	58.5	Gypsum (NG)*	—	—	16.03
C-184582	EA (An)	62.0	Grey mudstone (CBL)	-0.51	-12.70	—
C-184508	EA (An)	62.0	Grey lam. mdst. (CBL)	-1.58	-15.95	—
C-184583	LA	180	Black wackestone (FL)	+1.92	-4.13	—

APPENDIX 5: SAMPLE LOCATIONS

Lithology, facies assemblage and stratigraphic level of each hand sample (HS), thin section (TS), polished slab (PS), conodont sample (CS), and geochemistry sample (GS). Cgl= conglomerate; Sst= sandstone; Mdst= mudstone; Lmst= limestone; Cal= caliche; Pal= terrigenous paleosol.

SECTION 1

SAMPLE # (PT- / C-)		LITH	ASSM	LEVEL	HS	TS	PS	CS	GS
15.3	184530	Lmst	LA	20m				X	
15.4	184601	Cgl-Cal ?	LA	30m	X	X			

SECTION 2

SAMPLE # (PT- / C-)		LITH	ASSM	LEVEL	HS	TS	PS	CS	GS
29.1	184602	Cgl	LA	31m	X				
29.2	184531	Lmst	LA	33m				X	

SECTION 3

SAMPLE # (PT- / C-)		LITH	ASSM	LEVEL	HS	TS	PS	CS	GS
16.4	184607	Lmst	Franklin.	0m	X				
16.1	184603	Cgl	CA	11m	X				
16.2	184604	Cgl	CA	38m	X				
16.2b	184606	Lmst-Cal	CA	50m	X	X	X		
16.2c	184605	Sst-Cal	CA	50m	X	X	X		
16.3	184532	Lmst	LA	60m				X	

SECTION 4

SAMPLE # (PT- / C-)		LITH	ASSM	LEVEL	HS	TS	PS	CS	GS
21.1	184533	Lmst	LA	35m				X	

SECTION 5

SAMPLE # (PT- / C-)		LITH	ASSM	LEVEL	HS	TS	PS	CS	GS
30.1	184609	Cgl-Cal	CA	0.5m	X	X	X		
30.3	184610	Lmst	LA	1m	X				
30.2	184535	Lmst	LA	1.5m		X (2)		X	
30.4	184611	Lmst-Cal	LA	1.5m	X	X (2)			
30.5	184612	Lmst-Cal	LA	6m	X	X (5)	X		

SECTION 6

SAMPLE	# (PT- / C-)	LITH	ASSM	LEVEL	HS	TS	PS	CS	GS
14.1	184613	Lmst	Franklin.	0m	X				
14.2	184614	Cgl	CA	5m	X				
14.3	184615	Mdst	CA	26m	X				
14.3b	184616	Cgl	CA	34m	X	X			
14.4	184617	Cgl	CA	34m	X				
14.7	184620	Lmst-Cal	CA	39m	X				
14.8	184536	Lmst-Cal	CA	39m		X		X	
14.5	184618	Lmst-Cal	CA	41m	X	X			
14.6	184619	Lmst-Cal	CA	41m	X	X			
14.9	184621	Cgl	CA	42m	X	X			
14.9b	184622	Cgl-Cal	CA	65m	X	X			
14.9c	184623	Cgl	CA	65m	X				
14.10	184624	Cgl	CA	90m	X				
14.11	184625	Cgl	CA	103m	X				
14.12b	184627	Cgl	CA	120m	X				
14.12	184626	Cgl	CA	124m	X				
14.13	184628	Cgl-Cal	CA	155m	X	X			
14.14	184629	Lmst-Cal	CA	155m	X				
14.14b	184537	Lmst-Cal	CA	155m	X	X (3)			
14.15	184630	Lmst-Cal	CA	157m	X				
14.16	184631	Mdst	CA	169m	X				
14.17	184632	Cgl	CA	169m	X				
14.18	184633	Cgl-Cal	CA	169m	X	X			
14.19	184634	Cgl	CA	181m	X				
14.20	184635	Cgl	CA	200m	X				
14.21	184636	Lmst-Cal	CA	202m	X	X			
14.22	184637	Cgl-Cal	CA	209m	X				
14.24	184638	Cgl	CA	210m	X	X			
14.23	184538	Lmst	LA	211m				X	
14.25	184639	Cgl	CA	221m	X				
14.26	184640	Cgl	CA	221m	X				
14.27	184641	Lmst	LA	222m	X				
14.28	184539	Lmst	LA	222m		X		X	
14.29	184642	Lmst-Cal	LA	222m	X	X			
14.30	184643	Mdst-Cal	CA	223m	X	X			
14.30b	184644	Cgl	CA	224m	X				
14.31	184645	Cgl	CA	229m	X				
14.31b	184646	Mdst	CA	230m	X				
14.32	184647	Mdst	CA	236m	X				
14.32b	184648	Mdst-Pal	CA	Scree	X				
14.33	184540	Lmst	LA	245m				X	

SECTION 7

SAMPLE	# (PT- / C-)	LITH	ASSM	LEVEL	HS	TS	PS	CS	GS
32.1	184649	Cgl	CA	4m	X				
32.1b	184650	Cgl	CA	8m	X				
32.2	184651	Cgl	CA	26m	X				

32.3	184652	Cgl	CA	36m	X				
32.4	184541	Lmst	LA	37m		X		X	
32.5	184653	Lmst	LA	37m	X				
32.6	184654	Cgl	CA	39m	X				
32.7	184655	Cgl-Cal	CA	45m	X	X			
32.8	184542	Lmst	LA	53m		X		X	
32.9	184656	Lmst	LA	54m	X				
32.10	184657	Cgl	CA	55m	X				
32.11	184658	Cgl	CA	93m	X	X			
32.14	184660	Lmst	LA	127m	X				
32.13	184659	Lmst	LA	134m	X				
32.12	184543	Lmst	LA	136m				X	

SECTION 8

SAMPLE # (PT-/C-)		LITH	ASSM	LEVEL	HS	TS	PS	CS	GS
31.1	184661	Cgl-Cal	CA	6m	X	X			
31.2	184662	Cgl-Cal ?	CA	18m	X				
31.3	184663	Cgl	CA	28m	X				
31.4	184664	Lmst-Cal ?	CA	28m	X	X			
31.5	184544	Lmst	LA	74m				X	
31.6	184665	Lmst	LA	76m	X	X			
31.7	184666	Cgl-Cal	CA	?	X	X			
31.8	184545	Lmst	LA	?				X	

SECTION 9

SAMPLE # (PT-/C-)		LITH	ASSM	LEVEL	HS	TS	PS	CS	GS
19.1	184667	Cgl	CA	52m	X				
19.2	184668	Cgl-Cal	CA	58m	X	X			
19.3	184669	Cgl	CA	72m	X				
19.5	184670	Cgl-Cal	CA	90m	X	X	X		
19.6	184546	Lmst	LA	92m	X				

SECTION 10

SAMPLE # (PT-/C-)		LITH	ASSM	LEVEL	HS	TS	PS	CS	GS
15.5	184680	Sst-Cal	LSA	6m	X		X		
3.1	184672	Sst-Cal	LSA	~10m	X	X	X		
3.2	184673	Sst-Cal	LSA	~10m	X	X (2)	X		
3.2a	—	Sst-Cal	LSA	~10m			X		
3.2b	184674	Sst-Cal	LSA	~14m	X		X		
15.6	184681	Cgl-Cal	CA	~15m	X	X	X		
15.7	184682	Cgl-Cal	CA	~15m	X		X		
15.8	184683	Cgl-Cal	CA	~15m	X				

15.9	184684	Cgl-Cal	CA	~15m	X	X	X		
15.10	184685	Cgl-Cal	CA	~15m	X		X		
3.3	184675	Cgl-Cal	CA	15m	X	X			
3.4	184676	Cgl	CA	15m	X				
3.5	184677	Cgl	CA	15m	X				
3.6	184678	Sst	USA	scree	X				
3.6b	184547	Lmst	LA	31m				X	
3.7	184679	Sst	USA	37m	X				
3.30	184713	Mdst-Pal	USA	61m	X				
15.11	184686	Sst	USA	122m	X				
15.12	184687	Sst	USA	141m	X				
15.13	184688	Lmst	LA	143m	X				
15.14	184689	Sst	USA	145m	X				
15.15	184690	Sst	USA	145.0m	X				
15.16	184691	Sst	USA	146.0m	X				
15.17	184692	Sst	USA	147.0m	X				
15.18	184693	Sst	USA	148.0m	X	X			
15.19	184694	Sst	USA	148.5m	X				
15.20	184695	Sst	USA	149.0m	X	X			
15.21	184696	Sst	USA	149.2m	X				
15.22	184697	Sst	USA	149.5m	X				
15.23	184698	Sst	USA	149.8m	X	X			
15.24	184699	Sst	USA	150.0m	X	X			
15.25	184700	Sst	USA	150.5m	X	X			
15.26	184701	Lmst	USA	150.7m	X	X			
15.27	184702	Lmst	USA	151.0m	X	X			
15.28	184703	Lmst	USA	151.5m	X				
15.29	184704	Lmst	USA	152.0m	X				
15.30	184705	Lmst	USA	152.5m	X				
15.31	184706	Lmst	LA	153.0m	X				
15.32	184707	Lmst	LA	153.7m	X				
15.33	184548	Lmst	LA	153.7m				X	
15.34	184708	Sst	USA	155m	X				
15.35	184709	Sst	USA	163m	X				
15.36	184710	Lmst	LA	173m	X				
15.37	184711	Sst-Cal	USA	177m	X	X			
15.38	184712	Sst	USA	185m	X				

SECTION 11

SAMPLE	# (PT- / C-)	LITH	ASSM	LEVEL	HS	TS	PS	CS	GS
7B.5	184729	Sst	Franklin.	0m	X				
7.0a	184714	Sst-Cal	LSA	18m	X	X	X		
7.0b	184715	Lmst-Cal	LSA	18m	X	X	X		
7.1	184716	Sst-Cal	LSA	40m	X		X		
7.2	184717	Sst	LSA	41m	X				
7.3	184718	Cgl-Cal	CA	42m	X	X			
7.4	184719	Sst-Cal	CA	44m	X	X			
7.5	184720	Cgl	CA	57m	X				
7.6	184721	Cgl	CA	111m	X				
7.7	184722	Cgl	CA	117m	X				
7.8	184723	Sst-Cal	CA	135m	X				
7B.1	184725	Cgl	CA	159m	X				
7B.2	184726	Cgl	CA	169m	X				

7B.3	184727	Sst	USA	189m	X				
7B.4	184728	Lmst	LA	198m				X	
7.9	184549	Lmst	LA	198m				X	
7.10	184550	Lmst	LA	201m				X	
7.11	184724	Sst	Trold F. Fm.		—	X			

SECTION 12

SAMPLE # (PT- / C-)		LITH	ASSM	LEVEL	HS	TS	PS	CS	GS
2.1	184730	Sst	CA	28m	X				
2.2	184731	Cgl	CA	41m	X				
2.3	184732	Lmst	LA	62m	X				
2.4	184733	Sst	USA	78m	X				
2.5	184734	Lmst	LA	82m	X				
2.6	184735	Lmst	LA	90m	X				

SECTION 13

SAMPLE # (PT- / C-)		LITH	ASSM	LEVEL	HS	TS	PS	CS	GS
1.1	184736	Mdst	Franklin.	0m	X				
1.2	184737	Cgl	CA	17m	X				
1.3	184738	Cgl	CA	21m	X				
1.3b	184739	Mdst	CA	21m	X				
1.4	184740	Sst-Cal	CA	58m	X	X			
1.4b	184741	Mdst-Cal	CA	58m	X		X		
1.6b	184745	Cgl	CA	61m	X				
1.5	184742	Cgl	CA	63m	X				
1.5b	184743	Sst-Cal ?	CA	63m	X				
1.25	184768	Sst	CA	64m	X				
1.6	184744	Sst	CA	64m	X				
1.7	184746	Cgl	CA	75m	X				
1.8	184747	Cgl	CA	75m	X				
1.9	184748	Sst-Cal	CA	109m	X				
1.10	184749	Sst	CA	113m	X				
1.10b	184750	Sst-Cal	CA	113m	X	X	X		
1.11b	184752	Sst	CA	114m	X				
1.12	184753	Sst-Cal	CA	114m	X				
1.26	184769	Sst-Cal	CA	114m	X		X		
1.11	184751	Cgl	CA	115m	X				
1.13	184753	Cgl	CA	125m	X				
1.14	184754	Cgl	CA	165m	X				
1.15	184755	Cgl	CA	167m	X				
1.16	184756	Sst-Cal ?	USA	175m	X		X		
1.27	184770	Sst-Cal ?	USA	175m	X				
1.16b	184757	Sst-Cal	USA	178m	X				
1.17	184758	Sst	USA	197m	X				
1.18	184759	Sst	USA	205m	X				
1.19	184551	Lmst	LA	209m				X	
1.19b	184760	Sst	USA	214m	X				
1.20b	184762	Sst	LA	221m	X				

1.20c	184763	Sst-Cal	LA	221m	X	X
1.20a	184761	Cgl	USA	222m	X	X
1.21	184764	Sst	LA	230m	X	
1.22	184765	Lmst	LA	233m	X	
1.23	184766	Cgl-Cal ?	CA	246m	X	X
1.24	184767	Cgl-Cal ?	CA	247m	X	X

SECTION 14

SAMPLE # (PT- / C-)		LITH	ASSM	LEVEL	HS	TS	PS	CS	GS
27.1	184553	Lmst	LA	1m				X	
27.2	184554	Lmst	LA	6m				X	

SECTION 15

SAMPLE # (PT- / C-)		LITH	ASSM	LEVEL	HS	TS	PS	CS	GS
18.1	184552	Lmst	LA	73m				X	
18.2	184771	Cgl-Cal	LA	76m	X	X			
18.3	184772	Lmst	LA	76m	X				
18.4	184773	Lmst	LA	76m	X				
18.5	184774	Cgl	LA	81m	X				
18.6a	184775	Cgl	LA	81m	X				
18.6b	184776	Cgl	LA	82m	X				

SECTION 16

SAMPLE # (PT- / C-)		LITH	ASSM	LEVEL	HS	TS	PS	CS	GS
6.1a	184777	Mdst	Franklin.	0m	X				
6.1b	184778	Lmst	Franklin.	0m	X				
6.2	184779	Lmst-Cal	LSA	2m	X	X	X		
6.4	184780	Cgl-Cal ?	LSA	5m	X	X			
6.4b	184781	Sst-Cal ?	LSA	47m	X				
6.5	184782	Cgl	LSA	~65m	X				
6.6	184783	Lmst-Cal	LSA	~65m	X		X		
6.7b	184785	Sst-Cal	LSA	~65m	X		X		
6.7	184784	Sst-Cal	LSA	81m	X				
6.7c	184786	Sst-Cal	LSA	81m	X	X	X		
5.0	184787	Sst	LSA	130m	X				
5.0b	184788	Cgl	CA	131m	X				
5.0c	184789	Cgl-Cal	CA	163m	X	X	X		
5.1	184790	Cgl	CA	190m	X				
5.2	184791	Cgl	CA	205m	X				
5.3	184792	Sst	USA	210m	X				
5.4	184793	Sst	USA	~210m	X	X			
5.5	184555	Lmst	LA	221m				X	

5.6	184793	Cgl	CA	230m	X				
5.7	184794	Cgl-Cal	CA	235m	X	X			

SECTION 17

SAMPLE # (PT- / C-)		LITH	ASSM	LEVEL	HS	TS	PS	CS	GS
4.1b	184557	Lmst	LA	10m				X	
4.1	184556	Lmst	LA	15m				X	

SECTION 18

SAMPLE # (PT- / C-)		LITH	ASSM	LEVEL	HS	TS	PS	CS	GS
12.2	184797	Cgl	CA	18m	X				
12.1	184796	Mdst	CA	19m	X				
12.3	184798	Cgl	CA	43m	X				
12.4	184799	Sst	USA	scree	X				
12.5	184558	Lmst	LA	60m				X	

SECTION 19

SAMPLE # (PT- / C-)		LITH	ASSM	LEVEL	HS	TS	PS	CS	GS
11.1	184800	Cgl	CA	15m	X	X			
11.2	184801	Lmst-Cal	CA	57m	X	X	X		
11.3a	184802	Cgl	CA	76m	X				
11.5	—	Sst	USA	126m	X				
11.6	184803	Sst	USA	127m	X				
11.3b	184559	Lmst	LA	146m				X	
11.7	184561	Lmst	LA	146m				X	
11.4	184560	Lmst	LA	154m				X	
11.8	184804	Sst	Sst	156m	X				

SECTION 20

SAMPLE # (PT- / C-)		LITH	ASSM	LEVEL	HS	TS	PS	CS	GS
33.1	184805	Cgl	CA	2m	X				
33.2	184806	Sst-Cal	USA	11m	X		X		
33.3	184807	Sst-Cal	USA	17m	X				
33.4	184562	Lmst	LA	31m				X	

SECTION 21

SAMPLE # (PT- / C-)		LITH	ASSM	LEVEL	HS	TS	PS	CS	GS
23.2	184809	Lmst	Franklin.	0m	X				
23.1	184808	Cgl	CA	1m	X				
23.3	184810	Cgl	CA	1m	X				
23.4	184563	Lmst	LA	11m		X		X	
23.5	184811	Cgl	CA	11m	X				
23.6	184812	Mdst-Cal	CA	17m	X	X	X		
23.7	184813	Cgl-Cal	CA	17m	X	X			
23.8	184814	Cgl	CA	37m	X				
23.9	184815	Sst	USA	46m	X	X			
23.10	184564	Lmst	LA	59m		X		X	
23.11	184816	Sst	USA	64m	X				
23.12	184817	Lmst	LA	scree	X				

SECTION 22

SAMPLE # (PT- / C-)		LITH	ASSM	LEVEL	HS	TS	PS	CS	GS
9.1	184819	Cgl	CA	6m	X				
9.2	184820	Lmst-Cal	CA	15m	X		X		
9.3	184565	Lmst-Cal	CA	15m		X	X	X	
9.4	184821	Lmst-Cal	CA	~15m	X		X		
9.5	184822	Cgl	CA	24m	X	X			
9.6	184823	Cgl	CA	39m	X				
9.6b	184825	Sst	USA	40m				X	
9.6c	184566	Lmst	LA	51m				X	
9.6c	184826	Lmst	LA	51m	X				
9.7	184824	Sst	USA	75m	X				
9.8	184567	Lmst	LA	108m				X	
9.9	184827	Sst	USA	scree	X				

SECTION 23

SAMPLE # (PT- / C-)		LITH	ASSM	LEVEL	HS	TS	PS	CS	GS
26.1	184828	Lmst	Franklin.	0m	X				
26.2	184829	Cgl-Cal ?	CA	1m	X		X		
26.3	184830	Cgl-Cal	CA	5m	X	X			
26.4	184831	Cgl-Cal	CA	15m	X	X	X		
26.5	184568	Lmst-Cal ?	LA	28m			X	X	
26.6	184832	Lmst-Cal ?	LA	28m	X	X			
26.7	184833	Cgl	CA	38m	X				
26.8	184834	Sst	USA	43m	X				
26.9	184569	Lmst	LA	62m				X	
26.10	184835	Sst	USA	76m	X				

SECTION 24

SAMPLE # (PT- / C-)		LITH	ASSM	LEVEL	HS	TS	PS	CS	GS
13.2	184570	Lmst	LA	3m				X	

SECTION 25

SAMPLE # (PT- / C-)		LITH	ASSM	LEVEL	HS	TS	PS	CS	GS
25.1	184836	Cgl-Cal	CA	33m	X	X	X		
25.2	184837	Lmst-Cal	CA	36m	X	X	X		
25.3	184571	Lmst	LA	37m				X	

SECTION 26

SAMPLE # (PT- / C-)		LITH	ASSM	LEVEL	HS	TS	PS	CS	GS
24.1	184572	Lmst	LA	5m				X	

SECTION 27

SAMPLE # (PT- / C-)		LITH	ASSM	LEVEL	HS	TS	PS	CS	GS
13.3	—	Mdst-Pal	EA	2m	X				
13.5	184840	Mdst-Pal	EA	2m	X				
13.6	184840	Evap	EA	8m	X				
13.4	184839	Sst	?	scree (35m)	X				

SECTION 28

SAMPLE # (PT- / C-)		LITH	ASSM	LEVEL	HS	TS	PS	CS	GS
8.1	184575	Lmst-Cal ?	CA	1m				X	X
8.2	184576	Cgl-Cal	CA	2m		X	X	X	X
10.2	184841	Cgl-Cal	CA	~2m	X				
10.4	184843	Lmst-Cal	CA	~2m	X	X			
8.2b	184849	Cgl-Cal	CA	3m	X		X		
8.3	184850	Lmst-Cal	CA	5m	X		X		
10.5	184844	Lmst-Cal	CA	~5m	X	X			
8.0	184848	Lmst-Cal	CA	6m	X				X
10.3	184842	Lmst-Cal	CA	~6m	X	X			

8.4a	184577	Lmst	EA	12m		X (2)	X	X
8.4b	184578	Lmst	EA	12m			X	
8.4c	184501	Lmst	EA	12m	X			X
8.5	184502	Lmst-Cal	EA	12m	X	X		X
G-1	184591	Lmst	EA	12.0m				X
G-2	184592	Evap	EA	12.3m				X
G-3	184593	Evap	EA	15.0m				X
G-4	184594	Evap	EA	18.0m				X
G-5	184595	Evap	EA	21.0m				X
G-6	184596	Evap	EA	24.0m				X
10.8a	184846	Mdst	EA	~28m	X			
10.8b	184847	Mdst	EA	~28m	X			
10.6	184845	Lmst	EA	~30m			X	X
10.7	184573	Lmst	EA	~31m		X	X	X
10.7b	—	Lmst	EA	~31m	X			
8.12	184581	Lmst	EA	31m		X	X	X
8.11	184506	Lmst	EA	31m	X	X		X
8.6	184579	Lmst	EA	36m		X	X	
G-7	184597	Evap	EA	36.0m				X
G-8	184598	Lmst	EA	36.1m				X
G-9	184599	Evap	EA	39.0m				X
G-10	184600	Evap	EA	42.0m				X
G-11	184751	Evap	EA	45.0m				X
G-12	184752	Evap	EA	48.0m				X
8.9	184505	Evap	EA	48m	X	X		
8.9b	—	Evap	EA	48m		X		
G-13	184753	Lmst	EA	49.0m				X
G-14	184754	Evap	EA	49.2m				X
G-15	184755	Lmst	EA	49.3m				X
8.7	184580	Lmst	EA	50m	X	X		X
8.7b	184503	Lmst	EA	50m	X			X
8.8	184504	Lmst	EA	50m	X	X		X
G-16	184756	Lmst	EA	50m				X
G-17	184757	Evap	EA	51.0m				X
G-18	184758	Lmst	EA	51.5m				X
G-19	184759	Lmst	EA	52.5m				X
G-20	184760	Evap	EA	53.0m				X
G-21	184761	Evap	EA	54.5m				X
G-22	184762	Evap	EA	57.0m				X
G-23	184763	Evap	EA	58.5m				X
10.9b	184582	Brecc	EA	61m	X	X	X	X
10.9c	184507	Brecc	EA	61m	X	X		
10.9d	184508	Brecc	EA	61m	X	X		X
10.9	184574	Lmst	EA	~62m			X	
22.1	184509	Sst-Cal ?	USA	132m	X	X		
22.2	184510	Sst	USA	138m	X	X		
22.3	184511	Sst	USA	138m	X			
22.4	184512	Sst	USA	146m	X	X		
22.5	184513	Sst	USA	180m	X			
22.6	184583	Lmst	LA	181m			X	X

LOCALITY "A" (Northern Blind Fiord belt: 78°32'N / 85°09'W)

SAMPLE # (PT- / C-)		LITH	ASSM	LEVEL	HS	TS	PS	CS	GS
15.1	184608	Sst	?	scree (2m)	X				
15.2	184534	Lmst	LA	~15m				X	

LOCALITY "B" (NNE of Trold Fiord: 78°44'N / 84°15'W)

SAMPLE # (PT- / C-)		LITH	ASSM	LEVEL	HS	TS	PS	CS	GS
20.1	184671	Sst	Upper Cc	—	X				

LOCALITY "C" (Northern Trold Fiord belt: 78°36'N / 84°41'W)

SAMPLE # (PT- / C-)		LITH	ASSM	LEVEL	HS	TS	PS	CS	GS
—	—	—	—	—					

LOCALITY "D" (Svendsen Peninsula: 78°03'N / 85°07'W)

SAMPLE # (PT- / C-)		LITH	ASSM	LEVEL	HS	TS	PS	CS	GS
10.1	184584	Lmst	LA	—				X	

LOCALITY "E" (Bjorne Peninsula: 77°25'N / 86°47'W)

SAMPLE # (PT- / C-)		LITH	ASSM	LEVEL	HS	TS	PS	CS	GS
28.1	184585	Lmst	—	21m				X	
28.2	184514	Lmst	—	48m	X				
28.3	184515	Sst	—	61m	X				
28.4	184516	Sst	—	67m	X				
28.5	184517	Sst	—	75m	X				
28.6	184518	Sst	—	78m	X				
28.7	184519	Sst	—	88m	X				
28.8	184586	Lmst	—	111m	X				
28.9	184520	Sst	—	116m	X				
28.10	184521	Lmst	—	249m	X				
28.11	184522	Lmst	—	253m	X				
28.12	184523	Sst	—	296m	X				
28.13	184524	Lmst	—	297m	X				
28.14	184587	Lmst	—	300m				X	
28.15	184525	Sst	—	368m	X				
28.16	184526	Sst	—	405m	X				

28.17	184527	Sst	—	478m	X	
28.18	184588	Sst	—	530m		X
28.19	184528	Sst	—	565m	X	
28.20	184529	Lmst	—	618m	X	
28.21	184589	Lmst	—	755m		X